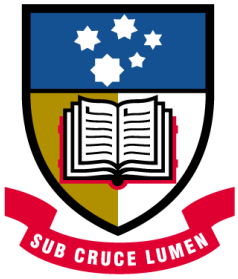

Leak Detection and Condition Assessment for Water Distribution Pipelines using Fluid Transient Waves

Jinzhe Gong

B.Eng., M.Eng.

Thesis submitted in fulfilment of the requirements for the degree of Doctor of Philosophy

The University of Adelaide

Faculty of Engineering, Computer and Mathematical Sciences

School of Civil, Environmental and Mining Engineering

To my beloved wife He Shi and son Keming Gong

Abstract

The focus of this PhD research is to develop non-invasive and cost-effective techniques for assessing the structural condition of pressurised pipelines using fluid transient pressure waves. The specific objectives include the detection of leaks and localised deterioration that is distributed along a pipeline, such as extended sections of corrosion or the spalling of cement lining. The latter is described by *pipeline condition assessment* in this thesis.

The transient behaviour of a leak is studied in the frequency domain. Numerical studies conducted in this research demonstrate that two leak-induced patterns (on the resonant and the anti-resonant responses) can exist in a frequency response diagram (FRD). The amplitudes of the responses are related to the impedance of the valve in a reservoir-pipeline-valve (RPV) system.

A new leak detection technique has been developed in this research based on the further understanding of the leak-induced patterns. This technique uses the relative sizes of the first three resonant responses to determine the location and size of a single leak in RPV systems. In reservoir-pipeline-dead end systems, the information required for single event leak detection is further reduced to the first two resonant responses.

A new measurement strategy for the extraction of the FRD of single pipelines is proposed in this research. The boundary valve loss is used to adjust the amplitude of the leak-induced pattern on the resonant responses and also the sharpness of the resonant peaks. A specific type of pseudo-random binary sequence (PRBS) termed the inverse repeat sequence (IRS), is used as the excitation signal. The antisymmetric property of IRS enables part of the nonlinear responses of the system under excitation to be cancelled out, yielding a measured FRD close to the theoretical linear system response. A

side-discharge valve based transient generator is designed and fabricated in this research to implement the new FRD measurement strategy. Laboratory experiments are conducted on an intact pipeline and a pipeline with a leak.

This research also conducts analysis of the characteristics of distributed pipe wall deterioration and develops new detection techniques. In a measured pressure trace, the size of the reflection resulting from a section of pipeline with a change in wall thickness is indicative of the characteristic impedance of this section. Once the impedance of this section is determined, the wave speed and wall thickness can be estimated. A technique for the detection of a single deteriorated section in pipelines is developed based on the above analysis.

Two other condition assessment techniques are developed to deal with the complexities induced by multiple deteriorated sections. The first technique is termed *reconstructive MOC* (method of characteristics) *analysis*, which uses the pressure trace measured at the upstream face of the valve in a RPV system to determine the distribution of the impedance along the pipeline. The algorithm reconstructs a MOC grid by calculating the MOC compatibility equations backwards in time, estimating the properties of the pipeline (impedance, wave speed) and the length of each pipe reach as discretised by the MOC grid from the valve towards the reservoir. Preliminary experimental verification is conducted to verify the applicability of the new technique.

The second technique is *reconstructive transient analysis* (RTA), which can be conducted at any interior accessible points along a pipeline, and does not require a RPV boundary condition. The RTA uses two pressure transducers in close proximity to measure two transient pressure traces in one test. A signal processing algorithm is developed to extract the directional transient waves (traveling upstream and downstream). The use of the directional transient waves enables the step response function (SRF) of the section of pipe upstream or downstream of the paired pressure transducers to be obtained. The *reconstructive MOC analysis* is then adapted to interpret the SRF to yield the distribution of the impedance, from which the location and severity of distributed deterioration can be identified.

Statement of Originality

I, *Jinzhe Gong*, hereby declare that this work contains no material which has been accepted for the award of any other degree or diploma in any university or other tertiary institution in my name and, to the best of my knowledge and belief, contains no material previously published or written by another person, except where due reference has been made in the text. In addition, I certify that no part of this work will, in the future, be used in a submission in my name, for any other degree or diploma in any university or other tertiary institution without the prior approval of the University of Adelaide and where applicable, any partner institution responsible for the joint-award of this degree.

I give consent to this copy of my thesis when deposited in the University Library, being made available for loan and photocopying, subject to the provisions of the Copyright Act 1968.

The author acknowledges that copyright of published works contained within this thesis resides with the copyright holder(s) of those works.

I also give permission for the digital version of my thesis being made available on the web, via the University's digital research repository, the Library catalogue, the Australian Digital Thesis Program (ADTP) and also through web search engines, unless permission has been granted by the University to restrict access for a period of time.

Signed: .....Date: ...../.....

Acknowledgments

First of all, I would like to show my gratitude to my supervisors, Prof. Martin Lambert, Prof. Angus Simpson and Dr. Aaron Zecchin. This PhD thesis would not be possible without their guidance and support. They have reviewed all my manuscripts and given comments for improvement. They also provided financial support to me for attending international conferences.

I gratefully acknowledge the support from Ms. Barbara Brougham. She has given me many helpful advices on academic writing. She helped me gain not only skills but also confidence in writing academic papers.

I would like to thank technicians Brenton Howie, Simon Order and Stan Woithe in the Robin Hydraulics Laboratory at the University of Adelaide. They provided support throughout my laboratory experiments, especially for the design and fabrication of the customised transient signal generator used in my research.

I thank all my fellow postgraduate students within the School for keeping company and sharing experiences with me. I also thank all the staff in the School of Civil, Environmental and Mining Engineering for their support and help over the years of my PhD study.

I would like to thank the emotional and financial support from my parents, Mr. Qi Gong and Ms. Jinying Zhang. I greatly appreciate my wife, He Shi, for her unwavering support and encouragement since we were married. Lastly, I thank my baby boy, Keming, who brought me joy and hope.

Table of Contents

List of Publications

Journal papers

The following peer-reviewed journal papers are the major outcomes of this research and they form the main body of this thesis.

1. Gong, J., Zecchin, A. C., Simpson, A. R., and Lambert, M. F. (2013). "Frequency response diagram for pipeline leak detection: comparing the odd and the even harmonics." *Journal of Water Resources Planning and Management*, DOI: 10.1061/(ASCE)WR.1943-5452.0000298 (accepted for publication).

2. Gong, J., Lambert, M. F., Simpson, A. R., and Zecchin, A. C. (2013). "Single event leak detection in a pipeline using the first three resonant responses." *Journal of Hydraulic Engineering*, 139(6), 645-655.

3. Gong, J., Simpson, A. R., Lambert, M. F., and Zecchin, A. C. (2013). "Determination of the frequency response diagram of single pipelines using persistent transient excitation: a numerical investigation." *Journal of Hydraulic Research*, DOI: 10.1080/00221686.2013.818582 (accepted for publication).

4. Gong, J., Lambert, M. F., Simpson, A. R., and Zecchin, A. C. (2013). "A customized side-discharge valve for extracting the frequency response function of hydraulic pipelines using pseudorandom binary signals." *Journal of Hydraulic Engineering* (under review).

5. Gong, J., Lambert, M. F., Simpson, A. R., and Zecchin, A. C. (2013). "Single event leak detection in a pipeline using fluid transients with inverse-repeat binary sequences." *Journal of Hydraulic Engineering*, (under review).

6. Gong, J., Simpson, A. R., Lambert, M. F., Zecchin, A. C., Kim, Y., and Tijsseling, A. S. (2013). "Detection of distributed deterioration in single pipes using transient reflections." *Journal of Pipeline Systems Engineering and Practice*, 4(1), 32-40.

7. Gong, J., Simpson, A. R., Zecchin, A. C. and Lambert, M. F. (2013). "Detection of extended structural deterioration in a pipeline using fluid transients: a sensitivity analysis." *Journal of Hydraulic Engineering*, (under review).

8. Gong, J., Lambert, M. F., Simpson, A. R., and Zecchin, A. C. (2013). "Detection of localized deterioration distributed along single pipelines by reconstructive MOC analysis." *Journal of Hydraulic Engineering*, DOI: 10.1061/(ASCE)HY.1943-7900.0000806 (accepted for publication).

9. Gong, J., Zecchin, A. C., Lambert, M. F., and Simpson, A. R. (2013). "Condition assessment of hydraulic pipelines using paired pressure transducers and reconstructive transient analysis." *Journal of Hydraulic Engineering* (under review).

Conference papers

The following conference papers are also outcomes of this research.

1. Gong, J., Lambert, M. F., Simpson, A. R., and Zecchin, A. C. (2012). "Distributed deterioration detection in single pipelines using transient measurements from pressure transducer pairs." In: *11th International Conference on Pressure Surges*, 24-26 October 2012, Lisbon, Portugal. Cranfield, UK: BHR Group, 2012: 127-140.

2. Gong, J., Lambert, M. F., Simpson, A. R., and Zecchin, A. C. (2012). "Distributed deterioration detection and location in single pipes using the impulse response function." In: WDSA 2012: *14th Water Distribution Systems Analysis Conference,* 24-27 September 2012, Adelaide, South Australia. Barton, ACT, Australia: Engineers Australia, 2012: 702-719.

3. Gong, J., Zecchin, A. C., Lambert, M. F., and Simpson, A. R. (2012). "Signal separation for transient wave reflections in single pipelines using inverse filters." In: *World Environmental and Water Resources Congress 2012: Crossing Boundaries*, 20-24 May 2012, Albuquerque, New Mexico. Reston, VA: ASCE, 2012: 3275-3284.

4. Gong, J., Simpson, A. R., Lambert, M. F., Zecchin, A. C., and Kim, Y. (2011). "Detection of distributed deteriorations in single pipes using transient reflections." In: ICPTT 2011: *International Conference on Pipelines and Trenchless Technology 2011*, 26-29 October 2011, Beijing China. (Presented in the conference but not included in the conference proceedings. Published as Journal Paper No.6 after a major revision.)

5. Gong, J., Lambert, M. F., Zecchin, A. C., and Simpson, A. R. (2011). "Frequency response measurement of pipelines by using inverse-repeat binary sequences." In: CCWI 2011: *Computing and Control for the Water Industry 2011: Urban Water Management - Challenges and Opportunities*, 5-7 September, 2011, the University of Exeter, Exeter, UK. Exeter, UK: the University of Exeter, 2011: 883-888.

List of Tables

List of Figures

Chapter 1

Introduction

1.1 Research background

1.1.1 Significance of leak detection and condition assessment for water pipelines

Water distribution pipeline systems are widely used all over the world. They are critical infrastructure for industry and an indispensable facility for every household in modern cities. However, water distribution pipelines have become one of the most costly and difficult types of infrastructure to maintain in the modern world. Pipeline systems are subject to continual structural deterioration of the pipe wall from internal and external factors, such as internal and external corrosion, effects of natural disasters, excavation, and extreme high or low pressure resulting from inappropriate operation.

Leakage is one of the typical deterioration types in water transmission and distribution systems, and it is believed to be the major reason for water loss. According to publications released by the International Water Association (Lambert 2002) and the Asian Development Bank (McIntosh and Yniguez 1997), 'non-revenue water' (NRW) or 'unaccounted for water' (UFW) is between 20 % to 40 % for most of the countries or cities investigated. The significant loss of water in transmission and distribution increases cost for water utilities and imposes additional burden to the environment.

In addition to leaks, localised wall deterioration that is distributed along pipelines is also common in water transmission and distribution systems. Typical examples include internal or external corrosion (Swietlik et al. 2012) and the spalling of cement mortar lining (Stephens et al. 2008). Distributed deterioration may not impose imminent threats to the operation of a pipeline system, however it usually reduces water transmission efficiency (Tran et al. 2010), creates water quality problems (Vreeburg and Boxall 2007), and may also develop into more serious blockages or bursts over time (Zamanzadeh et al. 2007). In the US, there are an estimated 240,000 water main breaks per year, and the number of busts increases substantially near the end of the service life of the system (US EPA 2011).

The maintenance of water transmission and distribution systems can be very expensive. In a recent 12 months period, Australian urban utilities spent over one billion dollars on the maintenance and replacement of old and under-performing pipeline assets (WSAA 2008). In the US, it was estimated that $138 billion would be required to maintain and replace existing drinking water systems over the first 20 years of the 21st century (Selvakumar et al. 2002). The cost of maintenance is expected to increase with the aging of the infrastructure, most of which were laid in the post-war period and have been in the deterioration process for many decades. Given the remarkable costs and the significant social importance, strategically targeted programs of maintenance, replacement and rehabilitation are imperative to ensure the reliability and integrity of the critical but deteriorating infrastructure.

Accurate and cost-effective assessment of pipeline condition is essential to enable the development of targeted asset replacement programs. However, the detection of deterioration is challenging because the size and extent of the infrastructure are significant in scale, and much of the system is buried underground hence not easily observable.

1.1.2 Limitations in current technologies

Current pipeline inspection technologies cannot fully meet the needs of water utilities, which include, but not limited to, low-cost, low-intrusion capability, inspecting without disruption of service, and being able to provide comprehensive structural data (e.g. loss of linings or metal) (US EPA 2009). A number of commercial pipeline leak detection techniques are available, such as acoustic techniques (Fuchs and Riehle 1991; Tafuri 2000), ground penetrating radar (Eiswirth and Burn 2001), electromagnetic techniques (Atherton et al. 2000; Roubal 2002), tracer gas injection (Hargesheimer 1985). A detailed review of methods for leakage management in pipeline systems can be found in Puust et al. (2010). The current leak detection techniques are either inefficient for long transmission mains or too costly to implement (Colombo et al. 2009).

Current techniques for assessing the condition of the pipe wall also have limitations. Closed-circuit television (CCTV) inspection (Tran et al. 2009) captures images of a pipe's inner surface using a camera on a carrier that travels within the pipeline. However, this method is intrusive, costly and not reliable for identifying the severity of a deterioration (e.g. the depth of a crack) (Hao et al. 2012). Surface penetrating radar (SPR) (Donazzolo and Yelf 2010) and in-pipe GPR (Ekes et al. 2011) techniques apply electromagnetic sensors directly to the outside or inside surface of a pipeline, but they are mainly utilized for localized inspection and are inefficient and costly for long range applications. Magnetic flux leakage (MFL) testing is also a localized electromagnetic method which can assess the metal loss in a short section of pipe. However, the use of MFL in water pipelines is limited to cleaned, unlined pipes and also requires accessibility to the exterior of the pipeline (Liu and Kleiner 2013). The guided wave ultrasound method (Rose et al. 2009) uses ultrasonic waves propagating along the pipe wall and their reflections to determine the location and sizes of defects on the wall, but the range of inspection is limited in buried pipes due to the rapid signal attenuation (Liu and Kleiner 2013).

The United States environmental protection agency (US EPA) (2012) recently conducted research to identify and characterise the state of technology for structure condition assessment (including leak detection and wall condition assessment) of drinking water transmission and distribution systems. The research concluded that the cost of most inspection technologies is even higher than the failure consequences of small water distribution mains (less than 300 mm in diameter). The need to develop technologies for structure condition assessment of non-ferrous pipelines (such as asbestos cement and plastic pipes) and the need for low cost pipeline condition screening techniques were also identified by this research. It was highlighted that *cost-effective* and *non-destructive* techniques are the key directions of development for future technologies.

1.1.3 Leak detection and wall condition assessment using fluid transient waves

Development of new pipeline fault detection and condition assessment techniques that meet the needs of water utilities is necessary and of great importance. Among the pipeline condition assessment technologies that are being developed, fluid transient analysis (Chaudhry 1987; Wylie and Streeter 1993) based methods have shown considerable potential. The system characteristics of a pipeline can be determined by exploiting the hydraulic behaviour of the pipeline using transient pressure (or flow) waves. *Cost-effectiveness* and *non-invasiveness* are the two major advantages of the transient-based methods.

Fluid transients result from *unsteady flow* in pipelines, where flow conditions (such as pressure, velocity and discharge) at a point may change with time (Wylie and Streeter 1993). On the contrary, if the conditions do not change with time, the flow is termed *steady flow*. When steady flow has been established in a pipeline, any changes in the flow conditions at a point will introduce the presence of unsteady flow (or fluid transient). The unsteadiness propagates in the form of waves along the pipeline from the point where the change in the flow conditions occurs. These waves are termed *fluid transient*

waves. A well-known example is *water hammer*, which is the term to describe fluid transient waves introduced by an instantaneous stoppage of flow at a downstream valve (Chaudhry 1987; Wylie and Streeter 1993).

Transient-based testing is *cost-effective*, since the information from a pipeline section thousands of meters long can be obtained in a single transient test that takes only a few minutes. The fluid transient waves propagate in the water at the speed of up to 1,400 m/s in pressurised metal pipelines, and relatively slower in asbestos cement and plastic pipes. Theoretically, any physical changes in the structural properties of the pipe cross-section (such as variations in wall thickness or pipe diameter) can introduce wave reflections. The properties (such as size, shape, arrival time, duration, etc.) of these reflected waves are indicative of the variation in structural properties of the pipeline. By analysing these reflections using appropriate algorithms, the structural properties of the pipeline can be reconstructed. This process is akin to the use of sonar waves to detect remote objects within marine environments.

The transient-based pipeline inspection technology is also *non-invasive.* Transient pressure waves can be generated (typically by a side-discharge valve) and measured (by pressure transducers) at existing connection points, such as air valves and scour valves. No excavation or pre-cleaning of the pipeline is required. The pipeline can be tested with the presence of a base flow, i.e. without disrupting the water transmission.

In the last two decades, intensive simplified numerical simulations, some elaborately controlled laboratory experiments and a number of field tests have been conducted with the aim of developing fluid transient-based pipeline condition assessment techniques (Stephens 2008; Colombo et al. 2009; Puust et al. 2010). However, many challenges have impeded the implementation of these techniques on real world systems. As a result, further research has to be conducted to advance the transient-based pipeline condition assessment technology.

Generally speaking, deterioration in pipelines can be divided into two categories: discrete deterioration and distributed deterioration. Discrete deterioration describes faults that occur at points, such as leaks or discrete blockages (e.g. partially closed in-line valves). Distributed deterioration refers to localized deterioration that typically extends meters or tens of meters along the pipeline and can reoccur multiple times. Common distributed deterioration includes internal or external corrosion (Swietlik et al. 2012), the spalling of cement motor lining spalling (Stephens et al. 2008), extended blockages due to tuberculation or sedimentation (Arbon et al. 2007), graphitization (Zamanzadeh et al. 2007), and structurally weak sections caused by cracks in the pipe wall or backfill concrete (Hachem and Schleiss 2011).

Most fluid transient-based pipeline inspection techniques focus on the detection of discrete deterioration, in particular, the detection of leaks. In earlier studies, most transient-based leak detection techniques were developed in the time domain. Typical techniques include *time-domain reflectometry* (TDR) analysis (Jönsson and Larson 1992; Brunone 1999; Brunone and Ferrante 2001; Lee et al. 2007a), *inverse transient analysis* (ITA) (Liggett and Chen 1994; Vítkovský et al. 2000; Vítkovský et al. 2007; Covas and Ramos 2010), and *impulse response analysis* (IRA) (Liou 1998; Vítkovský et al. 2003b; Kim 2005; Lee et al. 2007b). The TDR and IRA have difficulty in detecting leaks if the measured pressure trace is complex. If a leak is small in size, the reflection from the leak is hard to distinguish from reflections introduced by other components (e.g. wall thickness changes). The ITA involves iterative calibration of the pipeline parameters through comparing the measured transient pressure trace with the results of numerical simulation on the calibrated pipeline model. The implementation can be very time consuming and the results may be non-unique when the parameters to be calibrated are great in number. In addition, as an inverse calibration algorithm, the ITA relies on accurate forward modeling of the transient behavior of the pipeline system. However, boundary condition and parameter uncertainties in real pipelines, and the difficulty in accurately simulating transient behavior numerically make the error in the forward modeling almost inevitable (Vítkovský et al. 2007). The model error is recognised as being the most

significant limiting factor in the successful field application of ITA (Puust et al. 2010).

After 2000, research on transient-based leak detection has begun to focus on the frequency domain. Representative techniques include *transient damping method* (Wang et al. 2002; Nixon and Ghidaoui 2006) and *frequency response analysis* (FRA) (Mpesha et al. 2001; 2002; Covas et al. 2005; Lee et al. 2005b; Duan et al. 2011; Gong et al. 2013e). The use of advanced signal processing techniques to enhance the accuracy of leak detection has also increased after 2000, such as wavelet analysis (Ferrante and Brunone 2003a; Taghvaei 2009), cepstrum analysis (Taghvaei et al. 2006; Shucksmith et al. 2012) and Hilbert-Huang transform methods (Ghazali et al. 2011). Detailed literature reviews on transient-based leak detection techniques can be found in Colombo et al. (2009) and Puust et al. (2010). Reviews on leak detection techniques that are relevant to the research presented in this thesis can be found in the *introduction* sections in Chapters 3 to 7.

The frequency response analysis has advantages over other transient-based leak techniques. A leak in a single pipeline introduces a sinusoidal pattern on the resonant frequency responses, where the period and size of the leak-induced pattern can be used to determine the location and size of the leak (Lee et al. 2005b). When multiple leaks exist, each leak will introduce a sinusoidal pattern and a superimposed pattern can be observed in the frequency response diagram (FRD) (Lee et al. 2005b). However, the FRD is not sensitive to pipe sections with diameter or wall thickness changes. Numerical simulations showed that junctions of series pipe sections can change the location of the resonant peaks, but have little impact on the period and phase of the leak-induced sinusoidal pattern (Duan et al. 2011). This finding indicates that the FRD-based leak detection technique has potential to be applied to real pipelines where both discrete and distributed deterioration exist.

There are, however, a few practical issues that impede the successful application of the FRD-based leak detection techniques. The bandwidth of the input transient signal for FRD extraction is a critical factor, since an accurate

FRD that covers a sufficient number of resonant responses is essential to successful leak detection. Discrete input signals like pulse and step signals have been used in past research, both numerically and experimentally (Lee et al. 2006). They are easy to generate (usually by a fast perturbation in the opening area of an in-line or side-discharge valve) but have limitations in bandwidth. The power spectrum of pulse or step signals is inversely proportional to the increase of frequency, and in real pipelines the transient generator (valves) typically lack of the necessary manoeuvrability to insure the signal is sharp (containing high frequency components) (Lee et al. 2008a). As a result, when using pulse or step signals, the signal-to-noise ratio (SNR) can be low for high frequency components, resulting in inaccurate estimation of the FRD. New types of transient signals that have wide bandwidth and sufficient SNR are needed to insure accurate extraction of the FRD of real pipelines.

The nonlinear response of real pipeline systems is also a practical issue that needs to be properly addressed. Like most systems in the real world, pipelines can be considered to consist of a combination of a linear response and a nonlinear response to an excitation (e.g. a predominantly linear response with some small nonlinear behaviour). Only the linear portion of the frequency response is desirable because all the FRD-based leak detection techniques have been developed using linear theory. It is known that the nonlinear response is proportional to the magnitude of perturbation if an oscillating valve is used as the transient generator (Lee et al. 2002; 2003; 2005a). Therefore, the magnitude of valve perturbation is suggested to be small. This restriction makes the generation of a transient signal that has sufficient bandwidth and SNR even more difficult.

The use of *steady oscillatory flow* (Chaudhry 1987; Wylie and Streeter 1993) has the potential to improve the current transient-based FRD extraction techniques. In the steady oscillatory flow regime, the flow conditions are varying with time and repeat after a fixed time interval (Chaudhry 1987). Steady oscillatory flow that contains multiple frequency components is suitable for the extraction of the FRD of a pipeline. The FRD extraction can

be efficient since multiple frequency responses of a pipeline can be determined simultaneously. This is attributable to its persistence and periodicity. Sufficient energy can be input into the system with a relatively small perturbation magnitude, and the SNR can be increased by synchronous averaging of the response periods.

The pseudo-random binary sequence (PRBS) (Godfrey 1993) can be used as one type of steady oscillatory flow. The PRBS can have a wide bandwidth and the energy is distributed over a long time-frame, allowing the magnitude of the perturbation to be small (Liou 1998). The most widely used PRBS signal is the maximum-length binary sequence (MLBS, in some literature, PRBS refers to MLBS). Lee et al. (2008a) developed a customised solenoid side-discharge valve to generate MLBS-based excitation signals. The valve was electronically controlled to produce pulses that follow a MLBS-based pattern; that is, only when the output of the embedded shift register is 1, is a sharp pulse generated by abruptly opening and then closing the side-discharge valve. The first three resonant responses of an intact pipeline in the laboratory were successfully extracted using this transient generator. However, Lee et al. (2008a) pointed out that the magnitude of the input signal must be carefully selected and relatively small.

In addition to the topic of leak detection using fluid transients, attention has also been paid to the assessment of the wall condition of pipelines in the past few years. Ferrous pipelines (either lined or unlined) have been used extensively in Australia, America, Europe and numerous other regions in the world, and represent a significant portion of the aging infrastructure. Distributed deterioration, such as internal or external corrosion and the spalling of cement lining, commonly exists in aged ferrous pipelines. Given the potential hazard to the operation of the system, water utilities have general interests in detecting this type of deterioration (US EPA 2009). The transient research group in the University of Adelaide has taken pioneering research in the area of pipeline condition assessment using fluid transient waves. Distributed deterioration can introduce complex transient wave reflections, making the measured pressure trace complex and difficult to interpret.

Stephens et al. (2008; 2013) were the first to apply ITA to the detection of changes in pipe wall thickness in a cement mortar lined steel water main in the field. However, similar to the application of ITA to leak detection, the high computational cost and model error can be impediments to efficient and effective field application of ITA for pipeline condition assessment. More literature review on techniques for pipeline condition assessment can be found in the *Introduction* sections in Chapters 8 to 11.

Overall, the research of pipeline condition assessment using fluid transients is still at its infancy and further research and experiments have to be conducted to advance this technology. It has been noticed that sections of pipe with diameter changes only introduce slight shifts in the resonant response peaks (Duan et al. 2011, 2012), which, however, are difficult to measure accurately in field applications. A more promising starting point is the analysis in the time domain. Better understanding of the characteristics of wave reflections from distributed deterioration would be a prerequisite to the successful development of new transient-based pipeline condition assessment techniques.

1.2 Research aims

The overall aim of this thesis is to develop non-destructive and cost-effective techniques for leak detection and condition assessment in water distribution pipelines using fluid transient waves. It is hoped that, in the near future, the transient-based leak detection and condition assessment technology can be used as a practical tool by water utilities for strategic maintenance of their water distribution systems. In order to fulfil the overall aim of this research, three main research aims have been proposed, with a number of specific sub-aims under the first two main aims, as listed below. The linkage between these research aims (and sub-aims) is illustrated in Figure 1.1.

Aim 1: To advance the transient-based leak detection technology for pressurised water pipelines using steady oscillatory flow and the frequency response diagram (FRD).

Aim 1.1: To have a better understanding of how the properties of the leak and the pipeline affect the leak-induced pattern in the FRD.

Aim 1.2: To develop new leak detection algorithms that requires less bandwidth of the input signal, hence more practical for implementation in real pipelines.

Aim 1.3: To develop a better strategy for accurate extraction of the linear FRD of real pipelines by using appropriate transient excitation signals and system configurations.

Aim 2: To develop efficient and effective transient-based pipeline condition assessment technology for pressurised water pipelines.

Aim 2.1: To have a better understanding of how the properties of extended pipe wall deterioration (changes in wall thickness) affect the characteristics of the wave reflection under transient events.

Aim 2.2: To develop new algorithms for the detection of distributed deterioration that are high in accuracy and low in computational cost.

Aim 3: To verify the newly developed transient-based leak detection and condition assessment techniques by experiments.

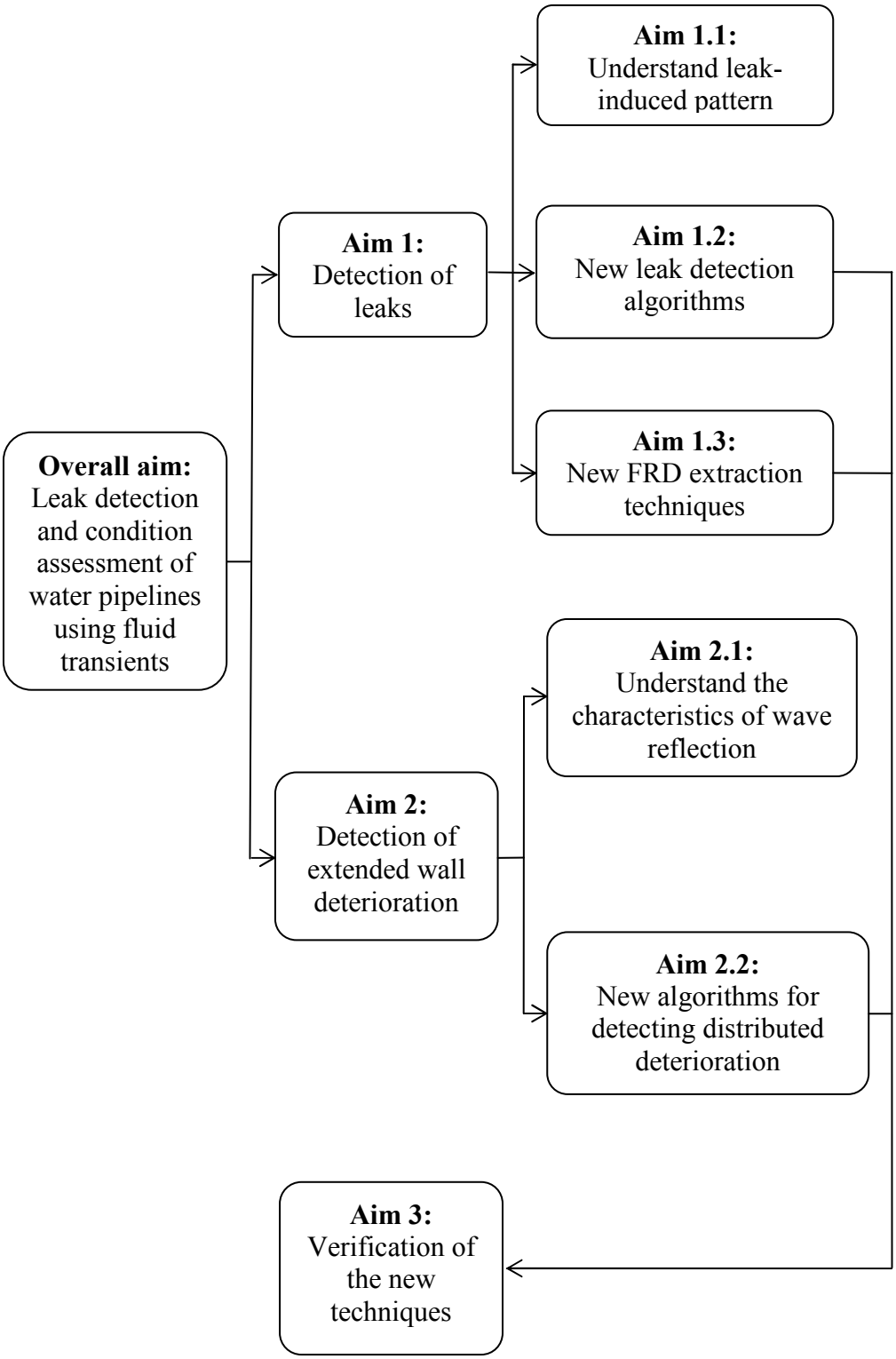

Figure 1.1 Research aims and their hierarchy

1.3 Organisation of thesis

This thesis has 12 chapters in total. The main body of this thesis is presented as a collection of the nine journal publications arising from the research undertaken. The manuscripts have been reformatted in accordance with University guidelines, and sections have been renumbered for inclusion within this thesis. The material of these manuscripts is otherwise as in the published or submitted journal papers.

Chapter 2 gives a synopsis of the publications that are included this thesis. A brief summary of each journal publication is given in this Chapter. The contributions of these publications to this research are illustrated by describing how they are linked to the specific aims of this research as presented in Figure 1.1.

The main body of this thesis consists of Chapters 3 to 11. Each chapter is formed by one of the nine journal publications produced in this research. **Chapters 3 to 7** are concerned with the leak detection in pressurized pipelines using fluid transient waves. **Chapter 3** (journal paper 1) investigates the characteristics of the leak-induced pattern in the FRD with respect to the configuration of the pipeline system. **Chapter 4** (journal paper 2) proposes a new FRD-based leak detection technique that only uses the first three resonant frequency response peaks. **Chapter 5** (journal paper 3) presents the results of a numerical study on the nonlinearity of pipeline systems and the selection of an appropriate transient signal for the extraction of the linear FRD of a pipeline. The invert repeat sequence (IRS, which is one type of PRBS) is found to be superior than other signals used for pipeline FRD extraction as it can suppress part of the nonlinear responses of the system. **Chapter 6** (journal paper 4) introduces a side-discharge valve-based transient generator that is developed in this research for FRD extraction using IRS. Comparison study between IRS an MLBS are conducted by extracting the FRD of an intact pipeline in the laboratory using these two types of signals. **Chapter 7** (journal paper 5) studies the appropriate pipeline configuration for FRD extraction and

conducts laboratory experiments on a leaking pipe. The experimental results provide further verification of the customised transient generator and the three-resonant-peaks-based leak detection technique.

Chapters 8 to 11 focus on the development of transient-based pipeline condition assessment techniques. **Chapter 8** (journal paper 6) investigates the characteristics of the wave reflections induced by a section of pipe with wall thickness changes under a step transient excitation. A technique for estimating the length, location and wall thickness of a single deteriorated section of pipe is developed based on the characteristic analysis. **Chapter 9** (journal paper 7) conducts a sensitivity analysis to study the relationship between the degree of change in wall thickness in a section of pipe and the sizes of the transient pressure waves reflected from and transmitted through that section. **Chapter 10** (journal paper 8) proposes a new pipeline condition assessment algorithm - reconstructive MOC (method of characteristics) analysis. This is achieved by estimating the distribution of pipeline properties (e.g. wave speed and wall thickness variations along a pipe) using a transient pressure trace measured at a closed end of a pipeline. **Chapter 11** (journal paper 9) describes another pipeline condition assessment algorithm that is adapted from the reconstructive MOC analysis, but does not require a dead end boundary condition. An algorithm that can extract the directional traveling waves (transient pressure waves traveling upstream or downstream along a pipeline) using two transducers in close proximity is also proposed in this chapter.

Chapter 12 is the last chapter in this thesis. It summarises the major contributions of this research. The limitations of this research and future directions in this research area are also discussed.

Chapter 2

Synopsis of Publications

This chapter provides a brief summary for each of the nine journal publications as given in the *List of Publications*. The link between the nine journal papers and how they are related to the specific aims of this research as listed in Section 1.2 are also discussed. These nine journal papers are presented in subsequent chapters of this thesis, with each of them composing one chapter.

2.1 Journal paper 1

Journal paper 1 (Chapter 3) aims to achieve a deeper understanding of the leak-induced sinusoidal pattern in the frequency response diagram (FRD) of a pipeline, which is the key information required for a successful FRD-based leak detection and location method. Lee et al. (2005b; 2006) observed the leak-induced pattern on the resonant response peaks and proposed that the period and magnitude of this pattern are indicative of the location and size of the leak. Sattar and Chaudhry (2008) found that, in some circumstances, the leak-induced pattern can be observed on the anti-resonant responses rather than the resonant responses. To date, no connection between the resonant and anti-resonant approaches has been discussed or explored. Journal paper 1 answers the question as to what factors, in addition to the leak, affect the presence and characteristics of the leak-induced pattern. It is found that, when an oscillating valve at the end of a pipeline is used as the transient generator, the mean impedance of the valve (or the steady-state impedance if the opening of the valve is at its mean in the steady state) determines where the leak-

induced pattern is shown (i.e. on the resonant peaks, or anti-resonant troughs) and how great the magnitude of the sinusoidal pattern is. When the ratio of the mean impedance of the oscillating valve to the characteristic impedance of the pipeline equals unity, leak-induced patterns are shown on both the resonant and anti-resonant responses with the same magnitude. With the ratio increasing from unity, the leak-induced pattern on the resonant responses grows in magnitude, while the pattern on the anti-resonant responses diminishes. The situation reverses if the ratio is decreasing from unity.

Journal paper 1 also studies the effects of the leak impedance and friction on the leak-induced pattern. Assumptions embedded in the development of the FRD-based leak detection and location techniques are summarised, in which system linearity is one of them. Challenges to existing FRD-based leak detection and location techniques are discussed in the conclusions. The bandwidth of the input transient signal is identified as one of the key factors and challenges exist in generating transient signals with a sufficient bandwidth for accurate FRD extraction in real systems.

Journal paper 1 achieves *Aim 1.1* by providing a better understanding of the characteristics of the leak-induced pattern in the FRD. The research contributes to the further development of the FRD-based leak detection and location techniques.

2.2 Journal paper 2

Journal paper 2 (Chapter 4) proposes a new FRD-based leak detection (including location and size estimation) technique that only uses the leak-induced pattern shown on the first three resonant response peaks. Since it is difficult to generate a transient signal with a bandwidth broad enough to cover a number of resonant response peaks, new techniques that use less information of the FRD (especially that in the high frequency portion) are desirable. The new technique proposed in journal paper 2 does not estimate the period or the magnitude of the leak-induced pattern, but rather it extracts the information of leak location and size from the relative sizes of the first

three resonant peaks (i.e. the ratios between the peak magnitudes). The three-resonant-peak-based leak detection technique is applicable to single event leak detection in reservoir-pipeline-valve (RPV) systems. If the valve at the end of the pipeline is fully closed, the information required can be further reduced to only the first two resonant peaks. A sensitivity analysis is conducted to study how the location of the leak affects the robustness of the new technique. An experimental FRD extracted by Lee et al. (2006) on a leaking pipeline in the laboratory is used to provide a preliminary verification of the new leak detection technique.

Journal paper 2 achieves *Aim 1.2* by developing a new leak detection technique that requires a reduced bandwidth measurement of the frequency response, therefore reducing the requirement on the bandwidth of the transient excitation signal. The research contributes to the development of practical leak detection techniques using fluid transients.

2.3 Journal paper 3

Journal paper 3 (Chapter 5) addresses the issue of non-linear responses of a pipeline system induced by the oscillation of a valve during the transient excitation process. To achieve accurate leak detection using frequency-domain methods, non-linear responses should be avoided as much as possible to yield an experimental FRD that is close to the theoretical linear FRD, since all the FRD-based leak detection techniques are based on linear theory. Earlier numerical studies by Lee et al. (2002; 2005a) have discovered that the non-linear response of a pipeline system is proportional to the amplitude of perturbation when an oscillating valve is used as the transient generator. One solution to mitigate the non-linear response of a system is to use excitation signals with an antisymmetric property. This type of signal can make part of the non-linear responses cancel out in the determination process for the frequency response function (Roinila et al. 2010).

Journal paper 3 also discusses appropriate transient signals for pipeline FRD extraction by taking the antisymmetric property into account and

incorporating other needs required by FRD-based leak detection (e.g. wide bandwidth and sufficient energy). The paper proposes that the inverse repeat sequence (IRS) (Godfrey 1993) is an appropriate type of transient signal for FRD extraction and leak detection. Numerical simulations are conducted to compare the IRS, the maximum length binary sequence (MLBS) and the single frequency sine signal in terms of the accuracy in frequency response extraction from a pipeline. All these three types of signals are persistent and periodic. Both of the IRS and sine signal are antisymmetric, while the MLBS is not. It is found that the IRS and the sine signal yield similar frequency response results, which are closer to the theoretical linear responses when compared with the results from MLBS. Compared to the single frequency sine signal, the IRS has an additional merit of wide bandwidth, therefore multiple frequency responses can be extracted simultaneously.

Journal paper 3 aligns with *Aim 1.3* by providing an appropriate type of transient signal for pipeline FRD extraction. The research contributes to the development of more accurate FRD extraction techniques and benefits to all FRD-based leak detection techniques.

2.4 Journal paper 4

Journal paper 4 (Chapter 6) reports a customised side-discharge valve-based transient generator for pipeline FRD extraction. The opening of this side-discharge valve is controlled by a rod vertical to the conduit for the side-discharge. The movement of the rod is then manoeuvred by two solenoids aligned with the long axis of the rod. One solenoid drives the valve opening and the other one drives the valve closure. The two solenoids are controlled by a programmable signal generator, which produces electrical signals of an MLBS or IRS structure. As a result, the opening of the side-discharge valve can be changed persistently in the form of MLBS or IRS. The movement of the rod is measured by a linear voltage displacement transducer (LVDT), from which the perturbation in the valve opening can be obtained.

The customised transient generator is applied to an intact pipeline in the laboratory to extract the FRD of the pipeline system. The experimental results show that greater amplitude in valve perturbation can introduce greater discrepancy between the experimental FRD and the theoretical linear FRD obtained from the transfer matrix method. The FRD extracted by the IRS is smoother and closer to the theoretical linear FRD when compared with the FRD extracted by the MLBS using the same amplitude of valve perturbation.

Journal paper 4 aligns with *Aim 3* by providing experimental verification for the numerical findings proposed in journal paper 3. This research contributes to the development of practical strategies for pipeline FRD extraction.

2.5 Journal paper 5

Journal paper 5 (Chapter 7) reports the findings of a numerical study and an experimental verification for FRD extraction and leak detection. The numerical study is a further development of the research reported in journal paper 1. It is found that the mean impedance of the valve in a RPV system affects not only the magnitude of the leak-induced pattern (as discussed in journal paper 1), but also the shape of the FRD. For greater values of the mean valve impedance, the leak-induced pattern shows more evidently on the resonant peaks, however, the resonant peaks are increasingly sharp. The resonant peaks contain critical information for successful leak detection and should be measured accurately in practice. However, if the mean valve impedance is too high, the resonant peaks could be too sharp to measure accurately, since in real systems the measurement is achieved by discrete sampling (resulting in only discrete frequencies being identified). As a result, there is a trade-off between the magnitude of the leak-induced pattern and the measurability of the resonant peaks. The numerical study in journal paper 5 suggests that the mean valve impedance should be within 1 to 10 times the characteristic impedance of the pipeline, while the specific value in practical applications should be determined on a case-by-case basis.

Journal paper 5 also presents the experimental results of FRD extraction using the IRS (as proposed in journal paper 3) and the customised transient generator (as developed in journal paper 4) for a pipeline with a leak. The mean impedance of the side-discharge valve (i.e. the customised transient generator) is adjusted so that the resonant peaks are rounded and can be robustly determined from discrete measurements. Two mean valve impedance values are used, and differences in the sharpness of the resonant peaks is observed. The experimental resonant peak values are then used to verify the three-resonant-peak-based leak detection technique (as proposed in journal paper 2). The location of the leak is determined with high accuracy.

Journal paper 5 aligns with *Aim 1.1*, *Aim 1.3* and *Aim 3*. The numerical study in journal paper 5 provides a better understanding of the characteristics of the FRD and contributes to the development of better strategies for pipeline FRD extraction. The experiments conducted in journal paper 5 verify the new FRD extraction strategy and the new FRD-based leak detection technique developed in previous journal papers.

2.6 Journal paper 6

Journal paper 6 (Chapter 8) presents the result of a numerical analysis of a transient pressure wave propagating across a section of pipeline with a change in wall thickness. The numerical study leads to the development of a new pipe wall condition assessment technique. It is found that a change in pipeline impedance can introduce a wave reflection, in which the size, reflection time and length of the reflected wave are indicative of the impedance change, the location and the length of the anomalous pipeline section. Once the change in impedance is determined, the wall thickness of this section of pipe can be estimated.

Experiments are conducted on a laboratory single pipeline system to verify the numerical findings. A section of pipe with a thinner wall thickness is placed in the system to simulate a deteriorated section. A step transient wave is generated by closing the valve at one end of the system, and transient pressure

traces are measured at the upstream face of the closed end. The wall thickness, location, and length of the thinner-walled section are determined successfully by applying the new technique to the experimental results. A sensitivity analysis is then conducted to study the effects of transient wave front on the wave reflection. It is found that the shape and size of the reflection are closely related to the shape of the input transient wave front, and a sharp transient wave front is preferred.

Journal paper 6 achieves *Aim 2.1* and aligns with *Aim 2.2* and *Aim 3*. The research provides an in-depth understanding of the characteristics of the wave reflections that result from extended wall deterioration. A new pipe wall condition assessment technique is developed for the detection of a single deteriorated section in pipelines. The experimental verification demonstrates the applicability of the new technique.

2.7 Journal paper 7

Journal paper 7 (Chapter 9) is an extension of the work presented in Journal paper 6 (Chapter 8). In this paper, a detailed sensitivity analysis is conducted to study the relationship between the degree of change in wall thickness in a structurally deteriorated section and the sizes of the transient waves reflected from, and transmitted through, that section. Two typical scenarios are discussed: a change in wall thickness from the internal side (constant external diameter) and that which occurs on the external side (constant internal diameter). Plots concerning the variation in the normalized magnitude of the reflected wave versus relative change in wall thickness are presented. The plots can be used as look-up charts for a fast and quantitative structural condition assessment of pipelines using fluid transient waves.

Journal paper 7 aligns with *Aim 2.1*. The research provides further understanding of the characteristics of the wave reflections that result from extended wall deterioration.

2.8 Journal paper 8

Journal paper 8 (Chapter 10) proposes a new pipeline condition assessment technique for the detection of multiple deteriorated sections in a pipeline. The new technique is termed *reconstructive MOC* (method of characteristics) *analysis*, in which the distribution of the properties of a pipeline, such as impedance and wave speed, are determined from a single pressure trace measured at the upstream face of the closed valve in a RPV system (where the valve closure is used to generate a step transient wave). The new algorithm is an inverse process of the traditional MOC modelling, which simulates the transient behaviour of a pipeline system with known properties and boundary conditions (Chaudhry 1987; Wylie and Streeter 1993). In contrast, in the reconstructive MOC analysis, the properties of the pipeline are unknown and yet to be determined by calculating the MOC compatibility equations backwards in time. Using the reconstructive MOC analysis, the MOC grid can be reconstructed and the properties of the pipeline can be determined reach by reach from the downstream closed end toward the upstream reservoir. One advantage of the reconstructive MOC analysis is that complex multiple reflections between deteriorated sections can be interpreted appropriately.

The reconstructive MOC analysis is verified by using an experimental transient pressure trace measured from a pipeline with a thinner-walled section (as also presented in journal paper 6). The plots for the distribution of the impedance and wave speed along the pipeline are obtained from the implementation of the algorithm, from which the thinner-walled section is identified and its location, length and impedance are successfully determined.

Journal paper 8 aligns with *Aim 2.2* and *Aim 3*. A new pipeline condition assessment technique, the reconstructive MOC analysis, is developed based on the understanding of the characteristics of the wave reflections induced by extended deterioration (as given in journal paper 6). The successful application to a laboratory pressure trace verifies the applicability of the new technique.

2.9 Journal paper 9

Journal paper 9 (Chapter 11) presents the development of a new pipeline condition assessment technique, *reconstructive transient analysis* (RTA), which is adapted from the reconstructive MOC analysis (as presented in journal paper 8) but does not require a dead end boundary condition. Associated with the RTA, a new transient wave measurement strategy for pipeline condition assessment is proposed. While the traditional measurement strategy only uses a single pressure transducer at each measurement station, in journal paper 9, two pressure transducers located in close proximity are used to measure transient pressure traces at arbitrary interior points in a pipeline. It is known that the pressure magnitudes measured by single transducers are a superposition of waves travelling in both the upstream and downstream directions. Given this fact, measured pressure traces can be extremely complex and difficult to interpret when multiple faults exist in the pipeline. The use of two pressure transducers in close proximity enables the decoupling and extraction of the two directional traveling waves. Using the two directional traveling waves as the input and output signals respectively, the step response functions (SRF) can be estimated for the pipe section upstream of the paired pressure transducers, and for that located in the downstream side. As a result, the complexity of the measured signal can be reduced significantly and condition assessment can be conducted separately for the two portions (upstream and downstream) of pipe.

The RTA is used to interpret the SRF, yielding the distribution of pipeline properties (e.g. impedance and wave speed). This is achieved by calculating the MOC compatibility equations backwards in time, which is similar to the strategy used in the reconstructive MOC analysis (as presented in journal paper 8). However, the difference lies in the fact that the information of transient flow at the measurement points is unknown and not required by the RTA, while the flow is known and remains zero in the reconstructive MOC analysis since the measurement is taken at the closed end. From the estimated

plots for the distribution of pipeline impedance or wave speed, properties of distributed deterioration in the pipe can be determined.

Journal paper 9 aligns with *Aim 2.2*. The research contributes to the development of advanced transient-based pipeline condition assessment techniques.

In summary, the research as reported in these nine journal publications align with the aims of this doctoral research. Each journal paper is related closely to one or more of the specific sub-aims and all of them contribute to the overall aim of this research, which is to advance the technology for leak detection and condition assessment of water pipelines using fluid transients. The contribution of these nine journal publications presented in this thesis in relation to the research aims of this doctoral research is summarised in Figure 2.1.

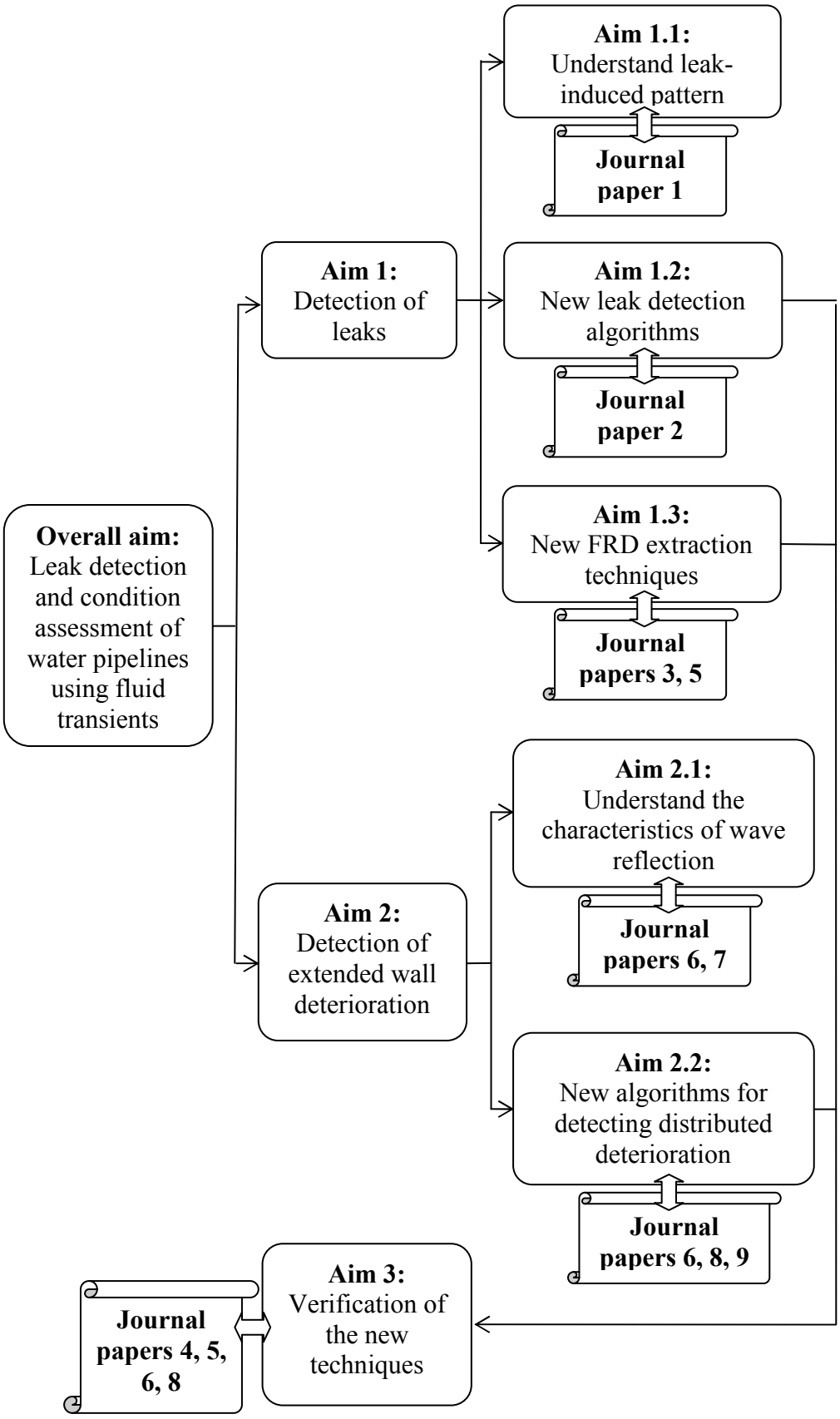

Figure 2.1 Contribution of the nine journal publications presented in this thesis in relation to the research aims of this doctoral research

Chapter 3

Frequency Response Diagram for Pipeline Leak Detection: Comparing the Odd and the Even Harmonics (Journal Publication 1)

Gong, J., Zecchin, A. C., Simpson, A. R., and Lambert, M. F.

School of Civil, Environmental and Mining Engineering, the University of Adelaide, Adelaide, SA 5005 Australia

Journal of Water Resources Planning and Management, DOI: 10.1061/(ASCE)WR.1943-5452.0000298 (published online)

Statement of Authorship

Title of Paper	Frequency Response Diagram for Pipeline Leak Detection: Comparing the Odd and the Even Harmonics
Publication Status	Accepted for Publication
Publication Details	Gong, J., Zecchin, A. C., Simpson, A. R., and Lambert, M. F. (2013). "Frequency response diagram for pipeline leak detection: comparing the odd and the even harmonics." *Journal of Water Resources Planning and Management*, DOI: 10.1061/(ASCE)WR.1943-5452.0000298 (published online).

Author Contributions

By signing the Statement of Authorship, each author certifies that their stated contribution to the publication is accurate and that permission is granted for the publication to be included in the candidate's thesis.

Name of Principal Author (Candidate)	Jinzhe Gong		
Contribution to the Paper	Developed and implemented the methodology, designed and conducted numerical simulations, interpreted and analysed results, prepared manuscript and acting as the corresponding author.		
Signature		Date	25/09/2013

Name of Co-Author	Aaron Zecchin		
Contribution to the Paper	Supervised development of work, helped to evaluate and edit the manuscript.		
Signature		Date	1·10·2013

Name of Co-Author	Angus Simpson		
Contribution to the Paper	Helped to evaluate and edit the manuscript.		
Signature		Date	25/9/2013

Name of Co-Author	Martin Lambert		
Contribution to the Paper	Helped to evaluate and edit the manuscript.		
Signature		Date	25/9/13

Abstract

Pipeline leak detection using hydraulic transient analysis is a relatively new detection technique. For single pipeline systems, recent work has led to two different approaches for determining leak parameters based on leak-induced patterns displayed in a pipeline's frequency response diagram (FRD). The major difference between the two techniques is that one uses the leak-induced pattern within the odd harmonics of an FRD, while the other one uses the leak-induced pattern at the even harmonics. In order to compare and contrast the two approaches, the current research analyses the relationship between the characteristics of the leak-induced patterns and the parameters of the pipeline system. A dimensionless analysis, based on hydraulic impedance, is adopted to simplify the equations. The amplitudes of leak-induced patterns at both the odd and the even harmonics in the FRD are found to be dependent on a critical parameter: the dimensionless steady-state valve impedance, Z_V^*. The value of Z_V^* is dependent on the steady-state valve opening. As a result, amplitudes of the leak-induced patterns within the FRD for any specific pipeline system can be controlled by the initial valve opening. This research also derives the equations for calculating the dimensionless leak size based on the value of Z_V^* and the amplitude of either leak-induced pattern. Finally, the two existing FRD-based leak detection methods are compared, and the approach using the odd harmonics is found to be superior.

3.1 Introduction

The problem of leakage in water distribution systems not only imposes a large economic cost on users and authorities, but also poses significant potential risks to public health due to possible contamination of the potable water supply. Attention to this problem has increased over the last decade due to a growing awareness of the need for water security. During this time, a number of transient based methods for leak detection have been developed (Colombo et al. 2009).

Transient based leak detection methods utilize transient pressure waves that travel at a high speed inside pipelines. Leaks, or any other physical changes in a pipe, can induce reflections on a travelling wave. In the time domain, these reflections are observed as discontinuities in the pressure signal measured along the pipe (Lee et al. 2007b). In the frequency domain, the frequency response diagram (FRD) of the pipeline system may be distorted due to the reflected signals (Lee et al. 2005b). Accordingly, numerous transient leak detection methods have been developed either in the time domain or the frequency domain.

Time domain transient leak detection methods mainly include time domain reflectometry techniques (Silva et al. 1996; Brunone 1999), impulse response techniques (Vítkovský et al. 2003b; Lee et al. 2007b) and inverse transient analysis (ITA) methods (Liggett and Chen 1994; Vítkovský et al. 2007; Jung and Karney 2008). Frequency domain techniques are usually based on the analysis of a pipeline system's FRD, which describes the amplitude of the pressure response fluctuation corresponding to each frequency component in an input signal. Compared with time domain methods, frequency domain methods require less computational time because the head and flow responses are determined directly through analytic relationships (Colombo et al. 2009).

Jönsson and Larson (1992) first proposed that the spectral analysis of a measured pressure trace could be used for leak detection. Several years later, Mpesha et al. (2001) proposed a leak detection method based on the analysis

of an experimental FRD of a pipeline system; Ferrante and Brunone (2003b) presented a leak detection method based on the analysis of hydraulic impedances of a pipeline; Covas et al. (2005) proposed a standing wave difference method (SWDM) which used the spectral analysis of an FRD to determine the leak-resonance frequency, thereby determining the leak location. However two solutions existed for a single leak in the SWDM.

In the same year, Lee et al. (2005b) introduced a method that could both determine the location and the size of a leak by analyzing the leak-induced pattern (pressure oscillations) at the resonant frequency components (the odd harmonics) in the FRD. In a later paper, Lee et al. (2006) presented the first experimental validation of the FRD based leak detection method. Sattar and Chaudhry (2008) then suggested a similar leak detection method but using the leak-induced pattern at the anti-resonant frequencies (the even harmonics).

According to the analyses presented in Lee et al. (2005b) and Sattar and Chaudhry (2008), a leak-induced pattern appears as sinusoidal oscillations at the odd or the even harmonic magnitudes in the FRD for a leaking pipe. The period of the leak-induced pattern can be used to determine the leak location. The amplitude of the pattern is indicative of the leak size. In Lee et al. (2005b) the leak-induced pattern at the odd harmonics is evident, while only slight perturbations can be observed at the even harmonics. In contrast, the leak-induced pattern at the even harmonics possesses a larger amplitude in Sattar and Chaudhry (2008). As a larger leak-induced pattern amplitude (which has a higher signal to noise ratio) is desirable in real applications, two questions naturally arise from this discrepancy between these two FRD based leak detection methods: Firstly, *what controls the amplitudes of the leak-induced patterns in the FRD for a single pipe with a leak?* Secondly, *if the amplitudes of the leak-induced patterns in the FRD for a specific pipe configuration can be controlled, which method would lead to a more accurate solution?*

The research reported here answers these questions by analyzing and comparing the leak-induced patterns at the odd and the even harmonics in the FRD. This study initially reviews the fundamental equations involved in the

analysis of steady oscillatory flow in a single pipe using the transfer matrix method (Chaudhry 1987). Analytic expressions for the magnitude of pressure response at the odd and even harmonics are adapted from Lee et al. (2005b) and Sattar and Chaudhry (2008).

Following this, a non-dimensionalization approach for the governing equations is performed, during which the amplitudes of the leak-induced patterns are observed to depend only on two dimensionless impedances: the dimensionless steady-state valve impedance (Z_V^*) and the dimensionless leak impedance (Z_L^*). For any specific pipeline system, the value of Z_L^* is constant, so that the relative sizes of the two amplitudes of the leak-induced patterns are controlled only by the value of Z_V^*. When Z_V^* is equal to unity, the amplitudes of the two leak-induced patterns at the odd and the even harmonics are equivalent. When it is larger than unity, the leak-induced pattern at the odd harmonics has a larger amplitude, while the oscillatory pattern at the even harmonics is more evident if Z_V^* is less than unity. As the value of Z_V^* is dependent on the steady-state valve opening, this finding indicates that the amplitudes of the leak-induced patterns in the FRD can be controlled by the initial steady-state valve opening.

Equations for determining the dimensionless leak size are also derived in this research. The dimensionless leak size can be determined from the amplitude of the leak-induced pattern at either the odd or the even harmonics. In order to illustrate the effects of the two dimensionless impedances (Z_V^* and Z_L^*) on the amplitudes of the leak-induced patterns, numerical simulations are conducted for the dimensionless system neglecting friction. A case study for a specific pipeline system with steady friction is also performed to determine the effect of Z_V^* on the accuracy of the two leak detection methods. Finally, the two leak detection methods are compared and contrasted. Recommendations for implementing the FRD based leak detection methods in the real world are outlined in the concluding section of this paper.

3.2 Fundamental equations

Unsteady flow in pipes can be described by simplified one-dimensional momentum and continuity equations, as shown by Chaudhry (1987):

$$\frac{\partial H}{\partial x}+\frac{1}{gA}\frac{\partial Q}{\partial t}+\frac{fQ^2}{2gDA^2}=0 \tag{3.1}$$

$$\frac{\partial Q}{\partial x}+\frac{gA}{a^2}\frac{\partial H}{\partial t}=0 \tag{3.2}$$

where H and Q represent the piezometric head and the flow rate; g is the gravitational acceleration; A and D are the cross sectional area and the inside diameter of the pipeline; f is the Darcy-Weisbach friction factor; a is the pressure wave speed; x and t are the spatial coordinate and time, respectively. Instantaneous H and Q values can be considered as the sum of the mean values, H_0 and Q_0, and the sinusoidal oscillations around the mean, $h^O=\mathrm{Re}[h(x)e^{j\omega t}]$ and $q^O=\mathrm{Re}[q(x)e^{j\omega t}]$, where h^O and q^O denote the head and flow sinusoidal oscillations; ω is the angular frequency, in radians per second; $j=\sqrt{-1}$; $h(x)$ and $q(x)$ are complex valued functions of x; $\mathrm{Re}[\ ]$ stands for the real part of the variable inside the brackets.

Provided the flow and head oscillation at the upstream end (entrance) of the ith pipe are known, the expressions for the amplitudes of head and flow fluctuation at the downstream end of the ith pipe can be written in the matrix notation as (Chaudhry 1987)

$$\begin{Bmatrix} q \\ h \end{Bmatrix}^{n+1}=\begin{bmatrix} \cosh(\mu_i L_i) & \dfrac{-1}{Z_{Pi}}\sinh(\mu_i L_i) \\ -Z_{Pi}\sinh(\mu_i L_i) & \cosh(\mu_i L_i) \end{bmatrix}\begin{Bmatrix} q \\ h \end{Bmatrix}^{n} \tag{3.3}$$

where the superscripts n and $n+1$ represent the upstream and downstream positions respectively; L_i is the length of the ith pipe; $Z_{Pi} = \mu_i a_i^2 / (j\omega g A_i)$ is the characteristic impedance for the ith pipe; and μ_i is the propagation operator given by $\mu = \sqrt{-\omega^2 / a^2 + j\omega g A R / a^2}$, in which R is a linearised resistance term. For turbulent flow and steady friction $R = fQ_0 / (gDA^2)$.

Similar matrices can be derived for other components such as inline valves and leaks. The point transfer matrix for a leak presented in Lee et al. (2005b) is

$$\mathbf{P_L} = \begin{bmatrix} 1 & -\dfrac{Q_{L0}}{2H_{L0}} \\ 0 & 1 \end{bmatrix} \tag{3.4}$$

in which Q_{L0} and H_{L0} are the steady-state flow through the leak and the head at the leak, respectively. The terms Q_{L0} and H_{L0} are related by the orifice equation $Q_{L0} = C_d A_L \sqrt{2gH_{L0}}$, where A_L is the area of the leak orifice; C_d is the coefficient of discharge; and $C_d A_L$ is called the lumped leak parameter. The transfer matrix for a sinusoidal oscillating valve can be written as (Lee et al. 2005b)

$$\begin{Bmatrix} q \\ h \end{Bmatrix}^{n+1} = \begin{bmatrix} 1 & 0 \\ -\dfrac{2\Delta H_{V0}}{Q_{V0}} & 1 \end{bmatrix} \begin{Bmatrix} q \\ h \end{Bmatrix}^{n} + \begin{Bmatrix} 0 \\ \dfrac{2\Delta H_{V0} \Delta\tau}{\tau_0} \end{Bmatrix} \tag{3.5}$$

where ΔH_{V0} and Q_{V0} represents the steady-state head loss across and flow through the valve, respectively; τ_0 is the mean dimensionless valve-opening coefficient; and $\Delta\tau$ stands for the magnitude of the dimensionless valve-opening oscillation generating the transients; the active input is given by the second vector term on the right side of the equation.

The overall transfer matrix $\mathbf{U}$ for a pipeline is obtained by an ordered multiplication of the individual field and point matrices starting at the downstream end. For a single pipeline with a leak (see Figure 3.1), $\mathbf{U} = \mathbf{F_2 P_L F_1}$, in which $\mathbf{F}_1$ and $\mathbf{F}_2$ are the field transfer matrices for the two pipe sections separated by the leak.

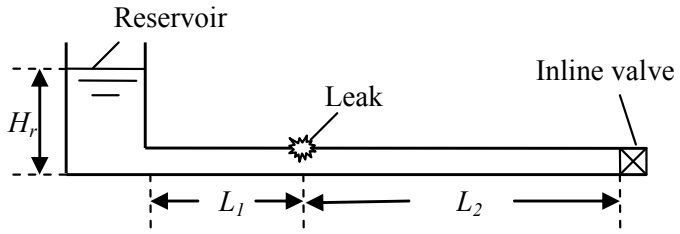

Figure 3.1 A reservoir-pipeline-valve system with a leak

3.3 Frequency response equations for a leaking pipe

Similar to the systems in Lee et al. (2005b) and Sattar and Chaudhry (2008), a reservoir-pipeline-valve system is adopted for the research described in this paper, as shown in Figure 3.1. For a frictionless intact pipeline (that is, without any anomalies such as leaks), the FRD has a uniform value of $2\Delta H_{V0}\Delta\tau/\tau_0$ at the odd harmonics and a zero value at the even harmonics (Lee et al. 2005b). Neglecting friction, where a leak exists in the pipe, the magnitude of the pressure fluctuation at the upstream side of the valve can be derived as (Lee et al. 2005b)

$$h = \frac{-2\Delta H_{V0}\Delta\tau/\tau_0}{1 - \dfrac{2\Delta H_{V0}\left[\cos\left(\dfrac{(L_1+L_2)\omega}{a}\right) + \dfrac{jQ_{L0}a}{2gAH_{L0}}\sin\left(\dfrac{L_1\omega}{a}\right)\cos\left(\dfrac{L_2\omega}{a}\right)\right]}{Q_{V0}\left[\dfrac{Q_{L0}a^2}{2H_{L0}g^2A^2}\sin\left(\dfrac{L_1\omega}{a}\right)\sin\left(\dfrac{L_2\omega}{a}\right) - \dfrac{ja}{gA}\sin\left(\dfrac{(L_1+L_2)\omega}{a}\right)\right]}} \tag{3.6}$$

where L_1 and L_2 are the lengths of the pipe sections upstream and downstream of the leak, as shown in Figure 3.1. The odd harmonics are defined as $\omega = \omega_r^{odd}\omega_{th}$, in which ω_{th} is the fundamental angular frequency of the reservoir-pipeline-valve system [$\omega_{th} = \pi a/(2L)$, where L is the total pipeline length] (Chaudhry 1987); ω_r^{odd} is the relative angular frequency for the odd harmonics ($\omega_r^{odd} = 1, 3, 5, \ldots$). By simplification and elimination of a small coefficient $(Q_{L0}a)/(4H_{L0}gA)$ [which is usually much smaller than unity under realistic combinations of leak size and head at the leak (Lee et al. 2005b)], the magnitude of the pressure fluctuation at the odd harmonics can be derived as

$$\left|h_{odd}\right| = \frac{2\Delta H_{V0}\Delta\tau/\tau_0}{\frac{\Delta H_{V0}Q_{L0}}{2Q_{V0}H_{L0}}\left[\cos\left(\omega_r^{odd}\pi x_L^* - \pi\right)+1\right]+1} \tag{3.7}$$

where $x_L^* = L_1/(L_1+L_2)$ is the dimensionless leak location.

Similarly, Sattar and Chaudhry (2008) derived the expression for the pressure fluctuation magnitude at the even harmonics:

$$\left|h_{even}\right| = \frac{2\Delta H_{V0}\Delta\tau/\tau_0}{\frac{1}{\left(\frac{a}{gA}\right)^2\frac{Q_{V0}Q_{L0}}{8\Delta H_{V0}H_{L0}}\left[\cos\left(\omega_r^{even}\pi x_L^*\right)-1\right]}-1} \tag{3.8}$$

where ω_r^{even} is the relative angular frequency for the even harmonics ($\omega_r^{even} = 2, 4, 6, \ldots$).

3.4 Dimensionless analysis of the leak-induced patterns

As part of conducting the research described in this paper, it is necessary to simplify the governing equations using a dimensionless analysis on the leak-induced patterns using hydraulic impedances (Wylie and Streeter 1993). Based on the characteristic impedance for a frictionless pipeline, $Z_C = a/(gA)$, the hydraulic impedance for a steady-state valve, $Z_V = 2\Delta H_{V0}/Q_{V0}$, and the hydraulic impedance for a leak (or a fixed orifice), $Z_L = 2H_{L0}/Q_{L0}$, dimensionless impedances for the valve and leak can be defined as

$$Z_V^* = Z_V / Z_C \tag{3.9}$$

$$Z_L^* = Z_L / Z_C \tag{3.10}$$

The magnitude of the pressure fluctuation h is non-dimensionalised by dividing it by the active input $2\Delta H_{V0}\Delta\tau/\tau_0$, i.e.

$$h^* = h/(2\Delta H_{V0}\Delta\tau/\tau_0) \tag{3.11}$$

3.4.1 Dimensionless analysis of frictionless leaking pipes

For a frictionless intact pipe, the values of h^* at the odd harmonics are all equal to unity, while those at the even harmonics are all zero. For a frictionless pipe with a leak, the expression of h^* can be obtained by substituting Eqs (3.9) to (3.11) into Eq. (3.6), which leads to

$$h^* = \frac{-1}{1 - Z_V^* \dfrac{\cos\left(\omega_r \dfrac{\pi}{2}\right) + j(Z_L^*)^{-1} \sin\left(\omega_r \dfrac{\pi}{2} x_L^*\right) \cos\left(\omega_r \dfrac{\pi}{2}(1 - x_L^*)\right)}{(Z_L^*)^{-1} \sin\left(\omega_r \dfrac{\pi}{2} x_L^*\right) \sin\left(\omega_r \dfrac{\pi}{2}(1 - x_L^*)\right) - j \sin\left(\omega_r \dfrac{\pi}{2}\right)}} \tag{3.12}$$

in which $\omega_r = \omega / \omega_{th}$ is the dimensionless relative angular frequency. For the head fluctuation at the odd harmonics, Eq. (3.7) can be written as

$$\left|h_{odd}^*\right| = \frac{1}{\dfrac{Z_V^*}{2Z_L^*}\left[\cos\left(\omega_r^{odd} \pi x_L^* - \pi\right) + 1\right] + 1} \tag{3.13}$$

Similarly, for the head fluctuation at the even harmonics, Eq. (3.8) yields

$$\left|h_{even}^*\right| = \frac{1}{\dfrac{2Z_V^* Z_L^*}{\cos\left(\omega_r^{even} \pi x_L^*\right) - 1} - 1} \tag{3.14}$$

Eqs (3.13) and (3.14) show that, in addition to the relative angular frequency, the dimensionless leak-induced patterns are dependent only on three dimensionless parameters: Z_V^*, Z_L^* and x_L^*. The periods of the sinusoidal patterns are both equal to $2/x_L^*$. The dimensionless amplitude of a leak-induced pattern can be defined as the maximum head value minus the minimum head value within the oscillatory pattern. From Eq. (3.13), the theoretical minimum head value at the odd harmonics is $1/\left(Z_V^* / Z_L^* + 1\right)$ when the cosine function $\cos(\omega_r^{odd} \pi x_L - \pi)$ equals 1. When the cosine function equals -1, the maximum head value is achieved as 1. As a result, the theoretical dimensionless amplitude of the leak-induced pattern at the odd harmonics is given as

$$\left|h^*_{odd}\right|_{amp} = 1 - \frac{1}{Z^*_V / Z^*_L + 1} = \frac{1}{Z^*_L / Z^*_V + 1} \tag{3.15}$$

The theoretical dimensionless amplitude for the leak-induced pattern at the even harmonics can be derived by a similar process, and written as

$$\left|h^*_{even}\right|_{amp} = \frac{1}{Z^*_L Z^*_V + 1} \tag{3.16}$$

Eqs (3.15) and (3.16) demonstrate that the amplitudes of the leak-induced pattern at the odd and the even harmonics are equal only if $Z^*_V = 1$. The expression of $\left|h^*_{odd}\right|_{amp}$ is a monotonically increasing function of Z^*_V, while $\left|h^*_{even}\right|_{amp}$ is a monotonically decreasing function of Z^*_V. When the value of Z^*_V is greater than 1, the amplitude of the leak-induced pattern at the odd harmonics is larger than that at the even harmonics; however, when Z^*_V is less than 1, the amplitude of the leak-induced pattern at the even harmonics is larger. These results indicate that, physically, the amplitudes of leak-induced patterns at the odd and even harmonics are controlled by the steady state valve opening, because the value of Z^*_V depends on the steady state head loss across the valve and the flow through the valve, which are in turn dependent on the steady state valve opening [see Eq. (3.17) in the next section].

3.4.2 Impedance parameter ranges

An analysis is now performed to determine the physical ranges for the above dimensionless impedances. The possible range of a parameter is presented as $O\{10^n, 10^m\}$, which indicates that the order of magnitude of the parameter is between 10^n and 10^m. Indicative values for n and m are discussed subsequently.

Considering the valve as an orifice and using the orifice equation, the expression of the dimensionless steady-state valve impedance can be written as

$$Z_V^* = \frac{\sqrt{2g\Delta H_{V0}}A}{aC_d A_{V0}} \tag{3.17}$$

where A_{V0} is the opening area of the steady-state valve; C_d is the coefficient of discharge for the valve opening, which is usually less than 1. It can be seen from Eq. (3.17) that the value of Z_V^* can be controlled by setting the valve opening A_{V0}. Similarly, the dimensionless leak impedance can be written as

$$Z_L^* = \frac{\sqrt{2gH_{L0}}A}{aC_{Ld}A_L} \tag{3.18}$$

In practice, the reasonable physical range for wave speed a is $O\{10^2,10^3\}$; for valve head loss ΔH_{V0} it is $O\{10^{-2},10^2\}$; for head at a leak H_{L0} it is $O\{10^{-2},10^2\}$. The size of $C_d A_{V0}$ can be either very small or comparable to A, so a reasonable estimate for the range of $A/(C_d A_{V0})$ is $O\{10^0,10^4\}$. In contrast, $C_{Ld}A_L$ should be much smaller than A, so the range of $A/(C_{Ld}A_L)$ is assumed to be $O\{10^2,10^4\}$. In addition, note that when simplifying Eq. (3.6) to obtain Eq. (3.7) and Eq. (3.8), the eliminated small coefficient $(Q_{L0}a)/(4H_{L0}gA)$ is equivalent to $1/(2Z_L^*)$. It must be small enough for the elimination to be satisfied, so the value of Z_L^* is assumed to be larger than 10^0. By substituting all these elements into Eq. (3.17) and Eq. (3.18), the ranges for the dimensionless steady-state valve and leak impedance are derived as

$$Z_V^* \in O\{10^{-4},10^4\} \tag{3.19}$$

$$Z_L^* \in O\{10^0,10^4\} \tag{3.20}$$

3.4.3 Leak size derivation

The dimensionless leak size $C_{Ld}A_L / A$ is a critical parameter that needs to be estimated during the leak detection procedure. Lee et al. (2005b) offered a procedure and equations for determining $C_{Ld}A_L / A$ using the leak-induced pattern at the odd harmonics for dimensional systems. Sattar and Chaudhry (2008) published a way to estimate the leak size through the use of the leak-induced pattern at the even harmonics, but by using a semi-empirical look-up curve rather than an analytical approach.

In contrast, the current research derives the equations for determining the dimensionless leak size $C_{Ld}A_L / A$ by utilizing the dimensionless impedances and either of the two dimensionless amplitudes of the leak-induced patterns. Rearranging the expression for the dimensionless leak impedance [Eq. (3.10)] yields $Q_{L0} = 2H_{L0}gA/(aZ_L^*)$. By substituting it into the orifice equation for the leak, $C_{Ld}A_L / A$ can be written as

$$C_{Ld}A_L / A = \sqrt{2H_{L0}g} \Big/ (aZ_L^*) \tag{3.21}$$

It is possible to estimate the value of H_{L0} once the leak location has been confirmed. The value of Z_L^* can then be obtained from the dimensionless amplitude of the leak-induced pattern either at the odd harmonics or at the even harmonics. Two new equations are developed using Eq. (3.15) and Eq. (3.16):

$$Z_L^* = Z_V^*(1 - \left|h_{odd}^*\right|_{amp}) \Big/ \left|h_{odd}^*\right|_{amp} \tag{3.22}$$

$$Z_L^* = (1 - \left|h_{even}^*\right|_{amp}) \Big/ (\left|h_{even}^*\right|_{amp} Z_V^*) \tag{3.23}$$

Values of the leak-induced pattern amplitudes can be read from the experimental FRD, and the value of Z_V^* can be calculated by the steady-state head loss across, and flow through, the inline valve. As a result, the

dimensionless leak size $C_{Ld}A_L / A$ can be determined mathematically either from the leak-induced pattern at the odd harmonics or that at the even harmonics. The above procedure is equivalent to the leak size determination procedure in Lee et al. (2005b), but with dimensionless parameters.

3.5 Dimensionless modeling of frictionless leaking pipes

In order to demonstrate the effects of the two dimensionless impedances (Z_V^* and Z_L^*) on the leak induced patterns, a frictionless reservoir-pipeline-valve system is described here. A specific set of impedance values is described first, followed by an explanation of the value of the dimensionless impedances one by one.

A leak with a dimensionless impedance of 12.12 (which comes from the pipeline system in the later *case study* section) is located at the dimensionless leak location $x_L^* = 0.1$. According to Eqs (3.15) and (3.16), the location of the leak does not impact on the amplitudes of the leak-induced patterns. The value of Z_V^* is set at 1.0. The dimensionless FRD for this system is obtained from Eq. (3.12) and shown in Figure 3.2.

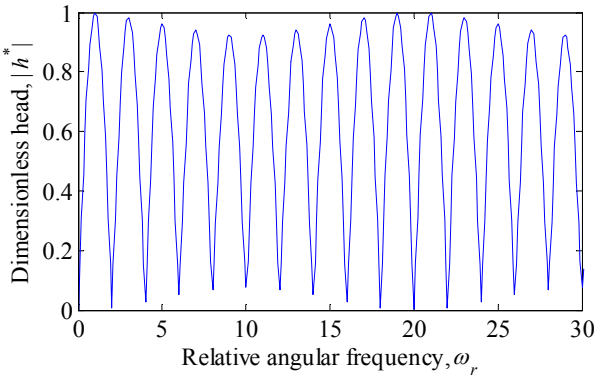

Figure 3.2 A dimensionless FRD with same leak-induced pattern amplitudes at the odd and even harmonics for a frictionless pipe simulation

The leak-induced patterns at the odd and even harmonics are illustrated in Figure 3.3. The circle points are values at the harmonics, and the solid lines are the sinusoidal fitted lines of the form $Y_{data} = x_1 \sin(x_2 \omega_r + x_3) + x_4$, where $x_1, \ldots, x_4$ are coefficients determined from a least squares fit to the data; ω_r is equal to ω_r^{odd} for the pattern at the odd harmonics and ω_r^{even} is the value for the even harmonics; and Y_{data} is the magnitude of head oscillation at the harmonics.

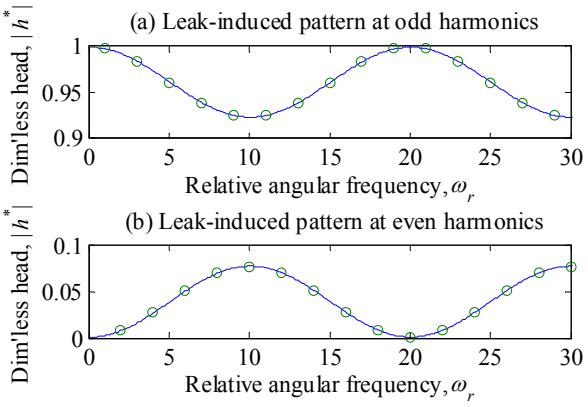

Figure 3.3 Dimensionless leak-induced patterns at the odd and even harmonics (frictionless pipe). The circles are values at harmonics, and the solid lines are the sinusoidal fitted lines

The amplitudes of the leak-induced patterns at the odd and even harmonics are both 0.076 (from the sinusoidal fitting line). This result validates the finding that when Z_V^* equals unity, the amplitudes of the leak-induced patterns are the same.

When Z_L^* is assigned the value of 12.12 and Z_V^* is increased from 10^{-4} to 10^4, the behavior of the leak-induced patterns is determined and shown in Figure 3.4. The theoretical amplitude of the leak-induced pattern at the odd harmonics (the thick solid line) rises, while that at the even harmonics (the thin solid line) drops, both monotonically. When Z_L^* is decreased to 6.06, the amplitudes of leak-induced patterns (dashed lines) show the same pattern but

with larger values. The intersections occur only when $Z_V^* = 1.0$ (Figure 3.4). These results confirm the finding that when Z_V^* is greater than unity, the leak-induced pattern at the odd harmonics is more evident, while when Z_V^* is less than unity, the pattern at the even harmonics has a larger amplitude. As mentioned in previous sections, the value of Z_V^* is controlled by the initial valve opening. The results shown in Figure 3.4 also verify the finding that the amplitudes of the leak-induced patterns can be adjusted by the initial steady-state valve opening.

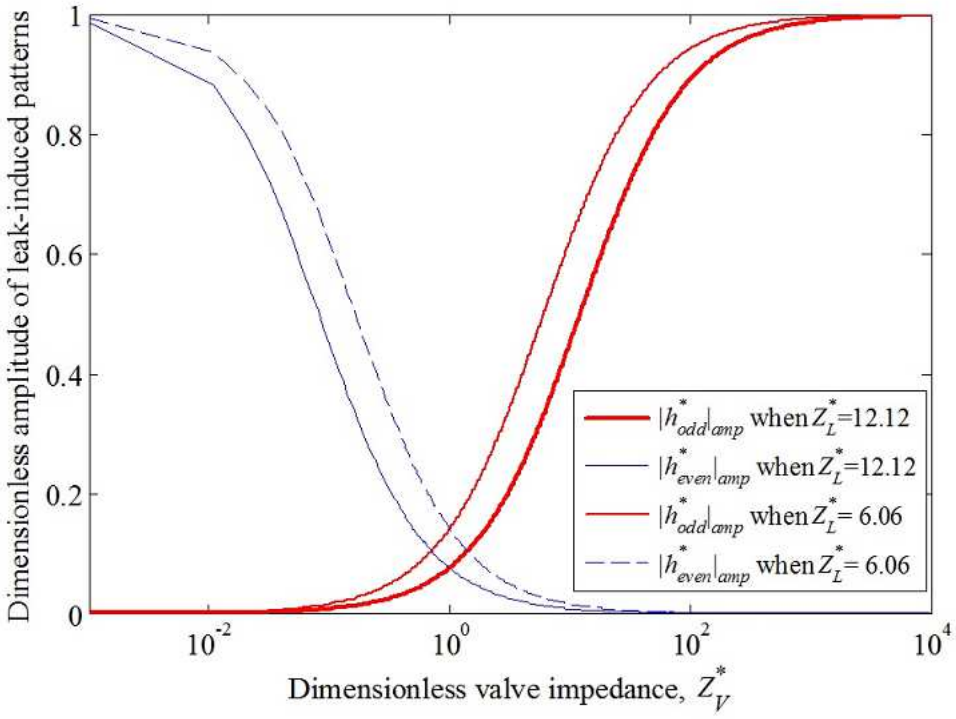

Figure 3.4 Variation of the leak-induced pattern amplitudes as the dimensionless valve impedance (Z_V^*) varies for a frictionless pipe simulation

When the value of Z_V^* remains constant and the value of Z_L^* is changed, the effect of Z_L^* on the amplitudes of the leak-induced patterns can be determined and is demonstrated in Figure 3.5. The amplitudes of the two leak-induced patterns alter with varying Z_L^* values, but are equal for the entire range of Z_L^* as long as Z_V^* equals unity (see the solid lines in Figure 3.5). The amplitudes

decrease monotonically with the increase of Z_L^* (equivalent to a decrease in leak size). When Z_V^* is equal to 2.0, the amplitude of the leak-induced pattern at the odd harmonics is always larger than the pattern amplitude at the even harmonics (see the dashed lines in Figure 3.5), as expected.

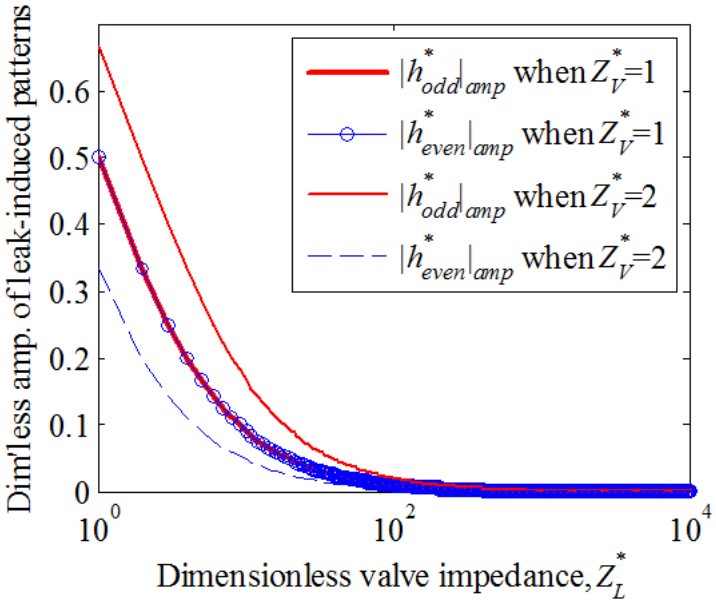

Figure 3.5 Variation of the leak-induced pattern amplitudes according to changes in the dimensionless leak impedance (Z_L^*) for a frictionless pipe simulation

The plots in Figure 3.5 indicate that a smaller value of Z_L^* (a larger leak size) leads to greater values for the leak-induced pattern amplitudes, for both patterns at the odd and the even harmonics. Note that in frictionless systems, ΔH_{V0} and H_{L0} are both constant and equal to the head of the reservoir, so that Z_V^* and Z_L^* are independent variables. For a given system, Z_L^* is always constant [Eq. (3.18)], while Z_V^* is a function of the valve opening [Eq. (3.17)].

3.6 Case study of a specific pipeline with steady friction

The previous dimensionless analysis is for frictionless pipes. In order to investigate the effect of Z_V^* on the leak-induced patterns for real pipelines, a case study is now presented for a leaking pipeline with steady friction. The steady-state valve opening is changed to obtain various steady-state flow rates as well as various values of Z_V^*. Leak detection procedures are performed based on the leak-induced pattern at the odd harmonics and the pattern at the even harmonics, respectively. The accuracies of the derived leak sizes are contrasted. The results are presented with dimensionless parameters to be consistent with the previous dimensionless analysis.

A reservoir-pipeline-valve system similar to that in Sattar and Chaudhry (2008) is adopted. The pipeline system layout is the same as that in Figure 3.1. The parameters of this system are summarized in Table 3.1, where H_r is the reservoir head.

Table 3.1 System parameters for the case study

Parameter	Value
L	160 m
L_1	16 m
L_2	144 m
D	25.4 mm
H_r	30 m
a	1000 m/s
f	0.024
$\Delta\tau/\tau_0$	0.05
$C_{Ld}A_L/A$	0.002

When the steady-state valve discharge Q_{V0} is set to be 0.2995 L/s by adjusting the steady-state valve opening, the value of Z_V^* is almost 1.0 and the value of Z_L^* is 12.07 (it is 12.12 if friction is neglected). The dimensionless FRD is determined numerically by using the original transfer matrices shown in Eqs (3.3) to (3.5) and the result is depicted in Figure 3.6.

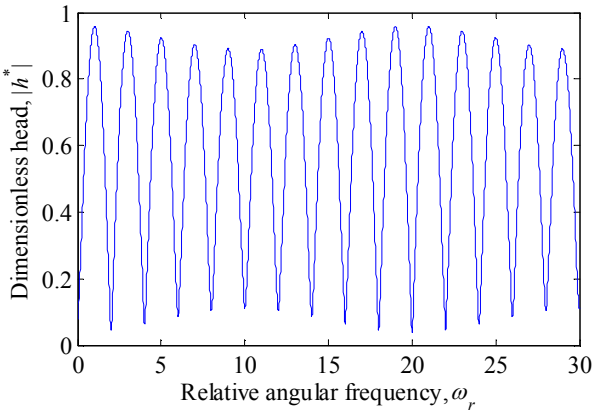

Figure 3.6 A dimensionless FRD for the pipeline system in the case study, $x_L^* = 0.1$

The values of $\left|h_{odd}^*\right|_{amp}$ and $\left|h_{even}^*\right|_{amp}$ determined by the fitting functions are 0.0701 and 0.0702, respectively. The equivalence indicates that, for a specific pipeline system with steady friction, the amplitudes of the leak-induced patterns are still very close to being the same when Z_V^* equals unity. The dimensionless leak location is determined to be 0.1 or 0.9 (a symmetric location due to the symmetric nature of the cosine function) by the periods of the leak-induced patterns. The aliased leak location ($x_L^* = 0.9$) can be eliminated using the leak-induced pattern at the odd harmonics and the phase-based technique presented in Lee et al. (2005b). Figure 3.7 shows the dimensionless FRD for the same pipeline system but the leak is now located at $x_L^* = 0.9$. The leak-induced pattern at the odd harmonics has a different phase compared with the pattern at the odd harmonics shown in Figure 3.6, while the leak-induced patterns at the even harmonics are identical.

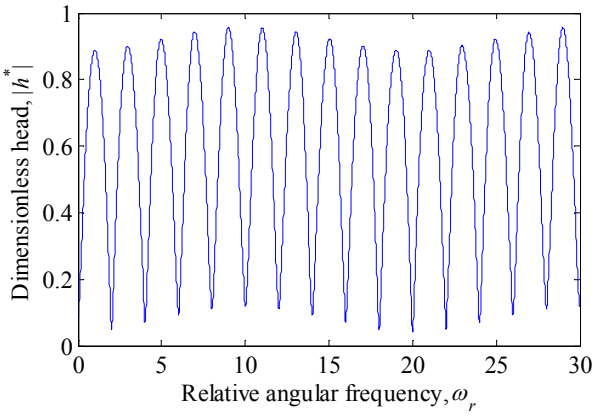

Figure 3.7 A dimensionless FRD for the pipeline system in the case study, $x_L^* = 0.9$

Once the leak location has been determined, the head at the leak H_{L0} can be estimated by linear interpolation, which yields a value of 29.73 m. The value of Z_L^* derived from the dimensionless amplitudes at the odd and the even harmonics are 13.27 and 13.25 by using Eq. (3.22) and Eq. (3.23), respectively. Finally, $C_{Ld}A_L / A$ comes to 0.0018 with both Z_L^* values using Eq. (3.21), which indicates the leak size can be determined relatively accurately from both leak-induced patterns when Z_V^* equals unity.

To determine the behavior of the dimensionless amplitudes of the leak-induced patterns for a specific pipeline system, various values of Z_V^* are now adopted (obtained by changing the steady-state opening of the valve). The range of Z_V^* is selected to be around unity in order to give a clear view about the behavior of the dimensionless amplitudes of the leak-induced patterns around this critical Z_V^* value, and the results are demonstrated in Figure 3.8.

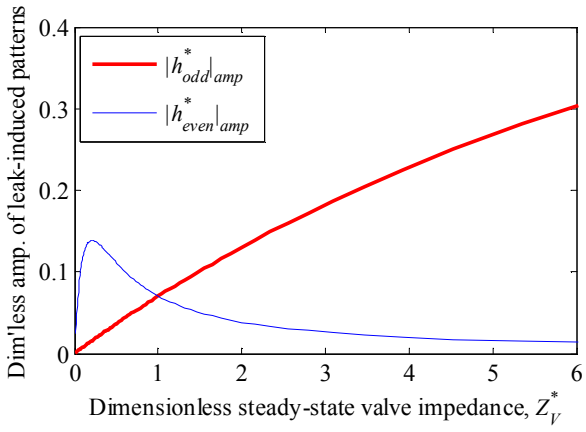

Figure 3.8 Variation of the dimensionless leak-induced pattern amplitudes according to changes in the dimensionless valve impedance (Z_V^*), for case study with steady friction

The dimensionless amplitude of the leak-induced pattern at the odd harmonics, $\left|h_{odd}^*\right|_{amp}$ (derived by using fitted functions), shows a monotonic increasing trend as Z_V^* increases, which is similar to the trend shown in Figure 3.4. In contrast, the changing curve of $\left|h_{even}^*\right|_{amp}$ is not monotonic and different compared with the corresponding trend line for frictionless systems shown in Figure 3.4. With an increasing value of Z_V^*, an increasing trend is observed at the beginning of the $\left|h_{even}^*\right|_{amp}$ curve. A decreasing trend starts when the value of Z_V^* reaches around 0.25. The discrepancy between the curve of $\left|h_{even}^*\right|_{amp}$ for friction systems (Figure 3.8) and that for frictionless systems (Figure 3.4) is caused only by the effect of friction. When friction is included, the values of ΔH_{V0} and H_{L0} change along with the varying of the steady-state valve opening, while they are constant and equal to the reservoir head in the frictionless analysis. A larger valve opening corresponds to a larger steady-state discharge and a smaller Z_V^* value, in which the effect of steady friction is also enlarged.

When the effect of steady friction is severe, or when the value of Z_V^* is less than 0.25 as shown in Figure 3.8, the governing equations derived in the frictionless analysis are no longer applicable for depicting the behavior of real pipelines with friction. This discrepancy is mainly exhibited in the distortion of the leak-induced pattern at the even harmonics in the FRD. In contrast, the leak-induced pattern at the odd harmonics is not affected to any significant degree. The above hypothesis is verified by calculating the dimensionless leak sizes within the whole range of Z_V^* and determining the accuracy. The results are presented in Figure 3.9.

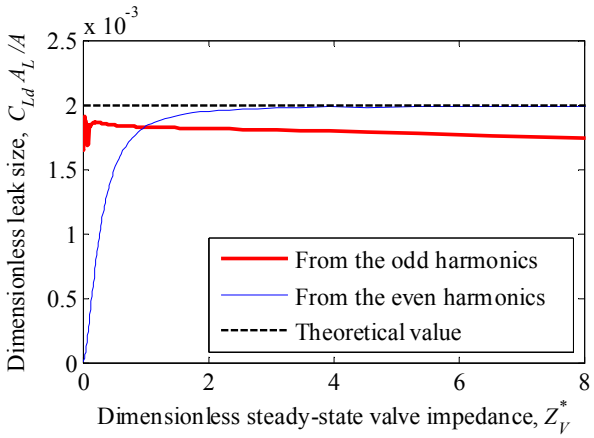

Figure 3.9 Variation of the dimensionless leak size ($C_{Ld}A_L / A$) (derived from the odd and the even harmonics, respectively) for changes in the dimensionless steady-state valve impedance (Z_V^*), for the case study with steady friction

When Z_V^* equals 1, the values of $C_{Ld}A_L / A$ determined from the leak-induced patterns at the odd and even harmonics are equivalent and close to the theoretical leak size (0.002). When Z_V^* is increased from 1, a slight decreasing trend that deviates from the theoretical leak size is observed for the dimensionless leak size determined from the odd harmonics, which indicates that values of Z_V^* that are too large are not desirable. Meanwhile, the leak size derived from the leak-induced pattern at the even harmonics seems to be more accurate. However, as can be seen in Figure 3.8, the value of $\left|h_{even}^*\right|_{amp}$ is small

and keeps on decreasing as the value of Z_V^* increases from 1.0. Considering that the head values at the even harmonics in the FRD are small values and close to zero [refer to the FRD showed in Lee et al. (2005b)], the amplitude of the leak-induced pattern at the even harmonics is hard to observe accurately from experimental data due to a poor signal to noise ratio (SNR).

When Z_V^* decreases from 1, the value of $C_{Ld} A_L / A$ derived from the odd harmonics remains steady but fluctuates when $\left|h_{odd}^*\right|_{amp}$ is too small. In contrast, the value of $C_{Ld} A_L / A$ derived from the even harmonics drops dramatically, even though the value of $\left|h_{even}^*\right|_{amp}$ is larger than $\left|h_{odd}^*\right|_{amp}$ when Z_V^* is smaller than 1. The relative error of the leak size derived from the even harmonics when compared to the real dimensionless leak size is around 30% when Z_V^* is 0.5. The deviation from the real leak size is more obvious for smaller Z_V^* values, which corresponds to greater friction effects.

The above case study on a specific pipeline system with steady friction verifies that the amplitudes of the leak-induced patterns can be adjusted in real applications by adjusting the steady-state valve opening. The steady friction has more effect on the leak-induced pattern at the even harmonics for values of Z_V^* less than 1. The fluctuation and large error in the derived leak sizes presented in Figure 3.9 demonstrate that, for small values of Z_V^* (less than 0.5), the influence of the steady friction is so great that the expression for the leak-induced pattern at the even harmonics derived by frictionless analysis is insufficient to depict the behavior of the head response or to be used to determine the leak size accurately.

3.7 Comparison of the two existing leak detection methods

The leak detection method proposed by Lee et al. (2005b) and that presented in Sattar and Chaudhry (2008) are now compared to illustrate which harmonics (odd or even) possess the greater utility for leak detection. Leak detection consists of two main goals: (1) to detect the leak location, and (2) to estimate the leak size. The dimensionless leak location can be determined from the period of the leak-induced pattern. The periods of the leak induced patterns at the odd and the even harmonics are the same regardless of whether steady friction is included or not. However, this approach leads to two possible symmetric locations for a leak corresponding to a single oscillation period due to the symmetric nature of the cosine function. In the method proposed by Lee et al. (2005b), the phase of the inversed leak-induced pattern at the odd harmonics can be used to determine in which half of the pipeline the leak is located. For the method presented in Sattar and Chaudhry (2008), however, the aliased position cannot be eliminated.

Regarding the estimation for the leak size, there are two different strategies. In Lee et al. (2005b), Eq. (3.7) together with the orifice equation were used to calculate the lumped leak parameter $C_{Ld}A_L$, which is equivalent to the procedure proposed in this paper but in the dimensional domain. The distortion in the FRD caused by unsteady friction can be corrected numerically by using a least squares regression of a scale- and trend-corrected sinusoid to the inverted peak data points (Lee et al. 2006). The procedure for determining the leak size has a strong mathematical foundation and the results are observed to be relatively accurate for a wide range of Z_V^* values in the case study described in this research. The mathematics and the results of the case study indicate that the method based on odd harmonics is robust and reliable in estimating the leak size.

The leak size estimation technique in Sattar and Chaudhry (2008) is not based on rigorous mathematical equations. Firstly, the amplitudes of the leak-induced pattern at the even harmonics are derived numerically with various leak sizes. Then, a semi-empirical relationship between the dimensionless amplitude (non-dimensionalised by dividing the head of the reservoir) and the dimensionless damage [$(C_{Ld} A_L / A)^{0.5}$] requires derivation by curve fitting. In Sattar and Chaudhry (2008), when an experimental FRD was obtained from a real pipeline system, the leak size was read from a look-up curve after the amplitude of the leak-induced pattern at the even harmonics had been determined. The effect of unsteady friction was neglected, which led to an average error of 7%, as mentioned in their work. Moreover, as illustrated in this research, the amplitude of the leak-induced pattern (either at the odd or the even harmonics) is not only dependent on the leak size but also influenced by the steady-state valve opening or the impedance of the valve. A simple semi-empirical curve is not sufficient to predict the leak size for arbitrary pipeline configurations.

The above analysis indicates that the leak detection method proposed by Lee et al. (2005b) using the leak-induced pattern at the odd harmonics has more advantages. It can eliminate the aliased leak location, and provide a leak size with acceptable accuracy with appropriate valve opening settings.

3.8 Challenges to current FRD-based leak detection techniques

This research indicates that the leak detection technique based on the analysis of the leak-induced pattern of resonant responses is promising, and extraction of the leak-induced pattern can be improved by using the appropriate valve impedance. However, it should be noted that challenges exist for the application to real pipelines. These challenges result from two major aspects: the assumptions made in the development of the mathematical leak detection algorithms, and practical limitations due to the complexities of real pipeline systems in the field. Details about these two aspects are discussed below.

3.8.1 Summary of the assumptions

A number of assumptions have been made during the development of the FRD-based leak detection algorithms. The major assumptions are summarized and presented below.

Main assumptions associated with the momentum and continuity equations [Eqs (3.1) and (3.2)]: (i) The flow is one dimensional and pressure is uniform at cross sections; (ii) The fluid is slightly compressible and the conduit walls are linearly elastic, but variations of the mass density ρ and the flow area A due to variations of the inside pressure are negligible during the mathematical deviation; (iii) The head losses during the transient state for a given flow velocity are the same as in steady flows at that velocity.

Main assumptions associated with the transfer matrix method [Eqs (3.3) to (3.5)]: (i) Sinusoidal steady-oscillatory flow can be established in pipelines, in which the instantaneous pressure head $H = H_0 + h^O$ and the instantaneous discharge $Q = Q_0 + q^O$, where H_0 and Q_0 are the mean values of head and discharge (i.e. the steady-state head and discharge), and h^O and q^O are the sinusoidal oscillations around the mean; (ii) The friction term and the non-linear boundary conditions are linearized, which requires that the amplitude of oscillations (h^O and q^O) to be small; (iii) The pipeline system is a linear system, so that any periodic forcing function (input signals) can be decomposed into various harmonics by Fourier analysis and analyzed separately. The overall system response is determined by superposition of individual responses; (iv) The pipeline section described by the field matrix Eq. (3.3) is constant and uniform in cross-sectional area, wall thickness, wave speed and wall material.

The orifice equation: It is assumed that the head at the leak and the flow through the leak is governed by the orifice equation $Q_{L0} = C_d A_L \sqrt{2gH_{L0}}$. This equation is developed for steady-state conditions, and can be accurate if

the lumped leak parameter $C_d A_L$ is calibrated appropriately. This equation is assumed to be still valid in the FRD-based leak detection using transient waves, where the value of $C_d A_L$ may vary during transient event. To make this assumption applicable, the transient waves used to excite the pipeline must be low in amplitude compared with the steady-state head. The IRS-based persistent signals proposed in this paper are suitable options.

The FRD-based leak detection techniques [Eqs (3.6) to (3.8)]: (i) The effects of friction are negligible, i.e, the pipeline is lossless; (ii) The size of the leak is small compared with the cross-sectional area of the pipeline; (iii) The pipeline under test is a single pipeline with simple boundary conditions (reservoir-pipeline-valve or reservoir-pipeline-reservoir).

3.8.2 Challenges in practical applications

As presented in the previous sub-section, current FRD-based leak detection techniques are developed based on a number of assumptions. These assumptions facilitate the deviation of the mathematical equations; however, they also impose challenges on the application of the FRD-based leak detection techniques on real pipelines. Major challenges and possible solutions to date are summarized below.

Effects of friction: The effects of friction are neglected in the FRD-based leak detection techniques. However, the effects of friction exist in every pipeline and affect the shape of the measured FRD. Lee et al. (2005b) found that steady friction can cause a uniform decrease of the amplitude of a FRD, but that it has negligible effects on the leak-induced pattern at the odd harmonics, while unsteady friction is frequency-dependent and cause a non-uniform distortion of the amplitude of resonant responses. To deal with the non-uniform distortion, a least squares regression fitting algorithm was proposed by Lee et al. (2006) through an experimental study. An equation with ten unknown parameters was calibrated to fit the measured data, so that the frequency of the leak-induced pattern, which is indicative of the location of the leak, could be estimated. This technique was successful in the

laboratory. This technique leads to another practical challenge: it requires the input signal to have a wide bandwidth, as a number of resonant responses need to be measured for the calibration of the ten unknowns.

Bandwidth in the input signal: The bandwidth required depends on the fundamental frequency of the pipeline under test. A shorter pipeline has a higher fundamental frequency, thus requires a higher bandwidth in the input signal. Traditional input transient signals, such as discrete step or pulse pressure waves generated by an abrupt valve movement, cannot fulfill this requirement for short pipelines. The discrete step or pulse pressure waves are not sharp enough to gain a wide enough bandwidth due to the limitation in the maneuverability of the valve. In addition, the energy distribution of these two types of signal is uneven in the frequency domain. The energy drops rapidly as the frequency increases, yielding low signal-to-noise-ratio (SNR) for high frequency components. A potential solution of this problem is to use persistent signals that have wide bandwidth and lower amplitude to replace the traditional discrete signals. Lee et al. (2008a) have used pseudo-random binary signal (PRBS)-based input transients to extract pipeline FRD in the laboratory. A laboratory-sized customized side-discharge valve-based transient generator was developed to produce the persistent and periodical signal. The experiments were successful as the estimated FRD was consistent with the theoretical FRD. However, some practical issues still exist, such as the effects of nonlinearities in real pipelines and the potential need to rapidly maneuver the side-discharge valve.

Pipeline parameter variations: The FRD-based leak detection techniques developed by Lee et al. (2005b) and Sattar and Chaudhry (2008) both assume that the pipeline is uniform in cross-sectional area, wall thickness, wave speed and wall material. However, these properties may vary along a pipeline in the field, for example, due to wall deterioration. Duan et al. (2011) have studied the effects of complex series pipelines on the FRD-based leak detection, which shows that the reflections resulting from internal series junctions modify the system resonant frequencies but have a small effect on the leak-induced information contained within the system frequency responses.

Numerical simulations performed by Duan et al. (2011) indicate that single or multiple leaks in complex series pipelines can still be detected by the FRD-based technique developed by Lee et al. (2005b), provided that the location and size of the resonant peaks of the system frequency responses are accurately determined.

Pipeline networks: The current FRD-based leak detection techniques are developed for single pipelines lying between well-defined boundary conditions (reservoir or valve). However, in practice, few systems exist within this narrow category. In contrast, pipelines often contain multiple sections or form a complex network. Due to the complexities in boundary conditions, until now, no field tests have been conducted for the FRD-based leak detection techniques.

Another challenge in pipeline networks is the demand-induced operational noise. Transients can be introduced into a pipeline system because of the use of water by an unknown consumer. The demand-induced transient noise is usually small in large scale systems, but need to take into account where necessary.

The extension of the FRD-based leak detection techniques to pipeline networks is important. Lee et al. (2005a) have studied this problem and outlined a FRD extraction procedure for pipelines in a network. An individual pipeline can be partially separated from the network by closing the valve at one end of the pipe section. A side-discharge valve located adjacent to the closed valve is then used to generate a transient pulse. The transient trace is measured by a transducer located at the same location as the generator from the beginning of the excitation (time 0) up to a time of $2L/a$, where L is the length of the single pipe section (from the closed valve to the junction in the other end) and a is the wave speed in this section. This initial length of data contains only the reflections within the pipe section but excludes reflections from the rest of the network. The FRD of the specified pipe section can be obtained by assuming that a reservoir exists at the open boundary, and extending the original data to a length of $4L/a$ through inverting the

measured data and attaching it to the end of the original data (Lee et al. 2005a). Although further studies and testing are necessary to validate this technique, it shows a potential of applying the FRD-based leak detection techniques to pipelines in the real world.

3.9 Conclusions

Leak-induced patterns at the odd and the even harmonics in the frequency response diagram (FRD) of a leaking pipe are analyzed and compared in this paper. A non-dimensionalization approach is performed to simplify the governing equations of the FRD, and to analyze the leak-induced patterns with dimensionless parameters. Equations for determining the dimensionless leak size $C_{Ld} A_L / A$ are derived utilizing the dimensionless impedances and the dimensionless amplitudes of the leak-induced patterns.

The dimensionless analysis conducted as part of this research illustrates that the amplitudes of the leak-induced patterns can be controlled by the steady-state valve opening. The amplitudes of the leak-induced patterns at the odd and the even harmonics are equivalent when the dimensionless steady-state valve impedance, Z_V^*, equals unity. When Z_V^* is greater than unity, the leak-induced pattern amplitude at the odd harmonics is larger than that at the even harmonics; whereas when Z_V^* is smaller than unity, the leak-induced pattern at the even harmonics is more evident. The value of Z_V^* can be adjusted by changing the steady-state opening of the inline valve. This finding is applicable to both frictionless pipeline systems and systems with steady friction.

A case study of a specific pipeline system is analyzed to investigate the effect of steady friction on the amplitudes of the leak-induced patterns. The results indicate that when the effect of steady friction is severe, where the value of Z_V^* is much less than unity, the leak sizes determined from the leak-induced

pattern at the odd harmonics have some fluctuations, and those determined from the leak-induced pattern at the even harmonics have huge errors.

Two existing leak detection methods are compared. The method proposed by Lee et al. (2005b), which uses the leak-induced patterns evident at the odd harmonics, is found to be more robust. It can provide a unique leak location and a relatively accurate leak size through mathematical calculations. Challenges to the existing FRD-based leak detection techniques are summarized, including physical assumptions made during mathematical deviation and typical practical issues in real pipeline systems.

This research suggests that, in real applications, the leak detection method proposed by Lee et al. (2005b) with a value of Z_V^* larger than unity should be employed. The opening of the inline valve needs to be small, ensuring a large steady-state valve head loss, a small valve discharge, and the slight effect of steady friction. However, in cases where Z_V^* cannot be over 1.0, i.e. the steady-state discharge is required to be large, the method presented in Sattar and Chaudhry (2008) can be employed to determine whether there is a leak and to estimate the location.

Acknowledgements

The research presented in this paper is supported by the Australian Research Council through the Discovery Project Grant DP1095270.

Notations

The following symbols are used in this paper:

A = inside pipe cross sectional area;
a = wave speed;
A_L = area of a leak orifice;
A_{V0} = opening area of a steady-state valve;

C_d, C_{Ld} = coefficient of discharge for a valve opening and for a leak orifice;

D = internal pipe diameter;

$\mathbf{F_1}$, $\mathbf{F_2}$ = field matrices of the two pipe sections divided by a leak;

f = Darcy-Weisbach friction factor;

g = gravitational acceleration;

H = instantaneous head;

H_0 = steady-state head;

H_r = reservoir head;

H_{L0} = steady-state head at a leak orifice;

h, h^* = amplitude and dimensionless amplitude of head fluctuation;

h^O = head oscillation around the mean;

$h(x)$ = complex head amplitude;

$|h_{odd}|$, $|h^*_{odd}|$ = magnitude and dimensionless magnitude of head fluctuation at the odd harmonics;

$|h_{even}|$, $|h^*_{even}|$ = magnitude and dimensionless magnitude of head fluctuation at the even harmonics;

$|h^*_{odd}|_{amp}$, $|h^*_{even}|_{amp}$ = dimensionless amplitude of leak-induced pattern at the odd harmonics and the even harmonics;

j = imaginary unit, $\sqrt{-1}$;

L = total length of pipe;

L_1, L_2 = lengths of the two pipe sections divided by a leak;

$O\{10^n, 10^m\}$ = an order of magnitude range from 10^n to 10^m;

$\mathbf{P_L}$ = point matrix for a leak;

Q = instantaneous flow rate;

Q_0 = steady-state discharge;

Q_{L0} = steady-state flow out of a leak;

Q_{V0} = steady-state flow through a valve;

q^O = discharge oscillation around the mean;

$q(x)$ = complex discharge amplitude;

R = linearised resistance term;

Re[] = real part of the variable inside the brackets;

t = time;

$\mathbf{U}$ = overall transfer matrix for a pipeline;

x = distance along pipe;

$x_1, \ldots x_4$ = coefficients to be determined in fitting function;

x_L^* = dimensionless position of a leak;

Y_{data} = oscillatory head values at harmonics;

Z_C = characteristic impedance of a frictionless pipe;

Z_L, Z_L^* = hydraulic impedance and dimensionless hydraulic impedance for a leak orifice;

Z_{Pi} = the characteristic impedance for the i th pipe;

Z_V, Z_V^* = hydraulic impedance and dimensionless hydraulic impedance for a steady-state valve;

Greek symbols:

ΔH_{V0} = steady-state head loss across a valve;

$\Delta\tau$ = magnitude of the dimensionless valve-opening oscillation;

μ_i = propagation operator for the i th pipe;

τ_0 = mean dimensionless valve-opening coefficient, centre of oscillation;

ω, ω_r = angular frequency and dimensionless relative angular frequency;

ω_r^{odd}, ω_r^{even} = relative angular frequency for odd harmonics and for even harmonics;

ω_{th} = fundamental angular frequency for a reservoir-pipeline-valve system;

Chapter 4

Single Event Leak Detection in a Pipeline using the First Three Resonant Responses (Journal Publication 2)

Gong, J., Lambert, M. F., Simpson, A. R., and Zecchin, A. C.

School of Civil, Environmental and Mining Engineering, the University of Adelaide, Adelaide, SA 5005 Australia

Journal of Hydraulic Engineering, 139(6), 645-655.

Statement of Authorship

Title of Paper	Single Event Leak Detection in a Pipeline using the First Three Resonant Responses
Publication Status	Published
Publication Details	Gong, J., Lambert, M. F., Simpson, A. R., and Zecchin, A. C. (2013). "Single event leak detection in a pipeline using the first three resonant responses." *Journal of Hydraulic Engineering*, 139(6), 645-655.

Author Contributions

By signing the Statement of Authorship, each author certifies that their stated contribution to the publication is accurate and that permission is granted for the publication to be included in the candidate's thesis.

Name of Principal Author (Candidate)	Jinzhe Gong		
Contribution to the Paper	Developed and implemented the methodology, designed and conducted numerical simulations, interpreted and analysed results, prepared manuscript.		
Signature		Date	25/09/2013

Name of Co-Author	Martin Lambert		
Contribution to the Paper	Supervised development of work, helped to evaluate and edit the manuscript and acting as the corresponding author.		
Signature		Date	25/9/13

Name of Co-Author	Angus Simpson		
Contribution to the Paper	Helped to evaluate and edit the manuscript.		
Signature		Date	25/9/2013

Name of Co-Author	Aaron Zecchin		
Contribution to the Paper	Helped to evaluate and edit the manuscript.		
Signature		Date	1·10·2013

Abstract

Hydraulic transients (water hammer waves) can be used to excite a pressurized pipeline, yielding the frequency response diagram (FRD) of the system. The FRD of a pipeline system is useful for condition assessment and fault detection, because it is closely related to the physical properties of the pipeline. Most previous FRD-based leak detection techniques use the sinusoidal leak-induced pattern recorded on the FRD, either shown on the resonant responses or the anti-resonant responses. In contrast, the technique reported in the current paper only uses the responses at the first three resonant frequencies to determine the location and size of a leak. The bandwidth of the excitation only needs to be five times that of the fundamental frequency of the tested pipeline, which is much less than the requirement in conventional FRD-based techniques. Sensitivity analysis and numerical simulations are performed to assess the robustness and applicable range of the proposed leak location technique. The proposed leak location technique is verified by both numerical simulations and using an experimental FRD obtained from a laboratory pipeline.

4.1 Introduction

With rapid population growth, urbanization and industrialization, providing adequate water for domestic and industry use is increasingly becoming a challenge for water authorities around the world. Resources of fresh water are limited or even scarce in some countries, however, for almost every city, only part of the treated water is delivered to consumers successfully, since a large amount of water is lost during transmission.

The amount of water lost during transmission varies between systems, from lower than 10 % in well maintained systems such as those in The Netherlands (Beuken et al. 2006) to more than 50 % in some undeveloped countries or regions (Mutikanga et al. 2009). According to publications released by the International Water Association (Lambert 2002) and the Asian Development Bank (McIntosh and Yniguez 1997), 'non-revenue water' (NRW) or 'unaccounted for water' (UFW) is between 20 % to 40 % for most countries or cities investigated. Among various reasons for the water loss, leakage is considered to be the major one (Nixon and Ghidaoui 2006; Colombo et al. 2009).

In addition to water loss, leakage also costs extra energy for water treatment, storage and pumping (Colombo and Karney 2002). Moreover, leaks may lead to water quality problems, because toxins and bacteria can be introduced into water distribution systems via leaks in low pressure conditions during hydraulic transients (Karim et al. 2003; Colombo et al. 2009; Meniconi et al. 2011; Collins et al. 2012). As a result, leak detection in water distribution systems is of great interest in both industry and academic areas (Puust et al. 2010).

In the past two decades, a number of leak detection techniques have been developed, including acoustic techniques (Fuchs and Riehle 1991; Tafuri 2000), ground penetrating radar (Eiswirth and Burn 2001), electromagnetic techniques (Goh et al. 2011), fiber optic sensing (Inaudi et al. 2008), and hydraulic transient-based techniques (Colombo et al. 2009; Puust et al. 2010).

A major advantage of the transient-based methods is that the information of a long pipeline (usually thousands meters) can be obtained efficiently and cost-effectively, because transient waves travel at high speed along fluid-filled pipes. Up to now, intensive simplified numerical simulations, some elaborately controlled laboratory experiments and a few field tests have been conducted for leak detection using transient-based techniques (Colombo et al. 2009; Puust et al. 2010).

The existing transient-based leak detection techniques can be divided into two categories: the time-domain techniques and the frequency-domain techniques. In the time domain, leak-induced reflections are observed as discontinuities in the pressure traces measured along the pipe. A few leak detection techniques have been developed based on time-domain phenomena (Jönsson and Larson 1992; Brunone 1999), which are complicated by the fact that the size and shape of a leak-induced reflection not only depend on the properties of the leak, but also relate to the input signal (Lee et al. 2007b). For example, using a positive step transient wave as the input, the leak-induced reflections are shown as a small negative step in the measured pressure trace; while when a pulse input is injected, the leak-induced reflections are also pulses. By using signal processing, a leak location can be determined irrespective of the characteristics of the input signal. For example, the use of the wavelet analysis (Ferrante and Brunone 2003a) or the impulse response function (IRF) of the pipeline can improve the estimation of the leak location (Vítkovský et al. 2003b; Lee et al. 2007b). However, difficulties exist in real world applications, where leak-induced reflections are usually small in magnitude, and they can be hard to distinguish from the reflections introduced by other hydraulic components, such as joints, junctions, and entrapped air.

Several transient-based leak detection techniques have been developed in the frequency domain, based on analyzing the frequency response function (FRF) or the frequency response diagram (FRD) of a pipeline system. The FRF of a pipeline system is the Fourier transform of the IRF, which describes the magnitude of the system response to each oscillatory excitation at a specific frequency, and the FRD is the plot of a FRF. The FRF or FRD is dependent

on the physical configuration of the pipeline system, such as the boundary condition, the length, the location and size of the leak. As a result, the FRF or FRD can be used for leak detection.

Jönsson and Larson (1992) first proposed that it is possible to distinguish the leak-induced reflections in the spectrum at a frequency corresponding to the leak location. Mpesha et al. (2001) proposed that the FRD of a pipeline with leaks had additional resonant pressure amplitude peaks, and a method using the FRD was presented for detecting and locating leaks. Ferrante and Brunone (2003b) demonstrated that Fourier transform of transient pressure does not show further peaks unless leak size is larger than a critical value.

Covas et al. (2005) proposed a *standing wave difference method*, which uses the spectral analysis of an FRD to determine the leak-resonance frequency and indicate the leak location. However, two locations are estimated for a single leak, with one of them an alias and undistinguishable.

Lee et al. (2005a) proposed a *resonance peak-sequencing method* for leak location. The resonant responses in a FRD (peaks at the odd harmonics of the pipeline fundamental frequency) are ranked in order of magnitude. The rank sequence is indicative to the dimensionless leak location range, and the size of the leak has no effect on the order of the peaks. For example, using the rank sequence of the first three resonant peaks, the leak can be located to one of the six unequal ranges along the pipe, but the exact location cannot be pinpointed.

In the same year, Lee et al. (2005b) proposed a technique for leak location and size estimation using the sinusoidal leak-induced pattern shown on the resonant responses (frequency responses at the odd harmonics). The period and phase of the sinusoidal leak-induced pattern is indicative of the leak location, while the amplitude is related to the leak size. One year later, laboratory experiments were conducted by the same authors, which verified the odd harmonics-based leak detection technique (Lee et al. 2006). The experimental FRD were affected by the frequency-dependent behavior resulting from unsteady friction. In order to produce an accurate estimation of

the oscillation frequency and phase, a least squares regression algorithm was adapted to fit a cosine function to the inverted resonant responses. However, up to 10 coefficients need to be calibrated, which requires at least 10 resonant responses to yield a determined system for the regression process.

Sattar and Chaudhry (2008) suggested a similar leak detection method but using the leak-induced pattern on the anti-resonant responses (frequency responses at the even harmonics). The anti-resonant responses can be hard to measure accurately in practice, because they are usually low in amplitude.

The odd harmonics-based leak detection technique was extended to complex series pipe systems by Duan et al. (2011), in which the results of analytical analysis and numerical simulations suggest that internal junctions of series pipe sections can change the location of the resonant peaks, but have little impact on the period and phase of the leak-induced sinusoidal pattern.

Although the existing odd harmonics-based leak detection technique (Lee et al. 2005b; Duan et al. 2011) has its advantages, two major limitations are obstacles for real world applications. Firstly, a significant number of resonant responses need to be known, in order to provide sufficient information to identify the period and phase of the sinusoidal leak-induced pattern. This in turn requires the input signal to have a wide bandwidth that covers a significant number of harmonics of the pipeline's fundamental frequency. However, due to limitations in the maneuverability of existing transient generators, it is difficult to obtain a wide bandwidth input with enough signal-to-noise-ratio (SNR). Secondly, the distortion caused by the frequency-dependent behavior of real pipelines, such as the effects of unsteady friction, needs to be corrected in order to give a better estimation of the amplitude, period and phase of the sinusoidal leak-induced pattern. The frequency-dependent behavior of real pipelines is complicated, and more distortion is expected in the response at higher resonant frequencies.

The research presented in this paper proposes a novel FRD-based leak detection technique that is not affected significantly by problems with either

the bandwidth of the input or distortion due to unsteady friction. Only the first three resonant responses recorded in a FRD (which are the responses at the first three odd harmonics), are used to estimate the location and size of a single leak. The bandwidth of the input signal only needs to be greater than the third resonant frequency of the pipeline, which is five times the fundamental frequency. In addition, the effects of unsteady friction are usually not significant on the first three resonances, and the new leak location algorithm is robust to measurement errors (as shown in the sensitivity analysis in a latter section), so that the procedure for correction can be avoided. This new technique is verified by both numerical simulations and laboratory experiments.

4.2 Frequency response equations for a single pipe with a leak

This section reviews the frequency response equations for a single pipeline with a leak, which are the basis of most frequency-domain transient-based leak detection techniques. The reservoir-pipeline-valve (RPV) configuration is adopted, where two possible boundary conditions are discussed and compared.

4.2.1 System configurations

Typically, to extract the FRD of a pipeline, systems with two types of configuration can be used: the reservoir-pipeline-valve (RPV) system and the reservoir-pipeline-reservoir (RPR) system (Lee et al. 2006). The fundamental frequency of a RPV system is half that of a RPR system (Lee et al. 2006). As a result, the RPV system requires a smaller bandwidth for the input signal to cover the same number of resonant frequencies, and this type of configuration is the focus of the current research. A typical RPV system for leak detection is given in Figure 4.1, where H_r represents the head of the reservoir; L is the total length of the pipe; L_1 and L_2 are the length of the pipe sections upstream and downstream of the leak, respectively. A pressure transducer is located at

the end of the pipe to achieve the highest signal-to-noise ratio (Lee et al. 2006).

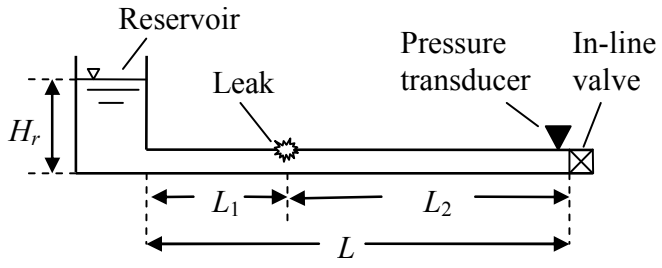

Figure 4.1 A reservoir-pipeline-valve system with a leak.

Pipeline systems with a RPV configuration can have two possible boundary conditions: the *RPV-High Loss Valve* boundary condition and the *RPV-Closed Valve* boundary condition. For RPV-High Loss Valve systems, the in-line valve has a small opening to achieve a high value of hydraulic impedance. The downstream side of the in-line valve can be connected to the atmosphere or a constant head reservoir. For *RPV-Closed Valve* systems, the in-line valve is fully closed to form a dead end.

The frequency responses equations for pipelines with the *RPV-High Loss Valve* and the *RPV-Closed Valve* boundary conditions are given below in sequence. The *RPV-Closed Valve* boundary condition can be regarded as a special case of the *RPV-High Loss Valve* boundary condition, where the opening of the valve is extremely small. The limitations and benefits of the *RPV-Closed Valve* boundary condition are analyzed and presented.

4.2.2 Frequency response equations for RPV-High Loss Valve systems

The frequency response equation of a pipeline system can be derived from the transfer matrix method (Chaudhry 1987; Wylie and Streeter 1993). The transfer matrix for an intact pipe section is given as

$$\begin{Bmatrix} q \\ h \end{Bmatrix}^{n+1} = \begin{bmatrix} \cosh(\mu L_i) & \frac{-1}{Z_P}\sinh(\mu L_i) \\ -Z_P \sinh(\mu L_i) & \cosh(\mu L_i) \end{bmatrix} \begin{Bmatrix} q \\ h \end{Bmatrix}^{n} \tag{4.1}$$

where q and h are complex discharge and head at either end of the pipe section; the superscripts n and $n+1$ represent the upstream and downstream positions respectively; L_i is the length of this pipe section; $Z_P = \mu a^2 / (j\omega gA)$ is the characteristic impedance of the pipe; μ is the propagation operator given by $\mu = \sqrt{-\omega^2 / a^2 + jgA\omega R / a^2}$, in which ω is the angular frequency; a is the wave speed; $j = \sqrt{-1}$ is the imaginary unit; g is the gravitational acceleration; A is the cross-sectional area of the pipe; and R is a linearised resistance term. For turbulent flow and steady friction $R = R_s = fQ_0 / (gDA^2)$, where f is the Darcy-Weisbach friction factor; Q_0 is the steady-state flow rate; and D is the inside diameter of the pipeline. If unsteady friction is included, an additional component R_{us} needs to be added into the linearised resistance term, i.e. $R = R_s + R_{us}$. Unsteady friction is studied in detail in the *numerical verification* section presented latter in this paper.

To highlight the impact of a leak on the frequency response, the pipeline is assumed to be frictionless in the following derivation. The transfer matrix for a frictionless and intact pipe is given as

$$\begin{Bmatrix} q \\ h \end{Bmatrix}^{n+1} = \begin{bmatrix} \cos\left(\frac{L_i\omega}{a}\right) & -\frac{j}{Z_C}\sin\left(\frac{L_i\omega}{a}\right) \\ -jZ_C \sin\left(\frac{L_i\omega}{a}\right) & \cos\left(\frac{L_i\omega}{a}\right) \end{bmatrix} \begin{Bmatrix} q \\ h \end{Bmatrix}^{n} \tag{4.2}$$

where $Z_C = a/(gA)$ is the characteristic impedance of a frictionless pipeline.

The matrix for a leak is

$$\begin{Bmatrix} q \\ h \end{Bmatrix}^{n+1} = \begin{bmatrix} 1 & -\dfrac{1}{Z_L} \\ 0 & 1 \end{bmatrix} \begin{Bmatrix} q \\ h \end{Bmatrix}^{n} \tag{4.3}$$

where $Z_L = 2H_{L0}/Q_{L0}$ is the impedance of the leak in the steady state, in which H_{L0} and Q_{L0} are the steady-state head and discharge at the leak.

An in-line valve can be used to generate steady oscillatory flow, where the transfer matrix is given as

$$\begin{Bmatrix} q \\ h \end{Bmatrix}^{n+1} = \begin{bmatrix} 1 & 0 \\ -Z_V & 1 \end{bmatrix} \begin{Bmatrix} q \\ h \end{Bmatrix}^{n} + \begin{Bmatrix} 0 \\ \dfrac{2\Delta H_{V0}\Delta\tau}{\tau_0} \end{Bmatrix} \tag{4.4}$$

where $Z_V = 2\Delta H_{V0}/Q_{V0}$ is the impedance of the in-line valve at the steady state, in which ΔH_{V0} and Q_{V0} are the steady-state head loss across the valve and the flow through the valve, respectively; τ_0 is the dimensionless valve opening size at the steady state; and $\Delta\tau$ is the amplitude of the dimensionless valve opening perturbation that generates the transients.

The matrices for all the components along a pipeline can be multiplied together from the downstream to upstream boundary to form an overall transfer matrix. At the upstream face of the in-line valve (where the transducer is located), the magnitude of the head response at resonant frequencies (odd harmonics) is given as

$$\left|h_{odd}\right| = \frac{2\Delta H_{V0}\Delta\tau/\tau_0}{1+\dfrac{Z_V}{2Z_L}\left[1-\cos\left(\pi x_L^* \omega_r^{odd}\right)\right]} \tag{4.5}$$

where x_L^* is the dimensionless leak location that is defined as $x_L^* = L_1/L$; and ω_r^{odd} represents the relative angular frequency for the odd harmonics, which is given as $\omega_r^{odd} = \omega^{odd}/\omega_{th}$ = 1, 3, 5…, where ω^{odd} represents the angular

frequency for the odd harmonics; and $\omega_{th} = a\pi/(2L)$ is the fundamental angular frequency of the RPV system.

In practice, it is difficult to control the oscillatory perturbation of an in-line valve. Instead, a side-discharge valve located upstream of and adjacent to the in-line valve can be used to generate the transients (Lee et al. 2006). The side-discharge valve can be modeled as a point where a discharge perturbation takes place:

$$\begin{Bmatrix} q \\ h \end{Bmatrix}^{n+1} = \begin{bmatrix} 1 & 0 \\ 0 & 1 \end{bmatrix} \begin{Bmatrix} q \\ h \end{Bmatrix}^{n} + \begin{Bmatrix} \hat{q} \\ 0 \end{Bmatrix} \tag{4.6}$$

where $\hat{q}$ represents the discharge perturbation at the side-discharge valve.

Once a side-discharge valve is used to generate the transients, the in-line valve can have a constant opening, of which the transfer matrix can be obtained from Eq. (4.4) by removing the last column vector on the right hand side. Then the overall transfer matrix of a RPV system with a side-discharge valve can be obtained, and the magnitude of the resonant response as measured at the upstream face of the in-line valve is written as

$$\left|h_{odd}\right| = \frac{\hat{q}Z_V}{1 + \dfrac{Z_V}{2Z_L}\left[1 - \cos\left(\pi x_L^* \omega_r^{odd}\right)\right]} \tag{4.7}$$

4.2.3 Frequency response equations for RPV-Closed Valve systems

For *RPV-Closed Valve* systems, the pipeline sections and the leak are modeled by their transfer matrices as described in Eq. (4.2) and Eq. (4.3), respectively. The in-line valve is not included in the deviation, as it is fully closed to form the dead end. A side-discharge valve that is located at the upstream face of the closed in-line valve is used to generate the transients, and Eq. (4.6) is adopted to describe the input discharge perturbation produced by the side-discharge

valve. Finally, the magnitude of the resonant response as measured at the upstream face of the closed in-line valve is derived as

$$\left|h_{odd}\right| = \frac{\hat{q}}{\frac{1}{2Z_L}\left[1-\cos\left(\pi x_L^* \omega_r^{odd}\right)\right]} \tag{4.8}$$

RPV-Closed Valve systems can be regarded as *RPV-High Loss Valve* systems but the opening of the valve is extremely small, and accordingly the impedance of the valve is extremely high. Under this assumption, Eq. (4.8) can be obtained directly from Eq. (4.7) by rearranging the equation and setting the impedance of the valve Z_V to infinite.

4.2.4 Comparison between the RPV-High Loss Valve and the RPV-Closed Valve boundary conditions

Compared with the *RPV-High Loss Valve* boundary condition, the *RPV-Closed Valve* boundary condition has two limitations: firstly, the dead end boundary condition cannot always be obtained because the in-line valve in real pipelines may not seal perfectly; secondly, theoretically, the magnitude of the resonant response can be infinite for *RPV-Closed Valve* systems according to Eq. (4.8) (when the cosine component in the denominator equals unity). In real pipelines, the magnitude of the resonant response will not be infinite due to the effects of friction, but it will still be large. The high magnitude of resonant response can introduce risks of pipe burst and significant fluid-structure interactions. In contrast, for *RPV-High Loss Valve* systems, the maximum magnitude of resonant response is controllable and it is related to the impedance of the valve according to Eq. (4.7).

However, the *RPV-Closed Valve* boundary condition has its own benefits. The governing equation for the resonant response of *RPV-Closed Valve* systems [Eq. (4.8)] is less complex than that of systems with the *RPV-High Loss Valve* boundary condition, as the impedance of the valve Z_V is not included. As a

result, theoretically less information is required for estimating the leak location and size in systems with the *RPV-Closed Valve* boundary condition.

Techniques are developed in this research for leak detection in pipelines with the *RPV-High Loss Valve* and the *RPV-Closed Valve* boundary conditions, respectively. The leak detection technique for *RPV-High Loss Valve* systems is presented first, following by the technique for *RPV-Closed Valve* systems as a special case.

4.3 Leak detection for *RPV-High Loss Valve* systems

The development of a technique for detecting leaks in *RPV-High Loss Valve* systems is presented in this section. It can be seen from Eqs (4.5) and (4.7) that the magnitude of each resonant response $|h_{odd}|$ is related to the impedance of the leak Z_L and the dimensionless location of the leak x_L^*. Provided the values of other parameters are known, including $(2\Delta H_{V0}\Delta\tau/\tau_0)$, $\hat{q}$ and Z_V, theoretically only two equations are required for solving the two unknowns, which means only two resonant responses are needed for leak location and size estimation.

In practice, however, the estimation of $(2\Delta H_{V0}\Delta\tau/\tau_0)$, $\hat{q}$ and Z_V may have errors, thus yielding errors in the estimated values of Z_L and x_L^*. This research proposes a leak location algorithm that uses solely the magnitude of the first three resonant responses, being independent of the values of $(2\Delta H_{V0}\Delta\tau/\tau_0)$, $\hat{q}$ or Z_V. However, the impedance of the leak Z_L cannot be derived using the magnitude of the first three resonant responses solely, but rather the ratio of Z_V to Z_L can be estimated.

Details about the new leak location and size estimation algorithms for *RPV-High Loss Valve* systems are described below. A sensitivity analysis is

performed to confirm the robustness and applicable range of the proposed technique.

4.3.1 Determination of the leak location for RPV-High Loss Valve systems

In the proposed new leak location technique, all the parameters on the right hand side of Eq. (4.5) or Eq. (4.7) are assumed to be unknowns. Although there are a number of symbols on the right hand sides of these equations, it is observed that they can be categorized into three independent variables. For Eq. (4.5), the three variables are $\left(2\Delta H_{V0}\Delta\tau/\tau_0\right)$, Z_V/Z_L and x_L^*. For Eq. (4.7), they are $\hat{q}Z_V$, Z_V/Z_L and x_L^*. As a result, to solve for x_L^*, three equations are required, which means the peak values of three resonant responses are needed.

Using the inverted peak values of the first three resonant responses given by Eq. (4.5) or Eq. (4.7) (obtained with ω_r^{odd} = 1, 3 and 5 respectively), the following equation can be written:

$$\frac{\dfrac{1}{|h|_1}-\dfrac{1}{|h|_5}}{\dfrac{1}{|h|_1}-\dfrac{1}{|h|_3}}=\frac{\cos(5\pi x_L^*)-\cos(\pi x_L^*)}{\cos(3\pi x_L^*)-\cos(\pi x_L^*)} \tag{4.9}$$

where the subscripts '$_{odd}$' for the head responses are removed for simplicity, and the new subscripts '$_1$, $_3$ and $_5$' representing the values of ω_r^{odd} are used. Simplifying the above equation and assuming $\cos(\pi x_L^*)\neq 0\ or\ \pm 1$, which means $x_L^*\neq 0$, 0.5 or 1, the following equation is obtained:

$$\frac{\left(|h|_5-|h|_1\right)|h|_3}{\left(|h|_3-|h|_1\right)|h|_5}=4\cos^2(\pi x_L^*)-1 \tag{4.10}$$

Eq. (4.10) gives the relationship between the peak values of the first three resonant responses and the location of the leak. This relationship is independent of any other parameters. In addition, x_L^* is only related to the relative sizes of the peaks, thus the absolute magnitude of the resonant response is not important. Solving Eq. (4.10) for x_L^* yields

$$x_L^* = \frac{1}{\pi} arc\cos\left(\pm\frac{1}{2}\sqrt{1+P_L}\right) \tag{4.11}$$

where P_L represents the left part of Eq. (4.10).

From Eq. (4.11), two values of x_L^* can be obtained for a specific value of P_L, provided the two values within the brackets in Eq. (4.11) are within the range of [-1, 1]. The summation of these two x_L^* values is unity, implying that they are two symmetric possible leak locations along the pipe. Numerical simulations performed in this research illustrate that, by comparing the size of the first two resonant responses $|h|_1$ and $|h|_3$, the alias can be eliminated. When $|h|_1 > |h|_3$, the leak is located within the range of $x_L^* \in (0, 0.5)$; while when $|h|_1 < |h|_3$, the leak is located within $x_L^* \in (0.5, 1)$. Details of the numerical simulations are given in Figure 4.2 in the sensitivity analysis presented in a latter section.

4.3.2 Determination of the leak size for RPV-High Loss Valve systems

Once the leak location has been identified, the leak size can be determined. In the steady state, the size of the leak is related to the steady-state head H_{L0} and discharge Q_{L0} at the leak through the orifice equation

$$Q_{L0} = C_{Ld} A_L \sqrt{2gH_{L0}} \tag{4.12}$$

where C_{Ld} is the discharge coefficient of the leak; and A_L is the flow area of the leak orifice. To estimate the lumped leak parameter $C_{Ld}A_L$, the values of H_{L0} and Q_{L0} need to be known.

The value of H_{L0} can be estimated once the location of the leak x_L^* has been determined. The value of Q_{L0} can be calculated if the value of the leak impedance Z_L is known ($Q_{L0} = 2H_{L0} / Z_L$). However, unlike the x_L^*, the value of Z_L cannot be estimated from the magnitude of the first three resonant responses directly, but rather only the value of Z_V / Z_L can be obtained. Using Eq. (4.5) or Eq. (4.7) with ω_r^{odd} = 1 and 3, the following equation can be derived:

$$Z_L = \frac{Z_V}{2} \frac{|h|_3 \left[\cos(3\pi x_L^*) - 1\right] - |h|_1 \left[\cos(\pi x_L^*) - 1\right]}{|h|_3 - |h|_1} \tag{4.13}$$

where the value of Z_V can be estimated from the steady-state head loss across the valve ΔH_{V0} and the steady-state flow through the valve Q_{V0} (which in turn can be estimated from ΔH_{V0} using the orifice equation).

Compared with the process for estimating the leak location [Eq. (4.11)], the estimation of the leak size depends on more parameters, and the procedure is more complex. However, in practice it is more important to detect the existence of a leak and estimate its location. A sensitivity analysis is performed and presented below for the proposed leak location algorithm to confirm its robustness and applicable range.

4.3.3 Sensitivity analysis for the three resonant responses-based leak location algorithm

A sensitivity analysis is now performed to assess the robustness and the applicable range of the proposed three resonant responses-based leak location

technique. The sensitivity analysis is based on the analysis of the total differential of x_L^*, which is presented as dx_L^*, with respect to all the dependent variables, which are the measured three resonant responses $|h|_1$, $|h|_3$ and $|h|_5$. By normalizing the total differential dx_L^* by x_L^*, the relationship between the fractional change in x_L^* (which is dx_L^*/x_L^*) and the fractional change in each dependent variable (which are $d|h|_1/|h|_1$, $d|h|_3/|h|_3$ and $d|h|_5/|h|_5$) can be obtained. The coefficient before the fractional change of a variable represents the degree of influence of this variable on the estimated x_L^*. The smaller the absolute value of the coefficient, the less sensitive the estimated x_L^* is to the corresponding dependent variable. The procedure for the total differential-based sensitivity analysis is detailed below.

Using Eq. (4.10), the total differential of x_L^* with respect to $|h|_1$, $|h|_3$ and $|h|_5$ can be obtained as presented in Eq. (4.14):

$$\frac{dx_L^*}{x_L^*} = C_1 \frac{d|h|_1}{|h|_1} + C_3 \frac{d|h|_3}{|h|_3} + C_5 \frac{d|h|_5}{|h|_5} \tag{4.14}$$

where the three coefficients before $d|h|_1/|h|_1$, $d|h|_3/|h|_3$ and $d|h|_5/|h|_5$ are

$$\begin{aligned} C_1 &= -\frac{2\cos(2\pi x_L^*)+1}{4\pi x_L^* \sin(2\pi x_L^*)} \frac{|h|_1 \left(|h|_5 - |h|_3\right)}{\left(|h|_3 - |h|_1\right)\left(|h|_5 - |h|_1\right)} \\ C_3 &= \frac{2\cos(2\pi x_L^*)+1}{4\pi x_L^* \sin(2\pi x_L^*)} \frac{|h|_1}{\left(|h|_3 - |h|_1\right)} \\ C_5 &= -\frac{2\cos(2\pi x_L^*)+1}{4\pi x_L^* \sin(2\pi x_L^*)} \frac{|h|_1}{\left(|h|_5 - |h|_1\right)} \end{aligned} \tag{4.15}$$

It can be seen from Eqs (4.14) and (4.15) that, for any leak position, if the fractional changes (relative errors) in the first three peak values are the same ($d|h|_1/|h|_1 = d|h|_3/|h|_3 = d|h|_5/|h|_5$), theoretically the estimation of x_L^* is free of error ($dx_L^*/x_L^* = 0$), because the summation of the three coefficients is zero

($C_1 + C_3 + C_5 = 0$). This indicates that theoretically steady friction does not have any effects on the proposed leak location technique, because steady friction only introduces uniform reduction on the overall magnitude of the resonant response (Lee et al. 2005b).

In practice, however, due to the effects of frequency-dependent behavior, the fractional changes in the first three peak values are usually different. Therefore, it is necessary to analyze the behavior of the three coefficients in detail. When the value of x_L^* is close to 0, 0.5 or 1, the coefficients C_1, C_3 and C_5 can be much greater than unity, as shown in Eq. (4.15). This indicates that the estimation of x_L^* from Eq. (4.11) is very sensitive to variations in the peak values for these cases. As a result, when the dimensionless leak location x_L^* is close to 0, 0.5 or 1, the proposed leak location algorithm is unstable and not applicable.

For other leak positions, the values of the three coefficients in Eq. (4.14) vary. To study the dependence of the three coefficients on the location of the leak x_L^*, a dimensionless analysis is performed. Dividing the resonant response $|h_{odd}|$ shown in Eq. (4.5) [or Eq. (4.7)] by $(2\Delta H_{V0}\Delta\tau/\tau_0)$ (or $\hat{q}Z_V$), the resonant response can be nondimensionalized to $|h_{odd}|^*$, and the result is shown as

$$|h_{odd}|^* = \frac{1}{1+\frac{Z_V}{2Z_L}\left[1-\cos\left(\pi x_L^* \omega_r^{odd}\right)\right]} \tag{4.16}$$

Figure 4.2 is obtained from Eq. (4.16), which shows how the dimensionless peak values of the first three resonant responses change when x_L^* varies from 0 to 1. The value of Z_V / Z_L is fixed to unity, which means that the impedance of the leak is the same as the impedance of the valve in the steady state. Note that the value of Z_V / Z_L can change the absolute magnitude of the FRD, but the order of the peaks remains unaffected (Lee et al. 2005a). The effects of

Z_V / Z_L on the values of the three coefficients (C_1, C_3 and C_5) is discussed later in this section.

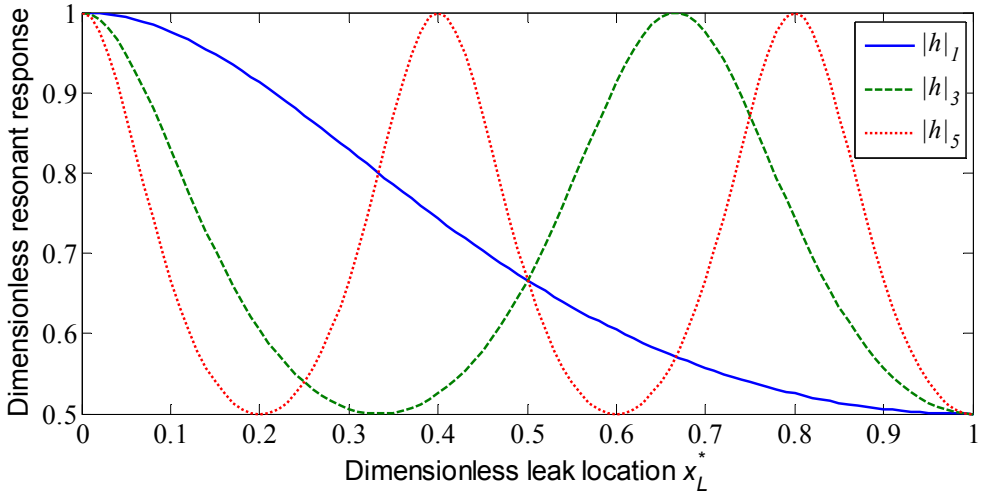

Figure 4.2 Impact of the dimensionless leak location x_L^* on the dimensionless peak values of the first three resonant responses, with $Z_V / Z_L = 1$

The changing patterns of the dimensionless peak values shown in Figure 4.2 are consistent with the curves shown in Figure 8 in Lee et al. (2005a), which are dimensional rather than dimensionless. As shown in Figure 4.2, the peak values are observed to intersect at five leak positions along the pipeline, dividing the pipeline into six unequal sections. Within each section, the order of the three peaks, i.e. the peak-ranking sequence, is unique. Lee et al (2005a) developed a *resonance peak-sequencing method* for locating a leak within a particular section using the rank of the measured first three resonant responses. In the current research, the rank of the first two resonant responses is used to eliminate the alias from the two possible leak locations estimated by the proposed three resonant responses-based leak location algorithm [Eq. (4.11)]. When $|h|_1 > |h|_3$, the leak is located within the range of $x_L^* \in (0, 0.5)$; while when $|h|_1 < |h|_3$, the leak is located within $x_L^* \in (0.5, 1)$.

The values of the coefficients C_1, C_3 and C_5 can then be estimated from Figure 4.2 for various leak positions, and the results are shown in Figure 4.3.

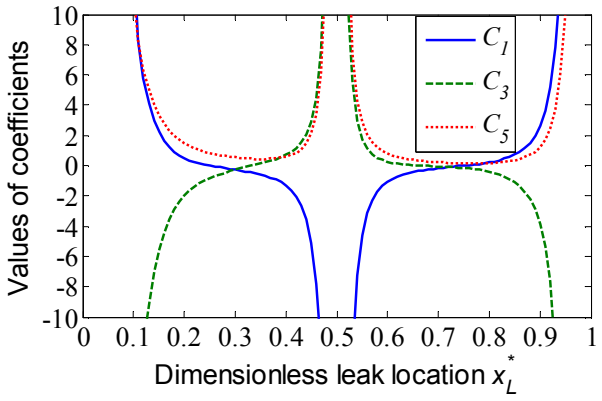

Figure 4.3 Impact of the dimensionless leak location x_L^* on the three coefficients C_1, C_3 and C_5 in Eq. (4.14), with $Z_V / Z_L = 1$

As seen in Figure 4.3 and as expected, for three x_L^* ranges [0, 0.1], [0.45, 0.55] and [0.9, 1], the values of the three coefficients C_1, C_3 and C_5 are very large (values exceeding ± 10 are not displayed). This confirms the previous statement that the leak cannot be detected when it is located near $x_L^* = 0$, 0.5, or 1. In contrast, for leak position ranges $x_L^* \in [0.1, 0.45]$ and $x_L^* \in [0.55, 0.9]$, most values for the three coefficients are within [-1, 1]. As a result, the proposed leak location algorithm is applicable within these two ranges.

The above numerical analysis also illustrates that the proposed leak location algorithm is tolerant of measurement errors. In real applications the measurement errors in the three peak values ($d|h|_1/|h|_1$, $d|h|_3/|h|_3$ and $d|h|_5/|h|_5$) usually share the same sign. For example, unsteady friction introduces reduction to all the resonant peak values, although non-uniform. However, from Figure 4.3, the values of C_1, C_3 and C_5 for any x_L^* are always a mixture of positive and negative values. According to Eq. (4.14), the final result of dx_L^* / x_L^* can be smaller than the summation of the measurement errors in the three peak values ($d|h|_1/|h|_1 + d|h|_3/|h|_3 + d|h|_5/|h|_5$), which indicates the fact that part of the effects of the error in the measured peak

values can be cancelled out through the transfer process to the error in the estimated leak location.

From additional numerical testing, increasing Z_V / Z_L increases the robustness of the new leak location algorithm [Eq. (4.11)]. Although the value of Z_V / Z_L does not affect the order of the peaks, it exerts an influence on the magnitude of the resonant responses and the values of the three coefficients. When the value of Z_V / Z_L increases from 1, the difference between $|h|_1$, $|h|_3$ and $|h|_5$ increases and the values of C_1, C_3 and C_5 decrease correspondingly. In practice, the increase of Z_V / Z_L can be achieved by reducing the opening of the in-line valve. The value of Z_V will be increased accordingly, while the value of Z_L is constant when the effects of friction are ignored, and it will not change significantly even when friction is included.

In summary, the proposed three resonant responses-based leak location technique for the *RPV-High Loss Valve* system is applicable when the leak is located within $x_L^* \in [0.1, 0.45]$ or $x_L^* \in [0.55, 0.9]$. To assure the robustness of the algorithm, the opening of the in-line valve is suggested to be small to yield a large value of Z_V / Z_L.

4.4 Leak detection for *RPV-Closed Valve* systems

A leak detection technique is developed for *RPV-Closed Valve* systems, which is a special case of *RPV-High Loss Valve* systems when the opening of the valve is extremely small. The frequency response equation for an *RPV-Closed Valve* system is given in Eq. (4.8). Compared with Eq. (4.7) for an *RPV-High Loss Valve* system, the impedance of the valve Z_V is not included on the right hand side of Eq. (4.8). The unknowns can be regarded as $\hat{q}Z_L$ and x_L^*, so that only two equations are required to solve these two unknowns from the measured resonant responses. The requirement for the signal bandwidth is

further reduced, as only the second resonant frequency needs to be covered. Details about the two resonant responses-based leak location and size estimation procedures for *RPV-Closed Valve* systems are given below.

4.4.1 Determination of the leak location for RPV-Closed Valve systems

As a special case of RPV systems, a single leak in a pipeline with the RPV-Closed Valve boundary condition can be detected from the magnitude of the first two resonant responses. Using Eq. (4.8) and substituting ω_r^{odd} with 1 and 3, the peak values of the first two resonant responses can be obtained as $|h|_1$ and $|h|_3$. Dividing $|h|_1$ by $|h|_3$, the unknown $\hat{q}Z_L$ can be eliminated, yielding an equation with a single unknown x_L^*, as shown in the equation below:

$$\frac{|h|_1}{|h|_3} = \left[2\cos(\pi x_L^*) + 1\right]^2 \tag{4.17}$$

Solving the above equation for x_L^* yields

$$x_L^* = \frac{1}{\pi} arc\cos\left[\frac{1}{2}\left(\pm\sqrt{\frac{|h|_1}{|h|_3}} - 1\right)\right] \tag{4.18}$$

According to Eq. (4.18), if $|h|_1 > |h|_3$, only one x_L^* can be obtained and it is within the range $x_L^* \in (0, 0.5)$. However, if $|h|_1 < |h|_3$, two x_L^* values may be obtained, but one of them is an alias. The two possible leak locations are both within the range $x_L^* \in (0.5, 1)$, so that the alias cannot be identified solely by using the rank of the first two resonant responses. The *resonance peak-sequencing method* would be helpful, but it requires the measurement of the third resonant response.

Notably, the three resonant responses-based leak location algorithm given in Eq. (4.11) for *RPV-High Loss Valve* systems is also applicable for *RPV-Closed Valve* systems, as the *RPV-Closed Valve* condition is a special case of the *RPV-High Loss Valve* condition when the impedance of the in-line valve is infinite or extremely high. One benefit of using three resonant responses is that the aliased leak location can be distinguished. On the other hand, a disadvantage is that it requires the input signal to have a wider bandwidth to cover the third resonant frequency.

4.4.2 Determination of the leak size for RPV-Closed Valve systems

To estimate the size of a leak, the impedance of the leak Z_L needs to be known. Once the location of the leak is estimated, the value of $\hat{q}Z_L$ can be estimated using either $|h|_1$ or $|h|_3$. Then, the value of the discharge perturbation $\hat{q}$ must be known to estimate the value of Z_L. Finally, using the value of Z_L and the orifice equation [Eq. (4.12)], the lumped leak parameter $C_{Ld}A_L$ can be estimated.

The value of $\hat{q}$ can be estimated from the measured pressure deviation resulting from the movement of the side-discharge valve, which is defined as the *input flow perturbation* in Lee et al. (2006). The input flow perturbation is related to the head perturbation during the generation of the transient by the Joukowsky formula. In the case where the side-discharge valve is located adjacent to a closed boundary with the valve perturbing in a pulse-like fashion, $\hat{q}$ can be estimated as $\hat{q} = -(gA/a)\Delta H$, where ΔH is the head perturbation from the mean state at the generation point.

4.4.3 Sensitivity analysis for the two resonant responses-based leak location algorithm

To study the robustness of the two resonant responses-based leak location algorithm, as given in Eq. (4.18), a sensitivity analysis is performed. The total differential dx_L^* is derived from Eq. (4.17) and then normalized by x_L^*, which is shown as

$$\frac{dx_L^*}{x_L^*} = C_1' \frac{d|h|_1}{|h|_1} + C_3' \frac{d|h|_3}{|h|_3} \tag{4.19}$$

where

$$\begin{aligned} C_1' &= -\frac{2\cos(\pi x_L^*)+1}{4\pi x_L^* \sin(\pi x_L^*)} \\ C_3' &= \frac{2\cos(\pi x_L^*)+1}{4\pi x_L^* \sin(\pi x_L^*)} \end{aligned} \tag{4.20}$$

It can be seen from Eq. (4.20) that the values of the two coefficients C_1' and C_3' are independent of the magnitude of the resonant responses, but rather depending only on the dimensionless leak location x_L^*. The plots for C_1' and C_3' are given in Figure 4.4.

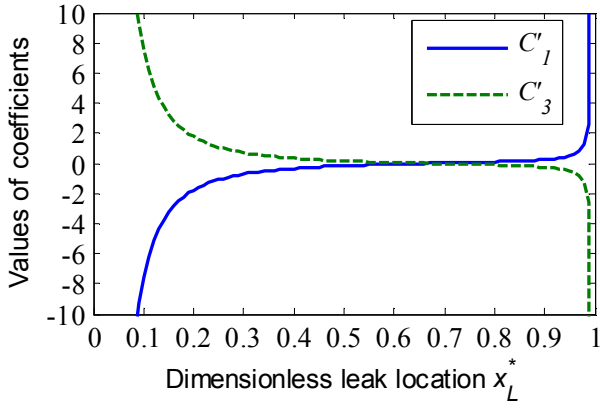

Figure 4.4 Impact of the dimensionless leak location x_L^* on the two coefficients C_1' and C_3' in Eq. (4.19)

The values of C_1' and C_3' represent the sensitivity of the estimated x_L^* to the measured resonant responses $|h|_1$ and $|h|_3$ for various leak positions. Most values of C_1' and C_3' are within the range of [-1, 1] when the leak location range is within [0.2, 0.95]. Therefore, the two resonant responses-based leak location algorithm is stable and applicable when the leak is located within $x_L^* \in [0.2, 0.95]$.

Similar to the leak location algorithm using three resonant responses, the two resonant responses-based leak location algorithm is also tolerant of measurement errors, as the values of C_1' and C_3' are the same in the absolute value but always opposite in sign. According to Eq. (4.19), part of the effects of the frictional variations (relative errors) in $|h|_1$ and $|h|_3$ can be cancelled out if they share the same sign, which is usually the case in real applications. However, two possible leak locations may be obtained from Eq. (4.18) for a pair of $|h|_1$ and $|h|_3$.

The values of C_1' and C_3' for the two resonant response-based algorithm shown in Figure 4.4 are small around x_L^* = 0.5, which indicates that the leak location can be estimated even if it is located at or around the middle of the

pipeline. However, if the actual leak location is x_L^* = 0.5, an alias x_L^* = 1 will exist. It cannot be removed because for both x_L^* = 0.5 and 1, all the resonant responses are the same, i.e. $|h|_1 = |h|_3 = |h|_5$.

In summary, the two resonant responses-based leak location algorithm is applicable to *RPV-Closed Valve* systems when the leak is located within $x_L^* \in [0.2, 0.95]$, however, if $x_L^* \geq 0.5$, two possible leak locations can be estimated and the alias is hard to be distinguished.

4.5 Numerical verification

Numerical simulations are performed to verify the proposed three resonant responses-based leak location [Eq. (4.11)] and size estimation [Eq. (4.13)] techniques for RPV-High Loss Valve systems. The transfer matrix method is used for the numerical modeling and unsteady friction is included.

The two resonant responses-based leak location [Eq. (4.18)] and size estimation techniques for *RPV-Closed Valve* systems are not modeled or discussed in this section, because: the *RPV-Closed Valve* condition is just a special case of the *RPV-High Loss Valve* condition; the two resonant responses-based leak location technique has difficulty in distinguishing the aliased leak location; the leak size estimation procedure for *RPV-Closed Valve* systems is complicated; and the three resonant responses-based leak location technique is still applicable for systems with the *RPV-Closed Valve* boundary condition. However, both the three and the two resonant responses-based leak location techniques are applied to the interpretation of an experimental FRD, as presented later in the *experimental verification* section in this paper.

4.5.1 Unsteady friction model

Unsteady friction is included in the numerical simulations performed in this section. Compared with frictionless pipeline models or models with steady friction only, the behavior of the numerical model with unsteady friction is

closer to that of real pipelines, thus yielding a better estimation of the validity of the proposed leak detection technique.

The unsteady friction model used in this research is adopted from Vítkovský et al. (2003a). Vítkovský et al. (2003a) derived the frequency-domain expression for the unsteady friction component (R_{us}) of the resistance term using the Zielke (1968) unsteady friction model and the Vardy and Brown (1996) weighting function for smooth-pipe turbulent flow, which is given below as

$$R_{us} = \frac{2j\omega}{gA}\left(\frac{1}{C} + \frac{j\omega D^2}{4\nu}\right)^{-1/2} \tag{4.21}$$

where ν is the kinematic viscosity and C is the shear decay coefficient, which depends on the Reynolds number of the mean flow and is given by $C = 7.41/\mathbf{Re}^{\kappa}$ and $\kappa = \log_{10}\left(14.3/\mathbf{Re}^{0.05}\right)$.

The summation of the unsteady friction component R_{us} and the steady friction component R_s composes the linearized resistance term R in Eq. (4.1). Together with the matrix for a leak Eq. (4.3) and the matrix for an oscillating valve Eq. (4.4), the governing equation for the resonant response at the upstream face of the valve can be derived. The numerical studies described in the following subsections are based on this numerical pipeline model.

Pipeline models with steady friction only are not considered in the numerical study. Steady friction is not dependent on frequency and only yields a uniform reduction on the overall magnitude of the frequency response. According to the sensitivity analysis shown in Eq. (4.14), the uniform distortion due to steady friction does not have any effects on the accuracy of the estimated leak location.

4.5.2 Case study

A case study is performed on a pipeline with a leak located at x_L^* = 0.2, where the unsteady friction model described in the previous subsection is used. The system layout is given in Figure 4.1. The in-line valve is used to generate the transient, and it is assumed to have a small opening in the steady state and connected to the atmosphere at the downstream side. The parameters used for the numerical simulations are listed in Table 4.1 below.

Table 4.1 System parameters for the numerical simulations

Parameter	Value
H_r	30 m
Q_{V0}	0.0034 m^3/s
L	2000 m
D	0.3 m
a	1200 m/s
f	0.02
$\Delta\tau/\tau_0$	0.05
$C_{Ld}A_L$	1.41×10^{-4} m^2

The frequency response diagrams (FRDs) for the case study (x_L^* = 0.2) are obtained numerically using the transfer matrix method. The results are presented in Figure 4.5, where the FRD in the solid line is for the pipeline with the system parameters shown in Table 4.1 and with unsteady friction (Vítkovský et al. 2003a); the FRD in the dotted line is for the same pipeline but under a frictionless assumption. The FRDs in Figure 4.5 are nondimensionalized, where the *y*-axis represents the dimensionless head response that is nondimensionalized by dividing the dimensional resonant response by the active input $\left(2\Delta H_{V0}\Delta\tau/\tau_0\right)$, and the *x*-axis denotes the relative angular frequency $\omega_r = \omega/\omega_{th}$.

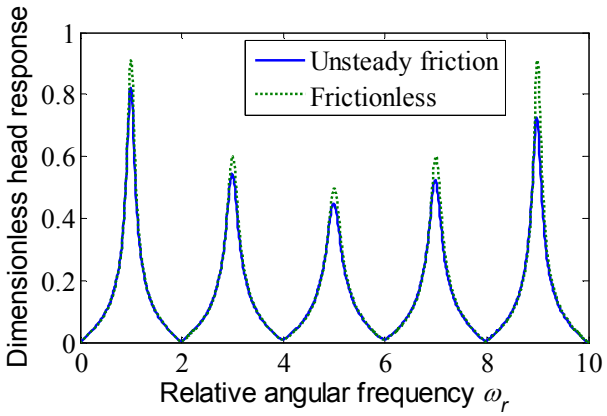

Figure 4.5 Numerical FRDs for the case study $x_L^* = 0.2$

From Figure 4.5, the dimensionless peak values for the first three resonant responses are $|h|_1 = 0.912$, $|h|_3 = 0.601$ and $|h|_5 = 0.496$ for the frictionless simulation (the dotted line), and $|h|_1^{us} = 0.821$, $|h|_3^{us} = 0.542$ and $|h|_5^{us} = 0.446$ for the simulation with unsteady friction (the solid line). Using Eq. (4.11) and $|h|_1^{us}$, $|h|_3^{us}$ and $|h|_5^{us}$, the possible dimensionless leak locations are estimated as $\left(x_L^*\right)^{us} = 0.199$ or $\left(x_L^*\right)^{us} = 0.801$. Then using the rank of the first two resonant response $|h|_1^{us} > |h|_3^{us}$, it is concluded that the leak should be within the range of (0, 0.5). Therefore, the leak is confirmed to be located at $\left(x_L^*\right)^{us} = 0.199$.

Compared with the actual leak location $x_L^* = 0.2$ m, $\left(x_L^*\right)^{us}$ is accurate as it only has a relative deviation of $\left[\left(x_L^*\right)^{us} - x_L^*\right] / x_L^* \times 100\,\%$ = -0.5 %. This deviation is much smaller than the deviation between the numerical peak values for the unsteady friction model ($|h|_1^{us}$, $|h|_3^{us}$ and $|h|_5^{us}$) and the results for the frictionless model ($|h|_1$, $|h|_3$ and $|h|_5$). In addition, the value of dx_L^*/x_L^* is calculated as -0.2 % using the estimated $\left(x_L^*\right)^{us}$, which is consistent with the result of Eq. (4.14) when the numerical peak values are substituted.

The impedance of the in-line valve is calculated as $Z_V = 1.78\times10^4$ s/m^2 from the steady-state analysis of the pipeline system shown in Table 4.1. The impedance of the leak is then estimated from Eq. (4.13) using the numerical results for the simulation with unsteady friction [$\left(x_L^*\right)^{us}$, $|h|_1^{us}$, $|h|_3^{us}$ and $|h|_5^{us}$] and it is $Z_L = 1.75\times10^4$ s/m^2. Using Z_L and assuming that the steady-state head at the leak H_L is the same as the reservoir head H_r, finally the lumped leak parameter can be estimated from Eq. (4.12) and it is $\left(C_{Ld}A_L\right)^{us} = 1.42\times10^{-4}$ m^2. Compared with the theoretical leak size given in Table 4.1, the estimation is accurate.

The above numerical case study with $x_L^* = 0.2$ and incorporating unsteady friction shows that the leak location and size are estimated accurately using the proposed three resonant responses-based leak detection technique. To study the behavior of the proposed leak detection technique for other leak positions, additional numerical testing is performed and reported in the following subsection.

4.5.3 Simulations for various leak locations

Numerical simulations are performed on pipelines with the dimensionless leak location x_L^* varying from 0.01 to 0.99, with a step of 0.01 each. The system parameters used in these simulations are the same as those given in Table 4.1. Unsteady friction is included in all the numerical simulations.

The relative deviation between the estimated leak location and the corresponding actual leak location is estimated for each simulation. Meanwhile, for each of the estimated leak size, the relative deviation from the actual leak size is also estimated. The relative deviation for the estimated leak size is defined as $\left[\left(C_{Ld}A_L\right)^{us} - C_{Ld}A_L\right] \Big/ C_{Ld}A_L \times 100\,\%$. The curves of the relative deviation for the estimated leak location and the estimated leak size are given in Figure 4.6.

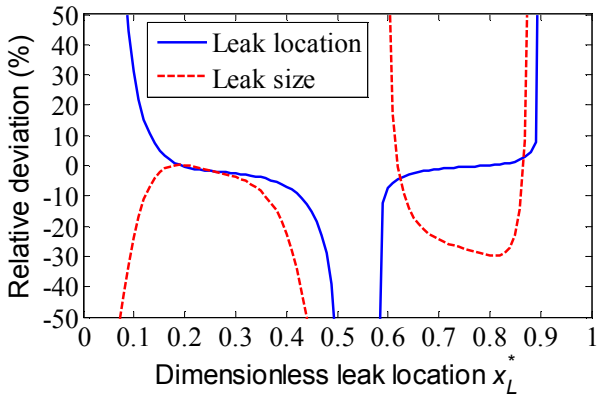

Figure 4.6 The relative deviation between the estimated leak location and the actual leak location (solid lines), and the relative deviation between the estimated leak size and the actual leak size (dashed lines)

The curves presented in Figure 4.6 are not continuous. One reason for the discontinuity is that the data out of the bounds of the *y*-axis are not shown, and another reason is that the leak location algorithm Eq. (4.11) and/or the leak impedance estimation algorithm Eq. (4.13) are not applicable mathematically when the leak is located at some specific positions. It can be seen from Figure 4.6 that when the leak is actually located within $x_L^* \in [0.15, 0.4]$ or $x_L^* \in [0.6, 0.9]$, the accuracy of the estimated leak location $\left(x_L^*\right)^{us}$ is acceptable (within $\pm 5\%$). In contrast, the estimated leak size is less accurate, as expected, and underestimated most times.

The numerical simulations indicate that the proposed three resonant responses leak location algorithm is applicable for pipelines with unsteady friction. The relative deviations of the estimated leak locations (solid lines in Figure 4.6) are consistent with the results of Eq. (4.14) in the sensitivity analysis. However, compared with the theoretical applicable ranges $x_L^* \in [0.1, 0.45]$ and $x_L^* \in [0.55, 0.9]$ for frictionless pipes given in the sensitivity analysis, when the effects of unsteady friction are considered, the applicable ranges is slightly reduced to $x_L^* \in [0.15, 0.4]$ and $x_L^* \in [0.6, 0.9]$. The estimation of the leak size is less accurate, and it is usually underestimated compared with the actual leak

size. The proposed leak detection technique is further verified using an experimentally determined FRD in the following section.

4.6 Experimental verification

The proposed three and two resonant responses-based leak location techniques are verified using an experimentally determined FRD. The laboratory experiments were conducted by Lee et al. (2006) in the Robin Hydraulics Laboratory at the University of Adelaide. The methods for extracting the FRD of a real pipeline have been discussed in detail in Lee et al. (2006). The system configuration and experimental data presented in Lee et al. (2006) are also described briefly in the subsection below.

4.6.1 System configuration and experimental data

The experimental pipeline was a copper pipeline in a tank-pipeline-(in-line) valve configuration. The length of the pipe is L = 37.53 m and the internal diameter is D = 0.022 m. The in-line valve is fully closed, so the pipeline system had a *RPV-Closed Valve* boundary condition. The upstream water tank is pressurized by air and the steady-state pressure head is H_r = 38.09 m. The wave speed in the experimental pipeline was a = 1328 m/s determined by experiment. A side-discharge valve was located at the upstream face of the closed in-line valve to generate the transient excitation (a pulse signal). A free discharging orifice with a diameter of 1.5 mm ($C_{Ld}A_L = 1.6\times10^{-6}$ m^2) was located at 28.14 m downstream from the reservoir to simulate the leak, thus the actual dimensionless leak location was $x_L^* = 0.75$.

The experimentally determined FRD was presented as Figure 17 in Lee et al. (2006). The peak values for the first resonant responses are estimated as $\left|h\right|_1^{lab} = 3.05\times10^6$ m^{-2}s, $\left|h\right|_3^{lab} = 7.75\times10^6$ m^{-2}s and $\left|h\right|_5^{lab} = 5.35\times10^6$ m^{-2}s from the experimental FRD. They represent the head response per unit discharge input [i.e. $\hat{q}$ = 1 m^3/s in Eq. (4.8)].

4.6.2 Leak location using the three resonant responses-based technique

Using the three resonant responses-based leak location technique given in Eq. (4.11), the dimensionless leak location is estimated as $\left(x_L^*\right)^{lab}$ = 0.27 or 0.73. The rank of the peak values of the first two resonant responses is $|h|_1^{lab} < |h|_3^{lab}$, so that the leak should be within a dimensionless range of $(0.5, 1)$. As a result, $\left(x_L^*\right)^{lab}$ = 0.73 is adopted. Compared with the actual dimensionless leak location x_L^*, the absolute error in the estimated x_L^* is $\left(x_L^*\right)^{lab} - x_L^*$ = - 0.02, and the relative error is $\left[\left(x_L^*\right)^{lab} - x_L^*\right] \Big/ x_L^* \times 100\ \%$ = -2.7 %. The size of the leak is not estimated, because the proposed leak size estimation formula [Eq. (4.13)] is not applicable to the experimental pipeline with the *RPV-Closed Valve* boundary condition.

4.6.3 Leak location and size estimation using the two resonant responses-based technique

For the two resonant responses-based leak location technique, Eq. (4.18) is used. The dimensionless location of the leak is estimated as $\left(x_L^*\right)^{lab}$ = 0.56 or 0.80. The alias cannot be removed. For the estimation $\left(x_L^*\right)^{lab}$ = 0.80 which is closer to the actual location, it is less accurate than the estimation derived from the three responses-based leak location technique.

To determine the size of the leak, the impedance of the leak is determined first. It is estimated as $Z_L = 2.53 \times 10^6$ s/m^2 by substituting the first resonant response $|h|_1^{lab} = 3.05 \times 10^6$ m^{-2}s and the unit discharge perturbation $\hat{q}$ = 1 m^3/s into Eq. (4.8). Then, under the assumption that the steady-state head at the leak is the same as the steady-state head at the reservoir ($H_{L0} = H_r = 38.09$ m), the steady-state flow at the leak is estimated as $Q_{L0} = 3.01 \times 10^{-5}$ m^3/s.

Finally, the lumped leak size is estimated as $\left(C_{Ld}A_L\right)^{lab} = 1.1\times10^{-6}$ m^2 using the orifice equation Eq. (4.12). Compared with the theoretical leak size ($C_{Ld}A_L = 1.6\times10^{-6}$ m^2), the estimated size is significantly smaller.

4.6.4 Summary of experimental verification

The experimental verification illustrates that the proposed leak detection technique is applicable to pipelines in controlled laboratory conditions. The location of the leak is estimated successfully using either the three or the two resonant responses-based algorithm. The leak location estimated from the three resonant responses-based algorithm is accurate, with an absolute error of 2 % of the total pipe length. However, the two resonant responses-based algorithm yields less accuracy. The size of the leak is estimated from the two resonant responses-based algorithm, but the estimated leak size is smaller than the theoretical value.

The error in the estimates comes from the distortion in the experimentally determined FRD, which in turn may be mainly sourced from the effects of frequency-dependent behavior in the experimental pipeline, such as unsteady friction. For pipelines with longer length in the field, the fundamental frequency is usually significantly lower and the effects of unsteady friction on the first three resonant responses will be relatively small. As a result, it is expected that the proposed leak location technique is also applicable in field applications.

4.7 Challenges in field applications

The proposed leak detection technique has been verified by numerical studies and controlled laboratory experiments; however, some challenges may exist for application of the proposed methodology in the field. The proposed technique is designed for the detection of a single leak in a single pipeline, while in the field, complex pipeline networks and multiple leaks may exist.

Lee et al. (2005a) have studied how to extract the FRD for a branched pipe network. By closing the valve at one end of the pipe section, an individual pipeline can be partially separated from the network. A side-discharge valve located adjacent to the closed valve is then used to generate a transient pulse, and a pressure transducer located at the same location as the generator is used to measure the transient pressure trace. By assuming that a reservoir exists at the open boundary, and using signal processing, the FRD of the specified pipe section can be obtained (Lee et al. 2005a).

When multiple leaks exist in a single pipeline, three resonant responses are not sufficient to be able to determine the location of all the leaks. In this case, more resonant responses need to be measured and further investigation is required. Nevertheless, using the first three resonant responses, the method proposed in this paper can determine whether the pipe is leaking or not.

Another challenge in the application of the newly proposed method is that the shape of the leak may have some impact on the accuracy of the detection. In the numerical study and the experimental verification presented in this paper, a leak is simulated by an orifice with a circular opening. If the leak has a different shape, Eq. (4.12) as used in this paper cannot accurately describe the relationship between the head and the flow through the leak. As a result, the estimation of the size of the leak will be in error. However, theoretically the relative size of the first three resonant responses will not be affected, so that the location of the leak can still be determined accurately. More experiments are necessary to study the effects of the shape of a leak.

4.8 Conclusions

A novel frequency response diagram (FRD)-based leak location and size estimation technique is proposed in this research. It is suitable for detecting of a single leak in single pipelines with a reservoir-pipeline-valve (RPV) configuration. Instead of using the sinusoidal leak-induced patterns on the FRD as in traditional techniques, the new technique only uses the magnitude of the first three resonant responses.

A RPV-high loss valve configuration is suggested for the extraction of the FRD. A side-discharge valve is used to generate an impulse transient excitation, which is located at the upstream face of a high loss in-line valve at the end of the pipe. A pressure transducer is located at the same location as the side-discharge valve to measure the transient pressure. The opening of the in-line valve should be small enough to make the leak-induced distortion obvious in the first three harmonics. In practice, this can be achieved by trial-and-error. In addition to the measured transient pressure, the steady-steady head and flow at the in-line valve, the head at the reservoir, the length and internal diameter of the pipe, and the wave speed in the pipe need to be known.

The requirement for the bandwidth of the transient excitation is reduced to five times of the fundamental frequency of the pipeline under test, because only the first three resonant responses are used. In addition, the distortion in the measured FRD due to unsteady friction does not need to be corrected before applying the leak detection algorithm, because the effects of unsteady friction is not significant for the first three resonant responses, and part of the effects are cancelled out through the calculation for leak location. Moreover, only the relative sizes of the first three resonant responses are required, rather than the absolute values of the frequency response. This is a great advantage, as it can simplify the procedure for determining the FRD and avoids error introduced through intermediate calculations. For example, the voltage output from a pressure transducer can be used in the calculation directly, avoiding the transfer from voltage data to pressure data.

When the in-line valve at the end of the pipeline is fully closed, the requirement for the number of resonant responses can be reduced to two. However, two possible leak locations may be obtained from a specific FRD, and the alias is hard to remove.

Numerical simulations with unsteady friction performed in this research show that the three resonant responses-based leak location technique is applicable when the actual leak is located within the dimensionless range of

$x_L^* \in [0.15, 0.4]$ or $[0.6, 0.9]$. Within the applicable ranges, the relative deviation between the estimated leak location and the actual location is within ± 5 %. However, the estimated size of the leak is less accurate, and shown to be underestimated most times.

The proposed leak detection technique is also verified using an experimentally determined FRD. The experimental verification indicates that the proposed technique is applicable to real pipelines in controlled laboratory condition, even though the pipeline is short and the effects of unsteady friction is relatively high. The three resonant responses-based technique performs better than the two resonant responses-based technique. For pipelines with longer length in the field, the fundamental frequency of the pipeline is much lower and the effects of unsteady friction on the first three resonant responses will be relatively small. It is expected that the proposed three resonant responses-based technique leak detection technique is also applicable in field applications, provided the first three resonant responses can be measured successfully.

Acknowledgements

The research presented in this paper has been supported by the Australia Research Council through the Discovery Project Grant DP1095270. The first author thanks the Chinese Scholarship Council and the University of Adelaide for providing a joint postgraduate scholarship.

Notations

The following symbols are used in this paper:

A = inside pipe cross sectional area;
a = wave speed;
A_L = area of a leak orifice;
C = shear decay coefficient;

C_1, C_3, C_5 = coefficients used in Eq. (4.14);

C_1', C_3' = coefficients used in Eq. (4.19);

C_{Ld} = coefficient of discharge for a leak orifice;

D = internal pipe diameter;

f = Darcy-Weisbach friction factor;

g = gravitational acceleration;

H_0 = steady-state head;

H_r = reservoir head;

H_{L0} = steady-state head at a leak orifice;

h = complex head amplitude;

$|h_{odd}|$ = amplitude of head fluctuation at the odd harmonics;

$|h|_1$, $|h|_3$, $|h|_5$ = amplitude of the head oscillation at the first, the third and the fifth harmonics;

j = imaginary unit, $\sqrt{-1}$;

L = total length of pipe;

L_1, L_2 = lengths of the two pipe sections divided by a leak;

P_L = left part of Eq. (4.10);

Q_0 = steady-state discharge;

Q_{L0} = steady-state flow out of a leak;

Q_{V0} = steady-state flow through a valve;

q = complex discharge amplitude;

$\hat{q}$ = discharge perturbation;

R = linearised resistance term;

$\mathbf{R_e}$ = Reynolds number;

R_s, R_{us} resistance factor components for steady friction and unsteady friction;

x_L^* = dimensionless position of a leak;

Z_C = characteristic impedance of a frictionless pipe;

Z_L = hydraulic impedance of a leak orifice;

Z_P = the characteristic impedance of a pipe;

Z_V = hydraulic impedance of a steady-state valve;

Superscripts:

* = dimensionless values;

^{lab} sourced from laboratory experiments;

^{n}, $^{n+1}$ the upstream and the downstream position of a pipe;

^{us} effects of unsteady friction are included;

Greek symbols:

ΔH = head perturbation from the mean state at the generation point;

ΔH_{V0} = steady-state head loss across a valve;

$\Delta\tau$ = amplitude of the dimensionless valve-opening oscillation;

κ = coefficient in Eq. (4.21);

μ = propagation operator;

ν = kinematic viscosity;

τ_0 = mean dimensionless valve-opening coefficient, centre of oscillation;

ω, ω_r = angular frequency and dimensionless relative angular frequency;

ω^{odd}, ω_r^{odd} = angular frequency and relative angular frequency for odd harmonics;

ω_{th} = fundamental angular frequency for a reservoir-pipeline-valve system;

Chapter 5

Determination of the Linear Frequency Response of Single Pipelines using Persistent Transient Excitation: a Numerical Investigation (Journal Publication 3)

Gong, J., Simpson, A. R., Lambert, M. F., and Zecchin, A. C.

School of Civil, Environmental and Mining Engineering, the University of Adelaide, Adelaide, SA 5005 Australia

Journal of Hydraulic Research, DOI: 10.1080/00221686.2013.818582 (published online).

Statement of Authorship

Title of Paper	Determination of the Frequency Response Diagram of Single Pipelines using Persistent Transient Excitation: a Numerical Investigation
Publication Status	Accepted for Publication
Publication Details	Gong, J., Simpson, A. R., Lambert, M. F., and Zecchin, A. C. (2013). "Determination of the frequency response diagram of single pipelines using persistent transient excitation: a numerical investigation." *Journal of Hydraulic Research*, DOI: 10.1080/00221686.2013.818582 (published online).

Author Contributions

By signing the Statement of Authorship, each author certifies that their stated contribution to the publication is accurate and that permission is granted for the publication to be included in the candidate's thesis.

Name of Principal Author (Candidate)	Jinzhe Gong		
Contribution to the Paper	Developed and implemented the methodology, designed and conducted numerical simulations, interpreted and analysed results, prepared manuscript and acting as the corresponding author.		
Signature		Date	25/09/2013

Name of Co-Author	Angus Simpson		
Contribution to the Paper	Supervised development of work, helped to evaluate and edit the manuscript.		
Signature		Date	25/9/2013

Name of Co-Author	Martin Lambert		
Contribution to the Paper	Helped to evaluate and edit the manuscript.		
Signature		Date	25/9/13

Name of Co-Author	Aaron Zecchin		
Contribution to the Paper	Helped to evaluate and edit the manuscript.		
Signature		Date	1·10·2013

Abstract

The linear frequency response of a fluid-filled pipeline extracted by fluid transient waves can be used to detect leaks in pipelines. This research conducts numerical analysis on how to accurately determine the linear frequency response diagram (FRD) of single pipelines using persistent transient pressure signals. Two types of persistent signals, the maximum-length binary sequence (MLBS) and the inverse-repeat sequence (IRS), are compared in terms of the accuracy in estimating the linear response of a pipeline at resonant frequencies. The IRS is found to be more appropriate for identifying the linear portion of the FRD of a pipeline, since its antisymmetric property can supress part of the nonlinear response. Numerical simulations are conducted to verify the findings.

5.1 Introduction

The need to test pipelines (water, oil or gas, for example) has resulted in a significant body of research into ways that pipes can be tested without violating the integrity of the system. One promising technique involves using fluid transients injected into the pipeline system and analysing the resulting frequency response diagram (FRD), which is the plot of the frequency response function (FRF) of the system. For any specific pipeline system, the FRD is unique and its characteristics are determined by the properties of the pipeline, including length, friction, boundary conditions and wave speed. The FRD can be used, therefore, to diagnose the condition of the pipeline.

In the last decade, several FRD-based pipeline leak detection techniques (Mpesha et al. 2001; Lee et al. 2005a; Sattar and Chaudhry 2008; Gong et al. 2013e) have been developed. The accuracy of the FRD estimation has become increasingly important, and is especially reliant on information that indicates the system linear dynamics at the fundamental frequency of the pipeline system and corresponding odd harmonics (Lee et al. 2005b; Gong et al. 2013b).

In earlier studies, the sine-stepping technique was commonly used to extract the FRD of a pipeline system. The sine-stepping technique uses single frequency sine oscillatory signals as the input, and this frequency is adjusted to cover the range of frequencies required (Chaudhry 1987). This technique is widely used in numerical modelling with the transfer matrix method to determine the theoretical FRD of a pipeline system (Lee et al. 2005b; Sattar and Chaudhry 2008). However, performing a sine-stepping is undesirable in real world applications. The system needs to be excited at various different frequencies sequentially, and the measurement can only be taken after a steady-oscillatory flow has been established. As a result, to cover a sufficient number of frequencies, the whole procedure for extracting one FRD can take a number of hours. Furthermore, the final FRD is prone to errors, because the

influence of noise can vary throughout independent tests for different frequencies.

An alternative to the sine-stepping technique is to use single step or pulse signals as the excitation, where the FRF can be extracted through a single operation within a few minutes. Mpesha et al. (2002) used a step transient (generated by closing or opening a valve) to excite a single pipeline, and the FRD was obtained by a simple fast Fourier transform of the measured head or discharge. Lee et al. (2003) analysed the limitation of the step transient-based technique, and a few years later, Lee et al. (2006) performed laboratory experiments on pipeline FRD measurement and leak detection using a sharp pulse transient and a correlation-based FRF determination algorithm. A major challenge for the discrete step or pulse excitation is that the bandwidth is usually limited so that the signal-to-noise ratio (SNR) is low for high frequency components. The step or pulse wave is usually not as sharp as desired attributable to the limitation in the manoeuvrability of real signal generation devices (e.g. a side-discharge valve).

One solution to overcome the limitations of the discrete transient excitation while keeping the efficiency of FRD extraction is to use persistent signals as the excitation. Lee et al. (2008a) developed a customised side-discharge valve that can generate persistent maximum-length (pseudo-random) binary sequence (MLBS)-based transient pressure waves into a laboratory pipeline system [referred to as pseudo-random binary sequences (PRBS) in that paper]. The MLBS is a type of wide bandwidth and periodic signal, so that multiple frequency responses of a pipeline can be determined simultaneously and the SNR can be increased by synchronous averaging of the response periods. However, the magnitude of the input signal must be carefully selected and relatively small, since large valve perturbations can lead to significant nonlinear responses (Lee et al. 2002; 2003; 2005a).

In this technical note, studies are conducted on the nonlinear response of a pipeline during transient events, and the selection of persistent transient excitation signals with the aim of minimising the effect of nonlinearities on

the FRD. It is found that another type of PRBS, namely the inverse repeat sequence (IRS), is better than the MLBS in extracting the linear frequency response of a fluid-filled pipeline. Numerical simulations are conducted to compare the MLBS and the IRS in terms of the accuracy in determining the linear frequency response of a pipeline.

5.2 Nonlinearities of a pipeline system and linearisation in FRD-based leak detection techniques

In this research, the nonlinear behaviour of a pipeline system is taken into account in the selection of transient excitation. Similar to most systems, in reality a pipeline system has nonlinearities that will be reflected in the extracted FRD. However, only the linear portion of the frequency response of a pipeline system is desired since all existing FRD-based leak detection techniques are based on linear theory. As a result, the nonlinear response in the FRD will introduce error in the leak detection analysis. The nonlinearities of a pipeline and the linearisation in FRD-based leak detection techniques are analysed in the following sections.

Unsteady pipe flow can be described by the governing equations of continuity and motion (Chaudhry 1987):

$$\frac{\partial Q}{\partial x}+\frac{gA}{a^2}\frac{\partial H}{\partial t}=0 \tag{5.1}$$

$$\frac{\partial H}{\partial x}+\frac{1}{gA}\frac{\partial Q}{\partial t}+\frac{fQ|Q|}{2gDA^2}=0 \tag{5.2}$$

where Q is flow, H is head, g represents gravitational acceleration, A is cross-sectional area of the pipe, a is wave speed, D is pipe diameter, f is the Darcy-Weisbach friction factor, x is distance and t is time. Eq. (5.2) is a nonlinear partial differential equation.

In the time domain, Eqs. (5.1) and (5.2) can be solved by the method of characteristics (MOC). In the MOC, the two partial differential equations are transformed to two ordinary differential equations that hold along characteristic lines, and are described as the MOC compatibility equations (Chaudhry 1987), which retain the nonlinear component associated with friction. The MOC compatibility equations are integrated and solved in a step by step manner in the time domain. Typically a finite-difference technique (e.g. the trapezoidal rule) is used in the integration process, which is sufficiently accurate when the time steps used in solving these equations are small and the friction losses are adequately approximated by a linear variation across a time step along the characteristic lines (Chaudhry 1987; Wylie and Streeter 1993). Although approximation is introduced, the MOC inherits the nonlinear nature from the original governing equation of motion when pipe friction is included.

FRD-based leak detection techniques (Mpesha et al. 2002; Covas et al. 2005; Lee et al. 2005b; Sattar and Chaudhry 2008; Gong et al. 2013e) are based on the analysis of steady-oscillatory flow, where the pipeline system is excited by periodic pressure fluctuations. For the study of steady-oscillatory flow, the linear theory has to be introduced. It is assumed that a pipeline is a linear system, so that the head H and flow Q are linear superposition of a steady component and an oscillatory component, which can be described as

$$Q = Q_0 + \mathrm{Re}(qe^{j\omega t}) \tag{5.3}$$

$$H = H_0 + \mathrm{Re}(he^{j\omega t}) \tag{5.4}$$

where Q_0 and H_0 are the steady components, q and h are the oscillatory components, j represents the imaginary unit, ω denotes the angular frequency and $\mathrm{Re}(\ )$ denotes the real value operator. Substitution of Eqs. (5.3) and (5.4) into Eqs. (5.1) and (5.2) and subsequent linearisation yields

$$\frac{dq}{dx} + \frac{gA\omega j}{a^2} h = 0 \tag{5.5}$$

$$\frac{dh}{dx} + \left(R + \frac{\omega j}{gA} \right) q = 0 \tag{5.6}$$

where R is a linearised resistance term, and it is $fQ_0 / (gDA^2)$ for turbulent flow. Details of the linearisation process can be found in Chaudhry (1987) and Wylie and Streeter (1993). The approximation embedded in the derivation is that q and h are much smaller than Q_0 and H_0.

The linearised equations for oscillatory flow in a pipeline, Eqs. (5.5) and (5.6), can be solved by the transfer matrix method (Chaudhry 1987). When friction is neglected, the solution for a pipe is given as

$$\begin{Bmatrix} q \\ h \end{Bmatrix}^{n+1} = \begin{bmatrix} \cos\left(\frac{L_i \omega}{a} \right) & -j \frac{gA}{a} \sin\left(\frac{L_i \omega}{a} \right) \\ -j \frac{a}{gA} \sin\left(\frac{L_i \omega}{a} \right) & \cos\left(\frac{L_i \omega}{a} \right) \end{bmatrix} \begin{Bmatrix} q \\ h \end{Bmatrix}^{n} \tag{5.7}$$

where the superscripts $n+1$ and n represent positions in the downstream and upstream ends of the section of pipe, respectively, L is the length of the pipe.

In the analysis of FRD-based leak detection techniques, typically a leak is introduced as the target for detection and a valve is used as the transient generator. Approximation and linearisation are necessary in the derivation of the governing equations for them. The orifice equation (Wylie and Streeter 1993) is used to describe the relationship between the head and flow across the leak or valve. For a leak, it is written as

$$Q_{L0} = C_{Ld} A_L \sqrt{2 g H_{L0}} \tag{5.8}$$

where Q_{L0} is leak discharge, C_{Ld} is discharge coefficient for leak, A_L is area of the leak orifice, and H_{L0} is the head at the leak. Linearising Eq. (5.8) gives the transfer matrix solution of a leak (Lee et al. 2002; 2005b):

$$\begin{Bmatrix} q \\ h \end{Bmatrix}^{n+1} = \begin{bmatrix} 1 & -\dfrac{Q_{L0}}{2H_{L0}} \\ 0 & 1 \end{bmatrix} \begin{Bmatrix} q \\ h \end{Bmatrix}^{n} \tag{5.9}$$

When an oscillating valve is used to excite the pipeline in a sine-stepping manner, it is assumed that the oscillating valve satisfies the orifice equation in steady-oscillatory flow condition. After linearization, the transfer matrix for an oscillating valve is given as (Wylie and Streeter 1993; Lee et al. 2005b)

$$\begin{Bmatrix} q \\ h \end{Bmatrix}^{n+1} = \begin{bmatrix} 1 & 0 \\ -\dfrac{2\Delta H_{V0}}{Q_{V0}} & 1 \end{bmatrix} \begin{Bmatrix} q \\ h \end{Bmatrix}^{n} + \begin{Bmatrix} 0 \\ \dfrac{2\Delta H_{V0}\Delta\tau}{\tau_0} \end{Bmatrix} \tag{5.10}$$

where ΔH_{V0} and Q_{V0} are the steady-state head loss across, and the flow through, the valve, the mean dimensionless valve opening size is τ_0 and the magnitude of the dimensionless perturbation in the valve opening is $\Delta\tau$. The assumption embedded within the derivation is that $\Delta\tau$ is much smaller than τ_0.

Lee et al. (2005b) derived the governing equation for the head perturbation at the upstream face of the valve by combining the transfer matrices for all the components in a pipeline system with a leak. Analysis of this governing equation indicated that a leak could introduce a sinusoidal pattern in the resonant response. The period of this sinusoidal leak-induced pattern is related to the location of the leak, and the magnitude of the pattern is governed by the size of the leak. As a result, the FRD of a pipeline system can be used to locate the leak as well as estimate its size.

It is clear that approximation and linearisation are involved throughout the analysis of a leaking pipe by the transfer matrix method. The FRD derived from the transfer matrix method actually represents the linear frequency response of a pipeline system. Lee *et al.* (2002; 2003; 2005a) studied the discrepancy between the frequency response of a pipeline derived from the linear transfer matrix method and that resulted from the nonlinear MOC. It is found that, when the magnitude of the sinusoidal driving function ($\Delta\tau$) was large and thus violated the linearisation approximations, the nonlinear effects could transfer energy between different frequency components and distort the FRD. The *linearisation error*, which was defined as the percentage reduction in the amplitude of the output (head oscillation) calculated by MOC from the linear output derived from the transfer matrix method at the input frequency, is proportional to the value of $\Delta\tau$ with an exponential pattern.

5.3 Selection of appropriate excitation signals to minimise the nonlinear response of a pipeline

This research demonstrates that the nonlinear behaviour of a pipeline system is related not only to the value of $\Delta\tau$, but also to the characteristics of the input signal. By using the appropriate excitation signal, part of the nonlinear response of a pipe system can be suppressed, thereby yielding frequency responses close to the linear dynamics.

In general, the output signal $y(n)$ of a sampled nonlinear system can be described by a Volterra series expansion (Godfrey 1993; Roinila et al. 2010), which is a summation of discrete convolutions of both the linear portion and the nonlinear components, and it can be written as

$$
\begin{aligned}
y(n) &= \sum_{k=0}^{M} s_1(k)u(n-k) \\
&+ \sum_{k_1=0}^{M}\sum_{k_2=0}^{M} s_2(k_1,k_2)u(n-k_1)u(n-k_2)+\cdots \\
&+ \sum_{k_1=0}^{M}\cdots\sum_{k_i=0}^{M} s_i(k_1,\cdots,k_i)u(n-k_1)\cdots u(n-k_i)
\end{aligned}
\tag{5.11}
$$

where $u(k)$ is system input, M is the length of total data sequence of interest, s_1 is linear kernel, and $s_2,\cdots,s_i$ are nonlinear kernels. If the system is linear, then it can be described by the first convolution only, which is consistent with classic linear system theory.

Applying the correlation algorithm (Godfrey 1993) to Eq. (5.11), the cross-correlation function $\phi_{uy}(n)$ between the input and the output can be written as

$$
\begin{aligned}
\phi_{uy}(n) &= \sum_{k=0}^{M} s_1(k)\phi_{uu}(n-k) \\
&+ \sum_{k_1=0}^{M}\sum_{k_2=0}^{M} s_2(k_1,k_2)\phi_{uu}(n-k_1)\phi_{uu}(n-k_2)+\cdots \\
&+ \sum_{k_1=0}^{M}\cdots\sum_{k_i=0}^{M} s_i(k_1,\cdots,k_i)\phi_{uu}(n-k_1)\cdots\phi_{uu}(n-k_i)
\end{aligned}
\tag{5.12}
$$

where $\phi_{uu}(n-k_1)\cdots\phi_{uu}(n-k_i)$ represents the i th order autocorrelation function of the input $u(n)$ and it can be described by the symbol $\phi_{uu}(n)_i$, which in turn may be written by

$$
\phi_{uu}(n)_i = \sum_{k_1,\cdots,k_i}^{M} u(k)u(n-k_1)\cdots u(n-k_i) \tag{5.13}
$$

It is known that, for a linear system, the FRF can be estimated by the ratio of the Fourier transform of the cross-correlation function between the input and the output [$\phi_{uy}(n)$] to the Fourier transform of the autocorrelation function of the input [$\phi_{uu}(n)$]. This algorithm was used for the estimation of the FRF of a real pipeline system by Lee et al. (2006). When the pipeline system has

nonlinear dynamics, as described by Eqs. (5.11) and (5.12), the FRF estimated using the preceding algorithm will have errors when it is compared with the theoretical linear FRF.

It has been verified by earlier research (Godfrey 1993; Roinila et al. 2010) that all the even kernel components shown in Eq. (5.12) can be cancelled out if the input signal $u(n)$ is persistent, periodic and antisymmetric, i.e. it can be written by

$$u(n) = -u(n + S/2) \tag{5.14}$$

where S is the length of one period of the input signal. Since the contributions of the lower-order kernels on the output are usually dominating, once the nonlinear effect caused by the second-order kernel is removed, the estimation of the linear part of the system dynamics can be obtained more accurately.

Among persistent, periodic and antisymmetric signals, the inverse repeat sequence (IRS) is suitable for extracting the linear portion of the FRF of a system and it has been successfully applied to system identification of electrical devices (Godfrey 1993; Roinila et al. 2010). One period of an IRS can be obtained by doubling a period of a maximum-length binary sequence (MLBS) and toggling every other digit of the doubled sequence. The MLBS is one special type of pseudo-random binary sequences (PRBS). PRBS are two-level, predetermined and periodic signals. A detailed definition of PRBS is given by Godfrey (1993).

The MLBS can be generated by an n-bit shift register with exclusive or (XOR) feedback from the last stage and one or more of the other stages to the first stage. The stages of feedback must be chosen in such a way that a maximum periodical length of $2^n - 1$ is achieved. The process for generating the MLBS using shift registers is illustrated in Figure 5.1.

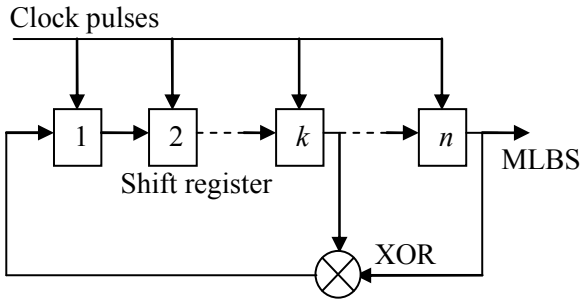

Figure 5.1 An *n*-Stage shift register with XOR feedback for MLBS generation

Lee et al. (2008a) developed a customised solenoid side-discharge valve to generate MLBS-based excitation signals. The valve was electronically controlled to produce pulses that follow a MLBS-based pattern; that is, only when the output of the shift register is 1, is a sharp pulse generated by abruptly opening and then closing the side-discharge valve. The movement of the valve was measured and the variation of the dimensionless valve opening throughout the test was used as the input signal.

This research proposes that the IRS is better than the MLBS in extracting the linear frequency response of a pipeline for the purpose of leak detection. The IRS inherits all the desirable properties for system identification from the MLBS, such as wide bandwidth, persistent and periodic. In addition, the IRS is antisymmetric, thereby enabling undesired effect of nonlinear dynamics of a pipeline to be suppressed.

5.4 Comparison of the MLBS and the IRS in the accuracy of linear FRD extraction

Numerical simulations are conducted to verify the fact that the IRS is superior to the MLBS in suppressing the nonlinear dynamics of a pipeline in the process of FRD extraction. Preliminary numerical studies have been performed by the authors on a leaking pipe in a reservoir-pipeline-valve (RPV) system (Gong et al. 2011b). It was demonstrated that when the dimensionless amplitude of the valve oscillation ($\Delta\tau$) is 0.2 and thus

exceeding the linearisation approximation, the FRD calculated from the nonlinear MOC model with IRS excitation was closer to the theoretical FRD derived from the linear transfer matrix method. This research conducts further investigation by comparing the accuracy of the frequency response extracted by the MLBS and the IRS under various values of $\Delta\tau$. Single frequency sine waves are also used in the study to provide reference information. Since a sine wave is also persistent, periodic and antisymmetric, its ability in suppressing the nonlinear dynamics of a pipeline should be similar to that of an IRS.

The pipeline system used in this study is a RPV system. The pipeline is intact and has a uniform internal diameter (D) of 40 mm and a total length (L) of 100 m. The head of the reservoir is 30 m. The wave speed (a) is 1000 m/s uniformly and the Darcy-Weisbach friction factor (f) is 0.02. The oscillating in-line valve has an initial opening of 6 mm in diameter and a discharge coefficient of 0.9. As a result, the steady-state opening area of the valve is 2.83×10^{-5} m^2, and the steady-state flow rate through the valve (Q_{V0}) is 6.1×10^{-4} m^3/s (velocity is 0.485 m/s, Reynold number is 17,017). The IRS-based excitation is generated by oscillating the dimensionless valve opening between two positions $\tau_0+\Delta\tau$ and $\tau_0-\Delta\tau$, where τ_0 is set to be unity in this study.

MOC simulations are conducted by oscillating the valve in patterns of MLBS, IRS and sine wave respectively, with various values of $\Delta\tau$. The MLBS used in this study is generated from a 10-stage shift register with a clock frequency of 100 Hz. As a result, the MLBS has a period of 10.23 s, an effective bandwidth of 44.3 Hz (the frequency where the power spectrum line drops to half of the maximum) and a resolution in its spectrum of 0.098 Hz (the interval between two power spectrum lines). The IRS used in this study is obtained by doubling one period of the MLBS and toggling each other digit of the double sequence. Accordingly, the period of the IRS is 20.46 s, but the effective bandwidth and frequency-domain resolution are the same as those of the MLBS. Considering that the fundamental frequency of the RPV model is 2.5 Hz [$a/(4L)$], the MLBS and the IRS are capable of determining the

frequency response of the preceding pipeline system up to its 17th harmonics. The sine wave used in the numerical simulation has a frequency same as the fundamental frequency of the pipe (2.5 Hz), so that the first resonant response can be extracted. Each MOC simulation has a time step of 1 ms and a modelling duration of 2000 s. As a result, 195 periods of the MLBS or 97 periods of the IRS are used in one MOC modelling.

The values of the percentage *linearisation error* [as defined in Lee et al. (2005a) and explained in Section 2 in this paper] are calculated for the first resonant response extracted from the preceding MLBS, IRS and sine signals with various values of $\Delta\tau$. The results are given in Figure 5.2. Since the FRD extracted from the MLBS and the IRS are sampled discrete sequences, linear interpolation is used to estimate the frequency response at the specific resonant frequency 2.5 Hz.

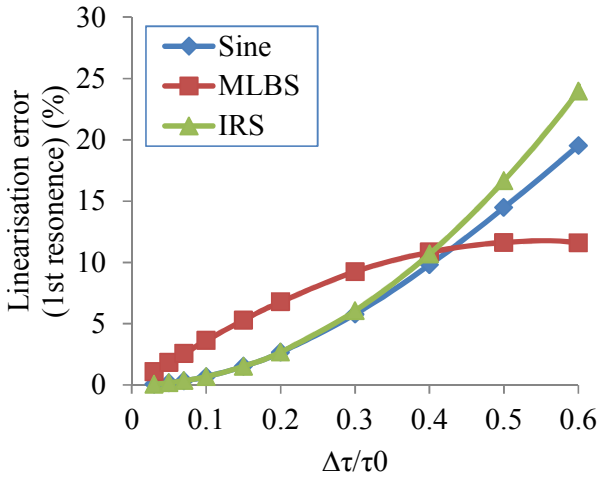

Figure 5.2 Percentage error at the first resonance (frequency response at 2.5 Hz) as a function of the magnitude of valve perturbation

The results shown in Figure 5.2 demonstrate that the linearisation error introduced by the MLBS, as expected, is in general higher than the error resulted from the IRS and the sine signal. The values of the linearisation error introduced by the IRS and the sine signal are comparable and proportional to the value of $\Delta\tau / \tau_0$ in an exponential pattern. The comparability is consistent

with the inference that the IRS and the sine signal have similar ability in suppressing the nonlinear dynamics because both of them are antisymmetic; while the exponential pattern is consistent with the results presented in Lee et al. (2005a). When the value of $\Delta\tau / \tau_0$ is greater than 0.4, it seems that the MLBS behaves better, although significant error is observed for all these three cases. However, it should be noted that the results shown in Figure 5.2 are for the first resonance only and the interpolation process is involved for the results from the MLBS and the IRS. The FRD (the first three resonances only) extracted from the MLBS and the IRS when the value of $\Delta\tau / \tau_0$ equals 0.4 are shown in Figure 5.3. It can be seen that the FRD extracted from the MLBS has greater discrepancy from the FRD obtained from the linear transfer matrix method. The discrepancy is attributable to the effect of nonlinearity in the nonlinear MOC simulation.

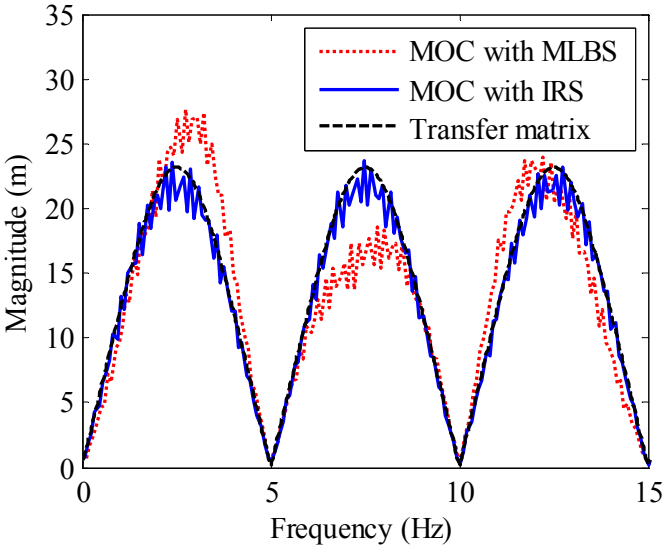

Figure 5.3 Comparison between the FRD from MOC using the MLBS and the IRS excitation with $\Delta\tau / \tau_0 = 0.4$ and the linear FRD from the transfer matrix method

5.5 Conclusions

This research has analysed the effect that transient excitation has on the nonlinear behaviour of a pipeline. A detailed analysis of the nonlinearity of a pipeline and its effect on the FRD-based leak detection techniques has been conducted. Because all the FRD-based leak detection techniques are based on linear theory, the FRD generated for leak detection is desired to only represent the linear response of the pipeline.

This research demonstrates that wide bandwidth, persistent, periodic and antisymmetric signals are suitable for the extraction of the linear FRD. The antisymmetric property enables even kernels of the nonlinear dynamics of a system to be cancelled out; therefore, the linear part of the system dynamics can be estimated more accurately. The inverse-repeat sequence (IRS), in particular, is found to be an appropriate excitation signal. Numerical studies conducted in this research demonstrate that the IRS is better than the maximum-length binary sequence (MLBS) that has been used in earlier research for FRD extraction.

Acknowledgements

The research presented in this paper has been supported by the Australian Research Council through the Discovery Project Grant DP1095270.

Notations

The following symbols are used in this paper:

A = cross-sectional area of a pipeline (m2)

A_L = opening area of a leak orifice (m2)

a = wave speed (m/s)

C_{Ld} = coefficient of discharge for a leak orifice (-)

D = internal pipe diameter (m)

f = Darcy-Weisbach friction factor (-)

g = gravitational acceleration (m/s2)

H = head (m)

H_0 = steady-state head (m)

H_{L0} = head across a leak (m)

h = complex head perturbation (m)

j = imaginary unit, $\sqrt{-1}$ (-)

L = length of pipe (m)

M = length of total data sequence of interest (-)

n = number of stages of a shift register, or a positive integer (-)

Q = flow (m3/s)

Q_0 = steady-state flow (m3/s)

Q_{L0}, Q_{V0} = discharge through a leak and a valve (m3/s)

q = complex discharge perturbation (m3/s)

R = linearised resistance term, $fQ_0 / (gDA^2)$ (s/m)

S = length of one period of a signal (-)

s_1 = linear kernel of a system (-)

$s_2, \cdots, s_i$ = nonlinear kernel of a system (-)

t = time (s)

u = input signal (-)

x = distance (m)

y = output signal (-)

Greek symbols:

ΔH_{V0} = steady-state head loss across a valve (m)

ϕ_{uu} = autocorrelation function of the input (-)

ϕ_{uy} = cross-correlation function between the input and the output (-)

ω = angular frequency (rad/s)

τ_0 = mean dimensionless valve aperture size (-)

$\Delta\tau$ = magnitude of the dimensionless valve aperture perturbation (-)

Chapter 6

A Customized Side-Discharge Valve for Extracting the Frequency Response Function of Hydraulic Pipelines using Pseudorandom Binary Signals (Journal Publication 4)

Gong, J., Lambert, M. F., Simpson, A. R., and Zecchin, A. C.

School of Civil, Environmental and Mining Engineering, the University of Adelaide, Adelaide, SA 5005 Australia

Journal of Hydraulic Engineering, (submitted).

Statement of Authorship

Title of Paper	A Customized Side-discharge Valve for Extracting the Frequency Response Function of Hydraulic Pipelines using Pseudorandom Binary Signals
Publication Status	Submitted for Publication
Publication Details	Gong, J., Lambert, M. F., Simpson, A. R., and Zecchin, A. C. (2013). "A customized side-discharge valve for extracting the frequency response function of hydraulic pipelines using pseudorandom binary signals." *Journal of Hydraulic Engineering*, (submitted).

Author Contributions

By signing the Statement of Authorship, each author certifies that their stated contribution to the publication is accurate and that permission is granted for the publication to be included in the candidate's thesis.

Name of Principal Author (Candidate)	Jinzhe Gong		
Contribution to the Paper	Developed and implemented the methodology, designed and conducted numerical simulations, designed the customised side-discharge valve, implemented laboratory experiments, interpreted and analysed results, prepared manuscript and acting as the corresponding author.		
Signature		Date	25/09/2013

Name of Co-Author	Martin Lambert		
Contribution to the Paper	Supervised development of work, helped to evaluate and edit the manuscript.		
Signature		Date	25/09/13

Name of Co-Author	Angus Simpson		
Contribution to the Paper	Helped to evaluate and edit the manuscript.		
Signature		Date	25/9/2013

Name of Co-Author	Aaron Zecchin		
Contribution to the Paper	Helped to evaluate and edit the manuscript.		
Signature		Date	1·10·2013

Abstract

The frequency response function (FRF) of a pressurized pipeline represents the physical characteristics of the system and is known to be able to indicate the existence and location of leaks and blockages. However, the extraction of the FRF for a pipeline is challenging because conventional transient (or controlled water hammer) wave generators have difficulty in generating a sufficiently wide enough bandwidth and high enough signal-to-noise ratio (SNR) excitation signals. This technical note presents the design of a side-discharge valve based transient generator that can generate two types of pseudorandom binary signals (PRBS): the maximum length binary signal (MLBS) and the inverse repeat signal (IRS). These two input signals are both wide bandwidth, persistent and periodic signals, and they have been used as the excitation to extract the linear FRF of a single water pipeline in an experimental apparatus in a hydraulics laboratory. By comparing the experimental results with the theoretical linear FRF of the single pipeline, it is found that in general the FRF extracted by the IRS is more accurate. This can be attributed to its ability to suppress part of the nonlinear behavior of a system. The experimental results confirm that the amplitude of the valve perturbation affects the magnitude of the head response and the shape of the FRF. This customized side-discharge valve provides possibilities for efficient and accurate extraction of the FRF for real pressurized pipelines, and therefore contributing to improving the integrity monitoring of water distribution systems by transient based techniques.

6.1 Introduction

The analysis of the dynamic response of pressurized pipeline systems is essential for the design, operation and also for the integrity monitoring of the system. In hydraulic pipeline systems, the dynamic analysis is typically conducted by introducing a transient or water hammer wave into the system and then measuring and analyzing the pressure response. The system response function describes the relationship between the input transient signal and the resultant pressure responses, and it gives detailed information of the physical characteristics of a pipeline system. The system response function is known as the impulse response function (IRF) in the time domain and the frequency response function (FRF) in the frequency domain (Ljung 1999).

The frequency-domain analysis is of particular interest since it allows the study of the frequency dependent effects, such as fluid-structure interaction (Tijsseling 1996) and unsteady friction (Vítkovský et al. 2006). In the last decade, the analysis of the FRF of pipeline systems under linear systems theory has also been used in integrity monitoring of water pipelines, such as the detection of leaks (Lee et al. 2005a; Lee et al. 2005b; Gong et al. 2013e; Gong et al. 2013b) and blockages (Lee et al. 2008b; Sattar et al. 2008), and more recently, general parameter identification (Zecchin et al. 2013). However, most previous studies have been limited to numerical analysis because the extraction of the linear FRF of a real pipeline is difficult.

The generation of an appropriate excitation transient signal is challenging. This can be attributed to aspects including high back-pressure in the pipeline and limitations in the lack of maneuverability of valves or other hydraulic components that are used as the signal generator (Lee et al. 2008a). In early studies, the extraction of the FRF of a pipeline was conducted through oscillating specially designed valves or hydraulic components at a number of frequencies in sequence. This procedure is known as a frequency sweep (or sine-sweep). For example, Svingen (1996) designed a variable periphery and frequency-controlled rotating disc placed in front of a free discharging orifice

to generate transient waves with specific frequencies. The frequency sweeping approach is time consuming because the system needs to be excited at many different frequencies sequentially, and the measurement can only be taken after a steady-oscillatory flow has been established. In an operating pipeline system, the flow conditions may change during the testing period so that the extracted response function may be impacted adversely.

An alternative to the frequency sweeping technique is to extract the FRF within a single operation using a wide bandwidth input signal. Side-discharge valves are typically used to generate pulse or step signals in pressurised pipelines. For example, Lee et al. (2006) performed laboratory experiments on FRF extraction and leak detection for a water pipeline using a sharp pulse transient and a correlation-based FRF determination algorithm. The pulse signal needs to be sharp and its amplitude has to be large enough to ensure a sufficient signal-to-noise ratio (SNR) in the high frequency components. However, the large amplitude requirements of the pulse signal may also risk damage to the pipeline system (Lee et al. 2008a).

A desirable transient excitation signal for the FRF extraction should have a wide bandwidth, high SNR and low amplitude. Developments in other disciplines have shown that the pseudorandom binary signal (PRBS) has the desired characteristics, and this type of signal is commonly used in determining the linear FRF of electrical systems (Godfrey 1993; Tan and Godfrey 2002). The PRBS is predetermined, persistent and periodic. Its spectrum has a wide bandwidth because the energy decay is relatively low towards the high frequency range. The periodicity enables the SNR to be increased by synchronous averaging of the response periods. The continuous form of the signal allows the energy to be distributed over a long time period so that the amplitude of the signal can be small.

Two specific types of PRBS are widely used. These are the maximum length binary signal (MLBS) and the inverse repeat signal (IRS) (Godfrey 1993). The MLBS can be generated by an *n*-bit shift register with “exclusive or” feedback from the last stage, and one or more of the other preceding stages.

The stages of feedback must be chosen in such a way that the maximum periodic length of $N = 2^n - 1$ is achieved. The IRS is generated by doubling the MLBS and inverting every other digit of the doubled sequence.

Liou (1998) conducted numerical studies on IRF extraction of a pressurized pipeline using MLBS (referred to as PRBS in that paper). Lee et al. (2008a) designed and fabricated the first side-discharge valve-based transient generator for the extraction of the linear FRF of a pipeline in the laboratory using MLBS (also referred to as PRBS in that paper). The valve was electronically controlled by a solenoid to produce discrete pulse sequences that follow a MLBS-based pattern. That is, only when the output of the shift register is 1, is a sharp pulse generated by abruptly opening and then closing the side-discharge valve. The FRF of a pressurized pipeline in the laboratory was successfully extracted.

Gong et al. (2011b) studied the linear FRF extraction for a pipeline using MLBS and IRS by numerical simulations. It is known that the nonlinear behavior of the pipeline system is proportional to the amplitude of the valve oscillation (Lee et al. 2002; Lee et al. 2005a). The nonlinearity is undesirable because all existing FRF-based leak and blockage detection techniques are developed under linear theory assumptions. The numerical results in Gong et al. (2011b) show that the IRS can yield more accurate estimation of the linear FRF than the MLBS when the nonlinearity introduced by the valve oscillation is significant. Gong et el. (2013d) consequently conducted a detailed sensitivity analysis of the nonlinear behavior of a pipeline with regard to the transient excitation generated by a side-discharge valve. It was shown numerically that the IRS can suppress part of the nonlinear behavior of a pipeline system because of its antisymmetic property in each period.

This technical note presents the design of a side-discharge valve-based transient generator and its application to FRF extraction of hydraulic pipelines. The opening of the valve is controlled by a vertical rod which is maneuvered by two solenoid coils. The rod then oscillates in a continuous MLBS or IRS form. The amplitude of the valve perturbation is adjustable.

Three case studies, with different values of perturbation amplitude, were conducted in the laboratory to extract the linear FRF of a pressurized water pipeline. The experimental results verify that the amplitude of valve perturbation can affect the accuracy of FRF estimation. Compared to MLBS, IRS can yield FRF estimation that is smoother and closer to the theoretical one predicted by linear theory. The magnitude of the head response and the shape of the FRF are also related to the amplitude of valve perturbation. This side-discharge valve-based transient generator provides a practical method for accurate extraction of the linear FRF of hydraulic pipelines.

6.2 Experimental apparatus

A customized side-discharge valve-based transient generator was developed in the laboratory to generate MLBS and IRS pressure signals within a pressurized pipeline for the purpose of FRF extraction. A schematic diagram of this transient generator is given in Figure 6.1. A brass block with a small diameter hole (2 mm as the minimum) drilled through the long axis forms the conduit for the water to escape the pipeline. The calibrated emitter coefficient ($C_d A_V$) of the valve, when fully open, is 2.7×10^{-6} m^2. A rod connected to two solenoids controls the valve opening. The lower solenoid drives the valve opening and the upper solenoid drives the valve closure. The rod is also connected with a linear voltage displacement transducer (LVDT) at the top to measure its movement during signal generation.

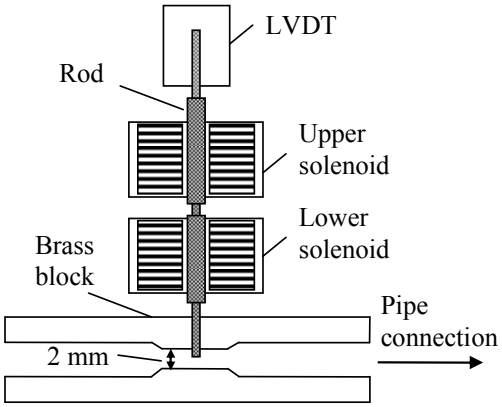

Figure 6.1 The customized transient generator used for generating MLBS and IRS

The two solenoids are electronically controlled by an external signal generator, driving the rod to oscillate between two positions (valve fully open and partially closed) to produce a persistent MLBS or IRS. The movement of the rod is converted into an equivalent dimensionless valve opening coefficient, τ (Chaudhry 1987), and the average value of τ is represented by τ_0. The normalized τ perturbation, $(\tau - \tau_0)/\tau_0$, is used as the input to the pipeline system. The amplitude of the input, $A_{in} = \max(\tau - \tau_0)/\tau_0$, is adjustable (i.e. the maximum displacement of the oscillating rod is adjustable).

The MLBS is generated by a 10-stage shift register based on a clock frequency of 100 Hz. As a result, there are 2^{10}-1 = 1023 binary digits within one period of the MLBS, and its period is 1023/100 = 10.23 s. The IRS is obtained by doubling the MLBS and reversing every other digit, so that the period of the IRS is 20.46 s. The bandwidth of the MLBS and the IRS are both 44.3 Hz, where the power of the signal drops to half the maximum. The MLBS and the IRS can be generated continuously to produce a persistent MLBS or IRS perturbation in the opening of the valve.

The customized valve is connected to an experimental pipeline in the Robin Hydraulics Laboratory in the University of Adelaide. A schematic diagram of

the experimental pipeline system is given in Figure 6.2. The pipeline is made of copper and has a length of 37.53 m and an internal diameter of 22 mm. The pipeline is bounded by a closed in-line valve at one end and a pressurized tank with a head of 38.50 m at the other end, forming a reservoir-pipeline-valve (RPV) system. The customized side-discharge valve-based generator is located 145 mm upstream from the closed in-line valve, and it has an elevation of 2.0 m above the upstream end of the pipeline. The head response of the pipeline system is measured at the same location as the generator by a flush-fitted pressure transducer (Druck PDCR 810). The output of the transducer is connected to a customized amplifier and then collected by a data acquisition card (Measurement Computing USB-1608FS). The output of the LVDT (movement of the rod) is also fed to the data acquisition card. The data acquisition is controlled by LabView software installed on a laptop computer. The internal roughness of the pipe is estimated as 1.5×10^{-6} m from the manufacturer. The sampling frequency used in this research is 5 kHz.

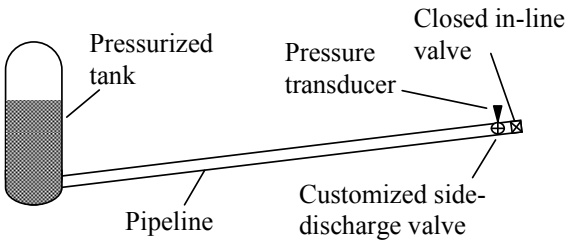

Figure 6.2 A schematic diagram of the experimental pipeline used in this research

6.3 Experimental extraction of the linear FRF using MLBS and IRS

Three case studies have been conducted in the laboratory with a range of amplitudes of the relative dimensionless valve perturbation, A_{in}. In each case study, both the MLBS and the IRS were used, and the experimental FRF of the pipeline was estimated and compared with the theoretical linear theory

FRF determined from the transfer matrix method (Chaudhry 1987). The repeatability was confirmed by conducting multiple tests in each case study. The frequency-domain unsteady friction model developed by Vítkovský et al. (2003a) was used in the numerical simulations to derive the theoretical FRD. This unsteady friction model is based on the smooth pipe unsteady friction weighting function proposed by Vardy and Brown (2003). More information about the application of the unsteady friction model to the transfer matrix method can be found in Gong et al. (2013e).

In the experimental study conducted, each individual experiment lasted for 10 minutes. The first a few seconds of data were measured under steady state (with the side-discharge valve open) to observe the initial steady-state head variation of the system. Then the IRS, or MLBS, excitation was started manually. It was observed that the pressure at the bottom of the pressurized tank became relatively stable after approximate 150 s of the IRS or MLBS excitation. As a result, in the process of the experimental FRF estimation, the first 245.52 s of data (24 periods of MLBS or 12 periods of IRS) in each test were removed to ensure that the data used in FRF calculation were under steady oscillatory flow condition. The algorithm for the linear FRF estimation was a logarithmic averaging procedure (Godfrey 1993; Gong et al. 2011b), which can be written as

$$H_{\log}(j\omega) = \left(\prod_{k=1}^{N_m} \frac{Y_{mk}(j\omega)}{X_{mk}(j\omega)} \right)^{1/N_m} \tag{6.1}$$

where $H_{\log}(j\omega)$ is the FRF determined by the logarithmic algorithm; j is imaginary unit $\sqrt{-1}$; ω is angular frequency; N_m is the number of averaged measurements; $Y_{mk}(j\omega)$ and $X_{mk}(j\omega)$ are the Fourier transforms of the measured output and input determined from the k^{th} measurement period.

6.3.1 Case study No.1: For an amplitude of input signal of $A_{in} \approx 0.5$

Discharge from the valve was measured using a volumetric method during each test. In this case study, the mean discharge out of the valve during MLBS or IRS excitation was measured as 4.8×10^{-5} m^3/s. The corresponding Reynolds number was 2,433. The Darcy-Weisbach friction factor was estimated as 0.040 and it was used in the determination of the theoretical linear FRF using the transfer matrix method.

Examples of the normalized IRS τ perturbation (input) and the corresponding head perturbation (output) in the case study are shown in Figure 6.3 and Figure 6.4 respectively. The measurements of the MLBS τ perturbation and its corresponding head response are not shown in the paper (for any of the three case studies) for the sake of brevity.

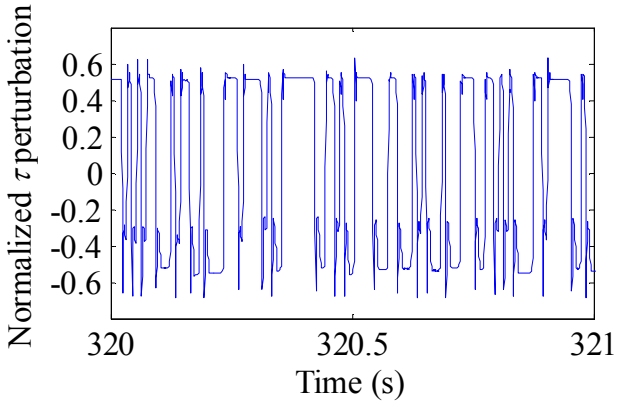

Figure 6.3 The normalized IRS τ perturbation (input) in the case study No.1

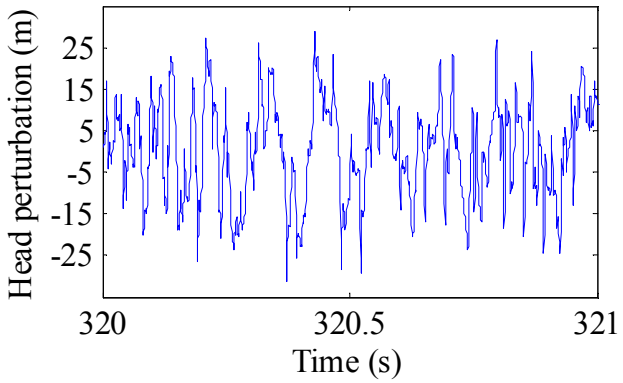

Figure 6.4 The head perturbation (output) in the case study No.1

The measured valve perturbation (Figure 6.3) follows an IRS pattern, but with small variations due to the mechanics of the side-discharge valve. The measured head response (Figure 6.4) shows little visible structure in the time domain, and the maximum magnitude is approximate ± 28 m. The logarithmic averaging procedure [Eq. (6.1)] was applied to the data obtained from the IRS and the MLBS experiments respectively to estimate the linear FRF of the pipeline. The results of the experimental FRF in this case study are shown in Figure 6.5 with comparison to the theoretical linear FRF. Each FRF is normalized by dividing it by the corresponding peak value around the first resonant frequency. The horizontal axis is normalized by dividing the frequency values by the fundamental frequency of the pipeline, which was estimated as 8.94 Hz from the extracted FRF.

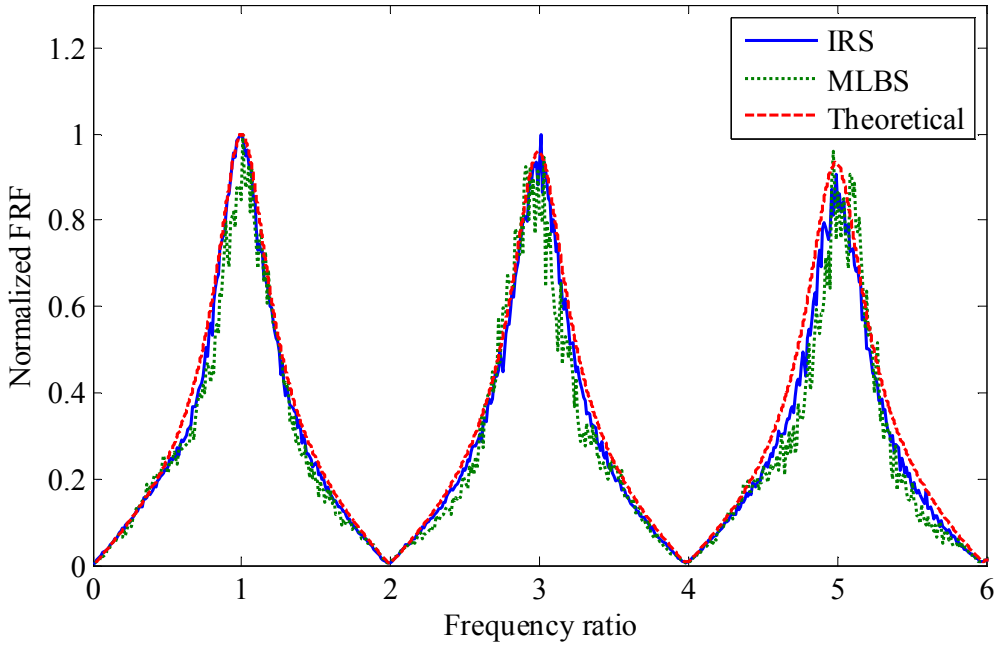

Figure 6.5 Comparison between the experimental FRF induced by IRS and MLBS excitation with the theoretical FRF in case study No.1

From Figure 6.5, the FRF induced by IRS is closer to the theoretical FRF when compared with that obtained from MLBS. To quantify the difference, the least squares error is calculated for both FRF results extracted by IRS and MLBS. The least squares error is defined as $sqrt\left(\sum\left[FRF_{Experimental}(i)-FRF_{Theoretical}(i)\right]^2\right)$, and the FRF data used in the calculation ranges from 0 to 49 Hz. The value of the least squares error is 1.03 for the FRF extracted by the IRS and it is 1.93 for the FRF resulted from the MLBS.

The FRF obtained from the IRS is smoother, although both the experimental results contain mild variations. One source of these variations is attributed to the nonlinearity of the dynamics of the experimental pipeline system. In this case study, the amplitude of the normalized τ perturbation (A_{in}) is approximately 0.5, which can introduce a significant nonlinear response (Lee et al. 2002; Lee et al. 2005a). The experimental results demonstrate that the IRS yields better estimation (smoother and closer to theoretical results) of the

FRF than the MLBS when the nonlinear effect is significant. This finding is consistent with the numerical analysis presented in Gong et al. (2013d). As a result, the use of IRS as an excitation signal can result in a more accurate estimation of the relative peak values in the FRF (resonant responses), which is the necessary information required by some FRF-based leak and blockage detection techniques (Lee et al. 2005b; Lee et al. 2008b; Gong et al. 2013e).

6.3.2 Case study No.2: For an amplitude of input signal of $A_{in} \approx 0.2$

In the second case study, the maximum allowable displacement of the rod in the customized side-discharge valve was reduced to lessen the nonlinear effects of the system. Both the IRS and the MLBS were generated to extract the experimental FRF. The mean discharge out of the valve was measured as $6.5\times10^{-5}\,\mathrm{m}^3/\mathrm{s}$. The corresponding Reynolds number was 3,294. The Darcy-Weisbach friction factor was estimated as 0.041 from the Moody diagram, and it was used in the determination of the theoretical FRF by the transfer matrix method. Sections of the normalized IRS τ perturbation (input) and its corresponding head perturbation (output) in this case study are shown in Figure 6.6 and Figure 6.7 respectively.

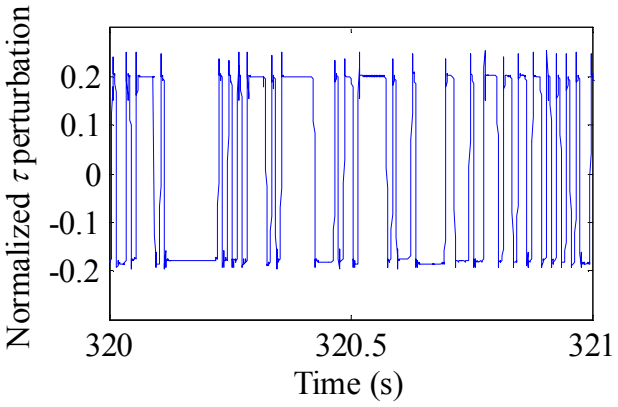

Figure 6.6 The normalized IRS τ perturbation (input) in the case study No.2

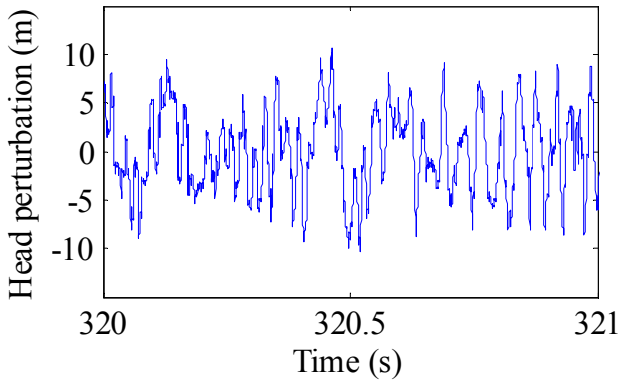

Figure 6.7 The head perturbation (output) in the case study No.2

In the second case study, the amplitude of the input signal (normalized τ perturbation, Figure 6.6) was reduced to $A_{in} \approx 0.2$. Accordingly, the magnitude of the head perturbation (Figure 6.7) was decreased to approximately ± 11 m. This indicates that the magnitude of the head perturbation under PRBS excitation is controllable by the value of A_{in}, and thus it can be adjusted to cater for various situations to minimize the risk of damaging the pipeline. This experimental finding is consistent with the theoretical analysis presented in Lee et al. (2005b), which concludes that the magnitude of the resonant head response induced by an oscillating valve is proportional to the amplitude of valve perturbation.

The experimental FRF induced by the IRS and the MLBS are estimated by using the logarithmic averaging procedure [Eq. (6.1)]. The results are compared with the theoretical linear FRF in Figure 6.8.

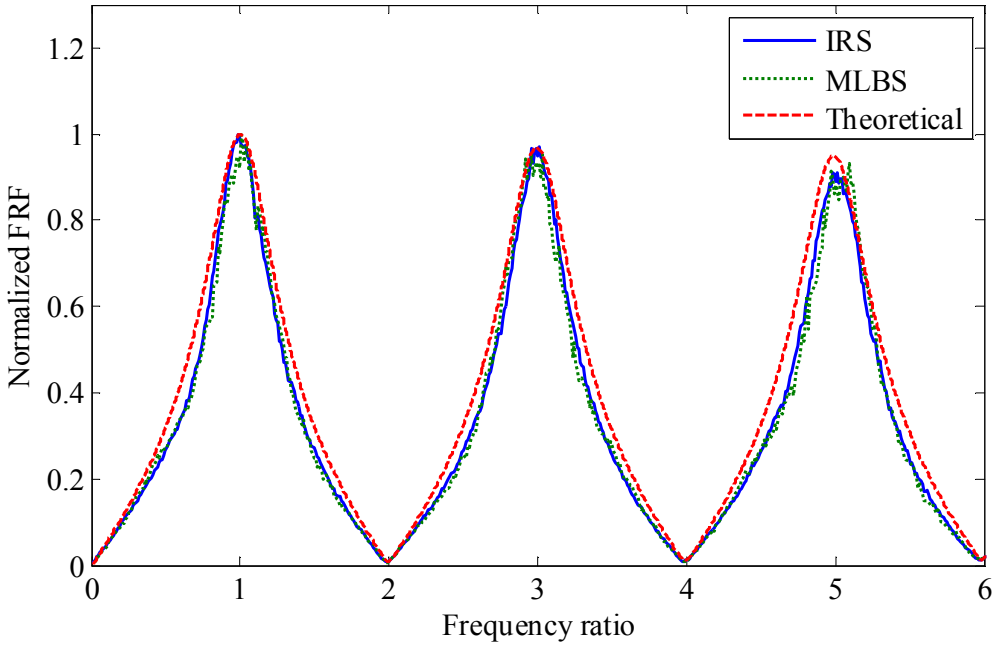

Figure 6.8 Comparison between the experimental FRF induced by IRS and MLBS excitation with the theoretical FRF in case study No.2

The results in Figure 6.8 show that both the experimental FRF values are close to the theoretical results around the peak values and they are much smoother than those for the larger valve perturbation shown in Figure 6.5. This finding provides experimental verification that the magnitude of the valve perturbation can affect the accuracy of the FRF estimation. A smaller magnitude in the valve perturbation yields a better estimate of the FRF (with less variation), because it introduces a reduced nonlinear response of the pipeline system (Lee et al. 2002; Lee et al. 2005a; Gong et al. 2013d). The experimental FRF extracted using IRS is even smoother than that induced by MLBS. The least squares error in the FRF extracted by the IRS is calculated as 1.41, which is lower than the error of 1.68 in the FRF extracted by the MLBS. As a result, the estimation of the peak values (resonant responses) in the FRF extracted by IRS are more accurate. This verifies that the IRS is better than the MLBS in FRF extraction of pipeline systems.

It is also observed that the shape of the FRF peaks extracted using a greater valve perturbation [Figure 6.5] is sharper than that obtained by using a smaller

amplitude of valve perturbation [Figure 6.8]. This is consistent with the numerical analysis presented in Gong et al. (2013d), which proposes that a higher valve impedance (the steady-state impedance when the opening of the oscillating valve is at its mean) yields sharper FRF peaks. In case study No.1, where the side-discharge valve has a greater value of perturbation amplitude, the mean opening of the valve (corresponding to τ_0) is lower than that in case study No.2. As a result, the impedance of the valve in case study No.1 is higher and the FRF peaks are sharper.

In both Figure 6.5 and Figure 6.8, the experimental values of the third peak (the third resonant response) are slightly lower than that in the theoretical FRF. However, this is consistent with the experimental results reported in Lee et al. (2008a).

6.3.3 Case study No.3: For an amplitude of input signal of $A_{in} \approx 0.06$

A third case study was performed with an even smaller amplitude of the valve perturbation ($A_{in} \approx 0.06$). Both the IRS and the MLBS were generated to extract the experimental FRF. The mean discharge out of the valve was measured as 7.0×10^{-5} m^3/s. The corresponding Reynolds number was 3,548. The Darcy-Weisbach friction factor was estimated as 0.041 from the Moody diagram, and it was used in the determination of the theoretical FRF. Sections of the normalized IRS τ perturbation (input), and its corresponding head perturbation (output), in this case study are shown in Figure 6.9 and Figure 6.10 respectively.

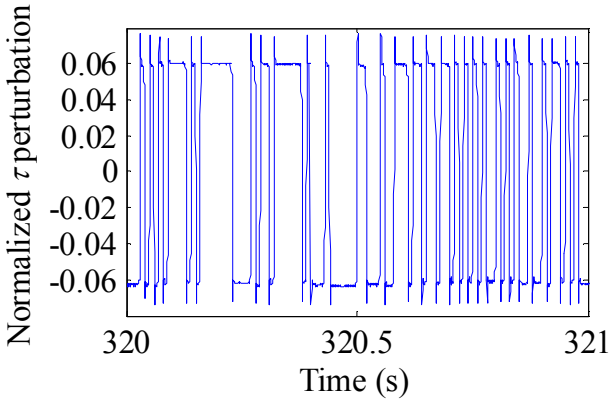

Figure 6.9 The normalized IRS τ perturbation (input) in the case study No.3

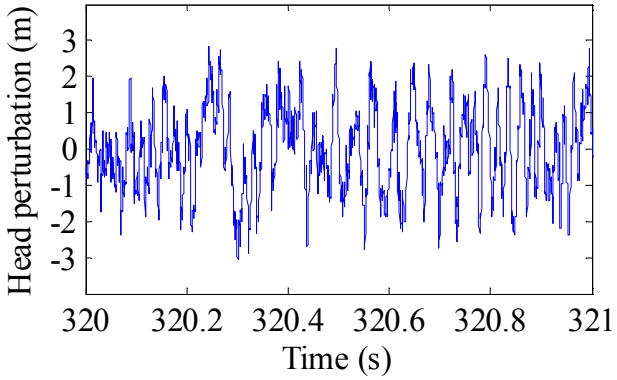

Figure 6.10 The head perturbation (output) in the case study No.3

In the third case study, the magnitude of the head perturbation (Figure 6.10) was further decreased to approximately ± 3 m. The experimental FRF extracted by using the IRS and the MLBS are estimated by the logarithmic averaging procedure [Eq. (6.1)], and the results are compared with the theoretical FRF in Figure 6.11.

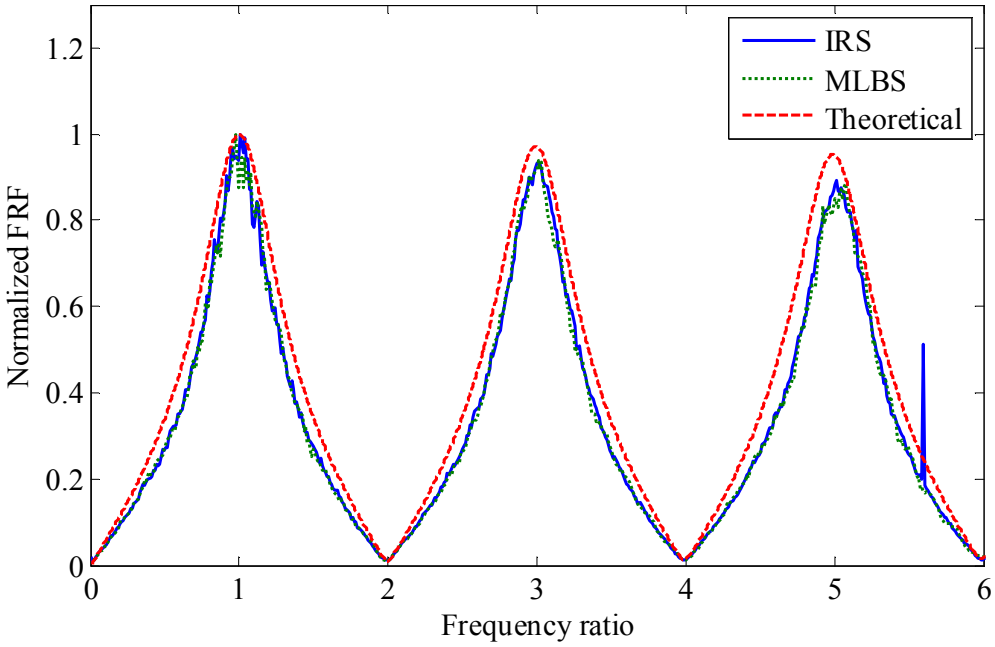

Figure 6.11 Comparison between the experimental FRF induced by IRS and MLBS excitation with the theoretical FRF in case study No.3

Compared to the results obtained in the second case study (Figure 6.8), both the experimental FRF results extracted in case study No.3 show a greater discrepancy from the theoretical FRF. The values of the least squares error for the FRF results extracted by IRS and MLBS are 1.77 and 1.89 respectively. Other than the effects of nonlinearity, which is believed to be mild in this case study since A_{in} is small, the error in the experimental FRF is related to the low signal-to-noise ratio (SNR) in the measurement. It was observed that the magnitude of head fluctuation under steady-state (with the side-discharge valve open) was approximately ± 1 m, which is one third of the signal under excitation. In the experimental FRF extracted by IRS, a spike is observed at 50 Hz. This is attributable to the low signal power of the IRS at this frequency (therefore low SNR). Theoretically, the power of IRS is zero at the frequency of half of the clock frequency, which is 100 Hz in the PRBS signal generator and it results in a half value of 50 Hz. The results shown in Figure 6.11 also verify the fact that less amplitude of valve perturbation (which leads to lower

valve impedance in this customized side-discharge valve) introduces more rounded FRF peaks (compared to Figure 6.5).

6.4 Conclusions

In this research, a solenoid controlled side-discharge valve has been designed and fabricated as a transient generator for frequency response function (FRF) extraction of hydraulic pipelines for frequencies up to 50 Hz. A vertical rod inserted in the side-discharge valve is used to control the opening of the valve, and two solenoids are used to maneuver the push and pull movements of this rod respectively. This side-discharge valve-based transient generator can produce two types of pseudorandom binary signals (PRBS) by perturbing the size of its opening. These signals are the maximum length binary signal (MLBS) and the inverse repeat signal (IRS) (Godfrey 1993). They are persistent, periodic and wideband, and therefore suitable for FRF extraction. This customized transient generator provides a method for accurate and efficient estimation of the FRF of hydraulic pipelines, facilitating the application of pipeline integrity monitoring techniques that utilizes the FRF.

Laboratory experiments have been implemented in a reservoir-pipeline-valve (RPV) system to determine its FRF using the customized transient generator. Three case studies were conducted with different values of the amplitude of valve perturbation (A_{in}). In each case study, experimental FRF results extracted by using MLBS and IRS respectively were compared with the theoretical linear FRF obtained from the transfer matrix method.

The experimental results show that greater amplitude of valve perturbation leads to a greater magnitude of head response and sharper FRF peaks, which are consistent with the numerical results presented in Lee et al. (2005b) and Gong et al. (2013d), respectively. Large amplitude valve perturbations can introduce a significant nonlinear system response, which can lead to errors in the linear FRF estimation (see case study No.1). Compared to the MLBS, the IRS can yield more accurate estimation of the FRF (see Figure 6.5 and Figure

6.8), since the IRS can suppress part of the nonlinear response of a system (Gong et al. 2013d). However, if the amplitude of valve perturbation and the magnitude of the corresponding head response are too small, the signal-to-noise ratio (SNR) could be poor and the estimated FRF can be affected by measurement noise (see Figure 6.11).

Acknowledgments

The research presented in this paper has been supported by the Australian Research Council through the Discovery Project Grant DP1095270. The first author thanks the Chinese Scholarships Council and the University of Adelaide for providing a joint postgraduate scholarship. The authors also thank technicians Brenton Howie, Simon Order and Stan Woithe in the Robin Hydraulics Laboratory in the University of Adelaide for their support in the design and fabrication of the customized transient generator.

Notation

The following symbols are used in this paper:

A_V = area of valve orifice;

A_{in} = amplitude of the input [normalized valve perturbation, $= \max(\tau - \tau_0)/\tau_0$];

C_d = coefficient of discharge for valve;

$H_{\log}$ = frequency response function determined by logarithmic averaging procedure;

j = imaginary unit ($\sqrt{-1}$);

N_m = the number of averaged measurements;

X_{mk} = Fourier transforms of the measured input;

Y_{mk} = Fourier transforms of the measured output;

Greek symbols:

τ = dimensionless valve opening;

τ_0 = mean dimensionless valve opening;

ω = angular frequency.

Chapter 7

Single Event Leak Detection in a Pipeline using Fluid Transients with Inverse-Repeat Binary Sequences (Journal Publication 5)

Gong, J., Lambert, M. F., Simpson, A. R., and Zecchin, A. C.

School of Civil, Environmental and Mining Engineering, the University of Adelaide, Adelaide, SA 5005 Australia

Journal of Hydraulic Engineering, (submitted).

Statement of Authorship

Title of Paper	Single Event Leak Detection in a Pipeline using Fluid Transients and Inverse-repeat Binary Sequences
Publication Status	Submitted for Publication
Publication Details	Gong, J., Lambert, M. F., Simpson, A. R., and Zecchin, A. C. (2013). "Single event leak detection in a pipeline using fluid transients and inverse-repeat binary sequences." Journal of Hydraulic Engineering, (submitted).

Author Contributions

By signing the Statement of Authorship, each author certifies that their stated contribution to the publication is accurate and that permission is granted for the publication to be included in the candidate's thesis.

Name of Principal Author (Candidate)	Jinzhe Gong		
Contribution to the Paper	Developed and implemented the methodology, designed and conducted laboratory experiments, interpreted and analysed results, prepared manuscript and acting as the corresponding author.		
Signature		Date	25/09/2013

Name of Co-Author	Martin Lambert		
Contribution to the Paper	Supervised development of work, helped to evaluate and edit the manuscript.		
Signature		Date	25/9/13

Name of Co-Author	Angus Simpson		
Contribution to the Paper	Helped to evaluate and edit the manuscript.		
Signature		Date	25/9/2013

Name of Co-Author	Aaron Zecchin		
Contribution to the Paper	Helped to evaluate and edit the manuscript.		
Signature		Date	1.10.2013

Abstract

The frequency response diagram (FRD) of a fluid-filled pipeline extracted by measured fluid transients (water hammer waves) can be used for the detection of leaks. This paper presents experimental results on single event leak detection in a reservoir-pipeline-valve (RPV) system. A customized side-discharge valve is used to generate persistent transient signals that are based on inverse-repeat binary sequences (IRS). The FRD of the laboratory pipeline is extracted and the first three resonant peaks are used to estimate the location and size of the leak. In addition, a numerical sensitivity analysis is conducted to study the effect that a boundary valve loss has on frequency-domain leak detection techniques. By adjusting the boundary valve loss, the resonant peaks on the FRD can be rounded, ensuring the experimental results of sampling to be robust and tolerant of noise. These numerical findings are verified by the laboratory experiments.

7.1 Introduction

Leak detection in water distribution systems is a topic of great interest in both industry and academia (Puust et al. 2010). A number of leak detection techniques have been developed in the past two decades, such as acoustic techniques (Fuchs and Riehle 1991; Tafuri 2000), ground penetrating radar (Eiswirth and Burn 2001), electromagnetic techniques (Goh et al. 2011) and fluid transient-based techniques (Colombo et al. 2009). The transient-based leak detection techniques have gained popularity over the last decade as the information of a long section of pipeline (usually thousands meters) can be obtained efficiently and cost-effectively through a single transient test.

A number of fluid transient-based leak detection and location techniques are reported in the literature, including *time-domain reflectometry* (TDR) analysis (Jönsson and Larson 1992; Brunone 1999; Brunone and Ferrante 2001; Lee et al. 2007a), *transient damping method* (Wang et al. 2002; Nixon and Ghidaoui 2006), *inverse transient analysis* (ITA) (Liggett and Chen 1994; Vítkovský et al. 2000; Vítkovský et al. 2007; Covas and Ramos 2010), *impulse response analysis* (Liou 1998; Vítkovský et al. 2003b; Kim 2005; Lee et al. 2007b) and *frequency response analysis* (Mpesha et al. 2001; 2002; Covas et al. 2005; Lee et al. 2005b; Duan et al. 2011; Gong et al. 2013e). The use of the frequency response of a pipeline for leak detection is typically faster than the ITA since no iteration is involved in the determination of the frequency response diagram (FRD), and it is more robust than the other transient-based techniques since pipeline parameter variations (such as wall thickness variations) have little effect on the leak-induced information in the FRD (Duan et al. 2011). A detailed literature review of transient-based leak detection techniques can be found in the paper by Colombo et al. (2009).

Lee et al. (2005b) proposed a systematic FRD-based technique that is able to estimate not only the locations but also the sizes of leaks in a pipeline. It was found that a leak in a single pipeline could introduce a sinusoidal leak-induced pattern on the resonant responses of the FRD. The size of the leak is related to

the amplitude of the sinusoidal leak-induced pattern, while the location of the leak is associated with the period of the pattern. In a subsequent paper, Lee et al. (2006) verified the resonant response-based leak detection technique in the laboratory. A single pulse signal was generated by a side-discharge valve to extract the experimental FRD. However, a practical challenge was that, in a short pipeline where the fundamental frequency is relatively high, the number of observable resonant peaks may be low due to the limitation in the bandwidth of the input transient signal. The power spectrum of a pulse signal drops with inverse proportionality to an increase in frequency, yielding low signal-to-noise ratio (SNR) for high frequency components. Raising the magnitude of the pulse can help increase the SNR, however, transient signals with high magnitude are not desirable in aging pipelines since they may cause damage to the system. The limitation in bandwidth also exists in other types of discrete signals, such as step transient signals that have been used by other researchers (Mpesha et al. 2002; Brunone et al. 2008).

One solution to increase the bandwidth of the excitation signal without introducing pressure variations of too high a magnitude is to use broadband and persistent signals. Lee et al. (2008a) developed a customized side-discharge valve that could generate periodic pulse sequences based on maximum-length pseudorandom binary sequences (MLBS). The MLBS is a specific type of pseudorandom binary sequence (PRBS) (Godfrey 1993), which is made up of predetermined periodic binary signals (e.g. with values being either 1 or 0). The PRBS has a wide bandwidth and its autocorrelation is similar to that of white noise, making the PRBS suitable for system identification in the frequency domain (Godfrey 1993). When applied to pipeline FRD extraction, multiple frequency responses of a pipeline can be determined simultaneously and the signal-to noise ratio (SNR) can be increased by synchronous averaging of the response periods. The customized side-discharge valve developed by Lee et al. (2008a) was used to extract the FRD of an intact pipeline in the laboratory. The valve was electronically controlled by a solenoid. When the value of the MLBS was a value of 1, a sharp pulse was generated by abruptly opening and then closing the side-discharge valve. However, because the laboratory pipeline was short (37.5 m)

and the fundamental frequency was relatively high (8.87 Hz), only the first four resonant responses were extracted.

Gong et al. (2013e) proposed an FRD-based leak detection technique that used only the first three resonant response peaks recorded in a FRD. The requirement for the bandwidth of the input signal was reduced significantly. In addition, the leak detection was based on the use of the relative sizes of these three peaks, making the technique robust and easy to implement (Gong et al. 2013e). Preliminary verification of the three-resonance-peaks-based leak detection technique was conducted by using an experimental FRD extracted by a single pulse signal as presented in Lee et al. (2006).

Recent work by Gong et al. (2011b; 2013d) demonstrated that the inverse-repeat sequence (IRS), another type of PRBS, is superior to the MLBS in minimizing nonlinear influences, and extracting the linear portion of the frequency response of a pipeline system. One period of an IRS can be obtained by doubling the period of MLBS and reversing every other digit of the doubled sequence (Godfrey 1993). As a result, the IRS is antisymmetric within one period. It is known that a valve oscillation can also excite a nonlinear response of the pipeline system, which affects the extracted FRD (Lee et al. 2002; Lee et al. 2005a). However, only the linear part of the FRD is desirable because all existing frequency response analysis techniques for pipelines are developed under linear theory assumptions. The antisymmetric property of IRS enables part of the nonlinear response of a system to be cancelled out (Godfrey 1993; Roinila et al. 2010), resulting in an experimental FRD that contains less nonlinear dynamics (Gong et al. 2013d).

The numerical findings have been verified by Gong et al. (2013c) through comparing the FRD results extracted from an intact laboratory pipeline using MLBS and IRS respectively. In Gong et al. (2013c), a dual-solenoid controlled side-discharge valve was developed to generate persistent MLBS or IRS transient signals. A reservoir-pipeline-valve (RPV) system was adopted: a pressurized tank was located at one end of the laboratory pipeline system and the dual-solenoid controlled side-discharge valve was placed at the other end

as an oscillating boundary. The opening of the valve could be shifted between fully open (when the binary signal was 1) and partially closed (when the binary signal was 0). The experimental FRD results extracted by IRS were found to be smoother and closer to the theoretical linear FRD derived from transfer matrix method when compared with the FRD extracted by the MLBS.

The focus of this paper is to develop a technique for accurate and efficient extraction of the linear portion of the FRD of a pressurized pipeline. First, a numerical analysis to study the effect of boundary valve loss on the shape of the FRD is presented. The study discusses what extent of boundary loss is appropriate for frequency-domain leak detection techniques. Then the dual-solenoid controlled side-discharge valve is applied to the extraction of the FRD of a pipeline with a leak in the laboratory. The IRS is adopted as the excitation signal and two different boundary valve losses are applied respectively for the purpose of comparison. The experimental results are used to verify the results found in the numerical analysis and also provide further verification for the three-resonance-peaks-based leak detection technique.

7.2 Effects of boundary valve loss on the shape of the frequency response diagram

The reservoir-pipeline-valve (RPV) system is traditionally used for FRD extraction and leak detection in pipelines (Mpesha et al. 2002; Lee et al. 2005b; Lee et al. 2006; Sattar and Chaudhry 2008). Three types of configuration are possible in an RPV system: (1) a RPV-Open Valve configuration, where the in-line valve is fully or predominantly open; (2) a RPV-Closed Valve configuration, where the in-line valve is fully closed; (3) a RPV-High Loss Valve configuration, where the in-line valve is slightly open.

For most existing FRD-based pipeline fault detection techniques, the frequency response at the resonant frequencies (the fundamental frequency of the tested pipeline f_{th} and its odd harmonics) is of significant interest (Lee et al. 2005b; Lee et al. 2006; Lee et al. 2008b; Gong et al. 2013e). This section

shows that the boundary condition effects on the shape of the pipeline FRD, and the RPV-High Loss Valve is the preferred configuration for extracting pipeline responses at the resonant frequencies.

7.2.1 RPV-Open Valve configuration

When the valve at the end of the pipe is fully open, an RPV-Open Valve system is obtained and it is equivalent to a Reservoir-Pipe-Reservoir (RPR) system. The middle point of the pipe is the optimal excitation and measurement location for such systems (Lee et al. 2006), where the maximum SNR can be achieved. Figure 7.1 shows the layout of a RPR system. A transient generator and a pressure transducer are located at the middle of the pipe. Different positions along the pipeline are represented by n_1 to n_4. The distance between n_2 and n_3 is assumed to be negligible, and the distance between n_1 and n_2 is the same as that between n_3 and n_4, i.e. $L_1 = L_2 = L/2$, where L is the total length of the pipeline.

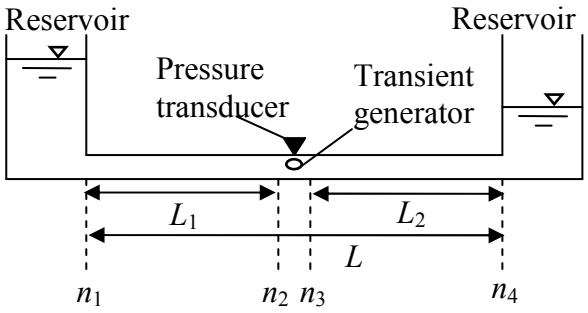

Figure 7.1 A Reservoir-Pipe-Reservoir system (which is equivalent to a RPV-Open Valve system) and the corresponding arrangement of the pressure transducer and a side-discharge valve transient generator for the extraction of the FRD

To determine the theoretical frequency response at the resonant frequencies, the pipe is assumed to be intact, uniform and frictionless. The field matrix for a section of uniform and frictionless pipe is given by Chaudhry (1987):

$$\begin{Bmatrix} q \\ h \end{Bmatrix}^{n+1} = \begin{bmatrix} \cos\left(\frac{L_i\omega}{a}\right) & -\frac{j}{Z_C}\sin\left(\frac{L_i\omega}{a}\right) \\ -jZ_C\sin\left(\frac{L_i\omega}{a}\right) & \cos\left(\frac{L_i\omega}{a}\right) \end{bmatrix} \begin{Bmatrix} q \\ h \end{Bmatrix}^{n} \tag{7.1}$$

where the superscripts $n+1$ and n represent positions in the downstream and upstream ends of the section of pipe, respectively; q and h are complex oscillatory discharge and head at either end of the pipe; L_i is the length of the ith section of pipe; ω is angular frequency; a is the wave speed; $j=\sqrt{-1}$ indicates the imaginary unit; and Z_C is the characteristic impedance of the pipe section which is defined as

$$Z_C = \frac{a}{gA} \tag{7.2}$$

where A is the cross-sectional area of the pipe section; and g is the gravitational acceleration.

Because the FRF of a pipeline system is independent of the format of the transient excitation (Lee et al. 2006), for simplicity, in the numerical study in this section, the transient source is modeled as a point where a unit discharge perturbation takes place. The point matrix of the transient source can be written as (Lee et al. 2006)

$$\begin{Bmatrix} q \\ h \end{Bmatrix}^{n3} = \begin{bmatrix} 1 & 0 \\ 0 & 1 \end{bmatrix} \begin{Bmatrix} q \\ h \end{Bmatrix}^{n2} + \begin{bmatrix} 1 \\ 0 \end{bmatrix} \tag{7.3}$$

By using the transfer matrices of all the components in the system and substituting the reservoir boundary conditions ($h_{n1}=h_{n4}=0$), the magnitude of the head oscillation at the middle point can be finally derived as

$$|h_{n2}| = \frac{1}{2} Z_C \frac{\cos\left(\frac{L\omega}{a}\right) - 1}{\sin\left(\frac{L\omega}{a}\right)} \tag{7.4}$$

It can be observed from Eq. (7.4) that, theoretically, the value of $|h_{n2}|$ equals infinity when ω reaches the fundamental angular frequency of a RPR system ($\pi a / L$) and its odd harmonics (the resonant frequencies). If the effect of friction is included, the head responses at the resonant frequencies will not be infinite but will have large values and appear as sharp spikes in the FRD [an example of the experimental FRD of a RPR system is given by Fig. 15 in Lee et al. (2006)]. It is difficult to determine the peak value of a resonant response accurately, as a very high resolution in the frequency domain is required to insure that the frequency responses, at or close to the sharp resonance peaks, are sampled. In addition, in real applications it may be difficult to access the optimal excitation and measurement location, that is, the middle of the pipe. As a result, the RPV-Open Valve (equivalent to RPR) configuration is not a desirable configuration for pipeline FRD extraction from a practical point of view.

7.2.2 RPV-Closed Valve configuration

Figure 7.2 illustrates a RPV system where an in-line valve is located at the downstream end. A transient generator and a pressure transducer are located at the upstream face of the in-line valve. The overall length of this pipeline is L. Different positions along the pipeline are represented by n_1 to n_4.

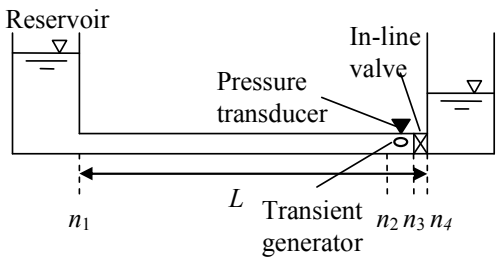

Figure 7.2 A Reservoir-Pipeline-(in-line) Valve (RPV) system and the corresponding arrangement of the pressure transducer and a side-discharge valve transient generator for the extraction of the FRD. When the in-line valve is fully closed, it forms a RPV-Closed Valve configuration; when the in-line valve is slightly open, it forms a RPV-High Loss Valve configuration

When the in-line valve is fully closed, it forms a RPV-Closed Valve system. Using the transfer matrix method (Chaudhry 1987), the magnitude of the head oscillation on the upstream side of the valve can be derived as

$$\left|h_{n3}\right| = Z_C \tan\frac{L\omega}{a} \tag{7.5}$$

Similarly as for the RPV-Open Valve configuration, challenges exist in the determination of the FRD for a RPV-Closed Valve configuration. Because the fundamental angular frequency for a RPV system is $\omega_{th} = 2\pi f_{th} = \pi a/(2L)$ (where f_{th} is the fundamental frequency), theoretically Eq. (7.5) is infinite when ω reaches any of the resonant frequencies (ω_{th} and its odd harmonics). In real pipelines where pipe friction and other losses exist, head responses at resonant frequencies will not be infinite but will still have large values and appear as sharp spikes in the FRD. Once again, a very high resolution in the frequency domain is required to ensure that the frequency responses at or close to the sharp peaks are sampled. An example of the experimental FRD determined from a RPV-Closed Valve configuration is given in Fig. 17 in Lee et al. (2006).

7.2.3 RPV-High Loss Valve configuration

An alternative to the RPV-Closed Valve configuration is a RPV-High Loss Valve configuration. This configuration can be achieved when the in-line valve shown in Figure 7.2 is slightly open (rather than fully closed) to introduce a high loss at the boundary. The transfer matrix for a high loss in-line valve can be written as (Lee et al. 2006)

$$\begin{Bmatrix} q \\ h \end{Bmatrix}^{n4} = \begin{bmatrix} 1 & 0 \\ -Z_V & 1 \end{bmatrix} \begin{Bmatrix} q \\ h \end{Bmatrix}^{n3} \tag{7.6}$$

where $Z_V = 2\Delta H_{V0} / Q_{V0}$ is defined as the impedance of the in-line valve; and ΔH_{V0} and Q_{V0} are the steady-state head loss across and the flow through the valve, respectively. By using the boundary conditions ($h_{n1} = h_{n4} = 0$), the transfer matrices of the pipe [Eq. (7.1)], the transient generator [Eq. (7.3)] and the in-line valve [Eq. (7.6)], finally the magnitude of the head oscillation at the end of the pipe yields

$$\begin{Bmatrix} q \\ h \end{Bmatrix}^{n4} = \begin{bmatrix} 1 & 0 \\ -Z_V & 1 \end{bmatrix} \begin{Bmatrix} q \\ h \end{Bmatrix}^{n3} \tag{7.7}$$

When ω is located at $\omega_{th} = \pi a / (2L)$ and its odd harmonics, the results of Eq. (7.7) are always equal to Z_V. As a result, the magnitude of the resonant response is controllable in real world applications by the steady-state opening of the in-line valve. In addition, numerical modeling has shown that, with proper values of Z_V, the frequency response around the resonant frequencies can be rounded rather than sharp (as will be shown in the following section). As a result, the frequency responses adjacent to a resonant frequency are close to the resonant response, and the estimation for the resonant response can be robust and accurate even when the resolution in the frequency domain is relatively low. In summary, the RPV-High Loss Valve configuration is suitable for extracting the pipeline FRD in practice.

7.3 Appropriate values of valve impedance for leak detection

This section presents a study of the appropriate values of Z_V for extracting the resonant response of a pipeline with a leak in a RPV-High Loss Valve configuration. An oscillating in-line valve is used as the transient generator, in which the mean dimensionless valve opening size is τ_0 and the magnitude of the dimensionless perturbation in the valve opening is $\Delta\tau$. It is typically assumed that the dimensionless valve opening remains at τ_0 in the steady state (before the oscillation), where Z_V is the steady-state impedance of the oscillating valve. The transfer matrix for an oscillating valve can be written as (Lee et al. 2005b)

$$\begin{Bmatrix} q \\ h \end{Bmatrix}^{n+1} = \begin{bmatrix} 1 & 0 \\ -Z_V & 1 \end{bmatrix} \begin{Bmatrix} q \\ h \end{Bmatrix}^{n} + \begin{Bmatrix} 0 \\ \dfrac{2\Delta H_{V0}\Delta\tau}{\tau_0} \end{Bmatrix} \tag{7.8}$$

where ΔH_{V0} is the steady-state head loss across the valve.

The transfer matrix for a leak can be written as (Lee et al. 2002; Lee et al. 2005b)

$$\begin{Bmatrix} q \\ h \end{Bmatrix}^{n+1} = \begin{bmatrix} 1 & -\dfrac{1}{Z_L} \\ 0 & 1 \end{bmatrix} \begin{Bmatrix} q \\ h \end{Bmatrix}^{n} \tag{7.9}$$

where $Z_L = 2H_{L0}/Q_{L0}$ is the impedance of the leak, and Q_{L0} and H_{L0} are the steady-state discharge through and the steady-state head across the leak.

By combining the transfer matrices of the pipe [Eq. (7.1)], the oscillating valve [Eq. (7.8)] and the leak [Eq. (7.9)] using the transfer matrix method, the expression for the head fluctuation at the upstream face of the valve can be

obtained (Lee et al. 2005b). The magnitude of the head fluctuation can be non-dimensionalized by dividing it by the active input $2\Delta H_{V0}\Delta\tau/\tau_0$. The impedance of the oscillating valve and the leak can be non-dimensionalized by dividing them by the characteristic impedance of the pipe (Z_C). From previous research conducted by the authors (Gong et al. 2013b), the theoretical dimensionless head fluctuation for a frictionless pipeline with a leak can be written as

$$h^* = \frac{-1}{1 - Z_V^* \dfrac{\cos\left(\omega_r \dfrac{\pi}{2}\right) + j(Z_L^*)^{-1}\sin\left(\omega_r \dfrac{\pi}{2} x_L^*\right)\cos\left(\omega_r \dfrac{\pi}{2}(1-x_L^*)\right)}{(Z_L^*)^{-1}\sin\left(\omega_r \dfrac{\pi}{2} x_L^*\right)\sin\left(\omega_r \dfrac{\pi}{2}(1-x_L^*)\right) - j\sin\left(\omega_r \dfrac{\pi}{2}\right)}} \tag{7.10}$$

where h^* is the dimensionless head fluctuation at the upstream face of the oscillating valve; $Z_V^* = Z_V/Z_C$ and $Z_L^* = Z_L/Z_C$ are the dimensionless impedance of the valve and the leak; $\omega_r = \omega/\omega_{th}$ is the dimensionless angular frequency; and $x_L^* = x_L/L$ is the dimensionless leak location downstream from the reservoir (x_L is the distance between the leak and the reservoir).

From Eq. (7.10), Gong et al. (2013b) found that a leak can introduce sinusoidal patterns on both resonant responses ($\omega_r = 1, 3, 5\cdots$) and anti-resonant responses ($\omega_r = 2, 4, 6\cdots$). The amplitude of the leak-induced pattern at the odd harmonics and that at the even harmonics are related to the value of Z_V^*. The former is proportional while the latter is inversely proportional to the value of Z_V^*. When the value of Z_V^* equals unity, the amplitude values of the two leak-induced sinusoidal patterns are the same. Because the leak-induced pattern in the odd harmonics is significant for leak detection, the value of Z_V^* should be greater than unity, so that the leak-induced pattern in the odd harmonics is more evident.

The research presented in his paper demonstrates that, in addition to the effects on the amplitude of the leak-induced pattern, the value of dimensionless impedance of the valve Z_V^* also affects the shape of the FRD. A greater value of Z_V^* can lead to a sharper pattern in the resonant response and a smoother pattern around the anti-resonant frequencies. However, to ensure that the resonant peaks can be accurately determined in practice, the resonant response should not be too sharp. As a result, the value of Z_V^* should not be too large.

Numerical simulations have been conducted to verify the above findings. The non-dimensional FRDs of an RPV system with a leak are presented in Figure 7.3 with respect to various values of Z_V^*. The leak has a dimensionless impedance of $Z_L^* = 10$ and the leak is located at a dimensionless location of $x_L^* = 0.3$ downstream from the reservoir. It can be seen from Figure 7.3 that as the value of Z_V^* increases, the amplitude of the leak-induced sinusoidal pattern at the resonant frequencies increases, but the curve of the FRD around resonant frequencies becomes sharper.

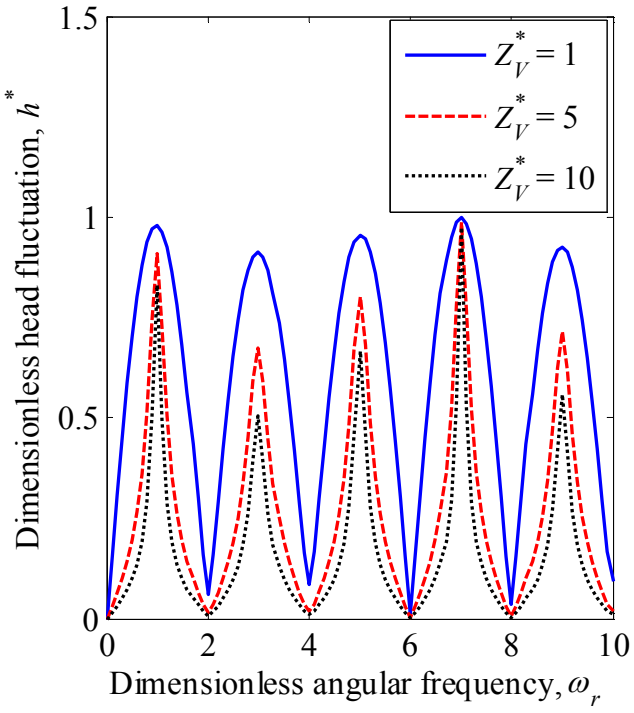

Figure 7.3 Dimensionless frequency response diagrams (FRDs) of a RPV system with a leak ($Z_L^* = 10$, $x_L^* = 0.3$). The shape of the FRD changes with the value of the dimensionless valve impedance Z_V^*

In summary, a greater value of Z_V^* results in a more obvious leak-induced pattern at the resonant frequencies (i.e. a greater amplitude), but if the value of Z_V^* is too large (for example, ≥ 10, as a guideline), the loss introduced by the throttled valve is so high that it behaves in a similar way to a RPV-Closed Valve system (i.e. the resonant responses have sharp spikes and it is difficult to determine accurately in practice). Consequently, it is suggested that the optimal range of Z_V^* for pipelines with a RPV-High Loss Valve configuration is between 1 and 10. In real applications, the specific value of Z_V^* should be evaluated case by case to provide the most appropriate shape of the FRD.

7.4 Extraction of the FRD of a pipe with a leak using a dual-solenoid controlled side-

discharge valve and inverse-repeat sequences

The preceding numerical analysis sheds light on how to choose the appropriate system configuration and the boundary loss for FRD extraction in real pipelines. Laboratory experiments have been conducted in the Robin Hydraulics Laboratory at the University of Adelaide to verify the numerical findings. While oscillating an in-line valve is difficult in real pipelines, the dual-solenoid controlled side-discharge valve developed in Gong et al. (2013c) has been used as the transient generator for the results presented in this paper.

The system layout of the experimental system is given in Figure 7.4. The experimental pipeline is a copper pipeline with a length (L) of 37.53 m and an internal diameter of 0.022 m ($A = 3.8\times10^{-4}$ m^2). The fundamental frequency of the pipeline (f_{th}) is 8.85 Hz measured by experiments. A pressurized tank with a pre-set head of 38.50 m is located at one end of the pipeline and a fully closed in-line valve is at the other end. The in-line valve has an elevation of 2 m above the upstream end of the pipeline. At 145 mm upstream from the closed in-line valve, a pressure transducer and the dual-solenoid controlled side-discharge valve were installed. The dual-solenoid side-discharge valve was used as the transient generator and the opening of the side-discharge valve could oscillate between fully open and partially closed. As a result, the pipeline system had a *RPV-High Loss Valve* configuration. A free discharging orifice with a diameter of 2 mm was located at 31.21 m downstream from the reservoir to simulate the leak, thus the actual dimensionless leak location was $x_L^* = 0.8316$. The equivalent opening (i.e., the area of the emitter times the coefficient of discharge) of the simulated leak was calibrated as 2.333×10^{-6} m^2 in the steady-state.

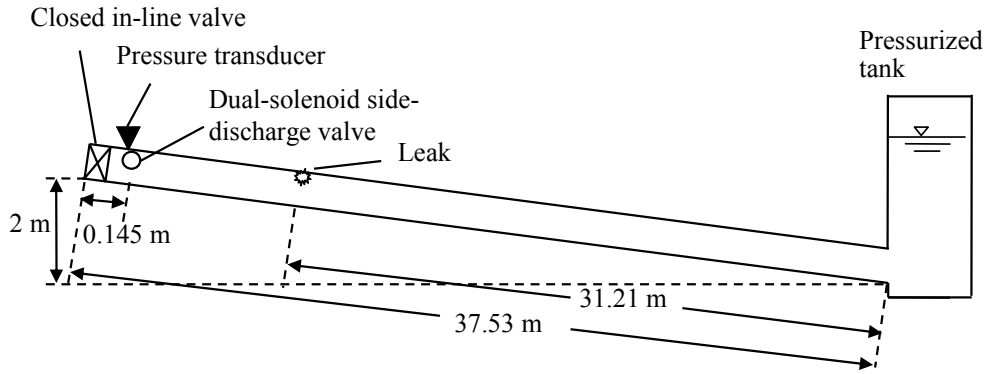

Figure 7.4 The system layout of the experimental pipeline

The dual-solenoid controlled side-discharge valve includes a brass block with a small diameter hole (2 mm at the minimum cross-section) drilled through the long axis forming the conduit. A metal rod vertical to the conduit was used to control the opening, and two solenoids aligned with the rod were used to drive it. The calibrated equivalent opening of the side-discharge valve was 2.7×10^{-6} m^2 when fully open. The two solenoids were controlled by an external signal generator that produces inverse-repeat sequence (IRS) (Godfrey 1993). The rod was also connected with a linear voltage displacement transducer (LVDT) to measure its movement during the transient event.

The external signal generator uses a 10-stage shift register to generate the IRS. The clock frequency used to drive the shift register is f_c = 100 Hz. As a result, the IRS-based transient excitation has a period of 20.46 s (with 2046 binary digits in one period), and a bandwidth of 44.3 Hz (0.443 f_c, at which frequency the power of the input drops to half the maximum). The IRS-based input signal enables the first three resonant responses of the laboratory pipeline to be extracted with reasonable signal-to-noise ratio. A detailed description of this customized device and examples of the experimental IRS-based transient excitation can be found in Gong et al. (2013c).

Two case studies have been conducted, with a low and a high dimensionless impedance (Z_V^*) of the dual-solenoid controlled side-discharge valve respectively. The steady-state impedance of the side-discharge valve cannot be used as Z_V since the valve was fully open in the steady state rather than kept at the mean opening. In this research, Z_V is defined as

$$Z_V = \frac{2\bar{H}_V}{\bar{Q}_V} \tag{7.11}$$

where $\bar{H}_V$ and $\bar{Q}_V$ are the mean head and discharge at the side-discharge valve when steady oscillatory flow has been established. $\bar{H}_V$ can be calculated from the pressure transient data measured by the transducer, and $\bar{Q}_V$ can be obtained using volumetric method. Once the value of Z_V is determined, the dimensionless valve impedance Z_V^* can then be calculated. In the laboratory, the value of Z_V can be changed by adjusting the magnitude of the valve oscillation.

The values of Z_V^* for the two case studies conducted in this research were 2.85 and 5.50 respectively, which were the lowest and greatest Z_V^* values achievable by the dual-solenoid controlled side-discharge valve. The dimensionless impedance for the leak was determined as Z_L^* = 3.22 in the steady state. The experimental FRD results for these two case studies are given in Figure 7.5 (only for the first three resonant responses). In order to compare the two experimental FRD results, each FRD was normalized by dividing the frequency responses by the value of the first resonant peak.

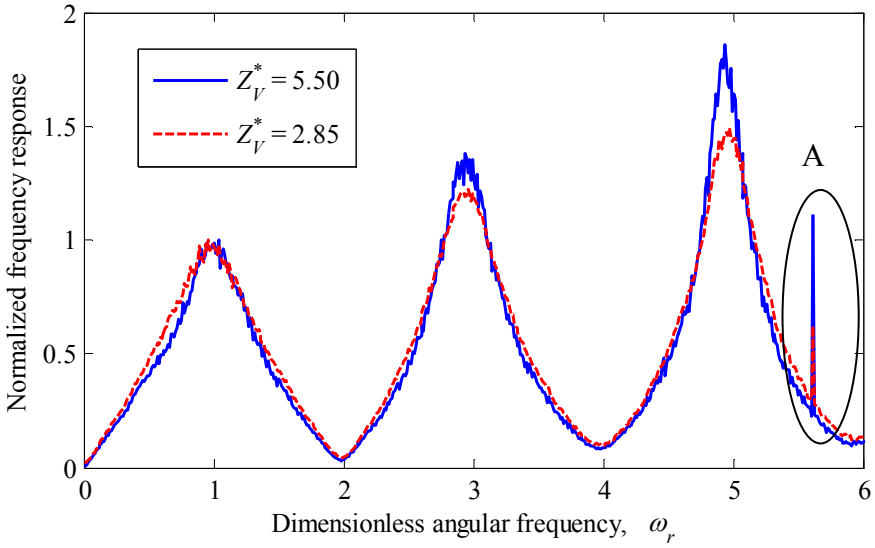

Figure 7.5 Normalized frequency response diagrams (including the first three resonant peaks) for the experimental pipeline. The peak at A is the result of low signal-to-noise ratio at the frequency of 0.5 f_c (i.e. 50 Hz in this experiment), where the theoretical power of the IRS is zero

The experimental FRD results shown in Figure 7.5 demonstrate that the experiment with the greater valve impedance value (Z_V^* = 5.50) yields greater leak-induced pattern but sharper resonant peaks. The experimental results are consistent with the numerical findings presented in previous sections. The spikes located between ω_r = 5 and 6 are the result of low signal-to-noise ratio at the frequency of 0.5 f_c (i.e. 50 Hz in this experiment), where the theoretical power of the IRS is zero (Godfrey 1993).

7.5 Estimation of the location and impedance of the leak using the three resonant responses-based technique

The FRD result of the laboratory pipe with a leak also provides valuable experimental data to further verify the three resonant responses-based leak detection technique proposed in Gong et al. (2013e). This leak detection

technique has been verified by using an experimental FRD extracted from a laboratory pipeline with a single leak in the *RPV-Closed Valve* configuration (Gong et al. 2013e). This paper presents verification using the FRD measured under the *RPV-High Loss Valve* configuration.

Once the first three resonant responses of a pipeline with a single leak have been extracted, the dimensionless leak location can be estimated by using Eq. (7.12) (Gong et al. 2013e):

$$x_L^* = \frac{1}{\pi} arc\cos\left(\pm\frac{1}{2}\sqrt{1+\frac{\left(|h|_5^*-1\right)|h|_3^*}{\left(|h|_3^*-1\right)|h|_5^*}} \right) \tag{7.12}$$

where $|h|_3^*$ and $|h|_5^*$ are the values of the normalized frequency responses at the third and the fifth harmonics of the fundamental frequency of the pipeline. The normalization is achieved by dividing the dimensional values of frequency response by the dimensional response at the first harmonic (which is same as the normalization used in Fig. 5). Two values of x_L^* can be obtained from Eq. (7.12) for a specific FRD. They are two symmetric possible leak locations along the pipe, since the summation of these two x_L^* values is unity. However, only one x_L^* value indicates the real leak location, while the other one is not a real location. The location of wrong leak position can be eliminated by comparing the normalized resonant responses $|h|_3^*$ with unity. When $|h|_3^* < 1$, the leak is located within the range of $x_L^* \in (0, 0.5)$, while when $|h|_3^* > 1$, the leak is located within $x_L^* \in (0.5, 1)$.

The impedance of the leak can also be estimated when the location of the leak has been determined. The equation for the dimensionless leak impedance can be written as (Gong et al. 2013e)

$$Z_L^* = \frac{Z_V^*}{2}\frac{|h|_3^*\left[\cos(3\pi x_L^*)-1\right]-\left[\cos(\pi x_L^*)-1\right]}{|h|_3^*-1} \tag{7.13}$$

The values of the normalized frequency responses at the third and the fifth harmonics can be read from Fig. 5. Then the dimensionless location and dimensionless impedance of the leak can be estimated from Eqs (7.12) and (7.13). The experimental values of $|h|_3^*$ in both cases are greater than unity, indicating that the leak is located within the range $x_L^* \in (0.5,1)$. The results of the estimated dimensionless location and impedance of the leak are summarized in Table 7.1.

Table 7.1 Experimental results for leak location and size estimation.

Case	Z_V^*	$\|h\|_3^*$	$\|h\|_5^*$	Experimental x_L^*	Relative error in location[a]	Experimental Z_L^*	Relative error in impedance[b]
1	2.85	1.222	1.494	0.8172	1.44%	5.15	59.9%
2	5.50	1.383	1.858	0.8042	2.74%	5.81	80.4%

[a]Relative error in location = |Experimental x_L^* - Real x_L^* |×100%, Real x_L^* = 0.8316

[b]Relative error in impedance = |Experimental Z_L^* - Steady-state Z_L^* |/ Steady-state Z_L^* ×100% , Steady-state Z_L^* = 3.22

It can be seen from Table 7.1 that the location of the leak has been estimated with good accuracy for both case studies, with an error of 1.44% and 2.74% of the total length of the pipeline respectively. The results verify that the three resonant responses-based leak detection technique can accurately locate a single leak in a pipeline with *RPV-High Loss Valve* configuration. Significant discrepancies have been observed between the experimentally estimated values and the steady-state value for the dimensionless impedance of the leak. The experimental results are much higher, which indicates that the size of the

leak is under-estimated. However, the magnitude of the discrepancy is as expected. The numerical studies conducted in Gong et al. (2013e) demonstrated that significant error in the estimated leak size could be encountered when the leak is located within $x_L^* \in (0.5,1)$ [see Fig. 6 in Gong et al. (2013e)]. Nevertheless, in practice it is more important to detect the existence of a leak and accurately estimate its location, rather than accurately estimating the leak rate.

An interesting finding is that the experiment with the greater valve impedance (Z_V^* = 5.50), thus more evident leak-induced pattern, yields less accurate estimation of the dimensionless leak location and impedance. This is because that the experimental FRD extracted with Z_V^* = 5.50 contains more significant nonlinear dynamics within the system than the FRD obtained with Z_V^* = 2.85. In order to obtain a greater value of Z_V^* in an oscillating valve, the mean valve opening has to be reduced. Since the customized side-discharge valve can only oscillate from fully open to partially closed, the greatest Z_V^* (5.50) was achieved when the valve opening was oscillating between fully open and almost fully closed. As greater valve oscillation introduces a more significant nonlinear response (Lee et al. 2002; Lee et al. 2005a; Gong et al. 2013d), the experiment with Z_V^* = 5.50 actually involved the greatest nonlinearity that could be excited in the laboratory system by the customized side-discharge valve transient generator.

7.6 Conclusions

This paper presents a new technique for the extraction of the frequency response diagram (FRD) of a fluid-filled pipeline. Numerical and experimental studies on how boundary losses affect the shape of the FRD have been conducted. It has been found that the reservoir-pipeline-high loss valve (*RPV-High Loss Valve*) configuration is the most suitable configuration for FRD extraction in real pipelines, since the size and shape of the FRD are controllable through the adjustment of the valve impedance. A greater

dimensionless valve impedance (Z_V^* , at the mean opening) can lead to a sharper FRD. The range between 1 and 10 is suggested for Z_V^* if an oscillating valve is used as the transient generator. When Z_V^* is properly adjusted based on the specific configuration of the system under test, the frequency responses around the resonant frequencies can be rounded, i.e. the frequency responses adjacent to a resonant frequency are close to the resonant response. As a result, the estimation of the resonant responses can be robust and accurate even when the resolution in the frequency domain is relatively low.

Frequency response diagrams (FRDs) of a laboratory pipeline with a leak have been extracted by using a customized dual-solenoid controlled side-discharge valve as the transient generator. The opening of the customized side-discharge valve is controllable and can oscillate between two positions (fully open and partially close). The inverse repeat sequence (IRS) was adopted as the excitation signal in the experiments. The IRS has a broad bandwidth so that multiple frequency responses can be extracted simultaneously. The persistency and periodicity of IRS enhance the signal-to-noise ratio (SNR) and its antisymmetric property suppresses part of the nonlinear response of the pipeline system. The side-discharge valve also forms the high loss boundary condition, in which the impedance of the valve is adjustable. Two sets of laboratory experiments have been conducted, with a low (2.85) and a high (5.50) dimensionless valve impedance respectively. The experiment with the greater valve impedance yields greater leak-induced pattern but sharper FRD around resonant frequencies. The experimental results are consistent with the results of the preceding numerical study.

The three resonant responses-based leak detection technique developed in Gong et al. (2013e) has been used to determine the location and impedance of the leak from the experimental FRDs. The dimensionless location of the leak has been determined successfully from both sets of experiments, with an error of 1.44% and 2.74% of the total length of the pipeline respectively. The dimensionless impedance of the leak has also been estimated, however, with

significant error. As a result, the size of the leak could not be accurately estimated. The experiments conducted in this research have verified that the three resonant responses-based leak detection technique is applicable in pipelines with *RPV-High Loss Valve* configuration.

Acknowledgements

The research presented in this paper has been supported by the Australia Research Council through the Discovery Project Grant DP1095270. The authors thank technicians Brenton Howie, Simon Order and Stan Woithe in the Robin Hydraulics Laboratory in the University of Adelaide for their support in the design and fabrication of the dual-solenoid controlled side-discharge valve.

Notations

The following symbols are used in this paper:

A = cross sectional area of a pipe;

a = wave speed;

f_c = clock frequency driving the shift register;

f_{th} = fundamental frequency of a pipeline system;

g = gravitational acceleration;

H_{L0} = steady-state head at a leak orifice;

$\bar{H}_V$ = mean head at an oscillating valve;

h = complex head amplitude;

h^* = dimensionless head fluctuation;

$|h|_1$, $|h|_3$, $|h|_5$ = amplitude of the head oscillation at the first, the third and the fifth harmonics;

j = imaginary unit, $\sqrt{-1}$;

L = total length of pipe;

L_1, L_2 = lengths of the two pipe sections on either side of a

leak;

$n_i, i = 1, 2, 3 \cdots$ = different positions along a pipeline;

Q_{L0} = steady-state flow out of a leak;

Q_{V0} = steady-state flow through a valve;

$\bar{Q}_V$ = mean discharge through an oscillating valve;

q = complex discharge amplitude;

x_L, x_L^* = location and dimensionless location of a leak;

Z_C = characteristic impedance of a frictionless pipe;

Z_L, Z_L^* = impedance and dimensionless impedance of a leak orifice;

Z_V, Z_V^* = impedance and dimensionless impedance of a valve;

Greek symbols:

ΔH_{V0} = steady-state head loss across a valve;

$\Delta\tau$ = amplitude of the dimensionless valve-opening oscillation;

τ_0 = mean dimensionless valve-opening coefficient, center of oscillation;

ω, ω_r = angular frequency and dimensionless relative angular frequency;

ω_{th} = fundamental angular frequency of a pipeline system;

Chapter 8

Detection of Distributed Deterioration in Single Pipes Using Transient Reflections (Journal Publication 6)

[1]Gong, J., [1]Simpson, A. R., [1]Lambert, M. F., [1]Zecchin, A. C., [1]Kim, Y., and [2]Tijsseling, A. S. (2013).

[1]School of Civil, Environmental and Mining Engineering, the University of Adelaide, Adelaide, SA 5005 Australia

[2]Department of Mathematics and Computer Science, Eindhoven University of Technology, The Netherlands

Journal of Pipeline Systems Engineering and Practice, 4(1), 32-40.

Statement of Authorship

Title of Paper	Detection of Distributed Deterioration in Single Pipes using Transient Reflections
Publication Status	Published
Publication Details	Gong, J., Simpson, A. R., Lambert, M. F., Zecchin, A. C., Kim, Y., and Tijsseling, A. S. (2013). "Detection of distributed deterioration in single pipes using transient reflections." *Journal of Pipeline Systems Engineering and Practice*, 4(1), 32-40.

Author Contributions

By signing the Statement of Authorship, each author certifies that their stated contribution to the publication is accurate and that permission is granted for the publication to be included in the candidate's thesis.

Name of Principal Author (Candidate)	Jinzhe Gong		
Contribution to the Paper	Developed and implemented the methodology, designed and conducted numerical simulations, interpreted and analysed results, prepared manuscript and acting as the corresponding author.		
Signature		Date	25/09/2013

Name of Co-Author	Angus Simpson		
Contribution to the Paper	Supervised development of work, helped to evaluate and edit the manuscript.		
Signature		Date	25/9/2013

Name of Co-Author	Martin Lambert		
Contribution to the Paper	Helped to evaluate and edit the manuscript.		
Signature		Date	25/9/13

Name of Co-Author	Aaron Zecchin		
Contribution to the Paper	Helped to evaluate and edit the manuscript.		
Signature		Date	1.10.2013

Name of Co-Author	Young-il Kim		
Contribution to the Paper	Conducted laboratory experiments.		
Signature		Date	25 Sep 2013

Name of Co-Author	Arris Tijsseling		
Contribution to the Paper	Helped to evaluate and edit the manuscript.		
Signature		Date	2/10/2013

Abstract

A number of different methods that use signal processing of fluid transients (water hammer waves) for fault detection in pipes have been proposed in the last two decades. However, most of them focus solely on the detection of discrete deterioration, such as leaks or discrete blockages. Few studies have been conducted on the detection of distributed deterioration, such as extended sections of corrosion and extended blockages. This is despite the fact that they commonly exist and can have a severe negative impact on the operation of pipelines. The research reported here proposes a method of detecting distributed deterioration by investigating the time-domain water hammer response trace from a single pipe with a deteriorated section. Through wave analysis using a step pressure input, a theoretical square-shaped perturbation is found to exist in the transient pressure trace as a result of distributed deterioration. The hydraulic impedance of this section can be derived from the magnitude of the reflected pressure perturbation, while the location and length of the corresponding deteriorated section can be determined by using the arrival time and duration of the perturbation. The proposed method has been validated by analyzing experimental data measured from a pipe with a section of wall thickness change.

8.1 Introduction

In the last two decades, a number of transient-based fault detection methods have been developed for water transmission pipelines (Colombo et al. 2009). Transient-based methods are promising and attractive because they are non-invasive, simple to perform and can provide information about a lengthy section of pipe (hundreds to thousands of meters). While most transient-based fault detection methods focus on the detection of discrete elements, such as leaks (Wang et al. 2002; Lee et al. 2005b; Lee et al. 2007b) and discrete (partial) blockages (Vítkovský et al. 2003b; Lee et al. 2008b), the detection of distributed elements has not attracted much attention. However, distributed deterioration, such as extended corrosion or blockages (Arbon et al. 2007), cement mortar lining spalling (Stephens et al. 2008), and pipeline sections with a lower pressure rating (mistakenly installed), sometimes exist in real pipelines and impose negative impacts on the operation of fluid transmission. According to a previous field study in South Australia (Stephens et al. 2008), sections with significant cement mortar lining spalling and internal corrosion, typically with a length around 10 meters each, were observed intermittently along the water transmission pipeline that was tested. Distributed deterioration can reduce water transmission efficiency (Tran et al. 2010), create water quality problems (Vreeburg and Boxall 2007), and critically, may also develop into bursts or severe blockages over time (Zamanzadeh et al. 2007). Techniques for the non-invasive detection of distributed deterioration are required.

The current paper presents a transient-based distributed deterioration detection method for single water transmission pipelines based on time-domain reflectometry (TDR) (Lee et al. 2007a). An incident wave is assumed to propagate along a pipeline that has a section of distributed deterioration, in which the hydraulic impedance is different from the impedance of other parts of the pipeline. The pressure transient trace of this pipeline is measured at the point of generation of the incident wave. The process of the wave propagating through the deteriorated section is analyzed using the method of

characteristics (MOC) (Wylie and Streeter 1993). The analysis illustrates that the properties of the distributed deterioration can be determined from the theoretical square-shaped perturbation in the measured pressure trace. Experimental verification of the proposed distributed deterioration detection method is performed by analyzing the data gathered from a pipeline with a section exhibiting changes in wall thickness. The impedance, wall thickness, wave speed, location and length of this section are successfully estimated.

8.2 Background

The physical foundation of the proposed TDR-based distributed deterioration detection method is presented here. A distributed deterioration in a single pipeline introduces an extended hydraulic impedance change. Reflections occur when a transient wave comes across impedance discontinuities, which are the boundaries of the distributed deterioration. The reflected signals are dependent on the location, length and hydraulic impedance of the deteriorated section, and so are indicators of the deterioration.

The characteristic impedance B of a uniform pipeline is defined as

$$B = a / (gA) \tag{8.1}$$

where a is the wave speed of the transient wave; A is the internal cross-sectional area of the pipeline; and g is the gravitational acceleration. The impedance is sensitive to the pipeline wall thickness. A change in wall thickness affects not only the internal cross-sectional area but it also affects the wave speed, where the wave speed and wall thickness are related by the wave speed formula (Wylie and Streeter 1993):

$$a = \sqrt{\frac{K / \rho}{1 + (K / E)(D / e)c_1}} \tag{8.2}$$

in which, K is the bulk modulus of the transmitted fluid; ρ is the density of the fluid; E is Young's modulus of the wall material; D is the internal diameter of the pipeline; e is the wall thickness; c_1 is an uncertain factor close to 1, depending on the structural restraint condition of the pipeline (Wylie and Streeter 1993).

The chemical and physical mechanisms of material deterioration, such as corrosion, tuberculation and graphitization, in water distribution pipelines are complex (Rajani and Kleiner 2001; Sarin et al. 2001; Nawrocki et al. 2010). However, when a section of extended corrosion or blockage is present, generally the wall thickness is changed. Young's modulus may also alter due to changes in the pipe wall material. All of these factors may lead to a change in the hydraulic impedance of the pipeline according to Eqs (8.1) and (8.2). For example, assuming that the bulk modulus of water and Young's modulus of the pipe wall remain constant, then according to Eq. (8.2), a thinner wall thickness due to internal corrosion results in a slightly larger internal diameter and a smaller wave speed, thereby yielding a smaller value of characteristic impedance. Similarly, a higher impedance value is expected if the wall becomes thicker.

In real pipes, the distribution and pattern of deterioration can be complex. For simplicity, this paper only considers uniformly distributed deterioration, i.e. sections with uniform anomalous impedance existing in a single pipeline.

8.3 Wave propagation analysis

The behavior of a transient wave propagating without attenuation through a deteriorated section with a lower impedance value is analyzed using the MOC. The process of wave reflection and transmission at the boundaries of the deteriorated section is illustrated in Figure 8.1. The two vertical solid lines in the pipeline stand for the two boundaries (interfaces) of the deterioration. The hydraulic impedance of the deteriorated section is B_1 and the impedance of the original pipeline is B_0 . Four wave propagating stages, and

corresponding hydraulic grade lines (HGLs), at different time stages are displayed.

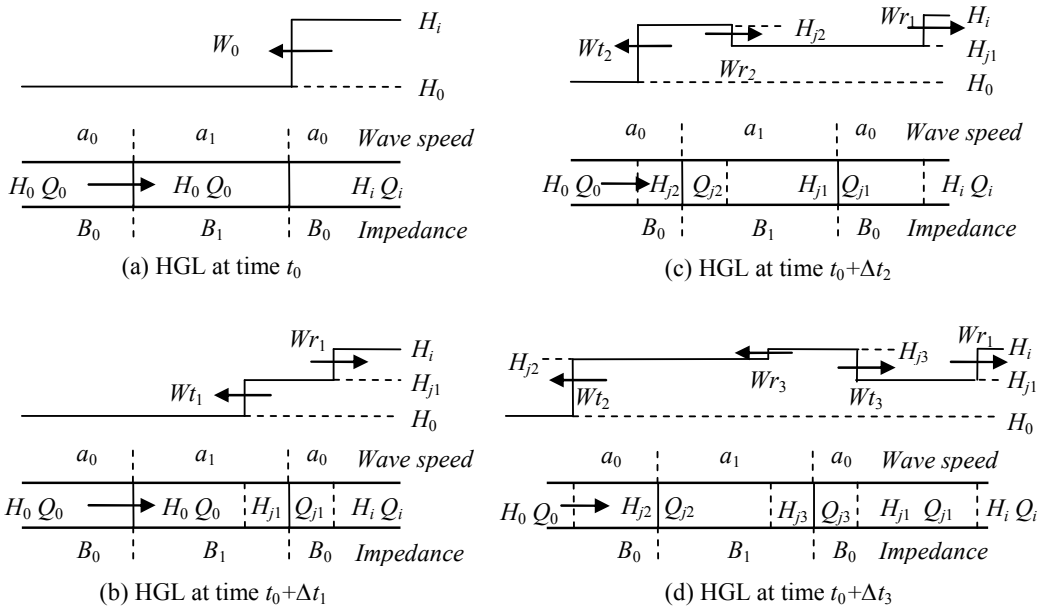

Figure 8.1 Wave propagating through a deteriorated section (designated with length L_1, impedance B_1, and wave speed a_1): (a) a step incident wave is approaching the deterioration from the right side; (b) the first reflection and transmission occur at the right boundary of the deterioration; (c) the second reflection and transmission occur at the left boundary of the deterioration; (d) the third reflection and transmission occur at the right boundary of the deterioration.

In Figure 8.1(a), the steady-state head is H_0 and the steady-state flow rate is Q_0, discharging from left to right. An incident wave W_0 with a magnitude of H_i is approaching the first interface (the right boundary) from the right side. In Figure 8.1(b), the first reflection occurred at the first interface. Part of the wave is reflected as W_{r1} and the remainder is transmitted as W_{t1}. Based on the MOC analysis of pipelines in series performed by Wylie (1983), three compatibility equations can be used to describe the wave reflection and transmission at the right boundary:

$$H_{j1} = H_0 + B_1 Q_0 - B_1 Q_{j1} \tag{8.3}$$

$$H_{j1} = H_i - B_0 Q_i + B_0 Q_{j1} \tag{8.4}$$

$$H_i = H_0 + B_0 Q_0 - B_0 Q_i \tag{8.5}$$

where H_{j1} and Q_{j1} are the head and flow after the first reflection and transmission. Solving the above equations for H_{j1} and Q_{j1} yields:

$$H_{j1} = H_0 + \frac{2B_1}{B_0 + B_1}(H_i - H_0) \tag{8.6}$$

$$Q_{j1} = Q_0 + \frac{2B_0}{B_0 + B_1}(Q_i - Q_0) \tag{8.7}$$

Eq. (8.6) illustrates the fact that the value of the head after the first reflection, H_{j1}, is dependent on the values of B_0 and B_1. Provided the deterioration has a lower impedance value than the original pipe (i.e. $B_1 < B_0$), the value of H_{j1} will be smaller than the value of the original incident wave head H_i. A step drop will occur in the HGL. The transmitted wave W_{t1} will be reflected again at the second boundary (left boundary) of the deteriorated section [see Figure 8.1(c)]. When W_{t1} is propagating from the low impedance section to the high impedance section, the value of the head after reflection and transmission, H_{j2}, will be higher than H_{j1}. Similarly, when the second reflected wave, W_{r2}, comes across the first boundary, the head will increase again [see Figure 8.1(d)]. A step rise will be observed in the HGL.

After the three steps, a head perturbation with a square shape will propagate along the pipeline. The head value of the perturbation wave is H_{j1} and the wave duration is the time required by the transient wave to travel twice the length of the deteriorated section

$$T_1 = 2L_1 / a_1 \tag{8.8}$$

where L_1 is the length of the anomalous deteriorated section and a_1 is the wave speed along this section. If the incident wave started from the measurement station (the location of the transducer) at time zero, the arrival time of the head perturbation is:

$$T_0 = 2L_0 / a_0 \tag{8.9}$$

where L_0 is the length between the transducer and the first encountered boundary of the deteriorated pipe section; and a_0 is the wave speed in the original intact pipeline.

8.4 Distributed deterioration detection procedures

Two distributed deterioration detection procedures with different detection configurations can be developed based on the previous wave propagation analysis. One procedure is used for detecting deterioration based on a transient generator and a pressure transducer located at a closed end of a pipeline; another procedure is used when the transient wave is generated and the pressure response is measured at any interior location along the pipe.

8.4.1 Detection at the end of a pipeline

For a reservoir-pipeline-valve system, an incident wave can be generated by a fast valve closure. A point just upstream from the valve is the best position for pressure wave observation, because the incident wave starts from this point and reflected signals will be reinforced at the closed valve (Lee et al. 2006). The head value of the incident wave caused by the valve closure can be calculated using either the Joukowsky head change equation (Wylie and Streeter 1993) or MOC analysis, and is written as

$$H_i = H_0 + B_0 Q_0 \tag{8.10}$$

The flow rate Q_i is zero after the valve is fully closed. Substituting Q_i = 0 into Eq. (8.7) yields the following expression for Q_{j1}:

$$Q_{j1} = \frac{B_1 - B_0}{B_0 + B_1} Q_0 \tag{8.11}$$

When the reflected wave W_{r1} [see Figure 8.1(d)] arrives at the end of the pipeline, where the transducer is located, the flow remains zero. Using the Joukowsky head change equation, the observed head of the reflection is:

$$H_p = H_{j1} + B_0 Q_{j1} \tag{8.12}$$

Substituting Eqs (8.6) and (8.11) into Eq. (8.12), and using $H_i - H_0$ to replace $B_0 Q_0$, H_p can be rewritten as

$$H_p = H_0 + \frac{3B_1 - B_0}{B_1 + B_0}(H_i - H_0) \tag{8.13}$$

This head level will last until the wave front W_{t3} [see Figure 8.1(d)] arrives at the transducer, which makes the completion of the theoretical square-shaped perturbation.

The impedance difference between the deteriorated section and the original pipeline is defined as $\Delta B = B_1 - B_0$. Substituting ΔB into Eq. (8.13) and rearranging it, the equation can be presented as

$$\frac{\Delta B}{B_0 + \Delta B / 2} = \frac{\Delta H}{\tilde{H}_i} \tag{8.14}$$

where $\Delta H = H_p - H_i$ is the magnitude of the deterioration-induced head perturbation; and $\tilde{H}_i = H_i - H_0 = B_0 Q_0$ is the magnitude of the incident wave, i.e. the head rise caused by the incident wave. Eq. (8.14) indicates that the impedance difference ΔB is only related to the impedance of the original pipeline B_0 and the magnitude ratio of the reflected disturbance to the incident wave $\Delta H / \tilde{H}_i$. The value of B_0 can be determined from Eq. (8.1) and the value of $\Delta H / \tilde{H}_i$ can be estimated from the measured pressure trace. Eq. (8.14) also illustrates that the ratio $\Delta H / \tilde{H}_i$ is independent of the steady-state head H_0 and flow rate Q_0, so that theoretically the impedance difference ΔB can be determined with arbitrary steady-state condition, provided the ratio can be accurately estimated from the measured pressure trace. Rearranging Eq. (8.14), finally the expression for ΔB is

$$\Delta B = \frac{2B_0 \, \Delta H / \tilde{H}_i}{2 - \Delta H / \tilde{H}_i} \tag{8.15}$$

If the change in impedance is caused only by a uniform wall thickness change, and the external diameter of the deteriorated section is known, the wall thickness and wave speed in this section can be determined using the definition of the pipeline impedance [Eq. (8.1)] and the wave speed formula [Eq. (8.2)]. The location and length of the deteriorated section can then be determined using Eqs. (8.8) and (8.9).

The above analysis applies only to wave reflections resulting from the deterioration within the first $2L/a$ of the transient trace (the first plateau), where L is the total length of the pipeline and a is the representative wave speed for the whole pipeline. Due to the effect of multiple reflections between the pipeline terminals and the boundaries of the deterioration, complex disturbances are expected in the pressure trace after the time of $2L/a$.

8.4.2 Detection at an interior location

A major advantage of generating the transient wave and measuring the pressure at an interior location is that the fluid transmission continues during the whole detection procedure, i.e. a base flow rate is maintained and only slight flow perturbations are imposed. A side-discharge valve and a transducer can be placed at any location along the pipeline. They can be situated at the same point or at different points. Figure 8.2 illustrates the layout of the detection system.

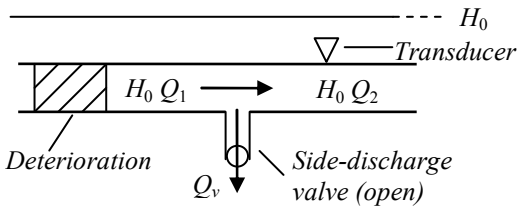

(a) HGL at time t_0

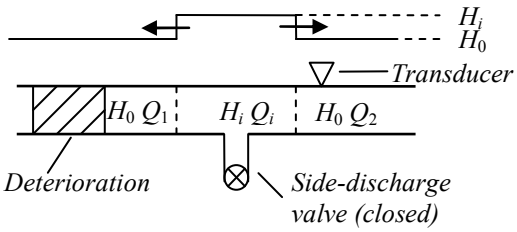

(b) HGL at time $t_0+\Delta t_1$

Figure 8.2 Distributed deterioration detection at an interior location within the pipeline: (a) the steady state condition; (b) the incident wave generated by the closure of the side-discharge valve.

Assume the steady-state head at the side-discharge valve is H_0, the flow through the valve is Q_v, and the flow rates at the upstream side and the downstream side of the valve are Q_1 and Q_2 respectively [Figure 8.2(a)]. A fast closure of the side-discharge valve leads to two symmetric incident waves propagating along two opposite directions in the main pipeline [Figure 8.2 (b)]. The head and flow of the incident waves can be derived as:

$$H_i = H_0 + B_0 Q_v / 2 \tag{8.16}$$

$$Q_i = (Q_1 + Q_2)/2 \tag{8.17}$$

If a deteriorated section is located at the upstream side of the side-discharge valve, reflections will occur at the boundaries of the deteriorated section. The whole procedure is the same as that shown in Figure 8.1. The head and flow for the reflected perturbation are:

$$H_p = H_0 + \frac{B_0 B_1}{B_0 + B_1} Q_v \tag{8.18}$$

$$Q_p = \frac{B_1 Q_1 + B_0 Q_2}{B_0 + B_1} \tag{8.19}$$

A transducer located at the downstream side of the deteriorated section can measure the reflected head perturbation H_p. The value of H_p can be used to determine the impedance of the deteriorated section. The location and length of the deteriorated section can be derived using the arrival time and duration of this head perturbation signal, provided the locations of the transducer and side-discharge valve are known.

In real applications, the relative location of the deteriorated section is unknown and generally three possible situations exist: The deteriorated section can be either between the transient generator and the transducer or at one side (upstream or downstream) of the two. Multiple solutions to the location of the deterioration can be obtained from a single time-domain transient trace. Lee et al. (2007a) analyzed this practical issue for leak detection and provided techniques to determine the origin of the reflection. However, more complex situations can be encountered in distributed deterioration detection. For example, the generator and/or the transducer may also be accidentally positioned within the deteriorated zone, and multiple deteriorated sections may introduce complex pressure responses.

8.5 Distributed versus discrete deterioration

In real world pipelines, both distributed (such as corrosion and extended blockages) and discrete deterioration (such as leaks and discrete blockages) may exist. The different types of deterioration can be determined from the measured transient pressure traces.

When a step wave is used as the excitation, a leak can introduce a pressure drop in the measured pressure trace (Lee et al. 2007b), while the reflection from a discrete blockage shows as a pressure jump (Kim et al. 2007). In contrast, a distributed deterioration introduces a square-shaped reflection. The square is either negative (lower than the head of the incident wave) for a deteriorated section with a lower impedance, or positive (higher than the head of the incident wave) when it has a higher impedance than the original pipeline. However, if both a leak and a discrete blockage exist in a single pipeline, the pattern of reflection could be similar to the square-shaped disturbance resulting from a distributed deterioration. In order to determine the type of the deterioration, the transient generation and pressure measurement needs to be performed on both the upstream and the downstream sides of the deterioration. For a distributed deterioration, the pattern of the square-shaped reflection is constant. For example, if the deterioration is a pipe section with a lower impedance, the reflection always has a negative square shape, no matter the transient generation and pressure measurement is taken at the upstream or the downstream side. In contrast, the two square-shaped reflections resulting from two local discontinuities will show opposite patterns, i.e. one is positive and the other is negative.

8.6 Experimental verification

8.6.1 System configuration

Laboratory experiments were conducted to validate the proposed distributed deterioration detection method. The test pipeline was a 37.46 m straight

copper pipe with an external diameter of 25.4 mm, an internal diameter D_0 = 22.14 mm, and a wall thickness e_0 = 1.63 mm. One end of the pipeline was connected to an electronically controlled pressurized tank and the other end was a closed in-line valve. The pipeline was fixed rigidly to a support structure on the wall to prevent vibration during transient events. A pipe section 1.649 m long with a thinner pipe wall thickness was placed 17.805 m upstream from the in-line valve. While the material and external diameter of this section were the same as those of the original pipeline, the internal diameter D_1 = 22.96 mm and the wall thickness e_1 = 1.22 mm. This section represents a pipe section with a lower pressure rating, or a section with uniform wall thickness that has decreased due to internal corrosion, neglecting the effects of spatial variability as would be present in realistic corroded sections.

A transient wave was generated by sharply closing a side-discharge solenoid valve 144 mm upstream from the closed in-line valve (the closure time was approximately 4 ms). Pressure responses were monitored at the side-discharge valve with a sampling rate of 2 kHz. The pressure transducer was a Druck PDCR 810 high integrity silicon flush mounted diaphragm transducer with an absolute pressure range of 0 to 15 bar. The rise time of the transducer was estimated to be 5 micro seconds (Lee et al. 2007a). A customized amplifier with carefully designed adjustable filtering and adjustable pressure ranges was used and the response frequency was 16 kHz. The pipeline system layout is illustrated in Figure 8.3.

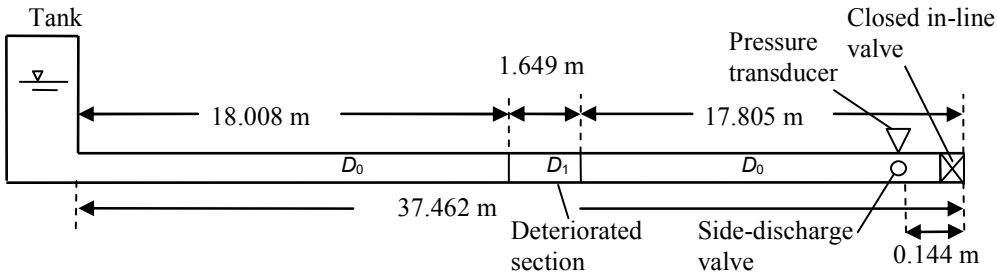

Figure 8.3 The experimental pipeline system layout.

8.6.2 Experimental pressure traces

Figure 8.4 gives an overview of the pressure transient trace as measured from Test 1. The transient response trace has a periodic pattern due to reflections at two pipeline ends. Signal attenuation, dissipation and dispersion can also be observed, but the influence of friction is negligible for the first plateau. In addition to the pressure perturbation that appears in the middle of the first plateau (of duration $2L/a$), complex perturbations due to multi-reflections are present in the following time.

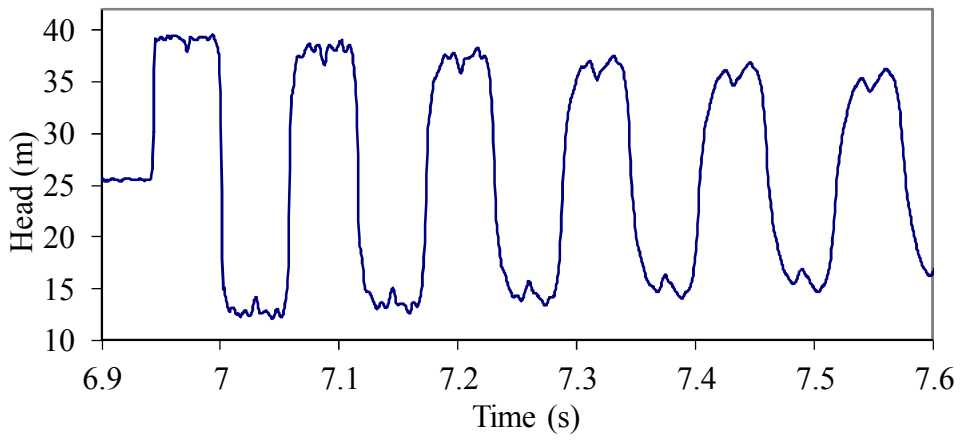

Figure 8.4 Experimental pressure trace of Test 1

To verify the repeatability of the experiments, a number of tests have been conducted with the same pipeline configuration. Experiments on an intact

pipeline were also performed for comparison. The first plateau (of duration $2L/a$) of the measured pressure traces for three tests on a pipeline with a thinner wall section (Tests 1 to 3) and of one test on an intact pipeline (marked as 'Intact') are shown in Figure 8.5. The pressure traces of Tests 1 to 3 are similar, with a pressure perturbation located at the middle of the plateau. The response from an intact pipe shows a nearly flat pattern, as is expected.

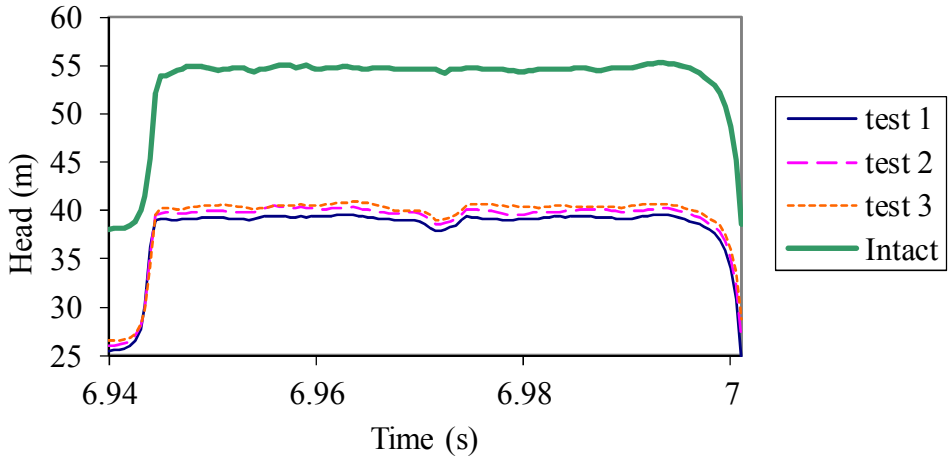

Figure 8.5 The first plateau of experimental head response traces. Three experiments (Tests 1 to 3) on a pipeline with a section of thinner wall thickness, compared to one experiment on an intact pipeline

8.6.3 Determination of the impedance, wave speed and wall thickness

Figure 8.6 gives an enlarged view of the pressure rise during valve closure measured in Test 1, and Figure 8.7 shows an enlarged view of the pressure perturbation in the first plateau of the pressure trace in Test 1. A pressure drop followed by a pressure rise (Figure 8.7) indicates that the reflection comes from a section with lower impedance. The reflected perturbation does not show a clear square shape as seen in the theoretical analysis (Figure 8.1), mainly because the wave front of the incident wave due to valve closure (Figure 8.6) is not a true vertical step, but rather it is a curve that has a total rise time T_r of around 4 ms (from 6.941 s to 6.945 s). The influence of the

shape and rise time of the initial wave front will be discussed later in the paper.

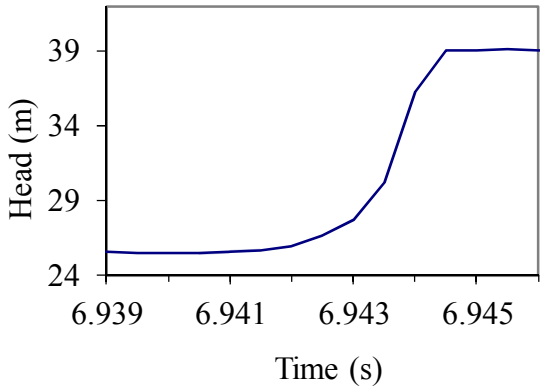

Figure 8.6 Enlarged view of the wave front in Test 1

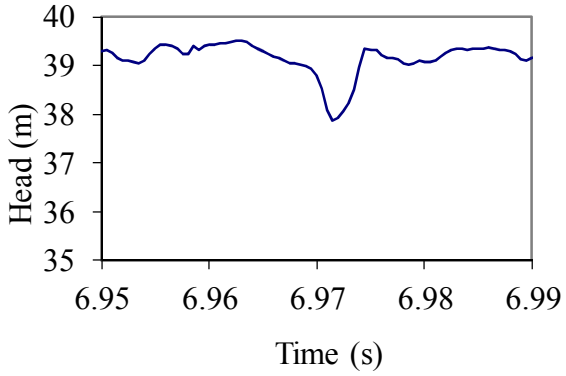

Figure 8.7 Enlarged view of the pressure perturbation in the first plateau of the pressure trace measured in Test 1

The wave speed (a_0) in the intact pipeline was 1328 m/s as determined by experiments (Lee et al. 2007a; Kim 2008). Using Eq. (8.1), the impedance of the original pipeline (B_0) is 3.516×10^5 s/m^2. The parameter c_1 in the wave speed formula [Eq. (8.2)] is estimated as 1.006 using the theoretical equation for thick-walled elastic pipeline provided in Wylie and Streeter (1993). The steady-state head is estimated to be H_0 = 25.55 m by averaging the pressure values within a short time interval before the wave front (6.92 s to 6.94 s). Similarly, the head value of the incident wave can be estimated from the first

plateau and it is H_i = 39.06 m (by averaging the pressure from 6.945 s to 6.947 s). As a result, the magnitude of the incident wave is $\tilde{H}_i = H_i - H_0$ = 13.51 m. The lowest head value in the reflected pressure disturbance shown in Figure 8.7 is H_p = 37.86 m, so that the magnitude of the disturbance is $\Delta H = H_p - H_i$ = –1.20 m. Finally, by using Eq. (8.15), the impedance difference between the deterioration and the original pipeline is estimated as ΔB = –29, 900 s/m^2. The impedance of the deterioration is determined to be B_1 = 3.217×10^5 s/m^2.

The deterioration is known to be a section with a uniform wall thickness change. Knowing B_1 and using the definition of impedance [Eq. (8.1)] and the wave speed formula [Eq. (8.2)], the wave speed and wall thickness of the deteriorated section are estimated as a_1 = 1292 m/s and e_1 = 1.29 mm, respectively. In this research, the *Goal Seek* function in Microsoft Excel is used to solve these equations.

The pressure traces in Tests 2 and 3 are also interpreted. Finally, the impedance B_1, wave speed a_1 and wall thickness e_1 of the deterioration that have been estimated from the three laboratory experiments are listed in Table 8.1. The analytical values of B_1, a_1 and e_1 for the actual wall thickness e_1 = 1.22 mm are also calculated and listed in the first row as the bench marks. The relative errors for the experimental results are calculated. The 'relative error' is defined as '|(value estimated from tests – analytical value) / analytical value|$\times$100%'.

Table 8.1 Impedance B_1, wave speed a_1 and wall thickness e_1 of the deteriorated section

Data source	Impedance B_1 (s/m^2)	Relative error[a]	Wave speed a_1 (m/s)	Relative error[a]	Wall thickness e_1 (mm)	Relative error[a]
Analytical values	3.151×10^5	N/A	1282	N/A	1.22	N/A
Test 1	3.217×10^5	2.1 %	1292	0.8 %	1.29	5.7 %
Test 2	3.234×10^5	2.6 %	1295	1.0 %	1.31	7.4 %
Test 3	3.217×10^5	2.1 %	1292	0.8 %	1.29	5.7 %

Note: Analytical values are theoretical results analytically calculated for the actual wall thickness of the deteriorated section e_1 = 1.22 mm; Tests 1-3 are experimental results estimated from the pressure traces measured in laboratory experiments.

[a]Relative error = |(value estimated from tests – analytical value)/ analytical value|$\times$100%

It can be seen from Table 8.1 that the estimated properties of the deteriorated section are close to the analytical results. It verifies that the distributed determination can be detected and its properties can be estimated from the water hammer pressure trace using the proposed technique. However, the relative errors in B_1, a_1 and e_1 are always small because their theoretical values are large compared with the absolute difference between the deterioration and the original pipeline. For example, the theoretical value of B_1 is approximately 10 times of the theoretical impedance difference between the deterioration and the original pipeline. The accuracy of the proposed technique can be further studied from the estimated impedance difference ΔB, wave speed difference Δa and wall thickness difference Δe.

The experimental results of the impedance difference ΔB, the wave speed difference Δa and the wall thickness difference Δe are compared with the analytical values for the actual B_1, a_1 and e_1 = 1.22 mm, as shown in Table 8.2. Relative errors are calculated using the same definition as used in Table 8.1.

It can be seen from Table 8.2 that ΔB, Δa and Δe all have a relative error of about 20 %. The error is acceptable, but it is much higher than the error shown in Table 8.1. In addition to the uncertainties in the laboratory pipeline, one source of error may come from the experimental wave front. Due to the limitation in the maneuverability of the valve, the initial wave front of the transient waves used in the experiments is curved rather than a theoretical vertical step. To study the effect of the initial wave front, numerical simulations are performed as described below.

Table 8.2 Difference in the impedance, wave speed and wall thickness between the deterioration and the original pipeline

Data source	Impedance difference $\Delta B = B_1 - B_0$ (s/m^2)	Relative error[a]	Wave speed difference $\Delta a = a_1 - a_0$ (m/s)	Relative error[a]	Wall thickness difference $\Delta e = e_1 - e_0$ (mm)	Relative error[a]
Analytical values	–36, 490	N/A	–46	N/A	–0.41	N/A
Test 1	–29, 900	18.1 %	–36	21.7 %	–0.34	17.1 %
Test 2	–28, 200	22.7 %	–33	28.3 %	–0.32	22.0 %
Test 3	–29, 900	18.1 %	–36	21.7 %	–0.34	17.1 %

Note: Analytical values are theoretical results analytically calculated for the actual wall thickness of the deteriorated section e_1 = 1.22 mm; Tests 1- 3 are experimental results estimated from the pressure traces measured in laboratory experiments.

[a]Relative error = |(value estimated from tests – analytical value)/ analytical value $|\times 100\%$

8.6.4 The influence of the initial wave front

As mentioned in the previous section, the initial wave front in Test 1 (Figure 8.6) is a 4 ms curve rather than a true vertical step. This is inevitable due to limitation in the maneuverability of real world valves. The curved wave front is assumed to be the major reason for the distortion in the reflected pressure disturbance, making it a smooth dip rather than a sharp square shape.

According to the wave propagation analysis shown in Figure 8.1, the interval between the first reflection and transmission [Figure 8.1(b)] and the third reflection and transmission [Figure 8.1(d)] is $2L_1 / a_1$, where L_1 = length of deteriorated section with impedance B_1 and wave speed a_1. If the rise time of the incident wave T_r is more than $2L_1 / a_1$, the wave W_{r2} (which is reflected from the left boundary of the deterioration), will overlap with the original incident wave W_0 at the right boundary. As a result, the theoretical spatial resolution (the theoretical shortest deterioration length that can be accurately detected) is $T_r a_1 / 2$.

The estimated value of $2L_1 / a_1$ is 2.6 ms for the experimental pipeline. It is smaller than the duration of the wave front T_r (4 ms), implying that wave overlapping did occur and the resulting impedance determined using Eq. (8.15) is compromised. However, it can be seen from Figure 8.6 that, although the whole wave front lasts 4 ms, the major pressure rise occurs within only 2.5 ms which is just less than $2L_1 / a_1$. As shown in Figure 8.6, the major pressure change occurred between 6.942 s and 6.9445 s. The pressure increased from 25.94 m to 39.00 m during the 2.5 ms, which is 97 % of the total pressure rise. As a result, it is expected that the experimental initial wave front will not have much influence on the accuracy in the estimation of ΔB, Δa and Δe.

To study in detail the influence of the initial wave front, numerical water hammer simulations have been conducted. The pipeline configuration used in the numerical simulations was the same as the experimental configuration as

illustrated in Figure 8.3, except that the side-discharge valve was removed and the transient wave was generated by the in-line valve at the end. The method of characteristics (MOC) was used to perform the numerical modeling and the resolution was 0.01 ms. Friction is neglected in the numerical simulations, because the influence of friction is negligible for the first plateau of the transient trace.

Three different cases were considered: Case 1, a vertical wave front (starting at 6.945 s, which is the time point of the full valve closure in Test 1) was adopted to determine the theoretical pressure response; Case 2, the measured wave front shown in Figure 8.6 was interpolated and used as the input in the MOC modeling; and Case 3, a third study has been performed on a modified pipeline configuration, in which the input was the measured pressure curve, but the length of the deteriorated section was doubled to 3.30 m to make $2L_1 / a_1$ (5.2 ms) longer than T_r (4 ms).

For these three case studies, the steady-state head (H_0) and the head of the incident wave (H_i) are all the same, so that the magnitudes of the incident wave are uniform ($\tilde{H}_i$ = 13.51 m). Three pressure traces were obtained numerically, one for each case, as shown in Figure 8.8. The pressure trace measured in the experimental Test 1 is also presented for comparison. The enlargement of the deterioration-induced pressure perturbations are shown in Figure 8.9.

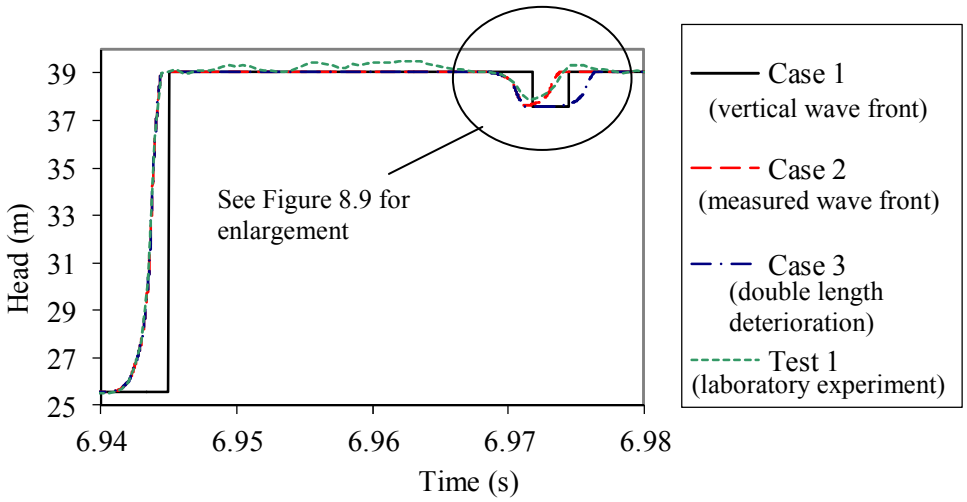

Figure 8.8 Pressure response traces obtained from numerical simulations: Case 1: Using the experimental pipeline configuration and a vertical wave front; Case 2: Using the experimental pipeline configuration and the measured wave front; Case 3: Using the measured wave front, and the modified pipeline configuration, in which the length of the deterioration is doubled; Test 1: The experimental pressure trace from Test 1

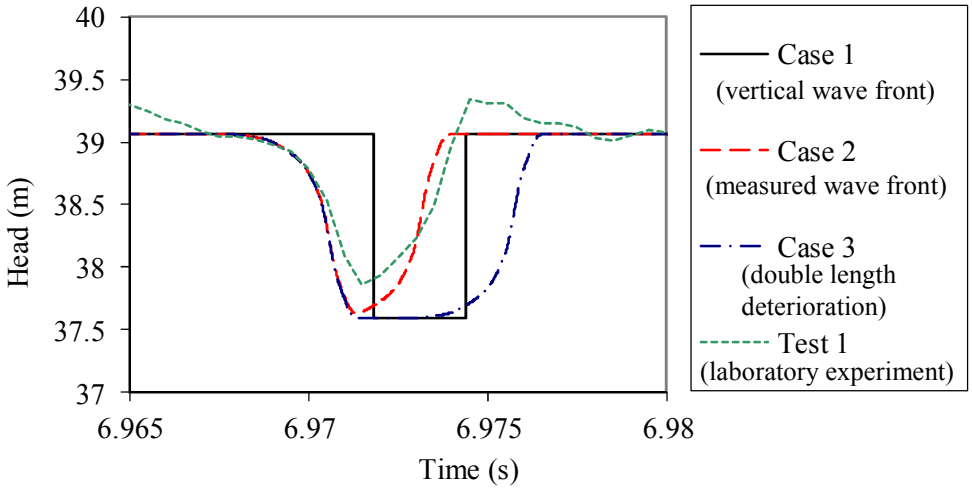

Figure 8.9 Deterioration-induced pressure perturbations obtained from numerical simulations (enlargement of Figure 8.8): Case 1: Using the experimental pipeline configuration and a vertical wave front; Case 2: Using the experimental pipeline configuration and the measured wave front; Case 3: Using the measured wave front, and the modified pipeline configuration, in which the length of the deterioration is doubled; Test 1: The experimental pressure trace from Test 1

To study the effect of the initial wave front on the accuracy of the estimated impedance difference ΔB, firstly the magnitude of the deterioration-induced perturbation ΔH is estimated for each case study from its numerical pressure trace. For Cases 2 and 3 with the curved initial wave front, the magnitude of the perturbation is defined as the head difference between the lowest pressure point in the perturbation and the head of the incident wave. Table 8.3 summarizes the values of ΔH for the three numerical case studies, and the corresponding estimated impedance difference ΔB. Analytical values are presented in the first row as bench marks, which are calculated for the theoretical impedance of the deteriorated section $B_1 = 3.151 \times 10^5$ s/m^2 using Eq. (8.14) and the magnitude of the incident wave $\tilde{H}_i = 13.51$ m. The relative deviation from the analytical value is calculated for each numerically determined ΔH, which is defined as '|(value estimated from numerical simulations – analytical value) / analytical value| $\times$ 100 %'.

Table 8.3 Magnitude of the reflected disturbance and the estimated impedance difference between the deterioration and the original pipeline

Data source	Magnitude of disturbance ΔH (m)	Relative deviation[a] (m)	Impedance difference ΔB (s/m^2)	Relative deviation[a]
Analytical values	–1.48	N/A	–36, 490	N/A
Case 1 (vertical wave front)	–1.48	0.0 %	–36, 490	0.0 %
Case 2 (measured wave front)	–1.44	2.7 %	–35, 580	2.5 %
Case 3 (double length deterioration)	–1.48	0.0 %	–36, 490	0.0 %

Note: Analytical values are theoretical results calculated for $B_1 = 3.151 \times 10^5$ s/m^2; Cases 1 - 3 are results estimated from the numerical pressure traces.

[a]Relative deviation = |(value estimated from numerical simulations – analytical value)/ analytical value | $\times 100\%$

It can be seen from Table 8.3 that the results derived from the numerical pressure trace in Case 1 (vertical wave front) are exactly the same as the analytical results, as is expected. This case study indicates that the impedance of the deterioration can be determined accurately when the incident wave has a vertical wave front. The numerical pressure trace of Case 1 can be used as the bench mark in Figure 8.9.

The deterioration-induced perturbation obtained numerically in Case 2 (measured wave front) is consistent with the experimental pressure perturbation in Test 1 (laboratory experiment) in shape and time, as is expected. However, the magnitude of the disturbance ΔH in Case 2 is only 2.7 % smaller than the analytical value. The impedance difference ΔB estimated in Case 2 also shows a high accuracy. These results verify the previous assumption that, although the curved experimental wave front has a total rise time (4 ms) that is greater than $2L_1 / a_1$, the effects of the wave overlapping is small because the major pressure rise (more than 97 % of the total head rise) occurs within a time interval less than $2L_1 / a_1$.

The result from Case 3 (double length deterioration) shows that when $2L_1 / a_1$ is longer than the rise time T_r, the reflected pressure disturbance does reach the theoretical straight bottom line (Case 1) and lasts for a short period of time before increasing again. From additional numerical testing, the duration is observed to be $2L_1 / a_1 - T_r$.

The magnitude of the reflected disturbance estimated in the laboratory experiment Test 1 is ΔH = –1.20 m, which has a relative error of 16.7 % compared with the theoretical value for Case 2 (–1.44 m). The error in the estimated ΔH leads to errors in the estimated ΔB, Δa and Δe, as depicted in Table 8.2. To these errors, the contribution from the curved wave front is small, as discussed previously in the numerical study of Case 2. Other sources of experimental error includes the effects from the small hydraulic components in the pipeline (such as joints and the customized brass block that is used to install the pressure transducer and the side-discharge valve), the

micro-perturbations that are always shown in the experimental pressure traces (even in the steady state), and the compromise in data due to sampling. It is expected that increasing the magnitude of the incident wave can increase the accuracy in the estimation assuming that the noise level remains the same, because the magnitude of the reflected disturbance is proportional to the magnitude of the incident wave.

8.6.5 Determination of the location and length

To estimate the location and length of the deteriorated section, the arrival time (T_0) and duration (T_1) of the reflected disturbance need to be estimated. From Figure 8.6 and Figure 8.7, the time between the end point of the wave front (6.945 s) and the lowest value in the reflected head disturbance (6.9715 s) is 0.0265 s. Then this value is used as T_0 in Eq. (8.9), and the deteriorated section is estimated to be 17.60 m upstream from the in-line valve.

The time T_1 in Eq. (8.8) is hard to estimate from the experimental pressure trace. From the numerical simulations shown in Figure 8.9, the duration of the deterioration-induced pressure dip can be the time interval between the start of the dip and the end of the straight bottom if $2L_1 / a_1$ is greater than T_r (this is Case 3 in Figure 8.9). The time from when the dip starts can be estimated from the first pressure datum in the experimental pressure disturbance that is lower than the head of the incident wave (H_i). From Figure 8.7 and using $H_i = 39.06$ m as a threshold, the starting time of the dip is 6.9675 s. However, the measured pressure dip shows a sharp tip at the bottom (at 6.9715 s in Figure 8.9) rather than a theoretical straight line, which suggests that $2L_1 / a_1$ is smaller than T_r in the experiment. If no prior information is known, this lowest point has to be used as the end point. As a result, the value of T_1 is estimated to be 0.0040 s. Using Eq. (8.8) and the estimated wave speed in the deterioration as shown in Table 8.1, the length of the pipe section with the thinner wall is estimated as 2.56 m, which is much larger than the actual value of 1.649 m. The experimental results of the location and length of

the deterioration are summarized in Table 8.4, along with a comparison with the actual values. The absolute error (|experimental value – actual value|) is presented instead of the relative error.

Table 8.4 Location and length of the deteriorated section

	Location L_0 (m)	Length L_1 (m)
Actual values	17.805	1.649
Experimental results	17.60	2.56
Absolute error[a]	0.205	0.911

Note: Actual values are the values measured in the experimental pipeline; Experimental values are the results obtained from the proposed technique using the experimental pressure trace.

[a]Absolute error = |experimental result – actual value|

The accuracy in the estimated location and length is acceptable in this clean laboratory experiment. However, in field and long pipelines, where the wave speed and impedance are not uniform and hard to estimate accurately, much more error can be expected. In addition to the shape and rise time of the wave front, sampling rate may also affect the accuracy, especially for the determination of the length of the deterioration.

8.7 Conclusions

A transient-based distributed deterioration detection method has been proposed. The transient response due to a deteriorated section with an impedance change has been analyzed by the method of characteristics. Two detection strategies have been adopted to cater for different equipment configurations. A theoretical square-shaped disturbance was found to appear within the first plateau of the water hammer trace due to reflection and transmission at the two boundaries of the distributed deterioration. The current study has shown that, in principle, the location, length and impedance of the deteriorated section can be estimated from the size of the measured deterioration-induced disturbance.

The formula used to estimate the impedance of the deterioration is given in Eq. (8.15). It is independent of the steady-state head and flow rate, but rather only related to the impedance of the original pipeline and the magnitude ratio of the reflected disturbance to the incident wave. The estimated impedance is accurate when the duration of the initial wave front is less than the time for the wave traveling twice the length of the deterioration. When the initial wave front has a longer duration, the results will be compromised.

The proposed distributed deterioration detection method was applied to the interpretation of experimental data measured from a pipeline with a section of decreased uniform wall thickness. The impedance of this deteriorated section was successfully estimated from three of the repeated experimental pressure traces. The wall thickness and wave speed were obtained, assuming that the uniform wall thickness change was the sole source of the impedance alternation. The location and the length of the deterioration were determined using time-domain reflectometry. The accuracy of these results was acceptable, indicating that the proposed technique is valid under controlled laboratory conditions.

Acknowledgements

The research presented in this paper has been supported by the Australia Research Council through the Discovery Project Grant DP1095270. The first author thanks the Chinese Scholarship Council and the University of Adelaide for providing a joint postgraduate scholarship.

Chapter 9

Detection of Extended Structural Deterioration in a Pipeline using Fluid Transients: a Sensitivity Analysis (Journal Publication 7)

Gong, J., Simpson, A. R., Zecchin, A. C. and Lambert, M. F.

School of Civil, Environmental and Mining Engineering, the University of Adelaide, Adelaide, SA 5005 Australia

Journal of Hydraulic Engineering, (submitted).

Statement of Authorship

Title of Paper	Detection of Extended Structural Deterioration in a Pipeline using Fluid Transients: a Sensitivity Analysis
Publication Status	Submitted for Publication
Publication Details	Gong, J., Simpson, A. R., Zecchin, A. C. and Lambert, M. F. (2013). "Detection of extended structural deterioration in a pipeline using fluid transients: a sensitivity analysis." *Journal of Hydraulic Engineering*, (submitted).

Author Contributions

By signing the Statement of Authorship, each author certifies that their stated contribution to the publication is accurate and that permission is granted for the publication to be included in the candidate's thesis.

Name of Principal Author (Candidate)	Jinzhe Gong		
Contribution to the Paper	Developed and implemented the methodology, designed and conducted numerical simulations, interpreted and analysed results, prepared manuscript and acting as the corresponding author.		
Signature		Date	25/09/2013

Name of Co-Author	Angus Simpson		
Contribution to the Paper	Supervised development of work, helped to evaluate and edit the manuscript.		
Signature		Date	25/9/2013

Name of Co-Author	Aaron Zecchin		
Contribution to the Paper	Helped to evaluate and edit the manuscript.		
Signature		Date	1·10·2013

Name of Co-Author	Martin Lambert		
Contribution to the Paper	Helped to evaluate and edit the manuscript.		
Signature		Date	25/9/13

Abstract

Fluid transient (water hammer) waves can be used as a tool for the detection of faults in pressurized pipelines, such as leaks or sections with structural deterioration. This technical note analyzes the relationship between the degree of change in wall thickness in a deteriorated section and the sizes of the transient waves reflected from and transmitted through that section. The analysis demonstrates that, while the transmitted wave is not very sensitive to a change in wall thickness, the magnitude of the reflected wave is related to not only the degree of change in wall thickness but also the wave speed in the intact pipeline. Plots are presented to describe variation in the magnitude of the reflected wave according to relative change in wall thickness. They can serve as look-up charts for direct estimation of the wall thickness of deteriorated sections from transient pressure traces as measured by a transducer.

9.1 Introduction

Water transmission and distribution systems are critical infrastructure for every city and town. Pipelines serving as a core component are of great importance for the successful operation of these systems. Structural deterioration of pipelines, such as leaks and corrosion of pipe wall, can reduce capacity of water distribution (Tran et al. 2010), increase energy consumption (Meniconi et al. 2010), and affect water quality (Vreeburg and Boxall 2007). To prevent these problems and maintain the system cost-effectively, accurate assessment of the structural condition of pipelines is essential.

Research in the past two decades has shown that fluid transients (also known as water hammer) (Chaudhry 1987; Wylie and Streeter 1993) can be used as a tool for non-destructive pipeline condition assessment. While a number of studies are focused on the detection of leaks (Jönsson and Larson 1992; Brunone 1999; Vítkovský et al. 2000; Covas et al. 2005; Lee et al. 2005b; Gong et al. 2013e), the research on the detection of localized deterioration that distributed along pipelines, such as the spalling of cement lining and extended pipe wall corrosion, is still in its infancy.

Stephens et al. (2008, 2013) were the first to apply the inverse transient analysis (ITA) to detect localized wall deterioration in a cement lined steel pipeline. The ITA calibrates pipeline parameters through an iterative process; therefore, it can be computationally costly for complex systems. Hachem and Schleiss (2012) proposed a technique for detecting a structurally weak section in a pipeline using a steep transient pressure wave. The wave speed in the deteriorated section was estimated by comparing the measured wave speed of the pipe with a weak section and that of an intact pipe. This strategy impedes the extension of the technique to detect multiple deteriorated sections, since the wave speeds in these sections would be difficult to determine by the proposed technique. Duan et al. (2012) proposed a technique to detect extended blockages (sections with greater wall thickness but the same external diameter as the intact part) in a pipeline using the frequency response diagram

(FRD). Numerical simulations in that study shown that extended blockages could cause the resonant frequencies of the system to shift. However, challenges are expected in real applications since the shifts of the resonant peaks are slight and difficult to measure accurately. Gong et al. (2012a; 2013f) developed a technique for detecting a single deteriorated section in a pipeline using a steep transient pressure wave. It was found that the magnitude of the wave reflection resulting from a deteriorated section was indicative of the impedance of that section. The impedance could then be used to determine the wall thickness and wave speed in the deteriorated section. A preliminary sensitivity analysis was conducted in Gong et al. (2012a) to study how a change in wall thickness affects the reflected and transmitted transient waves. However, the analysis was based on the assumptions that the external diameter was constant throughout the pipe and the ratio of the internal diameter to the wall thickness was known. Gong et al. (2013a) proposed an approach for detecting multiple deteriorated sections along a pipeline. However, a closed valve boundary condition was required and the transient pressure trace had to be measured at the upstream face of the closed valve.

This technical note is an extension of the work by Gong et al. (2012a; 2013f). The focus of this research is to study the characteristics of a pipe section with a change in wall thickness under fluid transient events. In particular, a detailed sensitivity analysis is conducted to study the relationship between the degree of change in wall thickness in a structurally deteriorated section and the sizes of the transient waves reflected from and transmitted through that section. Two typical scenarios are discussed: a change in wall thickness from the internal side (constant external diameter) and that occurs on the external side (constant internal diameter). Plots about variation in the normalized magnitude of the reflected wave versus relative change in wall thickness are presented. The plots can be used as look-up charts for a fast and quantitative structural condition assessment of pipelines using fluid transient waves.

9.2 Pipeline impedance and wave speed

The characteristic impedance of a uniform pipeline is given as (Chaudhry 1987; Wylie and Streeter 1993)

$$B = a / (gA) \tag{9.1}$$

where B is pipeline impedance; a is the wave speed; g is the gravitational acceleration; and A is the internal cross-sectional area of the pipeline. The impedance is sensitive to wall thickness, in which a variation affects not only the internal cross-sectional area but also the wave speed. The wave speed and the wall thickness are related by the wave speed formula (Chaudhry 1987; Wylie and Streeter 1993) , which can be written as

$$a^2 = \frac{K/\rho}{1 + (K/E)(D/e)c_1} \tag{9.2}$$

in which K is the bulk modulus of elasticity of fluid; ρ is the density of fluid; E is Young's modulus of the pipe material; D is the internal diameter of the pipeline; e is the wall thickness; and c_1 is a factor depending on the restraint condition (Wylie and Streeter 1993).

9.3 Transient wave reflection and transmission

When a steep incident transient pressure wave encounters a section of pipe with a variation in impedance, part of the wave is reflected and the rest is transmitted. Gong et al. (2012a; 2013f) conducted an analysis using the method of characteristics (MOC) in a frictionless pipeline, and expressions of the reflected and transmitted waves are derived as

$$H_r = H_0 + \frac{2B_1}{B_0 + B_1}(H_i - H_0) \tag{9.3}$$

$$H_t = H_0 + \frac{6B_0^2 B_1 + 2B_1^3}{(B_0 + B_1)^3}(H_i - H_0) \tag{9.4}$$

where H_r and H_t are the head of the reflected and transmitted waves respectively; H_0 is the head at the steady state; H_i is the head of the incident wave; B_0 and B_1 are the impedance of the intact pipe and the deteriorated section.

Values of H_r and H_t are dependent on the steady-state head and the head of the incident wave. In order to make the analysis general, normalized head perturbations are defined in this research and presented as

$$H_r^* = \frac{H_r - H_i}{H_i - H_0} \tag{9.5}$$

$$H_t^* = \frac{H_t - H_i}{H_i - H_0} \tag{9.6}$$

where H_r^* and H_t^* represent the normalized head perturbation of the reflected and transmitted waves respectively. They represent the ratio of the head variations in the reflected and transmitted waves to the magnitude of the incident wave.

The ratio between the impedance of the deteriorated section and that of the intact section is represented by B_r and written as

$$B_r = \frac{B_1}{B_0} \tag{9.7}$$

Substituting Eqs (9.3), (9.4) and (9.7) into Eqs (9.5) and (9.6), the normalized head perturbations of the reflected and transmitted waves can be rewritten as

$$H_r^* = \frac{B_r - 1}{B_r + 1} \tag{9.8}$$

$$H_t^* = -\frac{(B_r - 1)^2}{(B_r + 1)^2} \tag{9.9}$$

It can be seen from Eqs (9.8) and (9.9) that the normalized head perturbations of the reflected and transmitted waves are only dependent on the impedance ratio B_r. As a result, Eqs (9.8) and (9.9) are applicable for any types of deteriorated pipe section with a change in impedance. Plots of H_r^* and H_t^* according to variations in B_r from 0.5 to 1.5 are given in Figure 9.1.

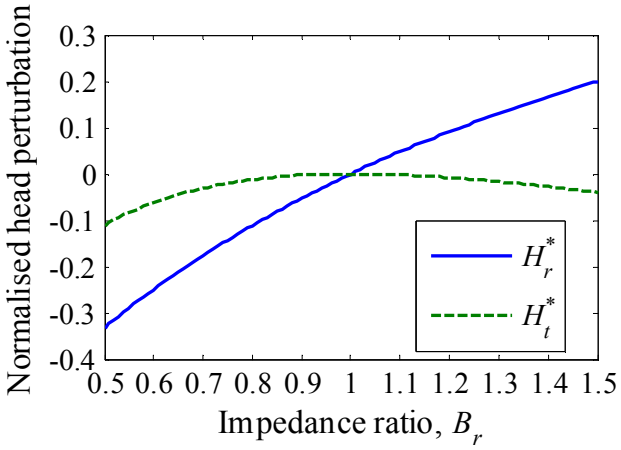

Figure 9.1 Variation of the normalized head perturbations for the reflected wave (H_r^*, solid line) and transmitted wave (H_t^*, dashed line) according to variations in the impedance ratio (B_r)

Figure 9.1 demonstrates that a deteriorated section introduces a negative reflection ($H_r < H_i, H_r^* < 0$) when the impedance in this section is lower than the impedance of the original pipe ($B_1 < B_0, B_r < 1$), and vice versa. The

transmitted wave always has a head lower than the incident wave ($H_t < H_i$, $H_t^* < 0$). For the reflected wave, the head perturbation is proportional to the variation in impedance and it is more sensitive to downward variation ($B_1 < B_0$). The size of the reflection is more than 30% that of the incident wave when $B_r = 0.5$, while the ratio is only around 20% for $B_r = 1.5$. On the contrary, the transmitted wave is not very sensitive to variations in impedance. The head difference between the transmitted wave and the incident wave is less than 2% when the impedance ratio (B_r) is within -0.75 to 1.33. This finding demonstrates that the head loss for an incident wave propagating through a deteriorated section of pipe can be neglected if the change in impedance is not significant (within $\pm 30\%$). As a result, for a pipeline with multiple deteriorated sections, the wave reflection resulted from a section can be transmitted through other sections with little loss. The reflected wave can be measured and analyzed as if there were only a single deteriorated section (provided that the reflection is not superimposed with other reflections). The pipeline condition assessment technique presented in Gong et al. (2013f), which was originally developed for the detection of a single deteriorated section, can then be extended to detect multiple deteriorated sections.

9.4 Sensitivity analysis of the effects of a change in wall thickness on the size of the transmitted and reflected waves

The preceding analysis demonstrates that a variation in impedance can introduce a wave reflection and affect the head of the wave transmitted under transient events. A typical cause for an impedance variation is a change in pipe wall thickness due to structural deterioration, such as extended corrosion. This research investigates the effects of a change in wall thickness on the sizes of the reflected and transmitted waves. Two typical scenarios are discussed in detail in the following sections: (1) an internal change in wall thickness

(constant external diameter); and (2) an external change in wall thickness (constant internal diameter). The analysis presented in this technical note only focuses on unlined pipelines. If necessary, however, the analysis can be extended to lined pipelines, such as mild steel cement lined (MSCL) pipes.

9.4.1 An internal change in wall thickness

In this subsection, it is assumed that a deteriorated section with an internal change in wall thickness occurs in a pipeline. Examples include: a section of pipe with a thinner wall thickness due to extended internal corrosion; and a mistakenly installed section of pipe under a different sub-classification, which has the same external diameter but a different wall thickness from the majority of the pipe. Since the original pipe and the deteriorated section with a change in wall thickness have the same external diameter, an equation relating the internal diameter and wall thickness of the original and damaged section can be obtained as

$$D_0 + 2e_0 = D_1 + 2e_1 \tag{9.10}$$

where D_0 and e_0 are the internal diameter and wall thickness of the original pipe, D_1 and e_1 are the counterparts of the deteriorated pipe section.

The relative change in wall thickness is defined as e_{rc} and represented by

$$e_{rc} = \frac{e_1 - e_0}{e_0} \tag{9.11}$$

Using the wave speed formula [Eq. (9.2)] and Eqs (9.10) and (9.11), the wave speed in the deteriorated section can be derived as

$$a_1^2 = \frac{(K/\rho)(1+e_{rc})a_0^2}{(K/\rho)+e_{rc}a_0^2\left(1-2c_1K/E\right)} \tag{9.12}$$

Substituting Eq. (9.1) into Eq. (9.7), the impedance ratio B_r can be rewritten as

$$B_r = \frac{a_1 D_0^2}{a_0 D_1^2} \tag{9.13}$$

Substituting Eqs (9.10) and (9.12) into Eq. (9.13) and rearranging the subsequent equation, B_r can be rewritten as

$$B_r = \frac{\sqrt{\dfrac{(K/\rho)(1+e_{rc})}{K/\rho + e_{rc}a_0^2\left(1-2c_1K/E\right)}}}{(1-2e_{rc}e_0/D_0)^2} \tag{9.14}$$

In Eq. (9.14), the numerator with the radical sign represents a_1/a_0 and the denominator is equivalent to D_1^2/D_0^2. Given the fact that the value of c_1 is usually around one and, for metal pipelines the ratio of E/K is typically ranging from 50 to 100 (Wylie and Streeter 1993), the small coefficient $(K/E)2c_1$ is in the order of $O\{10^{-2}\}$. As a result, $1-(K/E)2c_1 \approx 1$, and B_r can be simplified to

$$B_r = \frac{\sqrt{\dfrac{(K/\rho)(1+e_{rc})}{K/\rho + e_{rc}a_0^2}}}{(1-2e_{rc}e_0/D_0)^2} \tag{9.15}$$

If all the properties of the intact pipe are known, the value of e_0/D_0 can be calculated and the theoretical wave speed (a_0) in original pipeline can be determined by the theoretical wave speed formula [Eq. (9.2)]. In the field, however, some specifications of the pipeline may be unknown or difficult to obtain. As a result, the value of e_0/D_0 may be unknown, and the theoretical wave speed a_0 cannot be determined from the formula. An alternative solution is to measure the value of a_0 by conducting transient experiments in

pipe sections with 'good' condition. The value of e_0/D_0 can then be estimated from the measured a_0 by rearranging the theoretical wave speed formula. As a result, B_r can be rewritten as

$$B_r = \frac{\sqrt{\frac{(K/\rho)(1+e_{rc})}{K/\rho + e_{rc}a_0^2}}}{\left[1 - 2e_{rc}\frac{(K/E)a_0^2 c_1}{K/\rho - a_0^2}\right]^2} \tag{9.16}$$

The relationship between the relative change in wall thickness and the normalised head perturbation of the reflected or transmitted waves can be obtained by substituting Eq. (9.16) into Eqs (9.8) and (9.9). The expressions of the resulted equations are given in Eqs (9.17) and (9.18) respectively.

$$H_r^* = \frac{\sqrt{\frac{(K/\rho)(1+e_{rc})}{K/\rho + e_{rc}a_0^2}} - \left[1 - 2e_{rc}\frac{(K/E)a_0^2 c_1}{K/\rho - a_0^2}\right]^2}{\sqrt{\frac{(K/\rho)(1+e_{rc})}{K/\rho + e_{rc}a_0^2}} + \left[1 - 2e_{rc}\frac{(K/E)a_0^2 c_1}{K/\rho - a_0^2}\right]^2} \tag{9.17}$$

$$H_t^* = -\left\{\frac{\sqrt{\frac{(K/\rho)(1+e_{rc})}{K/\rho + e_{rc}a_0^2}} - \left[1 - 2e_{rc}\frac{(K/E)a_0^2 c_1}{K/\rho - a_0^2}\right]^2}{\sqrt{\frac{(K/\rho)(1+e_{rc})}{K/\rho + e_{rc}a_0^2}} + \left[1 - 2e_{rc}\frac{(K/E)a_0^2 c_1}{K/\rho - a_0^2}\right]^2}\right\}^2 \tag{9.18}$$

The plots of Eqs (9.17) and (9.18) are given in Figures 9.2 and 9.3, respectively. The plots are for a steel pipe ($E = 207$ GPa), anchored throughout ($c_1 = 1 - \mu^2 = 0.91$, where $\mu = 0.3$ is the Poisson's ratio of steel), and transmitting water at 20 ℃ ($K = 2.195$ GPa, $\rho = 998.2$ kg/m^3). Three specific wave speeds are considered, which are $a_0 = 800$, 1000 and 1200 m/s. The range of e_{rc} used is from -0.5 to 0.5, which means the thickness varies

from half the original wall thickness to one and half of the original wall thickness.

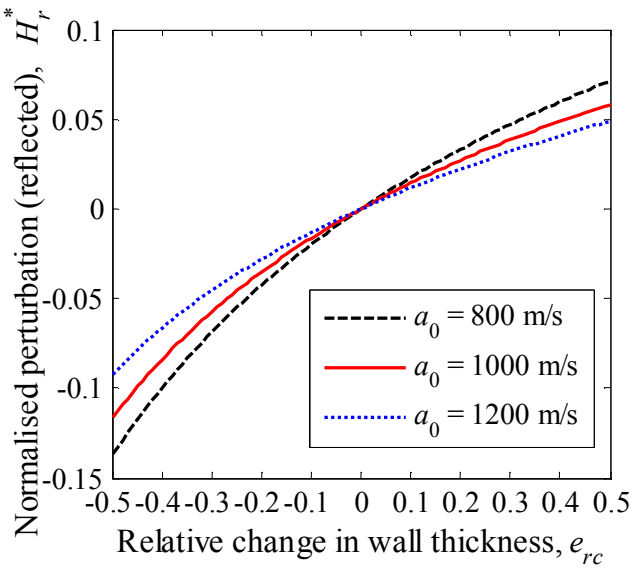

Figure 9.2 Variation of the normalized head perturbation of the reflected wave (H_r^*) according to a relative change in wall thickness (e_{rc}) from the internal side of a pipeline

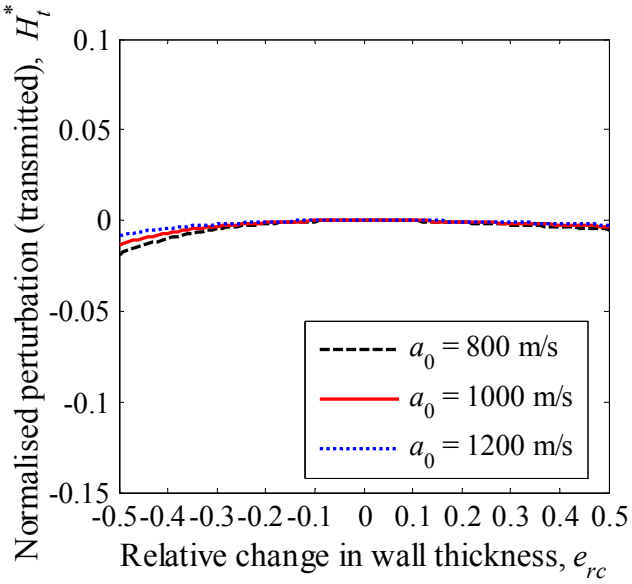

Figure 9.3 Variation of the normalized head perturbation of the transmitted wave (H_t^*) according to a relative change in wall thickness (e_{rc}) from the internal side of a pipeline

Figure 9.2 illustrates that, for the same degree of change in wall thickness from the internal side, the reflection is more evident in the pipeline that has a lower wave speed. A reduction in the thickness of the wall can introduce a perturbation of greater magnitude than that caused by an increase in wall thickness with the same degree. Figure 9.2 also shows that the magnitude of the reflection is proportional to the degree of change in wall thickness. When the variation of wall thickness is less than ± 10%, the head perturbation of the reflection has a magnitude of no more than ± 3% that of the incident wave. This observation can be used to distinguish severe deterioration from mild variations in wall thickness.

Figure 9.3 shows that the transmitted wave is not much affected by a change in wall thickness, which is consistent with the finding in Figure 9.1. The difference between the head values of the transmitted wave and the incident wave is no more than 1% for most e_{rc} values. This result demonstrates that, for an incident wave propagating through a deteriorated section of pipe with a change in wall thickness, the loss in head is typically negligible.

Discussion on the material of pipe wall

The results shown in Figures 9.2 and 9.3 are just for steel pipes ($E = 207$ GPa). In the field, pipes may be made from other types of material, such as copper and ductile iron. Among all the types of material that are commonly used to build pipelines, steel has the highest value of E (Wylie and Streeter 1993). Numerical simulations (not presented in this note) show that pipes with a lower value of E have even greater variation of H_r^* regarding to the same value of e_{rc}. The variation of H_t^* also increases but is still negligible.

The increase in the variation of H_r^* (or H_t^*) with a lower value of E can be explained mathematically. The partial derivative of H_r^* to E can be obtained from Eq. (9.17). The partial derivative is positive when $e_{rc} \in (-0.5, 0)$ and negative when $e_{rc} \in (0, 0.5)$. This demonstrates that the value of H_r^* is directly proportional to E when $e_{rc} \in (-0.5, 0)$, and inversely proportional to E when $e_{rc} \in (0, 0.5)$. Note that H_r^* is always negative when $e_{rc} < 0$ and positive when $e_{rc} > 0$. As a result, for any specific value of e_{rc} between -0.5 and 0.5 but other than 0, the variation in H_r^* (i.e. the absolute value of H_r^*) increases when the value of E decreases.

9.4.2 An external change in wall thickness

This subsection studies a deteriorated pipe section with an external change in wall thickness. For example, a section of pipe with a thinner wall thickness due to extended external corrosion (due to saltwater or acidic soils). The internal diameter is constant throughout the pipeline and denoted as D_0. The wall thickness of the original pipe and the deteriorated section are still represented by e_0 and e_1. Eq. (9.11) is still used to represent the relative change in wall thickness.

The expression of B_r shown in Eq. (9.13) can be simplified to

$$B_r = a_1 / a_0 \tag{9.19}$$

The expression of a_1 as shown in Eq. (9.12) is still applicable in this scenario. Substituting Eq. (9.12) into Eq. (9.19) and neglecting the small order term $(K/E)2c_1$, B_r can be described as

$$B_r = \sqrt{\frac{(K/\rho)(1+e_{rc})}{(K/\rho)+e_{rc}a_0^2}} \tag{9.20}$$

It can be seen that Eq. (9.20) is less complex than Eq. (9.16), which is the counterpart for the scenario of a change in wall thickness from the internal side. The denominator in Eq. (9.16) that represents the contribution of the change in internal diameter is not included in Eq. (9.20) (since the internal diameter is constant). Eq. (9.20) demonstrates that, when the wall thickness change is from the external side, the variation in the impedance is related to the relative change in wall thickness (e_{rc}) and the original wave speed (a_0), but not directly affected by the material of the pipe wall or the internal diameter of the pipe.

The relationship between the relative change in wall thickness and the normalised head perturbations of the reflected and transmitted waves can be obtained by substituting Eq. (9.20) into Eqs (9.8) and (9.9). The expressions of the subsequent equations are shown in Eqs (9.21) and (9.22).

$$H_r^* = \frac{\sqrt{\frac{(K/\rho)(1+e_{rc})}{K/\rho+e_{rc}a_0^2}}-1}{\sqrt{\frac{(K/\rho)(1+e_{rc})}{K/\rho+e_{rc}a_0^2}}+1} \tag{9.21}$$

$$H_t^* = -\left[\frac{\sqrt{\frac{(K/\rho)(1+e_{rc})}{K/\rho+e_{rc}a_0^2}}-1}{\sqrt{\frac{(K/\rho)(1+e_{rc})}{K/\rho+e_{rc}a_0^2}}+1}\right]^2 \tag{9.22}$$

The plots for H_r^* [Eq. (9.21)] are given in Figure 9.4. The plots for the transmitted wave are not presented, which are similar to Figure 9.3 and demonstrate that H_t^* is not sensitive to e_{rc}.

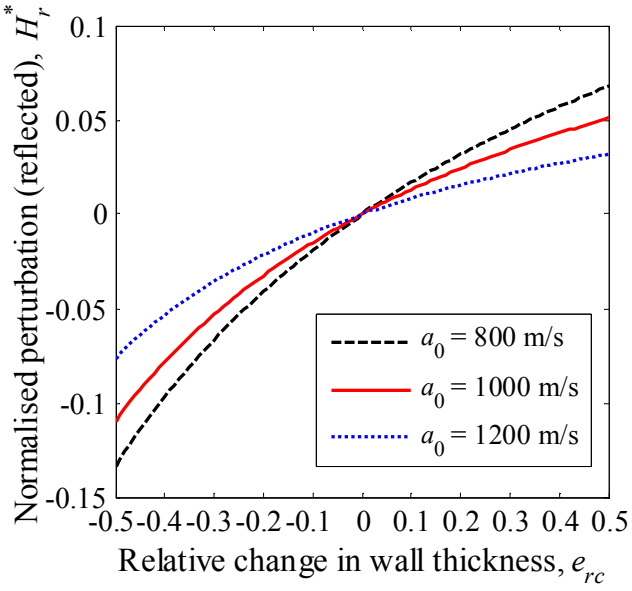

Figure 9.4 Variation of the normalized head perturbation of the reflected wave (H_r^*) according to a relative change in wall thickness (e_{rc}) from the external side of a pipeline

The results shown in Figure 9.4 have a similar pattern to that in Figure 9.2. However, the variation of H_r^* as shown in Figure 9.4 is slightly smaller than the counterpart in Figure 9.2 for any specific value of e_{rc}. Note that the results in Figure 9.2 are just for steel pipes, and as discussed in a previous section, pipes with a lower value of E have even greater variations of H_r^* regarding to the same value of e_{rc}. This demonstrates that, in general, a change in wall

thickness from the internal side of a pipeline can introduce a greater transient wave reflection than that resulted from a same degree change in wall thickness from the external side.

This finding can also be explained mathematically. The expressions of H_r^* for the two scenarios are given in Eqs (9.17) and (9.21) respectively. The absolute value of H_r^* in Eq. (9.17) (corresponding to a change in wall thickness from the *internal* side) is always greater than the absolute value of H_r^* in Eq. (9.21) (corresponding to a change in wall thickness from the *external* side) when e_{rc} is between -0.5 and 0.5 but other than 0.

9.5 Conclusions

A change in pipe wall thickness can introduce a variation in pipe impedance, which results in wave reflections and alters the head of the transmitted wave under fluid transient events. A sensitivity analysis has been conducted to study how a deteriorated pipe section with a change in wall thickness affects the sizes of the reflected and transmitted transient pressure waves. A change in wall thickness may be from either the internal or external sides of the pipeline, and sensitivity analyses have been conducted for these two scenarios respectively. The scenario in which changes in wall thickness occur on both internal and external sides is much more complex and was not discussed in this technical note. Nevertheless, it is expected that, in the combined scenario, the variations of H_r^* and H_t^* according to e_{rc} should behave between the two scenarios discussed in Figures 9.2 and 9.4.

The sensitivity analyses demonstrate that, when the variation in impedance is caused by a change in wall thickness, the size of the wave reflection is directly proportional to the degree of change in wall thickness and inversely proportional to the wave speed in the intact pipeline. A reduction in the thickness of the wall can introduce a perturbation of greater magnitude than that caused by an increase in wall thickness with the same degree. On the

contrary, the transmitted wave is not sensitive to variations in impedance or wall thickness. As a result, the head loss caused by wave transmission is typically negligible.

The results of this research can be used for fast and quantitative transient-based pipeline condition assessment. The plots describing the variation of the normalized head perturbation of the reflected wave according to relative change in wall thickness (Figures 9.2 and 9.4) can be used as look-up charts. Once a transient pressure traced induced by a steep pressure wave is measured from a pipeline, deteriorated sections can be identified from the reflected waves and the wall thickness of them can be read from the plots.

A variation in pipe impedance may also result from a physical change in material. For example, graphitization changes cast iron pipe wall to graphite flakes and iron oxides, but there may be no apparent change in wall thickness. Analysis of deterioration with a physical change in material is out of the scope of this research. However, the results of this research can be used to detect any types of extended structural deterioration that introduces a variation in impedance. The estimated wall thickness can be regarded as an equivalent wall thickness for deterioration with a physical change in material but not much change in wall thickness. If necessary, the equations can be reformulated to relate the impedance change to the change in material property.

Acknowledgements

The research presented in this paper has been supported by the Australian Research Council through the Discovery Linkage Grant LP130100567.

Notations

The following symbols are used in this paper:

A = cross sectional area of pipe;

a = wave speed;

B = pipeline impedance;

B_r = impedance ratio;

c_1 = coefficient of contain condition;

D = internal diameter of pipeline;

E = Young's modulus of pipe material;

e = pipe wall thickness;

e_{rc} = relative change in wall thickness;

g = gravitational acceleration;

H_0 = steady-state head;

H_i = head of incident wave;

H_r = head of reflected wave;

H_r^* = normalized head perturbation of reflected wave;

H_t = head of transmitted wave;

H_t^* = normalized head perturbation of transmitted wave;

K = Bulk modulus of elasticity of fluid;

Greek symbols:

ρ = density of fluid;

μ = Poisson's ratio.

Chapter 10

Detection of Localized Deterioration Distributed along Single Pipelines by Reconstructive MOC Analysis (Journal Publication 8)

Gong, J., Lambert, M. F., Simpson, A. R., and Zecchin, A. C.

School of Civil, Environmental and Mining Engineering, the University of Adelaide, Adelaide, SA 5005 Australia

Journal of Hydraulic Engineering, DOI: 10.1061/(ASCE)HY.1943-7900.0000806, (accepted for publication).

Statement of Authorship

Title of Paper	Detection of Localized Deterioration Distributed along Single Pipelines by Reconstructive MOC Analysis
Publication Status	Accepted for Publication
Publication Details	Gong, J., Lambert, M. F., Simpson, A. R., and Zecchin, A. C. (2013). "Detection of localized deterioration distributed along single pipelines by reconstructive MOC analysis." *Journal of Hydraulic Engineering*, DOI: 10.1061/(ASCE)HY.1943-7900.0000806.

Author Contributions

By signing the Statement of Authorship, each author certifies that their stated contribution to the publication is accurate and that permission is granted for the publication to be included in the candidate's thesis.

Name of Principal Author (Candidate)	Jinzhe Gong		
Contribution to the Paper	Developed and implemented the methodology, designed and conducted numerical simulations, interpreted and analysed results, prepared manuscript.		
Signature		Date	25/09/2013

Name of Co-Author	Martin Lambert		
Contribution to the Paper	Supervised development of work, helped to evaluate and edit the manuscript and acting as the corresponding author.		
Signature		Date	25/9/13

Name of Co-Author	Angus Simpson		
Contribution to the Paper	Helped to evaluate and edit the manuscript.		
Signature		Date	25/9/2013

Name of Co-Author	Aaron Zecchin		
Contribution to the Paper	Helped to evaluate and edit the manuscript.		
Signature		~~Date~~	1.10.2013

Abstract

The detection of localized deterioration that is distributed along pipelines, including wall thickness reduction caused by large scale corrosion, is essential for targeted pipeline maintenance and the prevention of pipe failure. This paper proposes a novel technique for the detection of distributed deterioration along a pipeline by estimating the distribution of pipeline properties using a measured pressure transient trace. The proposed technique is referred as *reconstructive MOC analysis* and it is an inverse process of the traditional forward MOC calculation. The reconstructive MOC analysis reconstructs the MOC grid and estimates the pipe parameters, such as impedance and wave speed, reach by reach from downstream to upstream. Numerical simulations are performed on a pipeline with three pipe sections of impedance changes. These deteriorated sections are accurately detected and located by using the new technique. Experimental verification is also performed by successfully detecting a section of pipe with a thinner wall thickness in a single pipeline.

10.1 Introduction

Deterioration in pipelines can be divided into two categories: discrete deterioration and distributed deterioration. Discrete deterioration describes faults that occur at points, such as leaks or partially closed valves. Distributed deterioration refers to localized deterioration that typically extends meters or tens of meters along the pipeline and can reoccur multiple times. Examples of distributed deterioration include internal or external widespread corrosion or the spalling of cement mortar lining, which are common in aging water distribution pipelines and can be large in number (Stephens et al. 2008). Distributed deterioration may not impose imminent threats to the operation of a pipeline system, however it usually reduces water transmission efficiency (Tran et al. 2010), creates water quality problems (Vreeburg and Boxall 2007), and may also develop into more serious blockages or bursts over time (Zamanzadeh et al. 2007). Detection of localized deterioration that is distributed along pipelines in its early stages helps authorities to cost-effectively maintain, replace and rehabilitate their pipeline assets, and prevents potential pipe failure.

At present, transient pressure waves are recognized as a potential tool for non-invasive detection of both discrete and distributed deterioration in pressurized pipelines. Jönsson and Larson (1992) proposed a spectral analysis technique of a measured pressure trace for leak detection. Pudar and Liggett (1992) suggested that leak detection in water distribution networks could be accomplished by solving an inverse problem using measurements of steady-state pressure (and/or flow). Liggett and Chen (1994) recommended that inverse calculation under transient events would be more suitable for leak detection because some system parameters (e.g. friction factor) could be calibrated through the inverse analysis rather than approximately estimated. The transient-based inverse approach has been further developed in the last two decades (Vítkovský et al. 2000; Covas and Ramos 2010) and is now known as the inverse transient analysis (ITA). Several other transient-based leak detection techniques have also been proposed, either in the time domain

(Brunone 1999; Lee et al. 2007b) or in the frequency domain (Ferrante and Brunone 2003b; Covas et al. 2005; Lee et al. 2005a; Gong et al. 2013e). The transient analysis has also been used in detection of discrete blockages in pipelines (Wang et al. 2005; Lee et al. 2008b; Sattar et al. 2008).

Investigating distributed deterioration detection in water transmission pipelines, Stephens et al. (2008; 2013) attempted the detection of changes in pipe wall thickness for pipelines in the field. The field study used fluid transients and the inverse transient analysis (ITA). It indicated that the loss of cement mortar lining could lead to wall corrosion and significant changes in wave speed. However, the structural complexity and parametric uncertainties of real pipes proved to be a serious obstacle to an efficient and accurate ITA.

Duan et al. (2012) proposed a technique for the detection of extended blockages by analyzing the frequency response of the pipeline system. Their analysis indicated that extended blockages can cause the resonant frequencies of the pipeline system to shift, and the locations and sizes of the blockages can be determined through an inverse calibration approach with optimization algorithms. However, a number of system resonant frequencies need to be accurately determined to provide sufficient information for the inverse calibration. This is difficult in practice due to the limitations in achieving an acceptably wide signal bandwidth and the effects of noise (Lee et al. 2008a).

Hachem and Schleiss (2012) advanced a transient-based technique for the determination of the location and stiffness of a structurally weak section in a single pipeline. The mean wave speed in the tested pipe and that in the intact pipe (without the weak section) were estimated from the pressure traces measured at the two ends. The location and length of the weak section were determined using the two mean wave speed values and the travel time of the reflections from the weak section. Thereafter, the wave speed in the weak section was estimated from the estimated length of this section and the two mean wave speed values. The stiffness was then estimated from the wave speed of the weak section. The major challenge for this technique is that the

wave speed values in weak sections are difficult to estimate accurately, especially when multiple deteriorated sections exist in the same pipeline.

Gong et al. (2013f) proposed a technique for detecting a single deteriorated section in a pipeline by analyzing the deterioration-induced reflections induced by a step transient wave. Wall thickness changes alter the impedance of the pipe section where the change exists. Using the measured pressure trace, Gong et al. (2013f) demonstrated that the size of the deterioration-induced transient wave reflection is related to the impedance of the deteriorated section, while the travel time of the perturbation is indicative of its location. The technique was verified using experimental data, and the location and impedance of a pipe section with a thinner wall thickness were estimated successfully. However, this technique is hard to extend to pipelines with multiple deteriorated sections, especially where the deterioration-induced perturbations are complex. This occurs due to the effects of multiple reflections within and between the deteriorated sections.

This paper proposes a novel and efficient transient-based distributed deterioration detection method for single water transmission pipelines. The method is based on the reconstruction of the impedance distribution along the pipe using backwards method of characteristics (MOC) calculation. The MOC is a conventional method for modeling transient events in pipeline systems where their properties (such as length, diameter, roughness height and wave speed) are known (Chaudhry 1987). The reconstructive MOC analysis proposed in this research is an inverse process, by which the distribution of the impedance and the wave speed can be estimated from the measured transient data. Plotting the distribution of the impedance or the wave speed allows the deteriorated sections to be identified and located. Numerical simulations show that this technique can deal with complex multiple reflections in the measured pressure traces, allowing multiple deteriorated sections to be accurately detected and located.

Experimental data from a single pipeline containing a section with a thinner wall thickness is used to verify the proposed technique. A side-discharge

valve was used to generate the incident transient wave in the experimental system. Because the transient generator valve is limited in its maneuverability, closing the valve to generate the incident wave is fast, but not instantaneous. The result is a wave front with a rise time of approximately 4 ms. This can be overcome by a signal preprocessing technique for estimating the step response function (SRF) of the pipeline from the measured pressure trace. The impedance, wave speed, location and length of the deteriorated section (a pipe section with a thinner wall thickness) in the experimental pipeline are estimated successfully.

10.2 Method of characteristics

This section gives the compatibility equations of the method of characteristics (MOC). The properties of a pipe are assumed to be distinct from reach to reach in the following derivation.

An example of the MOC grid in the $x-t$ plane for a single pipeline is shown in Figure 10.1. Assuming that properties of the pipe can be distinct from reach to reach, the MOC compatibility equations valid along the characteristic lines in the MOC grid [Figure 10.1(b)] are

$$C^+: \quad H_P - H_M + B_{MP}(Q_P - Q_M) + R_{MP}Q_P|Q_M| = 0 \tag{10.1}$$

$$C^-: \quad H_P - H_N - B_{PN}(Q_P - Q_N) - R_{PN}Q_P|Q_N| = 0 \tag{10.2}$$

where H_P , H_M and H_N are head values, and Q_P , Q_M and Q_N are discharges at points P , M and N , respectively, as shown in Figure 10.1; B and R denote the characteristic impedance of a reach of pipe and the pipe reach resistance, with the subscripts 'MP' and 'PN' representing the pipe reach MP and PN shown in Figure 10.1 respectively. Expressions for the impedance B and the reach resistance R for the ith pipe reach are given in Eq. (10.3) and Eq. (10.4), respectively.

$$B_i = a_i / (gA_i) \tag{10.3}$$

$$R_i = f_i \Delta x_i / (2gD_i A_i^2) \tag{10.4}$$

where a = wave speed; g = gravitational acceleration; A = pipe cross-sectional area; f = Darcy-Weisbach friction factor; D = internal diameter of the pipeline; and Δx represents the reach length, which is given by the x-t plane grid relationship

$$\Delta x_i = a_i \Delta t \tag{10.5}$$

where Δt is the time step in the MOC grid, as shown in Figure 10.1.

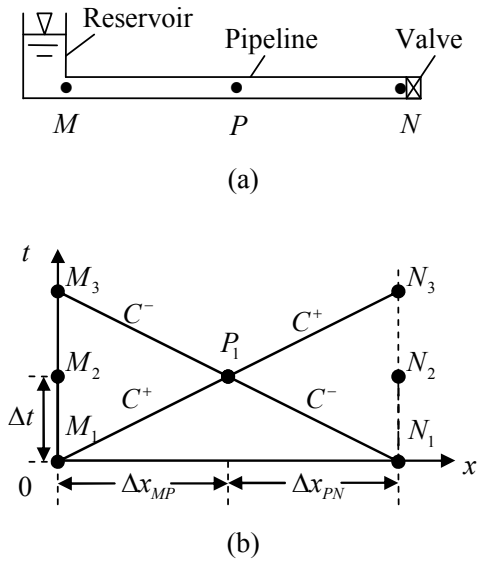

Figure 10.1 (a) An example pipeline system; and (b) its MOC grid for conventional MOC analysis.

In conventional MOC analysis, the structure of the MOC grid is predetermined and the properties of each reach (B_i , a_i , R_i and Δx_i) are known. The conventional MOC analysis is used to simulate the time-history of the transient pressure and flow at specific nodes.

10.3 Reconstructive MOC analysis

The reconstructive MOC analysis proposed in this research is the inverse process of the conventional MOC analysis described above. The MOC grid and the properties for pipe reaches are yet to be estimated from a measured time-history of transient pressure. In the following sections, previous research on performing MOC analysis backwards in time is reviewed; the problem to be solved in the proposed reconstructive MOC analysis is defined; the necessary assumptions are made; and then the detailed procedure of the reconstructive MOC analysis is presented.

10.3.1 Previous research on performing MOC analysis backwards in time

MOC analysis backwards in time has been used previously in valve stroking, a synthesis procedure that specifies the operation of control devices in order to prescribe the behavior of a transient to stay within a maximum head constraint (Wylie and Streeter 1993). The compatibility equations, Eqs (10.1) and (10.2), proved remarkably robust in calculating backwards in time, regenerating a transient effectively (Wylie and Streeter 1993).

Brunone and Morelli (1999) determined the characteristic curve of a valve (curve of the coefficient of discharge) by using the pressure traces measured at the upstream and downstream of the valve during an unsteady-state test. By solving the MOC capability equations and using the recorded time-history of pressure as the boundary condition, the instantaneous discharge at the valve can be calculated. The flow-rate curve is then obtained from the orifice equation.

Shamloo and Haghighi (2009) used a backwards transient approach for leak detection in a reservoir-pipeline valve (RPV) system, where the head perturbations at the reservoir were estimated from the transient trace measured at the valve end of the pipe. They then defined an objective function using the

theoretical constant head at the reservoir and the estimated head perturbations through a least-squares criterion. Thereafter, an inverse calibration process was performed to estimate the location and number of leaks. This is a complex problem involving the optimization of a significant number of parameters. An improvement was made by Haghighi et al (2012) on the backwards transient analysis-based leak detection technique, where a direct solution was used to replace the iterative optimization process. Leaks with unknown sizes are initially assumed at a number of characteristic nodes between the two ends of the pipeline. Equations for the estimated head at the upstream end were parametrically developed as a function of leak area using one period of the measured head data at the downstream end. Then a non-linear system of equations was achieved from the fact that the estimated head values (functions of leak area) should be equal to the measured (or theoretical) head values at the upstream end. As a result, the unknown leak sizes were solved directly from the non-linear system of equations by numerical methods.

All these uses of backwards MOC, however, assume that the MOC grid is explicit and the properties, including impedance, wave speed, diameter and friction factor, are known for every discretized reach. The innovation of the reconstructive MOC analysis proposed in this research is that this is the first time the MOC grid is reconstructed and the properties of each pipe reach are estimated using the first half period of the measured transient data. This one pass approach is quick and does not involve iteration or the calibration of a large number of parameters.

10.3.2 Problem definition

An example reservoir-pipeline-valve (RPV) system is shown in Figure 10.2(a). The MOC grid shown in Figure 10.2(b) is a plausible reconstruction of the MOC grid and presented here for illustration purposes only. The MOC grid is unknown at the beginning and it is constructed by the proposed method. Properties of each reach of pipe, including impedance B_i, wave

speed a_i, reach resistance R_i and the length Δx_i, are unknown. The aim of the proposed reconstructive MOC analysis is to estimate these properties of each reach by reconstructing the MOC grid.

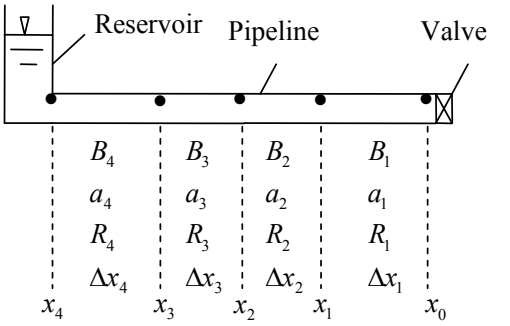

(a)

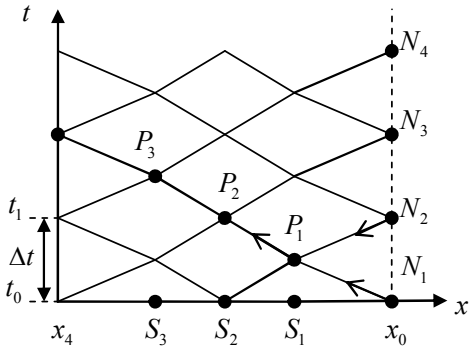

(b)

Figure 10.2 (a) An example pipeline system; and (b) a possible MOC grid reconstructed by the reconstructive MOC analysis (note that the pipeline properties can be different between reaches).

In order to conduct the reconstructive MOC analysis, a steady-state flow with a discharge of Q_0 is established first in the system. Then a step transient wave is generated at time $t = 0$ by abruptly shutting off the valve at the downstream end of the pipeline. Head perturbations are measured at the upstream face of the valve (at location x_0). The reconstructive MOC analysis utilizes the measured pressure transient trace to reconstruct the MOC grid. Perturbations shown in the plots of the estimated impedance and wave speed are indicative of the location and severity of deterioration throughout the pipe.

10.3.3 Assumptions

For simplicity, the inner diameter of the pipeline is assumed to be constant, uniform and known as D_0. This assumption is reasonable for pipelines where the wall thickness change attributable to deterioration is usually negligible when compared with the original diameter. As a result, the wave speed a_i in each reach can be estimated using Eq. (10.3) once the impedance value B_i has been determined, and the length of each pipe reach (or values of x_1 to x_3) can be estimated using Eq. (10.4).

Another assumption to be made is that the Darcy-Weisbach friction factor f is constant and uniform along the pipeline, and the effects of unsteady friction are negligible in the reconstructive MOC analysis. The value of the friction factor can be determined from steady-state conditions by

$$f = (H_r - H_{V0})\frac{2gD_0A_0^2}{LQ_0^2} \tag{10.6}$$

where H_r = reservoir head and H_{V0} = steady-state head at the valve. The steady-state discharge Q_0 has to be known to enable the calculation for f, and Q_0 is also used in the reconstructive MOC analysis, as presented later in this paper. Note that Eq. (10.6) is an alternative to determining f from the pipe roughness height and Reynolds number, which are difficult to accurately estimate in field situations.

When f is constant, the steady-steady hydraulic grade line (HGL) is linear and known along the pipeline. As a result, R_i in Eq. (10.4) is only a function of Δx_i. It is suggested that the steady-state discharge Q_0 is kept small, so that the effects of friction are minimized.

The third assumption is that the incident wave is introduced by an abrupt closure of a valve at the end of the tested pipeline. The abrupt valve closure

makes the wave front of the incident transient sharp and the rise time negligible. The sharp input signal can generate sharp reflections that are used by the reconstructive MOC analysis to build a picture of the pipe condition. In practice, however, due to limitations in the maneuverability of the transient generator valve, the incident wave usually has an inclined wave front. If the rise time of the wave front is greater than the sampling interval Δt of the measurement, error will be involved into the proposed reconstructive MOC analysis. This practical problem can be solved by converting the measured pressure trace to the step response function (SRF) of the system through signal processing, which is described in the *experimental verification* section later on in this paper.

The last assumption is that, in the pressure transient trace resulted from the closure of the valve, a measured pressure value remains until the next one is registered. In fact, the measured pressure data are always discrete sequences with a specific sampling interval. This assumption implies that the pipe properties are uniform within a pipe reach and the discontinuity occurs only at the interface between reaches. This assumption is applicable when the sampling rate of the pressure measurement is high enough to satisfy the required spatial resolution.

10.3.4 Analysis for the first reach

The reconstructive MOC analysis is performed reach by reach from the downstream valve to the upstream reservoir, and the analysis for the first reach between N_1 and S_1 in Figure 10.2(b) is presented here. Corresponding to the pipeline system and the MOC grid shown in Figure 10.2, a hypothetical pressure trace resulting from the rapid valve closure at x_0 at time $t = t_0$ and measured at the upstream face of the closed valve is assumed to be the trace given in Figure 10.3. Note that, in the hypothetical pressure trace, a measured pressure value remains until the next one is measured. As a result, all pipe properties are assumed to be constant within a reach.

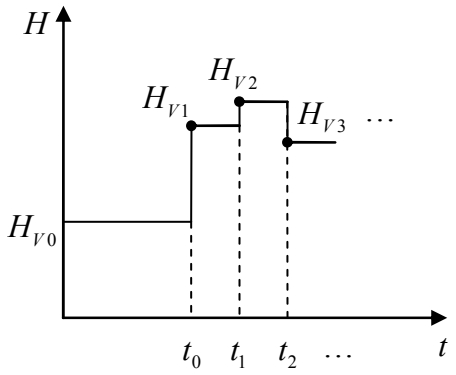

Figure 10.3 An example pressure trace resulting from a rapid valve closure and measured at the upstream face of the closed valve

For the first reach x_0x_1 as shown in Figure 10.2(a), the impedance B_1 can be determined from the steady-state head (H_{V0}) and flow (Q_0) at the valve, and the head value H_{V1}, which is measured at point x_0 and time t_0 (just after the valve closure). A positive characteristic line can be used to facilitate the analysis, as given in Figure 10.4.

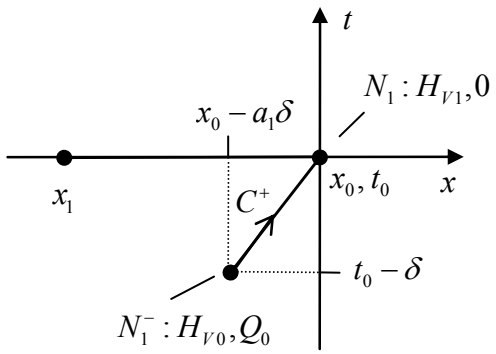

Figure 10.4 MOC analysis at point x_0 for determining B_1

In Figure 10.4, δ is a positive value of time but tends to zero. As a result, the length of the positive characteristic line (C^+ in Figure 10.4) is extremely short, the node N_1^- is very close to node N_1 and the effects of friction are negligible. The head and flow values for the two end points of this short positive characteristic line are shown in Figure 10.4. At node N_1^- (time

$t_0 - \delta$), the pipeline is still at the steady-state condition so the head and flow are H_{V0} and Q_0, while at node N_1 (time t_0) the head rises to H_{V1} and the flow becomes zero. Applying the positive compatibility equation [Eq. (10.1)] to this positive characteristic line, and neglecting the part associated with friction, the impedance B_1 for the first reach can be estimated as

$$B_1 = (H_{V1} - H_{V0}) / Q_0 \tag{10.7}$$

which actually is the same as the result from the Joukowsky head rise formula.

Once the impedance is determined, the wave speed in the first reach a_1 is estimated using Eq. (10.3), and the length of the reach, or the location of x_1, is estimated using Eq. (10.5). Then, the resistance factor R_1 for the first reach $x_0 x_1$ can be estimated using Eq. (10.4), so that the steady-state head H_{S1} at the upstream end of the first pipe reach [x_1 in the pipeline in Figure 10.2(a), which corresponds to node S_1 in the MOC grid in Figure 10.2(b)] can be estimated by

$$H_{S1} = H_{V0} + R_1 Q_0^2 \tag{10.8}$$

Now, all the properties in the first pipe reach are known, including B_1, a_1, x_1, R_1 and H_{S1}. These parameters will be used in the analysis for the next pipe reach.

10.3.5 Analysis for the second reach

For the second reach $x_1 x_2$, to determine the value of B_2, the head H_{P1} and discharge Q_{P1} at node P_1 [Figure 10.2(a)] are required. The characteristic lines between the three nodes N_1, N_2 and P_1 are given in Figure 10.5 to

facilitate the analysis. The arrows indicate the direction from known values to unknown values.

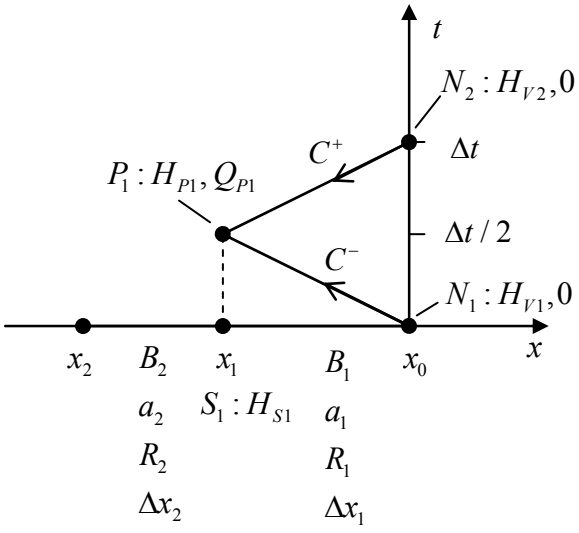

Figure 10.5 Reconstructive MOC analysis for the second pipe section

The information at node P_1 can be obtained from the information at nodes N_1 and N_2 by applying Eqs (10.1) and (10.2) to the characteristic lines N_2P_1 and N_1P_1, respectively. The impedance in the first reach B_1 is substituted into Eqs (10.1) and (10.2). The discharge values at nodes N_1 and N_2 are zero as the valve is fully closed. Finally, the equations for the characteristic lines N_2P_1 and N_1P_1 are:

$$H_{P1} - H_{V2} + B_1 Q_{P1} = 0 \tag{10.9}$$

$$H_{P1} - H_{V1} - B_1 Q_{P1} = 0 \tag{10.10}$$

Once H_{P1} and Q_{P1} at node P_1 are determined, the impedance B_2 of the second pipe reach x_1x_2 can be estimated using MOC analysis at point x_1 around $t = \Delta t / 2$. In the MOC grid shown in Figure 10.5, the change in the head and discharge at point x_1 occurs at $t = \Delta t / 2$ instantaneously. When $t < \Delta t / 2$, along the dashed line from node S_1 to node P_1, the head and

discharge at point x_1 remain at the steady state, which are H_{S1} and Q_0 respectively. Similar to the analysis for time t_0 shown in Figure 10.4, the instantaneous change in the head and discharge at $t = \Delta t / 2$ can be described by a positive characteristic line with an extremely small time span, as given in Figure 10.6.

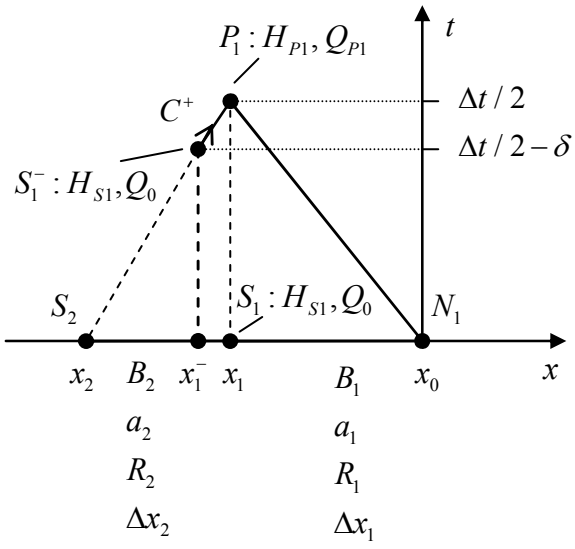

Figure 10.6 MOC analysis for point x_1 at $t = \Delta t / 2$

In the MOC grid shown in Figure 10.6, the area to the left of the characteristic line N_1P_1 has steady-state conditions when $t < \Delta t / 2$. Consider a node S_1^- in the vicinity of node P_1 and along the line S_2P_1 as shown in Figure 10.6, it represents the steady state information at point $x_1^- = x_1 - a_2\delta$ at time $t = \Delta t / 2 - \delta$. Since δ is positive but tends to zero, point x_1^- is located at the upstream of and in close proximity to point x_1, and the friction in the extremely short pipe reach between these two points can be neglected. As a result, the head and discharge at node S_1^- are the same as those at node S_1. Applying the positive compatibility equation [Eq. (10.1)] to the characteristic line $S_1^-P_1$ and neglecting the friction term R, the value of B_2 can be estimated as

$$B_2 = -(H_{P1} - H_{S1}) / (Q_{P1} - Q_0) \tag{10.11}$$

Other properties in this reach can be estimated using the same process as for the first reach, including a_2, x_2, R_2 and H_{S2}. The process of determining the properties of pipe reach x_1x_2 from the information at nodes N_1 and N_2 is the key component of the *reconstructive MOC analysis*, which means the MOC analysis is performed backwards in time and the properties of the pipeline are estimated from the measured head data.

10.3.6 Analysis for the subsequent pipeline reaches

The ways in which the properties of the other reaches of pipe are determined are similar to the methods used for the second reach, and the reaches are analyzed sequentially from downstream to upstream. For the analysis of the i th reach, the estimated properties of the (i -1) downstream pipe reaches are used, as well as the first i head data measured at the end of the pipeline. By conducting the MOC analysis backwards in time and towards the reservoir from the valve end, the head and discharge for the nodes on the characteristic line N_1P_i can be determined.

A similar process as illustrated in Figure 10.6 is then used to estimate the impedance B_i from the estimated information at node P_{i-1}, and the steady-state head and discharge at S_{i-1}, which are $H_{S(i-1)}$ and Q_0 respectively. Thereafter, Eqs (10.3) to (10.5) are used to determine other properties in this reach. The reconstructive MOC analysis continues until the properties of the final reach of pipe, that is adjacent to the reservoir, are estimated. At this point, plots of the impedance and wave speed distribution along the pipeline can be obtained, from which the number, location and severity of the deterioration can be estimated.

If only the condition of a specific section of the pipeline needs to be assessed, the reconstructive MOC analysis just needs to cover the length from the valve

to the upstream boundary of the targeted section. If the whole pipeline is covered, the total number of pipe reaches used in the reconstructive MOC analysis equals the number of pressure data in the first plateau of the measured pressure trace (from the initial pressure jump to the first reflection from the reservoir). Within this range, the effects of friction are usually negligible, especially for a small steady-state discharge.

The major advantage of the proposed reconstructive MOC analysis is that complex reflections caused by natural pipeline parameter variations and/or multiple deteriorated sections can be interpreted appropriately. Because both the wave reflections and transmissions are considered in the restoration of the information (head and flow) for each node in the MOC grid, multiple reflections are intrinsically included in the analysis. As a result, theoretically the complexities in the measured pressure trace resulting from pipeline parameter variations and multiple deteriorated sections can be resolved, revealing the correct impedance distribution along the pipeline. This advantage is demonstrated in the numerical simulations for the detection of multiple deteriorated sections in a single pipeline as presented in the following section.

10.4 Numerical simulations

Numerical simulations performed on a single pipeline with three deteriorated sections are used to verify the proposed reconstructive MOC analysis for detecting widespread corrosion or other extended damage in pipelines. Firstly, conventional MOC modeling (in which all the properties of the system are explicitly specified) is conducted to obtain the head response induced by a step transient wave. Then, the reconstructive MOC analysis is applied to the pressure trace to derive the impedance and the wave speed along the pipeline.

The layout of the pipeline system used for the numerical simulations is given in Figure 10.7. The deterioration is represented by three pipe sections with changes in wave speed (a_1 to a_3 and B_1 to B_3 as shown in Figure 10.7). The

total length of the pipeline is L = 1500 m; the diameter is D_0 = 600 mm and uniform along the pipe; the wave speed in normal sections is a_0 = 1000 m/s (impedance B_0 = 360.5 s/m^2); the steady-state flow rate is Q_0 = 0.05 m^3/s (velocity = 0.177 m/s); the Darcy-Weisbach friction factor used for the forward MOC modeling is f = 0.02.

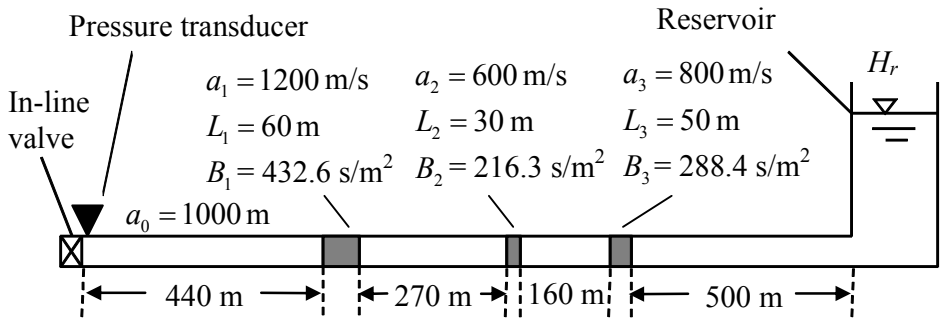

Figure 10.7 Pipeline configuration for the numerical simulation.

The time step for the MOC modeling was Δt = 1 ms, and the length of each reach in the grid was determined by $\Delta x_i = a_i \Delta t$. A step transient pressure wave is generated by shutting off the in-line valve at the end of the pipeline abruptly at time t_0 = 0.1 s. The duration of the closure is assumed to be zero, so that the wave front is steep and satisfies the third assumption made previously. The pressure trace is measured at the upstream face of the valve, and the first plateau (with time duration of 3.065 s) is presented in Figure 10.8.

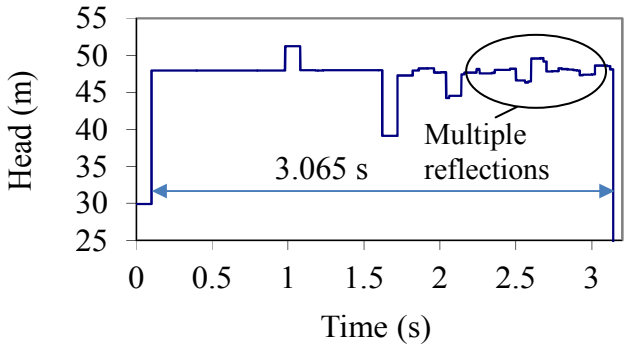

Figure 10.8 Pressure trace obtained in the forward MOC modeling (the first plateau, i.e. from the initial wave jump to the first reflection from the reservoir).

It can be seen from Figure 10.8 that the pressure trace is complex after about 1.7 seconds because of the multiple reflections within and between the three deteriorated sections. The perturbations in the oval, in particular, are just multiple reflections. It is difficult to estimate the number and various locations of the deteriorated sections using the single deterioration detection technique developed in Gong et al. (2013f). The reconstructive MOC analysis described in the previous section is therefore applied to interpret the pressure trace shown in Figure 10.8. The distributions of impedance and the wave speed along the pipeline are estimated and presented in Figure 10.9.

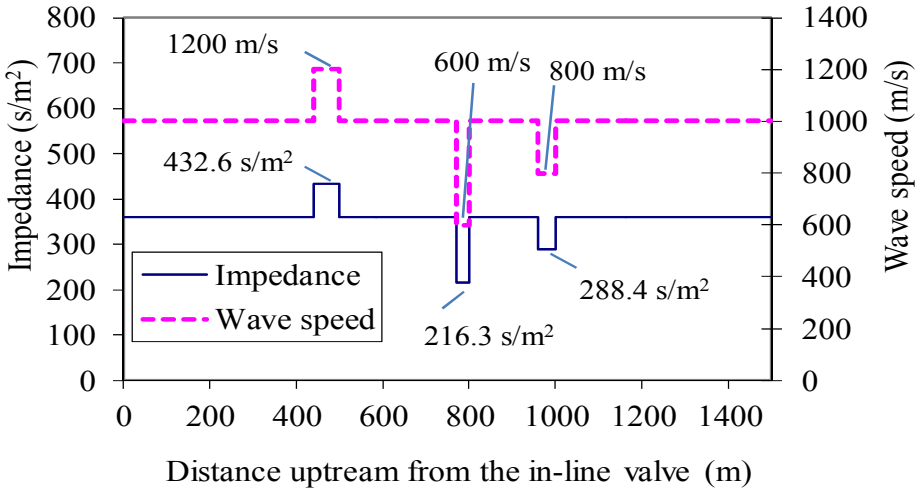

Figure 10.9 Impedance (B , on the left axis) and wave speed (a , on the right axis) estimated from the reconstructive MOC analysis for the numerical simulations

The three deteriorated sections can be identified and located accurately from the plots of the estimated distribution of the impedance and wave speed in Figure 10.9. The values of the estimated location, impedance and wave speed are consistent with the theoretical values in the pipeline model in Figure 10.3 (with discrepancy less than 0.05% between two numerical values). The successful numerical verification validates the proposed method of detecting widespread deterioration in a pipeline using the reconstructive MOC analysis. The method is able to deal with multiple reflections in the measured pressure trace. To further verify the proposed technique, data generated by an experimental pipeline in the laboratory is used, with details given in the following section.

10.5 Experimental verification

Experiments conducted on the single pipeline system in the Robin Hydraulics Laboratory at the University of Adelaide have produced data to verify the proposed technique for detecting widespread deterioration using the reconstructive MOC analysis. The experimental data has also been used in

Gong et al. (2013f) to verify a technique for detecting single distributed deterioration in pressurized pipelines.

The layout of the experimental pipeline system and the measured pressure traces are presented below. Because the proposed reconstructive MOC analysis requires a steep front in the incident wave, a preprocessing technique is developed to transfer the measured pressure trace to a step response function (SRF), in which the rising front slope of the experimental incident wave is corrected to a sharp step. The reconstructive MOC analysis is then performed on the SRF to estimate the impedance and wave speed distribution in the experimental pipeline.

10.5.1 Experimental pipeline configuration

The layout of the experimental pipeline system is given in Figure 10.10. The test pipeline is a 37.46 m in length of straight copper pipe with an internal diameter D_0 = 22.14 mm, and a wall thickness e_0 = 1.63 mm. One end of the pipeline is connected to an electronically controlled pressurized tank and the other to a closed in-line valve. A pipe section 1.649 m long with a thinner pipe wall thickness e_1 = 1.22 mm (the internal diameter D_1 = 22.96 mm) is placed 17.805 m upstream from the in-line valve. The material and external diameter of this section are the same as those of the original pipeline. This section represents a pipe section with a lower pressure rating, or could be interpreted as a section with uniform wall thickness reduction due to internal corrosion, disregarding the effects of spatial variability which would be present in realistic corroded sections. A side-discharge solenoid valve is located 144 mm upstream from the closed in-line valve for the generation of transient waves.

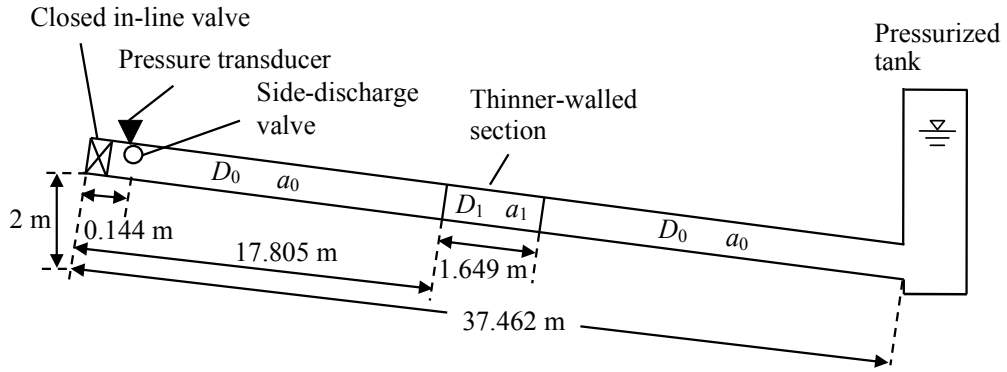

Figure 10.10 System layout of the experimental pipeline.

The wave speed in the intact pipeline is a_0 = 1328 m/s as determined by experiments (Lee et al. 2007a), which is very close to the theoretical wave speed 1329 m/s calculated from the theoretical wave speed formula for thick-walled pipes (Wylie and Streeter 1993). Using Eq. (10.3), the impedance of the original pipeline $B_0 = 3.516\times10^5$ s/m^2. The theoretical wave speed in the thinner-walled section is estimated as a_1 = 1282 m/s using the theoretical wave speed formula, while $B_1 = 3.151\times10^5$ s/m^2 using Eq. (10.3).

10.5.2 Experimental pressure trace

The transient wave is generated by closing the side-discharge solenoid valve rapidly but not instantaneously. Pressure responses are monitored at the side-discharge valve with a sampling frequency of 2 kHz. The closure time is approximately 4 ms, which is much greater than the sampling interval, so that a rising front slope is obtained rather than a steep step as used in the numerical simulations. The steady-state flow rate is not measured and yet to be estimated. The tests are repeated for a number of times and the measured pressure traces are consistent (Gong et al. 2013f). One of the measured pressure traces is presented in Figure 10.11 (only the first plateau) [which is the pressure trace of *Test* 1 in Gong et al. (2013f)]. The dip shown in the middle of the plot represents the reflections from the section with a thinner wall thickness.

The steady-state head at the valve is estimated to be H_{V0} = 25.55 m by averaging the head values within a short time interval before the wave front (6.92 s to 6.94 s). Similarly, the head value of the step incident wave can be estimated as H_i = 39.06 m (by averaging the head from 6.945 s to 6.947 s).

10.5.3 Preprocessing of the measured data

The experimental pressure trace shown in Figure 10.11 has a rising front slope of approximately 4 ms. The shape of the initial wave front affects the shape of reflections from the pipeline, and a detailed discussion is given in Gong et al. (2013f). In this experiment, the reflections from the thinner-walled section were not sharp because the original valve closure was not instantaneous. An improved estimation of the boundary between the normal pipe section and the thinner-walled section can be achieved if the measured pressure trace is pre-processed to build the steepness of the reflections before the reconstructive MOC analysis. In addition, the transient flow during this rising period is non-zero and unknown, so that the reconstructive MOC analysis described in the previous section cannot be performed directly on the measured trace.

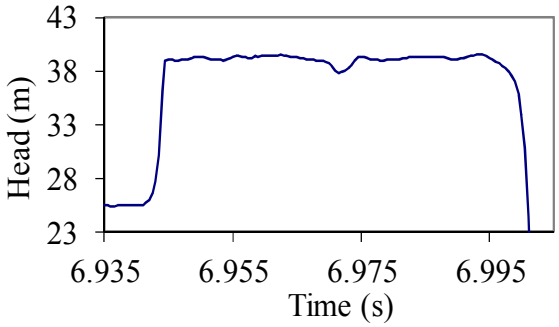

Figure 10.11 First plateau of the experimental pressure trace

A preprocessing procedure is proposed for deriving the step response function (SRF) of the pipeline from the measured pressure trace. The SRF is the response resulting from a theoretical step input transient wave, where the discharge is zero after the initial step head rise. The estimated SRF is then

used in the proposed reconstructive MOC analysis to determine the distribution of impedance and wave speed along the pipeline.

To obtain the SRF of a linear system, both the input and the output signals are required. For the experimental pipeline system, the measured pressure trace (Figure 10.11) can be used as the output. The *induced flow perturbation* at the side-discharge valve that is defined in Lee et al. (2006) can be used as the input. It is assumed that the flow perturbation is linearly related to the head perturbation during the generation of the transient (from 6.941 s to 6.945 s) by the Joukowsky formula, so that the input flow perturbation signal can be obtained by

$$\Delta Q = -\Delta H / B_0 \tag{10.12}$$

where ΔQ and ΔH are the discharge and head perturbation from the mean state at the generation point. Strictly speaking, B_1 should be used in Eq. (10.12) instead of B_0. However, since B_1 is unknown, an assumption that $B_1 = B_0$ has been made.

The unit SRF (which is the SRF of a system when the input is a step signal with a magnitude of unity) is then obtained from the estimated input flow perturbation and the measured pressure trace. The determination of the unit SRF is based on correlation analysis of the input and output signals, and details can be found in Ljung (1999). In this research, the system identification toolbox in Matlab (2010) was used to facilitate the signal processing. The plot of the estimated unit SRF is given in Figure 10.12.

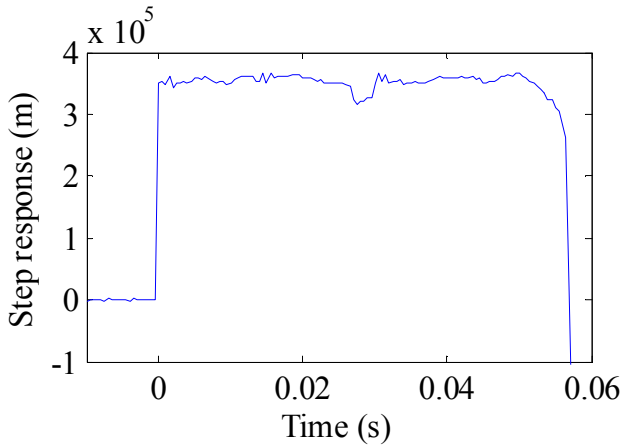

Figure 10.12 Plot of the unit step response function (SRF) estimated from the measured pressure trace (SRF for Q_0 = 1 m^3/s)

10.5.4 Reconstructive MOC analysis for the step response function

The proposed reconstructive MOC analysis is performed on the estimated step response function (SRF) from t = 0 up to t = 0.0565 s. The plots of the estimated impedance and wave speed are given in Figure 10.13.

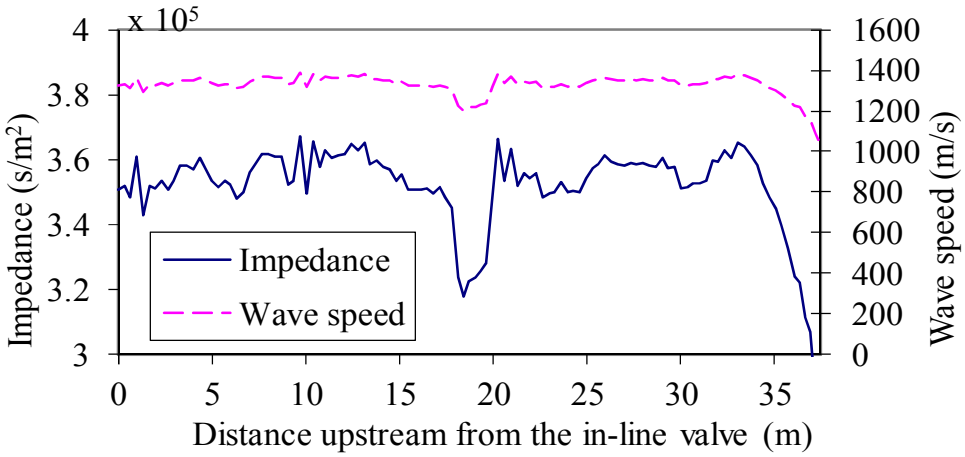

Figure 10.13 Impedance (B, on the left axis) and wave speed (a, on the right axis) estimated from the reconstructive MOC analysis for the experimental pipeline

The dip in the middle of each plot in Figure 10.13 indicates that a pipe section with lower impedance and wave speed values is located in the experimental pipeline. The impedance and the wave speed of this pipe section are estimated as approximately $B_1 = 3.235 \times 10^5$ s/m^2 and a_1 = 1233 m/s respectively by averaging the values at the bottom of the dip in the plots. The first derivative of the estimated distribution of wave speed is calculated to yield the gradient (changing rate) in wave speed along the pipeline, where the two points with local maximum gradient values indicate the boundaries of the thinner-walled section. The length of this section is then estimated as 1.85 m starting from 17.8 m upstream from the closed valve. These estimates are close to the theoretical values of the thinner-walled pipe section in the experimental pipeline system, as shown in Table 10.1.

Table 10.1 Estimated properties of the deteriorated section and corresponding error

Item	Impedance (m/s2)	Wave speed (m/s)	Length (m)	Starting location (m)
Theoretical values	3.151×10^5	1282	1.649	17.805
Estimated values	3.235×10^5	1233	1.85	17.8
Relative error[a]	2.7%	3.8%	12.2%	Not applicable

Note: [a]Relative error = |(estimated value – theoretical value)/ theoretical value|$\times 100\%$

Analysis of pressure traces obtained in repeated tests yields consistent and similar results. Compared with the results $B_1 = 3.217 \times 10^5$ s/m^2 and $a_1 = 1292$ m/s obtained from the single distributed deterioration detection technique in Gong et al. (2013f), the estimated impedance value for the thinner-walled pipe section are very close, while the wave speed estimated by the reconstructive MOC analysis is less accurate. The lower accuracy for the wave speed is because, in the reconstructive MOC analysis, it is derived from the estimated

impedance using Eq. (10.3) under the assumption that the diameter of the pipeline is constant. In contrast, in the experimental pipeline, the deteriorated section has a thinner wall thickness and a larger internal diameter. This violates the assumption of 'constant internal diameter'. Considering the experimental pipeline is small in diameter (D_0 = 22.14 mm), this introduces an error into the estimated wave speed which is unlikely to occur in larger diameter pipes. If the wall thickness of the deteriorated section is known and the theoretical wave speed formula is applicable, the wave speed can be estimated more accurately. However, this information is usually unknown or inapplicable; therefore, the assumption that the internal diameter is constant is more practical for pipelines in the field where the diameter is much larger. Nevertheless, the proposed reconstructive MOC approach has a wider applicable range, since the technique proposed in Gong et al. (2013f) is not able to interpret multiple reflections.

Small perturbations in the estimated distribution of impedance and wave speed are also observed in Figure 10.13. They are related to the joints, pipeline parameter variations, and uncertainties in the experiments, such as fluid-structure interactions and pressure fluctuations in the tank. The magnitude of these perturbations is much smaller than the perturbation resulting from the pipe section with a thinner wall.

Decreasing patterns are observed in both the estimated wave speed and impedance at the end of the plots (greater than approximately 34 m). They are related to the curved head drop shown at the end of the measured pressure trace (Figure 10.11, after about 6.995 s) and the estimated SRF (Figure 10.12, after about 0.05 s). The curved head drop results from the curved wave front and signal dispersion and dissipation during wave propagation. As a result, the estimated impedance and wave speed values for the pipe section close to the tank (located from approximately 34 m upstream from the in-line valve to the tank) are inaccurate. However, the curved head drop at the end of the plateau in the pressure trace has no effect on the estimates for the pipeline reaches downstream (from 0 m to 34 m), because the reconstructive MOC analysis is performed from downstream to upstream reach by reach.

In summary, the experimental verification indicates that the proposed reconstructive MOC analysis works in controlled laboratory conditions. A pipe section with a thinner wall thickness can be detected successfully and its impedance, wave speed, location and length estimated with reasonable accuracy. An error in a later section in the measured pressure trace has no effect on the estimates obtained from the former pressure data.

10.6 Conclusions

A novel distributed deterioration detection technique is proposed in this paper. A reservoir-pipeline-valve system is analyzed, and the pressure response resulting from the step transient wave generated by shutting off the valve abruptly is used. A reconstructive MOC analysis technique is proposed in this research, which is an inverse process of conventional MOC analysis. The novel inverse process calculates the transient head and flow backwards in time and estimates the pipe parameters, such as impedance and wave speed, from the downstream valve to the upstream reservoir reach by reach.

Numerical simulations support the observation that the proposed technique can deal with complex multiple reflections caused by natural pipeline parameter variations and multiple deteriorated sections. The impedance, wave speed, location and length of three deteriorated sections in a single pipeline are estimated accurately in a numerical study.

Experimental verification indicates that the reconstructive MOC technique provides a new and useful way to analyze data from pipelines suspected of experiencing widespread deterioration. A signal preprocessing technique is adapted, which transfers the measured pressure trace to the step response function (SRF), removing the effects of the rising front slope in the experimental incident wave. The impedance, wave speed, location and length of a pipe section with a thinner wall thickness in a laboratory experimental pipeline apparatus are estimated successfully.

The reconstructive MOC analysis is a step forward in assessing the condition of expensive and critical pipeline infrastructure non-invasively and cost-effectively. This technique is a promising alternative to existing pipeline condition assessment techniques, such as the inverse transient analysis, and is efficient in implementation.

Acknowledgements

The research presented in this paper has been supported by the Australia Research Council through the Discovery Project Grant DP1095270.

Notation

The following symbols are used in this paper:

A = pipe cross sectional area;

a = wave speed;

B = impedance of a pipe section;

C^+, C^- = positive and negative MOC characteristic lines;

D = internal pipe diameter;

e = wall thickness of a pipe;

f = Darcy-Weisbach friction factor;

g = gravitational acceleration;

H_{V0} = steady-state head at the valve;

H_i = head value of an incident pressure wave;

H_r = reservoir head;

L = length of pipe;

M, N, P, S = node labels on the MOC grid;

Q_0 = steady-state discharge;

R = resistance coefficient for a pipe reach;

t = time;

x = distance along a pipe;

Greek symbols:

δ	=	a positive real value that tends to zero;
ΔH	=	head perturbation from the mean state;
ΔQ	=	discharge perturbation from the mean state;
Δt	=	time step on the MOC grid;
Δx	=	length of a pipe reach on the MOC grid;

Chapter 11

Condition Assessment of Hydraulic Pipelines using Paired Pressure Transducers and Reconstructive Transient Analysis (Journal Publication 9)

Gong, J., Zecchin, A. C., Lambert, M. F., and Simpson, A. R.

School of Civil, Environmental and Mining Engineering, the University of Adelaide, Adelaide, SA 5005 Australia

Journal of Hydraulic Engineering, (submitted).

Statement of Authorship

Title of Paper	Condition Assessment of Hydraulic Pipelines using Paired Pressure Transducers and Reconstructive Transient Analysis
Publication Status	Submitted for Publication
Publication Details	Gong, J., Zecchin, A. C., Lambert, M. F., and Simpson, A. R. (2013). "Condition assessment of hydraulic pipelines using paired pressure transducers and reconstructive transient analysis." *Journal of Hydraulic Engineering*, (submitted).

Author Contributions

By signing the Statement of Authorship, each author certifies that their stated contribution to the publication is accurate and that permission is granted for the publication to be included in the candidate's thesis.

Name of Principal Author (Candidate)	Jinzhe Gong		
Contribution to the Paper	Developed and implemented the methodology, designed and conducted numerical simulations, interpreted and analysed results, prepared manuscript and acting as the corresponding author.		
Signature		Date	25/09/2013

Name of Co-Author	Aaron Zecchin		
Contribution to the Paper	Supervised development of work, helped to evaluate and edit the manuscript.		
Signature		Date	1·10·2013

Name of Co-Author	Martin Lambert		
Contribution to the Paper	Helped to evaluate and edit the manuscript.		
Signature		Date	25/9/13

Name of Co-Author	Angus Simpson		
Contribution to the Paper	Helped to evaluate and edit the manuscript.		
Signature		Date	25/9/2013

Abstract

Pipeline condition assessment assists authorities to maintain assets cost-efficiently and helps to prevent potential catastrophic failures. It is especially important for aging pipelines that are buried and undergoing internal and external corrosion. This paper describes (i) a method for extracting directional traveling waves in a single pipeline using two paired pressure transducers and (ii) a reconstructive transient analysis (RTA) method for non-invasive pipeline condition assessment using the traveling waves. A side-discharge valve is used to generate an incident pressure wave at an interior point in a pressurized pipeline, where two pressure transducers are located in close proximity on the upstream side of the generator to measure the pressure response. The measured transient pressure trace is decomposed into the reflected upstream and downstream traveling waves. The unit step response function (SRF) of the section of pipe upstream of the paired transducers is then estimated, which is free from the effects of the deterioration on the downstream side. Using the unit SRF, a RTA method is developed to determine the distribution of impedance (and consequently wave speed) along the section of pipeline, from which the location and severity of the deterioration can be assessed. The propose method is verified by numerical simulations conducted on a reservoir-pipeline-valve system with multiple deteriorated sections.

11.1 Introduction

Structural deterioration is a common problem for aging water distribution pipelines. Unlike leakages (Colombo and Karney 2005) or discrete blockages (Wang et al. 2005), structural deterioration can be large scale and distributed, and includes the following categories: internal or external corrosion (Swietlik et al. 2012); spalling of cement mortar lining (Stephens et al. 2008); extended blockages due to tuberculation or sedimentation (Arbon et al. 2007); graphitization (Zamanzadeh et al. 2007); and structurally weak sections caused by cracks in the pipe wall or backfill concrete (Hachem and Schleiss 2011).

Areas of distributed deterioration can impose a number of negative impacts on pipeline operation, such as a decrease in discharge capacity (Tran et al. 2010), an increase in energy consumption (Meniconi et al. 2010), and the problem of degraded water quality resulting in public health risks (Vreeburg and Boxall 2007). Moreover, distributed deterioration may also develop to the point of severe obstructions or bursts over time. As a result, it is preferable to detect distributed deterioration in water distribution systems at an early stage, with the intention of conducting targeted maintenance and rehabilitation before a catastrophic structural failure occurs.

At present, several pipeline condition assessment techniques are available, but they all have limitations. For example, closed-circuit television (CCTV) inspection (Tran et al. 2009) captures images of a pipe's inner surface using a camera on a carrier that travels within the pipeline. However, this method is costly and not reliable for identifying the severity of a deterioration (e.g. the depth of a crack) (Hao et al. 2012). Ground penetrating radar (GPR) (Metje et al. 2007) uses electromagnetic wave pulses and their reflections to identify the interface between different materials underground (such as regions of high soil moisture content resulting from a leak), but it is not accurate enough for assessing the wall condition of buried pipelines. Surface penetrating radar (SPR) (Donazzolo and Yelf 2010) and in-pipe GPR (Ekes et al. 2011)

techniques apply electromagnetic sensors directly to the outside or inside surface of a pipeline, but they are mainly utilized for localized inspection and are inefficient and costly for long range applications. The guided wave ultrasound method (Rose et al. 2009) uses ultrasonic waves propagating along the pipe wall and their reflections to determine the location and sizes of defects on the wall, but the range of inspection is limited in buried pipes due to the rapid signal attenuation (Liu and Kleiner 2013).

Among the different pipeline condition assessment technologies that are being developed, methods based on fluid transients (Chaudhry 1987; Wylie and Streeter 1993) show considerable potential. In fluid transient-based techniques, controlled transient pressure waves to interrogate the pipe system are created by artificially accelerating or decelerating the fluid. For example, an abrupt closure of an in-line or side-discharge valve can introduce a step pressure wave. These pressure waves travel at high speed inside a fluid-filled pipe and reflections occur when the wave encounters any physical anomalies along the pipe. The reflections can be measured by pressure transducers and then interpreted through signal processing methods to assess the condition of the pipe. The technique is efficient because the transient data, just lasting a few seconds, can provide information about the wall condition of a pipe stretching thousands of meters. The technique also has a wide operational range, since it can be applied to various types of pipes either elevated or buried.

Leak detection using fluid transients has been intensively studied in the past two decades (Jönsson and Larson 1992; Liggett and Chen 1994; Brunone 1999; Vítkovský et al. 2000; Lee et al. 2005b; Covas and Ramos 2010; Gong et al. 2013e; Gong et al. 2013b). In contrast, studies on the detection of distributed deterioration, such as wall thickness changes due to large scale corrosion, are limited.

Stephens et al. (2008, 2013) were the first to apply the inverse transient analysis (ITA) to the detection of changes in pipe wall thickness in a cement mortar lined steel water main in the field. The use of ITA requires an iterative

process for parameter calibration and can be computationally costly for systems with a large number of parameters, and may suffer from parametric identifiability issues.

Hachem and Schleiss (2012) proposed a technique for estimating the location and stiffness of a structurally weak section in a single pipeline using a steep pressure wave excitation and wavelet decomposition. The location and length of the weak reach were determined using the technique of time-domain reflectometry (TDR). Thereafter, the wave speed in the weak reach was estimated using the difference between the measured wave speed in the pipe under test and the theoretical wave speed in an intact pipe. The estimated wave speed was then used to estimate the stiffness of the weak section through the wave speed formula.

Gong et al. (2011, 2013) developed a technique for detecting a single deteriorated section in a pipeline that also uses a steep pressure wave and TDR. Unlike the technique of Hachem and Schleiss (2012), Gong et al. (2011, 2013) used the size of the deterioration-induced reflection, shown in the measured pressure trace, to estimate the impedance of the deterioration. The impedance could then be used to determine the wall thickness and wave speed in the deteriorated section.

A major limitation of the preceding techniques is that they have difficulty in dealing with pipelines with multiple deteriorated sections, where higher order reflections, within and in between, the deteriorated sections can increase the complexity of the measured pressure trace significantly. Gong et al. (2013a) proposed a method for identifying multiple deteriorated sections in single pipelines with a reservoir-pipeline-valve (RPV) configuration. The valve at the end of the pipe is abruptly closed to introduce a step wave and also form a dead end. A pressure transducer is located at the upstream face of the valve to measure the transient pressure response induced by the step wave. In addition to the direct (first order) deterioration-induced reflections that are used in Gong et al. (2011, 2013), the higher order reflections (termed mirco-

reflections), are also used in the method presented in Gong et al. (2013a) to enable the detection of multiple deteriorated sections.

The limitation of the method proposed in Gong et al. (2013a) is that it is only applicable to the RPV configuration with the transducer located at the dead end. When a pressure transducer is located at an interior point on the pipe, which is the typical scenario in real applications, the measured pressure trace is a superposition of the waves traveling upstream and those traveling downstream. It results in a much more complex trace than the pressure trace measured at a dead end.

This paper proposes an approach that is computationally efficient and able to estimate the location, length and severity of multiple deteriorated sections in a single pipeline using two paired transducers located at interior points. Preliminary studies conducted by the authors show that the pressure waves traveling upstream and downstream can be extracted from the measurements of two paired transducers (Gong et al. 2012c; Gong et al. 2012b). This research adapts the wave extraction algorithm and then uses the directional pressure waves for the detection of multiple deteriorated faults in a pipeline. The implementation of this new technique consists of four steps:

(1) Measurement of transient pressure traces using two paired pressure transducers that are located in close proximity.

(2) Extraction of the reflected axial plane waves: the wave traveling upstream and the wave traveling downstream.

(3) Determination of the unit step response function (SRF) of the pipe section on one side of the transducer pairs.

(4) Implementation of the reconstructive transient analysis (RTA) on the SRF to identify and locate multiple deteriorated sections.

These four steps are explained in detail in the rest of the paper. Numerical simulations are conducted on a single pipeline with multiple deteriorated sections to validate the new technique. The results confirm that the algorithms of signal separation and SRF determination are valid, and the RTA can handle complex micro-reflections properly. The location, length, impedance and wave speed of the deteriorated sections upstream from the pair of transducers (which is the target assessment section of the pipe) are estimated accurately.

11.2 Measurement of transient pressure traces

11.2.1 Pipeline configuration

A pipeline configuration suitable for the implementation of the new distributed deterioration detection technique is shown in Figure 11.1. A side-discharge valve (G_t) is used to generate a steep incident pressure wave that propagates both upstream and downstream simultaneously (W_u and W_d) by shutting off the valve abruptly. Two pressure transducers (T_{p1} and T_{p2}) are located in close proximity on one side of the generator, either upstream or downstream, but the case of upstream is used throughout this paper without loss of generality. The distance between T_{p1} and G_t and that between T_{p2} and G_t are represented by L_1 and L_2, respectively.

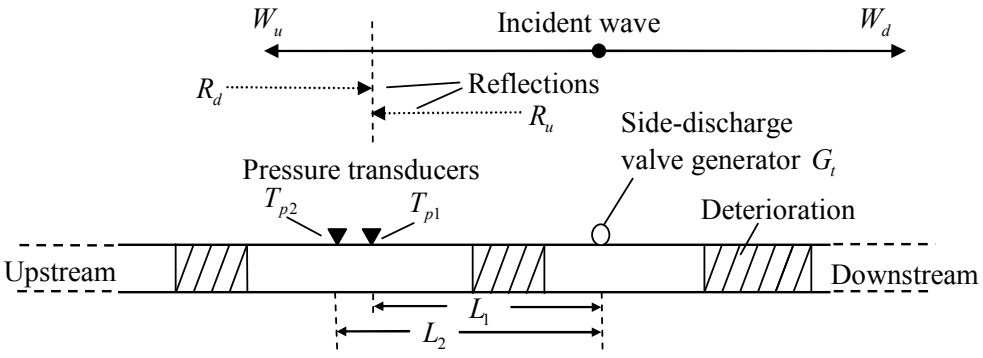

Figure 11.1 Pipeline configuration for transient wave measurement with illustration of wave propagation; R_u and R_d represent the reflected waves

traveling upstream and downstream respectively with respect to where transducer T_{p1} is located

The two boundaries of the pipeline are far away from the transducers and the generator, and reflections from boundaries are not considered. There are no constraints on the type of boundary condition, but a steady state is required before the generation of the transient excitation. After the excitation, reflected waves emanating from the deteriorated sections travel upstream or downstream along the pipeline (R_u and R_d). The pressure transducers measure the magnitude change of pressure at specific locations, which is the superposition of the incident wave and the two directional reflection waves.

The two paired transducers are located in the vicinity of each other such that the section of pipe in between can be assumed to be intact. The minimum distance between the two paired transducers depends on the sampling frequency of the pressure sensors, F_s . It should be greater than a few multiples of the step length of the wave propagation, which is the distance that a wave travels within one sampling interval and is given as a / F_s, where a is the wave speed in the section of pipe. Numerical simulations show that the distance between the two paired transducers can be as small as 1 m when the sampling frequency F_s = 2 kHz and the wave speed a = 1000 m/s (a / F_s = 0.5 m).

11.2.2 Pressure measurement

The pressure trace measured by a single transducer is a superposition of all traveling waves and as such it can be very complex when reflections occur from multiple deteriorated sections in the pipeline. In order to reduce the complexity of the signal and facilitate interpretation of the data, the proposed method decomposes a measured composite pressure signal into its individual components, including the incident wave (W_u), the reflected wave traveling upstream (R_u), and the wave traveling downstream (R_d) with respect to the

location of the pressure transducer. The reflected waves R_u and R_d are referred to as axial plane waves. To achieve the decomposition and obtain the individual axial plane wave, a signal processing algorithm is developed and described in the following section.

11.3 Extraction of the reflected axial plane waves

11.3.1 Expression of the measured pressure traces

The pressure traces measured at the transducers T_{p1} and T_{p2} include two reflected wave components $R_u(t)$ and $R_d(t)$. The measured pressure traces can be denoted as

$$H_1(t) = \begin{cases} H_0 & 0 \le t < t_0 + t_1 \quad (11.1a) \\ H_i + R_u(t) + R_d(t) & t \ge t_0 + t_1 \quad (11.1b) \end{cases}$$

and

$$H_2(t) = \begin{cases} H_0 & 0 \le t < t_0 + t_2 \quad (11.2a) \\ H_i + R_u(t - \Delta t) + R_d(t + \Delta t) & t \ge t_0 + t_2 \quad (11.2b) \end{cases}$$

respectively, in which t represents time; t_0 is the time point when the incident wave is generated; $t_1 = L_1 / a$ and $t_2 = L_2 / a$; and $\Delta t = t_2 - t_1$.

Because the two paired transducers are close to each other, the steady-state head and the head of the incident wave which they measure are assumed to be the same, and are denoted as H_0 and H_i respectively in Eqs (11.1) and (11.2). $R_u(t)$ and $R_d(t)$ represent the time-domain traces of the reflected pressure waves traveling upstream and downstream from T_{p1}. Note that

$R_u(t) = R_d(t) = 0$ when $t < t_0 + t_1$. To obtain the two axial plane waves $R_u(t)$ and $R_d(t)$ from the measured pressure traces $H_1(t)$ and $H_2(t)$, a signal separation algorithm is developed, and the procedure for estimating the axial plane wave $R_d(t)$ is detailed below.

11.3.2 Estimation of the axial plane waves

An intermediate signal $P_d(t)$ that only depends on $R_d(t)$ can be obtained from the two measured pressure traces. Firstly, the time-domain trace of $H_2(t)$ is moved forward in time by an interval of Δt, which may be achieved by substituting t by $t + \Delta t$ in Eq. (11.2), where the result becomes

$$H_2(t+\Delta t) = \begin{cases} H_0 & -\Delta t \le t < t_0 + t_1 \quad (11.3a) \\ H_i + R_u(t) + R_d(t+2\Delta t) & t \ge t_0 + t_1 \quad (11.3b) \end{cases}$$

Subtracting $H_1(t)$ from $H_2(t+\Delta t)$ yields the intermediate signal

$$P_d(t) = H_2(t+\Delta t) - H_1(t) = R_d(t+2\Delta t) - R_d(t) \quad t \ge t_0 + t_1 \tag{11.4}$$

Using the signal $P_d(t)$ the axial plane wave $R_d(t)$ can be derived. A Fourier transform $\mathrm{F}[\ ]$ is applied to $P_d(t)$, which can be described as

$$\mathrm{F}[P_d(t)] = (e^{j\omega 2\Delta t} - 1)\,\mathrm{F}[R_d(t)] \quad t \ge t_0 + t_1 \tag{11.5}$$

where j is the imaginary unit $\sqrt{-1}$; and ω is angular frequency. Rearranging Eq. (11.5) results in

$$R_d(t) = \mathrm{F}^{-1}\left[\Phi(\omega)\,\mathrm{F}[P_d(t)]\right] \quad t \ge t_0 + t_1 \tag{11.6}$$

where $F^{-1}[\,]$ represents the inverse Fourier transform and $\Phi(\omega) = 1/(e^{j\omega 2\Delta t} - 1)$. The procedure for deriving $R_u(t)$ is similar but not presented in this paper for brevity.

Compared with the measured pressure traces, the complexity in the axial plane waves $R_u(t)$ and $R_d(t)$ is significantly reduced. However, the two axial plane waves are coupled with one another. For example, $R_d(t)$ represents the reflections traveling downstream with regard to the location of transducer T_{p1}. These reflections emanate from the deterioration upstream of T_{p1}, but they are induced by not only the initial incident wave W_u, but also the wave $R_u(t)$ that travels upstream. Similarly, $R_u(t)$ is related to both W_d and $R_d(t)$.

To remove the coupling and facilitate the identification of distributed deterioration for the pipe section upstream from the pair of transducers, the unit step response function (SRF) of this pipe section is determined, which represents reflections emanating from the deterioration upstream of the transducers, and only induced by a step pressure wave with a magnitude of unity. In the unit SRF of the upstream section, the effects of the section of pipe downstream are totally removed. As a result, the wave reflections shown in the unit SRF can be directly attributed to their source upstream from the pair of transducers. The procedure for determining the unit SRF is described in the following section.

11.4 Determination of the unit step response function

The unit step response function (SRF) of a linear system can be derived once both the input and output of this system are known. For the pipeline system discussed in the previous sections, once the axial plane waves $R_u(t)$ and $R_d(t)$ are obtained, the input and the output for the pipe section upstream from the pair of transducers are explicit. Because the steady-state head H_0 is

arbitrarily selected and has no effect on the wave reflection, the input signal can be defined as $R_u(t)+(H_i-H_0)$ and the corresponding output is simply $R_d(t)$.

The procedure for determining the unit SRF from the input and output signals is standard and not discussed in this paper, interested readers are referred to Ljung (1999). In this research, the system identification tool box in Matlab software was used to facilitate the determination. Only the first few seconds of the unit SRF are used, which covers the length of the pipe section of interest.

The SRF of the pipe section downstream from the pair of transducers is difficult to determine. The input for this sub-system is implicit since the incident wave is generated at an interior point in this section. In practice, the generator can be relocated to a point upstream from the pair of transducers and then the algorithms presented previously can be adapted to estimate the SRF of the downstream section.

In the unit SRF of the pipe section upstream from the pair of transducers, the transient response of the deterioration is significantly simplified because the effects of the deterioration downstream are removed; however, higher order reflections between the deteriorated reaches in this section of pipe still exist in the SRF. At present, except for the inverse transient analysis (ITA), which involves iterative computation to find the optimum pipeline parameters, there is no other technique that can intrinsically compensate for the higher order transient reflection and yield an accurate estimation of the location and severity of multiple deteriorated sections. A novel reconstructive transient analysis (RTA) method is developed in this paper, which has the intrinsic ability to analyze all the wave reflections and transmissions, and can estimate the distribution of the impedance and wave speed for various sections along the pipeline from the SRF accurately.

11.5 Reconstructive transient analysis

The reconstructive transient analysis (RTA) proposed in this paper is based on the analysis of the unit step response function (SRF) of a pipe section. The method of characteristics (MOC) (Chaudhry 1987; Wylie and Streeter 1993) is used to develop the analysis method. In contrast to conventional MOC analysis which simulates the transient pressure and flow in a pipe model with explicit properties, the RTA estimates the properties of the pipeline (impedance and wave speed) from the transient pressure trace described by the SRF and does not require any information about the transient flow.

11.5.1 Transient wave behavior in pipes with a deteriorated section

Before discussing the RTA algorithm, the behavior of a transient wave crossing the boundary of a deteriorated section should be considered. The deteriorated section discussed in this paper is a pipe section with a change in the pipeline impedance, which is defined as

$$B = \frac{a}{gA} \tag{11.7}$$

where B represents the impedance of the section of pipe; g is gravitational acceleration; and A denotes the cross-sectional area of the pipe.

When a steep incident pressure wave arrives at the interface between the deteriorated section and the original intact pipe, where the discontinuity of the impedance exists, the phenomenon of wave reflection and transmission results. Figure 11.2 shows the wave reflection and transmission by illustrating the changes in the hydraulic grade line (HGL).

The sign and size of the wave after reflection are dependent on the impedance discontinuity. In previous research, the authors studied the behavior of a

transient wave passing a deteriorated section in detail using MOC analysis (Gong et al. 2013f). From this analysis the head value of the wave after the first reflection and transmission was derived as

$$H_{j1} = H_0 + \frac{2B_1}{B_0 + B_1}(H_i - H_0) \tag{11.8}$$

It can be seen from Eq. (11.8) that the head value of the wave after reflection and transmission is independent of any flow information, but only depends on the size of the incident wave ($H_i - H_0$) and the impedance values. When $B_1 < B_0$, the reflection is negative ($H_{j1} < H_i$), as shown in Figure 11.2. As a result, if the head value of the reflected wave can be measured and the impedance of the intact pipe is known, the impedance of the deteriorated section can be derived from Eq. (11.8). Similarly, when the incident wave arrives at the other boundary of the deterioration, another wave reflection and transmission process occurs. The relationship given by Eq. (11.8) forms the fundamental basis of the reconstructive transient analysis.

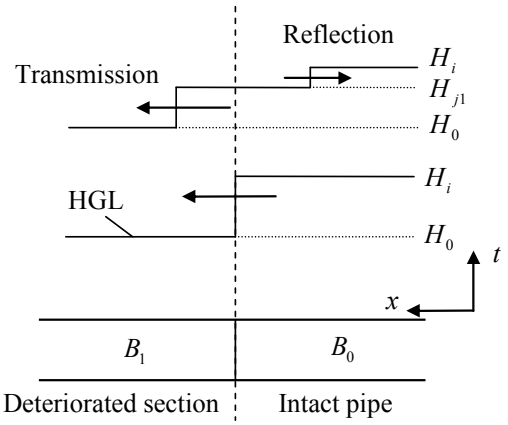

Figure 11.2 Theoretical behavior of a steep pressure wave crossing a discontinuity of impedance (H_0 = steady-state head; H_i = head of the incident wave; H_{j1} = head of the reflected and transmitted waves; $B_1 < B_0$)

11.5.2 Implementation of reconstructive transient analysis

The reconstructive transient analysis (RTA) proposed here is designed specifically for interpreting the unit step response function (SRF) of a section of pipeline. Through the RTA, the distribution of the impedance and wave speed can be determined, in which the location, length and severity of deteriorated sections are explicitly revealed. The RTA algorithm is presented below step by step. Friction is ignored initially in the derivation; however, the effects of friction are discussed later in this paper. The internal diameter of the pipe, D_0, is assumed to be known and constant. If the pipeline is composed of several pipe sections with various internal diameter values, then the diameter is assumed to be uniform within each section.

Discretization of the pipe

The section of pipe with a known unit SRF needs to be discretized in order to implement the RTA. The discretization starts from the pair of transducers and extends towards the upstream direction. The number of discretized reaches is equal to the number of the data points available in the unit SRF. However, the specific length of each reach is unknown and yet to be determined, as it depends on the sampling interval of the SRF and the wave speed within each reach (which are estimated by the RTA method). Along with the discretization of the section of pipe, an MOC grid can be drawn to facilitate the analysis as shown in Figure 11.3.

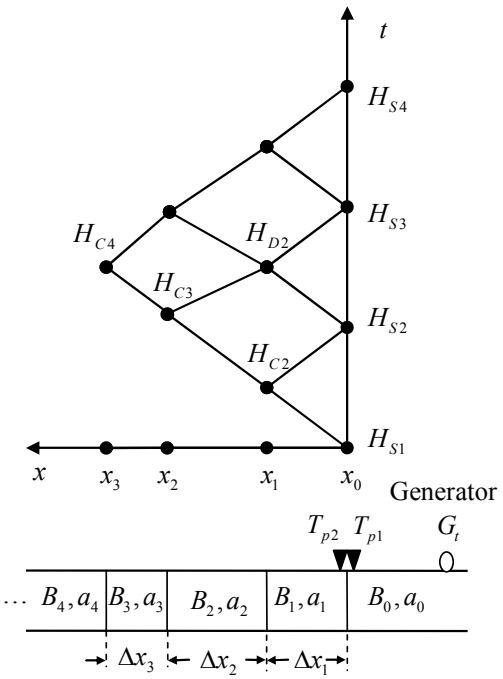

Figure 11.3 Discretization of a section of pipe using a MOC grid for the reconstructive transient analysis. Note that the properties of each pipe reach ($\Delta x_i, a_i, B_i$) are unknown and yet to be determined. The pair of transducers are T_{p1} and T_{p2}

In Figure 11.3, a single pipeline is discretized, and a MOC grid is presented above the discretized pipeline. The characteristic lines represent the transmission and reflection between the pipe reaches on the upstream side of the pair of transducers induced by a unit step pressure wave. Four data points (head values) of the unit SRF are presented as H_{S1} to H_{S4} along the vertical t axis of Figure 11.3, with H_{S1} representing the first measured head value at time $t = 0$. Accordingly, the section of pipe is discretized into four reaches along the x axis. The length of each reach is unknown at this stage but can be described as

$$\Delta x_i = x_i - x_{i-1} = a_i \Delta t \tag{11.9}$$

where Δx_i represents the length of the ith reach; x_i denotes the location of the left boundary of this reach; a_i designates the wave speed in the reach; and Δt is the sampling interval in the unit SRF sequence. After the discretization, the RTA can be conducted for these reaches in sequence.

Analysis of the first reach

The first value in the unit SRF, H_{S1}, represents the head value of the wave reflection at location x_0 when a unit step pressure wave arrives from the right hand side of the transducers. Substituting $H_0 = 0$ (i.e. taking this level as the datum), $H_i = 1$ and $H_{j1} = H_{S1}$ into Eq. (11.8), the impedance of the first reach of pipe can be derived as

$$B_1 = \frac{H_{S1} B_0}{2 - H_{S1}} \tag{11.10}$$

The wave speed in the first reach, a_1, can be estimated using Eq. (11.7) once the impedance B_1 is determined and the internal diameter is known as D_0. Thereafter, the length of this reach, Δx_1, can be obtained from Eq. (11.9).

Analysis of the second reach

To estimate the impedance of the second reach (B_2), the transient analysis needs to be performed backwards in time. To facilitate the analysis, the evolution of the wave propagation during the first time step is shown in Figure 11.4 using the characteristic lines.

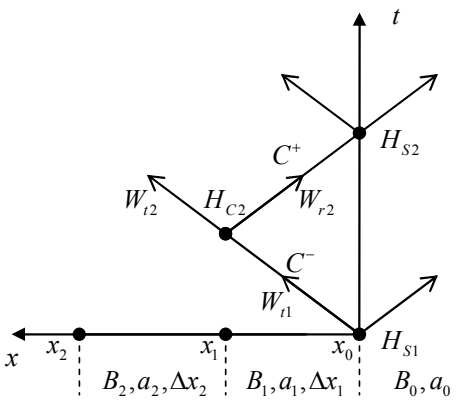

Figure 11.4 Evolution of the transient wave propagation within the first time step. Arrows represent the direction of the wave propagation

After the first reflection and transmission at location x_0, the first transmitted wave (W_{t1}) with a head value of H_{S1} propagates along the negative characteristic line C^-. At the interface between the first and the second reaches, i.e. at location x_1, wave reflection and transmission occurs again and the head value becomes H_{C2} for both the second transmitted (W_{t2}) and reflected (W_{r2}) waves. The second reflected wave (W_{r2}) propagates from x_1 to x_0 along the positive characteristic line C^+, and when it arrives at x_0, the process of wave reflection and transmission occurs, yielding a head value of H_{S2} that is registered in the unit SRF.

The value of H_{C2} is unknown but can be estimated from H_{S2} by calculating the transient backward in time along the line C^+. Applying the algorithm given by Eq. (11.8) to the reflection and transmission of wave W_{r2} at x_0, the head H_{S2} may be described as

$$H_{S2} = H_{S1} + \frac{2B_0}{B_0 + B_1}(H_{C2} - H_{S1}) \tag{11.11}$$

Rearranging Eq. (11.11) to solve for the head H_{C2} yields

$$H_{C2} = H_{S1} + \frac{B_0 + B_1}{2B_0}(H_{S2} - H_{S1}) \tag{11.12}$$

Similarly, applying Eq. (11.8) to the reflection and transmission of wave W_{t1} at x_1 gives

$$H_{C2} = \frac{2B_2}{B_1 + B_2} H_{S1} \tag{11.13}$$

Now substituting H_{C2} from Eq. (11.12) into Eq. (11.13), and rearranging the terms, the impedance of the second reach can be determined as

$$B_2 = B_1 \frac{(3B_0 + B_1)H_{S1} - (B_0 + B_1)H_{S2}}{(B_0 - B_1)H_{S1} + (B_0 + B_1)H_{S2}} \tag{11.14}$$

The wave speed a_2 and the length of the second reach Δx_2 can then be estimated in sequence, which finalizes the analysis of the second reach.

Analysis of the third reach

To estimate the impedance of the third reach, the head value of H_{C3} from Figure 11.3 is required. However, to calculate the value of H_{C3}, the value of H_{D2} needs to be known. The value of H_{D2} in Figure 11.3 can be obtained from H_{S3} through the same process described in Eq. (11.12), which can be written as

$$H_{D2} = H_{S2} + \frac{B_0 + B_1}{2B_0}(H_{S3} - H_{S2}) \tag{11.15}$$

Alternatively, using the characteristic line between H_{D2} and H_{C3}, and the line between H_{D2} and H_{S2}, the value of H_{D2} can also be expressed by

$$H_{D2} = H_{C2} + \frac{2B_1}{B_1 + B_2}(H_{C3} - H_{C2}) + \frac{2B_2}{B_1 + B_2}(H_{S2} - H_{C2}) \qquad (11.16)$$

Substituting Eq. (11.15) into Eq. (11.16), the value of H_{C3} can be obtained. Then the impedance of the third reach, B_3, can be estimated by applying Eq. (11.8) to the characteristic line lining H_{C2} and H_{C3}, which is the same process as described in Eq. (11.13). Once B_3 is known, the wave speed a_3 and length Δx_3 are then determined from Eq. (11.7) and Eq. (11.9) respectively. These equations are not presented in this paper for the sake of brevity.

Analysis of the subsequent reaches

The process for analyzing the subsequent reaches of pipe is similar to that for the third reach. The RTA continues reach by reach until the last reach of interest, or where the last value of the unit SRF is available. Finally, the distribution of the impedance and wave speed can be obtained, starting from the pair of transducers.

The process of RTA does not require any information related to the transient flow. This is an advantage of this algorithm because transient flow is difficult to measure in real systems. In the RTA transient analysis is conducted along characteristic lines one by one, where all the wave reflections and transmissions are considered. As a result, the RTA can appropriately handle the micro-reflections (i.e. higher order reflections) between the reaches. Throughout the analysis, there is no iterative process for parameter calibration; therefore, the algorithms are efficient in computation.

The prerequisite of a successful RTA is an accurate estimation of the unit SRF of the section of pipe under test, which requires a pair of transducers for transient measurement, a signal processing algorithm for the extraction of the two reflected axial plane waves, and a system identification process for the estimation of the unit SRF. All the above steps comprise the new technique for the detection of multiple deteriorated sections in single pipelines. Verification of the technique by numerical simulations is shown in the next section.

11.6 Numerical simulations

Numerical simulations have been conducted in a pipeline with five deteriorated sections. The boundary condition of the pipeline is not important for the proposed deterioration detection method, but a reservoir-pipeline-valve (RPV) configuration was used to facilitate the numerical simulations. Conventional forward MOC modeling was performed to obtain the transient response of the system. Then the preceding axial plane wave extraction algorithm was applied to the measured data and the reconstructive transient analysis (RTA) was conducted to detect the deterioration upstream from the pair of transducers. The system configuration and the pressure traces [$H_1(t)$ and $H_2(t)$] obtained from conventional MOC modeling are first given below. Then the axial plane waves [$R_u(t)$ and $R_d(t)$] and the estimated unit step response function (SRF) for the section of pipe upstream from the pair of transducers are determined. Finally, the impedance and wave speed estimated from the RTA are presented. The effects of friction are discussed in the last sub-section.

11.6.1 System configuration

The pipeline model used to verify the new distributed deterioration detection technique is given in Figure 11.5. It is an RPV system with five deteriorated sections, where the reservoir has a head of H_r = 30 m and the diameter of the

pipeline is D_0 = 0.6 m and uniform throughout. A deteriorated section is represented as a pipe section with a wave speed different from that of the intact pipe (as shown in Figure 11.5). The wave speed values in the intact sections are a_0 = 1000 m/s, and the values of a_1, a_2 and a_3 in the deteriorated sections are also given in Figure 11.5. The impedance values are calculated using Eq. (11.7), and they are B_0 = 360.5 s/m^2 for the intact sections and B_1 = 432.6 s/m^2, B_2 = 216.3 s/m^2, and B_3 = 288.4 s/m^2 in the deteriorated sections corresponding to the wave speed values of a_1, a_2 and a_3. Friction is ignored for the numerical simulations, so the steady-state head is $H_0 = H_r$ = 30 m throughout this pipe. The transient generator G_t is a side-discharge valve with an initial steady-state flow rate of Q_V = 0.05 m^3/s, and the incident wave is generated by shutting off the valve abruptly. The steady-state flow rate between the reservoir and the generator is Q_0 = 0.1 m^3/s. The in-line valve at the end of the pipe is partially open and the discharge is $Q_0 - Q_V$ = 0.05 m^3/s.

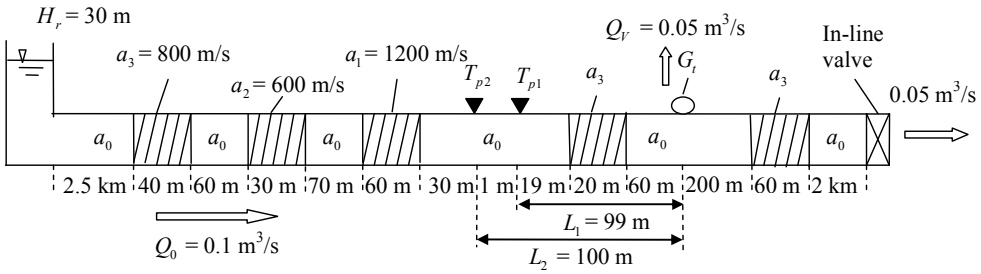

Figure 11.5 Pipeline configuration for the numerical simulations

11.6.2 Pressure traces from MOC modeling

Conventional MOC modeling is conducted on the pipeline system described in the previous sub-section. The sampling frequency in the MOC modeling is F_s = 2 kHz. The head of the step pressure wave is H_i = 39.0 m after the closure of the side-discharge valve at time t_0 = 0.1 s. Transient pressure traces

are measured at the pair of transducers (T_{p1} and T_{p2}) which are 1 m apart and the results are depicted in Figure 11.6.

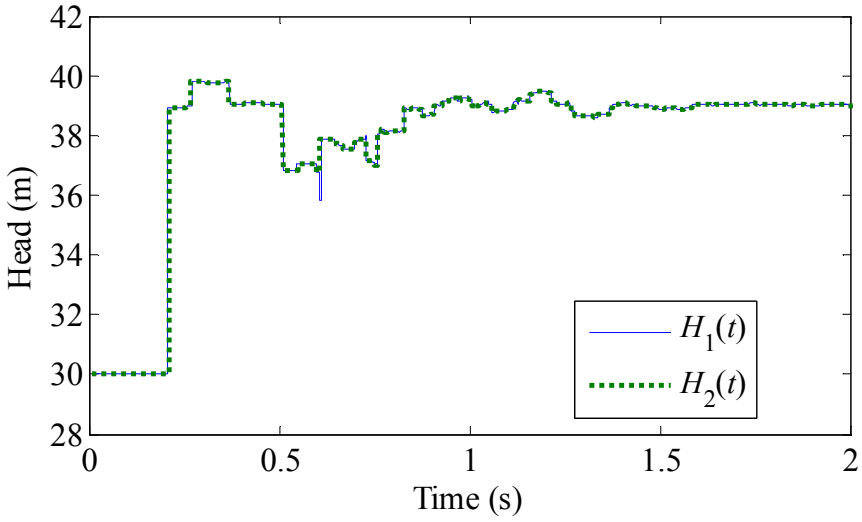

Figure 11.6 Pressure traces measured by the pair of transducers in the numerical simulation. $H_1(t)$ is from transducer T_{p1} and $H_2(t)$ is from transducer T_{p2}

The two pressure traces are similar because the two paired transducers are located in such close proximity (1 m apart). The raw pressure traces possess a complex structure, which is attributable to the superposition of the waves traveling along the pipe. As a result, it is difficult to interpret the raw pressure traces without further signal analysis.

11.6.3 Determination of the axial plane waves

To reduce the complexity, the axial plane waves $R_u(t)$ and $R_d(t)$ are estimated from the raw pressure traces, which represent the reflections traveling upstream from the transducers and the reflections traveling downstream. The signal processing algorithm described previously in Eqs (11.1) to (11.6) is applied to the numerical pressure traces $H_1(t)$ and $H_2(t)$.

The axial plane waves $R_u(t)$ and $R_d(t)$ are shown in Figures 11.7 and 11.8, respectively.

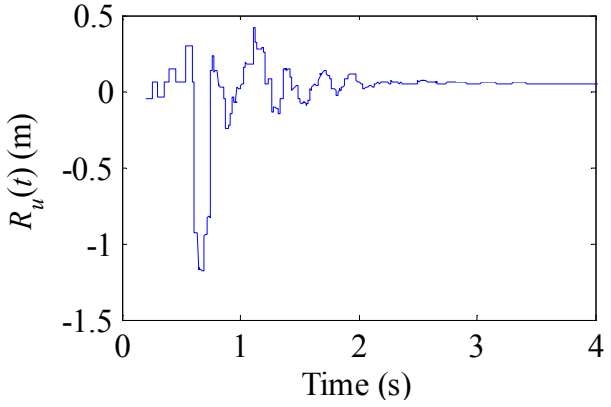

Figure 11.7 The pressure trace of the reflected wave $R_u(t)$ that travels upstream

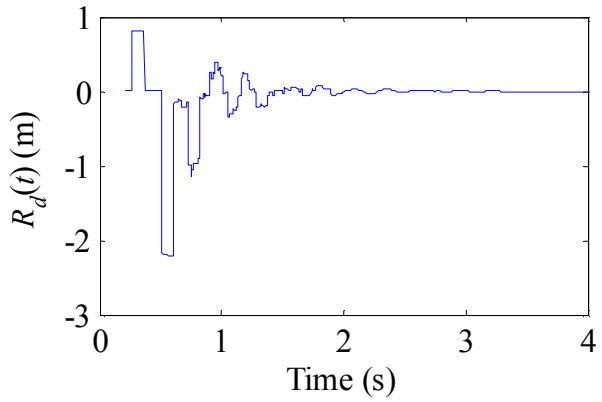

Figure 11.8 The pressure trace of the reflected wave $R_d(t)$ that travels downstream

In the trace of $R_d(t)$ in Figure 11.8, the reflections from the three deteriorated sections are clearer than those in the raw pressure traces. However, the trace is still complex because of the effects of higher order reflections and the interaction induced by the other axial plane wave $R_u(t)$.

11.6.4 Determination of the unit step response function

The unit step response function (SRF) is estimated from the axial plane waves for the section of pipe upstream from the transducers. The process was performed in Matlab using the system identification tool box. Firstly, a high-order, noncausal finite impulse response (FIR) model is established from the input and output using correlation analysis (Ljung 1999). Then the "step( )" internal function is used to estimate the unit SRF of this FIR model. In this study, the input signal is $R_u(t)+(H_i-H_0)$ and the corresponding output is $R_d(t)$, which are given in Figure 11.9.

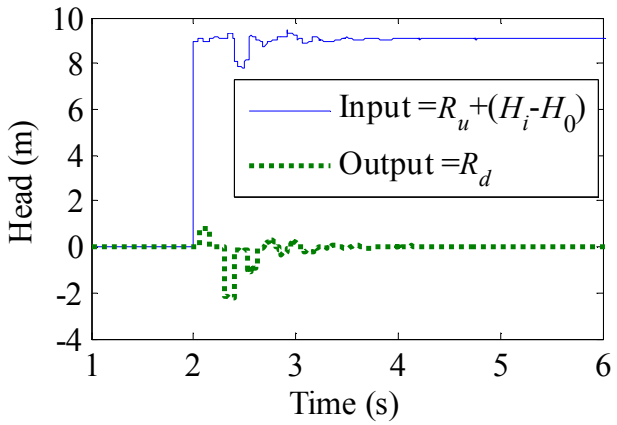

Figure 11.9 The input and the output signals for determining the unit step response function (SRF) of the pipe section upstream from the transducers

The estimated unit SRF is given in Figure 11.10, with a theoretical unit SRF presented for comparison. The theoretical unit SRF is obtained from a numerical simulation on a modified pipeline model where the entire section of pipe on the downstream side of the transducers is free of deterioration (wave speed = a_0, impedance = B_0), so that there is no reflection from the downstream side [$R_u(t)=0$ for all t]. The estimated unit SRF is observed to be equivalent to a high precision to the theoretical unit SRF, which confirms that all the signal processing performed previously is effective and accurate.

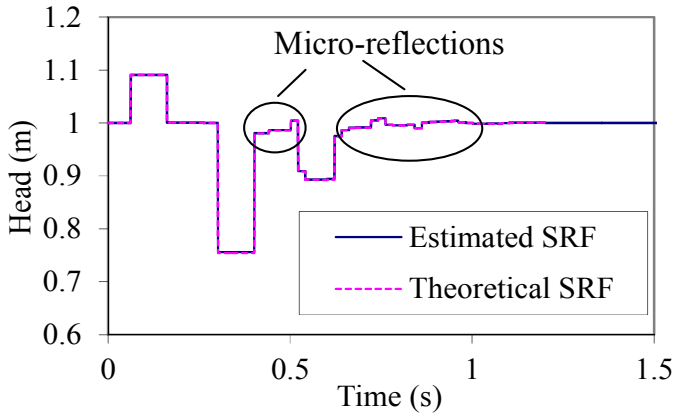

Figure 11.10 Comparison between the estimated unit step response function (SRF) with the theoretical unit SRF determined from MOC modeling

In the estimated unit SRF, the complexity is further reduced. However, micro-reflections are still observed as perturbations with small magnitudes. These micro-reflections are induced only by the higher order reflections reflecting between the three deteriorated sections in the section of pipe upstream from the transducer pair (see Figure 11.5). They can be appropriately interpreted by the reconstructive transient analysis (RTA).

11.6.5 Determination of the impedance and wave speed using RTA

The reconstructive transient analysis (RTA) was applied to the estimated unit SRF (Figure 11.10) to derive the distribution of the impedance and wave speed along the section of pipe upstream from the transducers. Before implementation of the RTA, the impedance and wave speed of the intact pipe (B_0 and a_0) are known but the impedance and the wave speed of the deteriorated sections (B_1 , B_2 , B_3 and a_1 , a_2 , a_3) are unknown. The algorithms of RTA described previously were implemented and the plot of the estimated distribution of impedance and wave speed is given in Figure 11.11. Data labels have been given for the estimated impedance distribution plot (solid line in Figure 11.11).

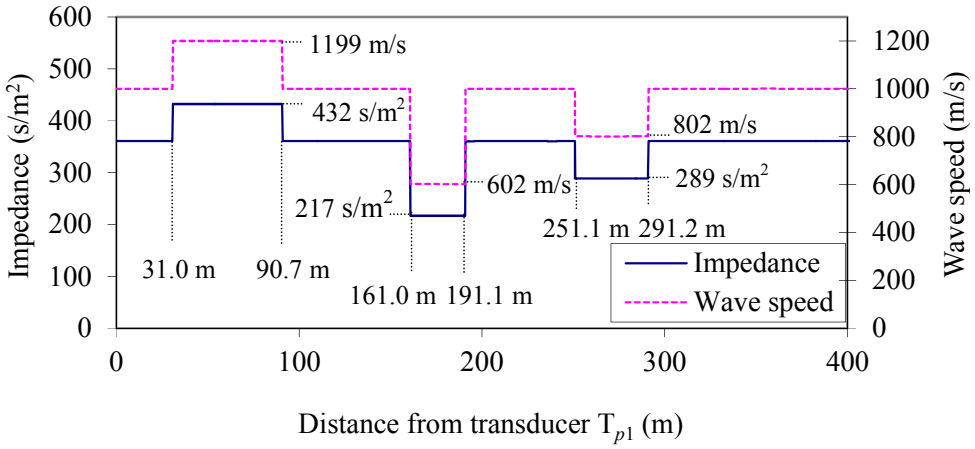

Figure 11.11 The distribution of impedance and wave speed estimated from the reconstructive transient analysis

The estimated values of impedance and wave speed are consistent with the theoretical values in the numerical model shown in Figure 11.5. The location and length of the three deteriorated sections are also determined accurately, with absolute error less than 0.5 m. The micro-reflections shown in the estimated unit SRF (small perturbations in Figure 11.10) do not have any effect on the accuracy of the estimation. The results shown in Figure 11.11 confirm that the proposed new technique can detect multiple deteriorated sections in a single pipeline accurately under assumption of zero friction.

11.6.6 Effects of friction

The effects of friction have been ignored in the analyses and the numerical simulations reported in the previous section of the paper. This is because on the timescales considered within this work (a few seconds after the transient excitation), the effects of friction are insignificant for the proposed deterioration detection technique. The effects of steady-friction are proportional to the square value of the steady-state discharge in the main pipeline, which can be controlled by the in-line valve at the end of the pipeline. In practice, the in-line valve can be fully closed to minimize the effects of steady-friction. The effects of unsteady friction are related to the transient flow induced by the side-discharge valve during the generation of

transients. The magnitude of the transient change in flow or pressure can be controlled by the size of the opening of the side-discharge valve. A smaller opening induces a smaller transient change in flow and pressure, which in turn reduces the effects of unsteady friction. In practice, the magnitude of the transient pressure induced by the side-discharge valve should be as small as possible, provided the desired signal-to-noise ratio (SNR) is satisfied.

For the pipeline model given in Figure 11.5, when a Darcy-Weisbach friction factor of f = 0.02 is used, the gradient of the steady-state hydraulic grade line (HGL) is just 2.13×10^{-4} for the section of pipe between the reservoir and the pair of transducers, which indicates that for a length of 1000 m of pipe, the head loss due to friction is just 0.213 m.

11.7 Conclusions

A novel technique for the detection of multiple deteriorated sections in single pipelines is proposed in this paper. Two pressure transducers located in close proximity are used to measure the transient response induced by a steep pressure wave generated by closure of a side-discharge valve-based generator at downstream. From the two measured pressure traces, the reflected wave traveling upstream and that traveling downstream can be obtained respectively (termed axial plane waves). Using these two axial plane waves, the unit step response function (SRF) can be estimated for the pipe section upstream of the transient generator. The reconstructive transient analysis (RTA), developed in this paper, can be applied to the SRF signal to determine the distribution of the impedance and wave speed in the pipe section. By reallocating the transient generator to the upstream side of the pair of transducers and repeating the preceding process, the condition of the pipeline section on the downstream side of the two paired transducers can be determined.

Numerical simulations have been conducted on a reservoir-pipeline-valve (RPV) system with five deteriorated sections to validate the new technique. The pair of transducers were located upstream from the transient generator (a side-discharge valve). Three deteriorated sections with wave speed values different from that of the intact pipeline were located upstream from the pair of transducers; the fourth deteriorated section was located between the transducers and the generator; and the fifth one was placed downstream from the generator. In the estimated unit SRF of the section of pipe upstream from the pair of transducers, the effects of the deterioration downstream from the transducers (including the deterioration between the generator and the transducers) were fully removed. When applying the RTA to the unit SRF, the complex micro-reflections between the three deteriorated sections were interpreted properly, and the location, length, impedance and wave speed of the deteriorated sections were estimated successfully.

The new technique only utilizes transient pressure responses and does not require any information about the transient flow. The effects of friction are not significant for the implementation of the proposed method, because the flow rate can be controlled by the in-line valve and side-discharge valve, and only the first few seconds of the pressure responses are used for the analysis. Compared with traditional transient-based distributed deterioration detection techniques, the new technique can deal with multiple deteriorated sections and is computationally efficient.

Acknowledgments

The research presented in this paper has been supported by the Australian Research Council through the Discovery Project Grant DP1095270. The first author thanks the Chinese Scholarship Council and the University of Adelaide for providing a joint postgraduate scholarship.

Notation

The following symbols are used in this paper:

A = inside pipe cross sectional area;

a = wave speed;

B = impedance of pipeline;

C^+, C^- = positive and negative characteristic lines;

D_0 = internal pipe diameter;

F_s = sampling frequency;

f = Darcy-Weisbach friction factor;

G_t = transient generator;

g = gravitational acceleration;

H_0 = steady-state head;

H_1, H_2 = pressure traces measured by transducers;

H_{Ci}, H_{Di}, $i = 2, 3, 4\ldots$ = estimated head values in the MOC grid;

H_i = head of the incident wave;

H_{j1} = head of the wave after the first reflection and transmission;

H_r = reservoir head;

H_{Si}, $i = 1, 2, 3\ldots$ = head values in the unit step response function;

j = imaginary unit, $\sqrt{-1}$;

L = length of pipe;

L_1, L_2 = distance between the generator and the transducers;

P_d = an intermediate signal related to R_d;

Q_0 = steady-state flow in the pipe section between the reservoir and the side-discharge valve;

Q_V = steady-state flow through the side-discharge valve;

R_u, R_d = reflected waves traveling upstream and downstream;

T_{p1}, T_{p2} = pressure transducers;

t = time;

W_{r2} = reflected wave;

W_{t1}, W_{t2} = transmitted waves;

W_u, W_d = incident waves traveling upstream and downstream;

x = distance;

Greek symbols:

$\Phi(\omega)$ = filter used in the signal extraction algorithm,

$\Phi(\omega) = 1/(e^{j\omega 2\Delta t} - 1)$

Δt = sampling interval;

Δx = length of a reach of pipe;

ω = angular frequency;

Chapter 12

Conclusions

Pipeline fault detection and structural condition assessment are essential for strategic and targeted maintenance of the critical infrastructure of water transmission and distribution systems. Current techniques for pipeline leak detection and condition assessment cannot fulfil the infrastructure health auditing needs of water utilities. Non-invasive and cost-effective techniques are of great interest to industry to not only facilitate asset management, but also prevent catastrophic events resulting from pressurised pipeline failure.

This PhD research focuses on the development of non-invasive techniques for pipeline leak detection and condition assessment using fluid transient waves. The hydraulic characteristics of leaks and localised pipe wall deterioration have been studied. New techniques for leak detection and structural condition assessment have been proposed based on the new knowledge developed through this research. Additionally, as part of this research, a transient signal generator has been designed and fabricated to facilitate the extraction of the frequency response diagram (FRD) of pressurised pipelines. Laboratory experiments have been conducted to verify the applicability of the transient generator and the leak detection techniques developed in this research. Preliminary experimental verification has also been performed for the new pipeline condition assessment technique that uses the reconstructive MOC analysis.

The specific contributions of this research are summarised in the next subsection. The limitations of this research and the recommendations for future work are also presented.

12.1 Research contributions

1. This research has advanced the knowledge of fluid transient behaviour in pressurised pipelines. In particular, the hydraulic characteristics of leaks and localised wall deterioration have been studied in detail in the frequency domain (Chapter 3) and the time domain (Chapters 8 and 9), respectively. The new findings obtained in this research have led to a better understanding of the characteristics of leaks and localised wall deterioration under transient events, and enables the exploitation of these unique characteristics for the development of non-invasive techniques for leak detection (Chapter 4) and condition assessment (Chapters 10 and 11).

2. A new technique has been developed for non-invasive leak detection in pressurised pipelines using fluid transients (Chapter 4). The new technique uses only the first three resonant peak magnitudes of a pipeline system. The information required by the new technique is much less than the FRD-based techniques developed in the past, which makes the proposed new technique more promising for practical implementation.

3. A new transient signal generator has been designed and fabricated as part of this research (Chapter 6). This device is based on a side-discharge valve and the opening of which is controlled by two solenoids. The adoption of the two solenoid valves enables a wider bandwidth of the signal to be achieved. Persistent, low magnitude and wide bandwidth signals, such as the maximum length binary sequence (MLBS) and the inverse repeat sequence (IRS), were produced by the new transient generator in the laboratory to enable the extraction of the FRD of pressurised pipelines (Chapters 6 and 7). A demonstrated advantage of the new transient signal generator is that, when the IRS is used as the excitation, part of the nonlinear response of the pipeline system can be suppressed, yielding a FRD close to a linear system

response, and hence suitable for FRD-based leak detection. As a tool for system identification of pipeline systems, it is believed that the new transient generator can be used not only for leak detection but also pipeline condition assessment and general system characterisation in the future.

4. New transient-based techniques for the detection of localised wall deterioration, that is distributed along pipelines, have been developed in this research (Chapters 10 and 11). These are termed reconstructive MOC analysis and the reconstructive transient analysis, respectively. While earlier studies were mainly focused on leak detection using fluid transient waves, this research explored the possibility of cost-effective structural condition assessment using fluid transients. The condition assessment techniques developed in this research do not require any iterative parameter calibration process (which is used in the inverse transient analysis for condition assessment in the past), therefore the algorithms are computationally efficient. The existence of multiple deteriorated sections in a single pipeline has been taken into account within these methods, and the complex multiple reflections were demonstrated to be appropriately interpreted by the newly developed techniques (Sections 10.3 and 11.6). A new transient pressure trace measurement strategy has been proposed by using two pressure transducers in close proximity (Section 11.2). This measurement strategy enables the extraction of directional traveling waves (pressure waves traveling upstream and downstream along a pipeline) and therefore reducing the complexities induced by multiple deteriorated sections. This new measurement strategy is combined with the reconstructive transient analysis, enabling pipeline structural condition assessment to be conducted at interior points in a pipeline (rather than only at boundary points as the reconstructive MOC analysis does).

5. Experimental verifications have been conducted in this research for the newly developed transient generator (Chapter 6), the three-resonant-

peak-based leak detection technique (Chapter 7), and the condition assessment technique using reconstructive MOC analysis (Chapter 10). The experimental results gave valuable information about the transient behaviour in real pipelines, provided a preliminary verification of the applicability of the new techniques developed in this research, and revealed challenges in real applications (Section 8.6.4). These experiments contribute to the development of practical transient-based pipeline fault detection and condition assessment techniques.

12.2 Research limitations and future work

Several limitations have been identified in this PhD research: (1) the three-resonant-peak-based leak detection technique presented in Chapter 4 is designed only for single event leak detection; (2) the new transient signal generator outlined in Chapter 6 was tested for FRD extraction only in a short (37.53 m) and small diameter (1 inch) laboratory pipeline; (3) the pipeline condition assessment technique using the reconstructive transient analysis (Chapter 11) requires the use of two pressure transducers in close proximity; however, to achieve two measurement points in closed proximity is challenging in the field; (4) in this research, deteriorated sections with uniform wall thickness are considered in the development of new pipeline condition assessment techniques; however, in real pipeline systems, localised deterioration, such as corrosion and the spalling of cement mortar lining, is typically non-uniform in shape and property.

It is recommended that the above research limitations should be addressed in future research. The specific directions recommended for future work are listed as follows:

1. Multiple leaks commonly exist in field pipelines. The development of new techniques that enable the detection of multiple leaks, but requires less information or less measurements than traditional transient-based leak detection techniques, is needed.

2. Until now, there is no experimental verification for pipeline FRD extraction in the field. This impedes the application of all the FRD-based leak detection techniques. In field applications, where the pipelines are much longer in length and larger in diameter, it may be difficult to establish steady oscillatory flow and extract the FRD for the whole pipeline system. However, it may be possible to extract the FRD for specific sections with relatively short length. More theoretical research focussing on using multiple pressure transducers to extract information as boundary conditions, and field tests focussing on system identification of specific sections in a long pipeline are recommended.

3. In the field, the connection of pressure transducers is limited to the points accessible along a pipe, such as air and scour valves. Two accessible points in close proximity are not common in real pipeline systems. As a result, challenges exist for the real application of the condition assessment techniques developed in this research. The development of new transient measurement equipment and undertaking of experiments are recommended for future work. The new transient measurement equipment is expected to achieve multi-sensor measurement but only use a single access point in a pipeline.

4. The research on pipeline structural condition assessment using fluid transients is still in its infancy. The transient trace measured in real pipelines can be complex and difficult to interpret. More research has to be conducted to obtain further understanding of the hydraulic characteristics of localised deterioration with non-uniform shape or property (e.g. pipe sections with partial cement mortar lining lost). The development of more sophisticated transient-based condition assessment techniques that are capable of dealing with the complex anomalies in field measurements has to be based on the enhanced understanding of the characteristics of deterioration in the field.

References

(2010). "MATLAB Release 2010a ", The MathWorks, Inc., Natick, Massachusetts, United States.

Arbon, N. S., Lambert, M. F., Simpson, A. R., and Stephens, M. L. (2007). "Field test investigations into distributed fault modeling in water distribution systems using transient testing." *Proceedings of the 2007 World Environmental and Water Resources Congress*, ASCE, Reston, VA.

Atherton, D. L., Morton, K., and Mergelas, B. J. (2000). "Detecting breaks in prestressing pipe wire." *Journal of the American Water Works Association*, 92(7), 50-56.

Beuken, R. H. S., Lavooij, C. S. W., Bosch, A., and Schaap, P. G. (2006). "Low leakage in the Netherlands confirmed." *Proceedings of the Water Distribution Systems Analysis Symposium 2006*, ASCE, Reston, VA.

Brunone, B., and Morelli, L. (1999). "Automatic control valve-induced transients in operative pipe system." *Journal of Hydraulic Engineering*, 125(5), 534-542.

Brunone, B. (1999). "Transient test-based technique for leak detection in outfall pipes." *Journal of Water Resources Planning and Management*, 125(5), 302-306.

Brunone, B., and Ferrante, M. (2001). "Detecting leaks in pressurised pipes by means of transients." *Journal of Hydraulic Research*, 39(5), 539-547.

Brunone, B., Ferrante, M., and Meniconi, S. (2008). "Portable pressure wave-maker for leak detection and pipe system characterization." *Journal / American Water Works Association*, 100(4), 108-116.

Chaudhry, M. H. (1987). *Applied Hydraulic Transients*, Van Nostrand Reinhold Company Inc, New York.

Collins, R. P., Boxall, J. B., Karney, B. W., Brunone, B., and Meniconi, S. (2012). "How severe can transients be after a sudden depressurization?" *Journal - American Water Works Association*, 104(4), E243-E251.

Colombo, A. F., and Karney, B. W. (2002). "Energy and costs of leaky pipes toward comprehensive picture." *Journal of Water Resources Planning and Management*, 128(6), 441-450.

Colombo, A. F., and Karney, B. W. (2005). "Impacts of leaks on energy consumption in pumped systems with storage." *Journal of Water Resources Planning and Management*, 131(2), 146-155.

Colombo, A. F., Lee, P., and Karney, B. W. (2009). "A selective literature review of transient-based leak detection methods." *Journal of Hydro-environment Research*, 2(4), 212-227.

Covas, D., Ramos, H., and Betamio de Almeida, A. (2005). "Standing wave difference method for leak detection in pipeline systems." *Journal of Hydraulic Engineering*, 131(12), 1106-1116.

Covas, D., and Ramos, H. (2010). "Case studies of leak detection and location in water pipe systems by inverse transient analysis." *Journal of Water Resources Planning and Management*, 136(2), 248-257.

Donazzolo, V., and Yelf, R. (2010). "Determination of wall thickness and condition of Asbestos Cement pipes in sewer rising mains using Surface Penetrating Radar." *Proceedings of the 13th Internarional Conference on Ground Penetrating Radar*, IEEE Computer Society, Washington, DC, 1-5.

Duan, H.-F., Lee, P. J., Ghidaoui, M. S., and Tung, Y.-K. (2011). "Leak detection in complex series pipelines by using the system frequency response method." *Journal of Hydraulic Research*, 49(2), 213-221.

Duan, H.-F., Lee, P. J., Ghidaoui, M. S., and Tung, Y.-K. (2012). "Extended blockage detection in pipelines by using the system frequency response analysis." *Journal of Water Resources Planning and Management*, 138(1), 55-62.

Eiswirth, M., and Burn, L. S. (2001). "New methods for defect diagnosis of water pipelines." *Proceedings of the 4th International Conference on Water Pipeline Systems*, BHR Group, Cranfield, UK, 137-150.

Ekes, C., Neducza, B., and Henrich, G. R. (2011). "Completing condition assessments using in-pipe GPR as pipe penetrating radar." *Proceedings of the Pipelines 2011 Conference*, ASCE, Reston, VA, 693-703.

Ferrante, M., and Brunone, B. (2003a). "Pipe system diagnosis and leak detection by unsteady-state tests. 2. wavelet analysis." *Advances in Water Resources*, 26(1), 107-116.

Ferrante, M., and Brunone, B. (2003b). "Pipe system diagnosis and leak detection by unsteady-state tests. 1. harmonic analysis." *Advances in Water Resources*, 26(1), 95-105.

Fuchs, H. V., and Riehle, R. (1991). "Ten years of experience with leak detection by acoustic signal analysis." *Applied Acoustics*, 33(1), 1-19.

Ghazali, M. F., Staszewski, W. W. J., Shucksmith, J. D., Boxall, J. B., and Beck, S. B. M. (2011). "Instantaneous phase and frequency for the detection of leaks and features in a pipeline system." *Structural Health Monitoring*, 10(4), 351-360.

Godfrey, K. (1993). *Perturbation Signals for System Identification*, Prentice Hall Inc., New York.

Goh, J. H., Shaw, A., Cullen, J. D., Al-Shamma'A, A. I., Oliver, M., Vines, M., and Brockhurst, M. (2011). "Water pipe leak detection using electromagnetic wave sensor for the water industry." *Proceedings of the 2011 IEEE Symposium on Computers and Informatics*, IEEE Computer Society, Washington, DC, 290-295.

Gong, J., Simpson, A. R., Lambert, M. F., Zecchin, A. C., and Kim, Y. (2011a). "Detection of distributed deteriorations in single pipes using transient reflections." *Presented in International Conference on Pipelines and Trenchless Technology (ICPTT) 2011*, ASCE, Reston, VA.

Gong, J., Lambert, M. F., Simpson, A. R., and Zecchin, A. C. (2012a). "Distributed deterioration detection and location in single pipes using the impulse response function." *Proceedings of the 14th International Conference on Water Distribution Systems Analysis*, Engineers Australia, Barton, ACT, Australia, 702-719.

Gong, J., Zecchin, A. C., Lambert, M. F., and Simpson, A. R. (2012b). "Signal separation for transient wave reflections in single pipelines using inverse filters." *Proceedings of the World Environmental & Water Resources Congress 2012*, ASCE, Reston, VA, 3275-3284.

Gong, J., Lambert, M. F., Simpson, A. R., and Zecchin, A. C. (2013a). "Detection of localized deterioration distributed along single pipelines by reconstructive MOC analysis." *Journal of Hydraulic Engineering*, DOI: 10.1061/(ASCE)HY.1943-7900.0000806(Accepted for publication).

Gong, J., Zecchin, A. C., Simpson, A. R., and Lambert, M. F. (2013b). "Frequency response diagram for pipeline leak detection: comparing

the odd and the even harmonics." *Journal of Water Resources Planning and Management*, DOI: 10.1061/(ASCE)WR.1943-5452.0000298(Accepted for publication).

Gong, J., Lambert, M. F., Simpson, A. R., and Zecchin, A. C. (2013c). "A customized side-discharge valve for extracting the frequency response function of hydraulic pipelines using pseudorandom binary signals." *Journal of Hydraulic Engineering*(Under review).

Gong, J., Simpson, A. R., Lambert, M. F., and Zecchin, A. C. (2013d). "Determination of the frequency response diagram of single pipelines using persistent transient excitation: a numerical investigation." *Journal of Hydraulic Research*, DOI: 10.1080/00221686.2013.818582(Accepted for publication).

Gong, J., Lambert, M. F., Simpson, A. R., and Zecchin, A. C. (2013e). "Single event leak detection in a pipeline using the first three resonant responses." *Journal of Hydraulic Engineering*, 139(6), 645-655.

Gong, J., Simpson, A. R., Lambert, M. F., Zecchin, A. C., Kim, Y., and Tijsseling, A. S. (2013f). "Detection of distributed deterioration in single pipes using transient reflections." *Journal of Pipeline Systems Engineering and Practice*, 4(1), 32-40.

Gong, J., Lambert, M. F., Simpson, A. R., and Zecchin, A. C. (2012c). "Distributed deterioration detection in single pipelines using transient measurements from pressure transducer pairs." *Proceedings of the 11th International Conference on Pressure Surges*, BHR Group, Cranfield, UK, 127-140.

Gong, J., Lambert, M. F., Zecchin, A. C., and Simpson, A. R. (2011b). "Frequency response measurement of pipelines by using inverse-repeat binary sequences." *Proceedings of the Computing and Control for the*

Water Industry (CCWI) 2011, University of Exeter, Exeter, UK, 883-888.

Hachem, F. E., and Schleiss, A. J. (2011). "A review of wave celerity in frictionless and axisymmetrical steel-lined pressure tunnels." *Journal of Fluids and Structures*, 27(2), 311-328.

Hachem, F. E., and Schleiss, A. J. (2012). "Detection of local wall stiffness drop in steel-lined pressure tunnels and shafts of hydroelectric power plants using steep pressure wave excitation and wavelet decomposition." *Journal of Hydraulic Engineering*, 138(1), 35-45.

Haghighi, A., Covas, D., and Ramos, H. (2012). "Direct backward transient analysis for leak detection in pressurized pipelines: from theory to real application." *Journal of water supply: research and technology—AQUA*, 61(3), 189-200.

Hao, T., Rogers, C. D. F., Metje, N., Chapman, D. N., Muggleton, J. M., Foo, K. Y., Wang, P., Pennock, S. R., Atkins, P. R., Swingler, S. G., Parker, J., Costello, S. B., Burrow, M. P. N., Anspach, J. H., Armitage, R. J., Cohn, A. G., Goddard, K., Lewin, P. L., Orlando, G., Redfern, M. A., Royal, A. C. D., and Saul, A. J. (2012). "Condition assessment of the buried utility service infrastructure." *Tunnelling and Underground Space Technology*, 28(1), 331-344.

Hargesheimer, E. E. (1985). "Identifying water main leaks with trihalomethane tracers." *Journal / American Water Works Association*, 77(11), 71-75.

Inaudi, D., Belli, R., and Walder, R. (2008). "Detection and localization of micro-leakages using distributed fiber optic sensing." *Proceedings of the 2008 7th International Pipeline Conference*, ASME, New York, NY, 599–605.

Jönsson, L., and Larson, M. (1992). "Leak detection through hydraulic transient analysis." In *Pipeline Systems*, B. Coulbeck and E. P. Evans, eds., Kluwer Academic Publishers, Dordrecht, the Netherlands 273-286.

Jung, B. S., and Karney, B. W. (2008). "Systematic exploration of pipeline network calibration using transients." *Journal of Hydraulic Research, IAHR*, 46(SUPPL. 1), 129-137.

Karim, M. R., Abbaszadegan, M., and Lechevallier, M. (2003). "Potential for pathogen intrusion during pressure transients." *Journal of American Water Works Association*, 95(5), 134-146.

Kim, S. H. (2005). "Extensive development of leak detection algorithm by impulse response method." *Journal of Hydraulic Engineering*, 131(3), 201-208.

Kim, Y. (2008). "Advanced Numerical and Experimental Transient Modelling of Water and Gas Pipeline Flows Incorporating Distributed and Local Effects," PhD thesis, University of Adelaide, Adelaide.

Kim, Y., Simpson, A. R., and Lambert, M. F. (2007). "The effect of orifices and blockages on unsteady pipe flows." *World Environmental and Water Resources Congress 2007*, ASCE.

Lambert, A. O. (2002). "International report: Water losses management and techniques." *Water Science and Technology: Water Supply*, 2(4), 1-20.

Lee, P. J., Vítkovský, J. P., Lambert, M. F., Simpson, A. R., and Liggett, J. A. (2002). "Leak detection in pipelines using an inverse resonance method." *Proceedings of the 1st Annual Environmental & Water Resources System Analysis Symposium*, ASCE, Reston, VA.

Lee, P. J., Vítkovský, J. P., Simpson, A. R., Lambert, M. F., and Liggett, J. A. (2003). "Discussion to 'leak detection in pipes by frequency response

method using a step excitation' by Mpesha, W., Chaudhry, M.H, and Gassman, S.L., 2002, 40(1), 55-62." *Journal of Hydraulic Research*, 41(2), 221-223.

Lee, P. J., Vítkovský, J. P., Lambert, M. F., Simpson, A. R., and Liggett, J. A. (2005a). "Frequency domain analysis for detecting pipeline leaks." *Journal of Hydraulic Engineering*, 131(7), 596-604.

Lee, P. J., Vítkovský, J. P., Lambert, M. F., Simpson, A. R., and Liggett, J. A. (2005b). "Leak location using the pattern of the frequency response diagram in pipelines: a numerical study." *Journal of Sound and Vibration*, 284(3-5), 1051–1073.

Lee, P. J., Lambert, M. F., Simpson, A. R., Vítkovský, J. P., and Liggett, J. A. (2006). "Experimental verification of the frequency response method for pipeline leak detection." *Journal of Hydraulic Research*, 44(5), 693–707.

Lee, P. J., Lambert, M. F., Simpson, A. R., Vítkovský, J. P., and Misiunas, D. (2007a). "Leak location in single pipelines using transient reflections." *Australian Journal of Water Resources*, 11(1), 53-65.

Lee, P. J., Vítkovský, J. P., Lambert, M. F., Simpson, A. R., and Liggett, J. A. (2007b). "Leak location in pipelines using the impulse response function." *Journal of Hydraulic Research*, 45(5), 643-652.

Lee, P. J., Vítkovský, J. P., Lambert, M. F., and Simpson, A. R. (2008a). "Valve design for extracting response functions from hydraulic systems using pseudorandom binary signals." *Journal of Hydraulic Engineering*, 136(4), 858-864.

Lee, P. J., Vítkovský, J. P., Lambert, M. F., Simpson, A. R., and Liggett, J. A. (2008b). "Discrete blockage detection in pipelines using the frequency

response diagram: numerical study." *Journal of Hydraulic Engineering*, 134(5), 658-663.

Liggett, J. A., and Chen, L.-C. (1994). "Inverse transient analysis in pipe networks." *Journal of Hydraulic Engineering*, 120(8), 934-955.

Liou, C. P. (1998). "Pipeline leak detection by impulse response extraction." *Journal of Fluids Engineering*, 120(4), 833-838.

Liu, Z., and Kleiner, Y. (2013). "State of the art review of inspection technologies for condition assessment of water pipes." *Measurement*, 46(1), 1-15.

Ljung, L. (1999). *System Identification - Theory for the User*, Prentice-Hall, Inc., Upper Saddle River, New Jersey.

McIntosh, A. C., and Yniguez, C. E. (1997). *Second Water Utilities Data Book : Asian and Pacific Region*, Asian Development Bank, Manila, Philippines.

Meniconi, S., Brunone, B., Ferrante, M., and Massari, C. (2010). "Fast transients as a tool for partial blockage detection in pipes: First experimental results." *Proceedings of the 12th International Conference on Water Distribution Systems Analysis*, ASCE, Reston, VA.

Meniconi, S., Brunone, B., Ferrante, M., Berni, A., and Massari, C. (2011). "Experimental evidence of backflow phenomenon in a pressurised pipe." *Proceedings of the Computing and Control for the Water Industry 2011*, University of Exeter, Exeter, UK.

Metje, N., Atkins, P. R., Brennan, M. J., Chapman, D. N., Lim, H. M., Machell, J., Muggleton, J. M., Pennock, S., Ratcliffe, J., Redfern, M., Rogers, C. D. F., Saul, A. J., Shan, Q., Swingler, S., and Thomas, A.

M. (2007). "Mapping the underworld – state-of-the-art review." *Tunnelling and Underground Space Technology*, 22(5–6), 568-586.

Mpesha, W., Gassman, S. L., and Chaudhry, M. H. (2001). "Leak detection in pipes by frequency response method." *Journal of Hydraulic Engineering*, 127(2), 134-147.

Mpesha, W., Chaudhry, M. H., and Gassman, S. L. (2002). "Leak detection in pipes by frequency response method using a step excitation." *Journal of Hydraulic Research*, 40(1), 55-62.

Mutikanga, H. E., Sharma, S., and Vairavamoorthy, K. (2009). "Water loss management in developing countries: Challenges and prospects." *Journal of American Water Works Association*, 101(12), 57-68.

Nawrocki, J., Raczyk-Stanisawiak, U., Swietlik, J., Olejnik, A., and Sroka, M. J. (2010). "Corrosion in a distribution system: Steady water and its composition." *Water Research*, 44(6), 1863-1872.

Nixon, W., and Ghidaoui, M. S. (2006). "Range of validity of the transient damping leakage detection method." *Journal of Hydraulic Engineering*, 132(9), 944-957.

Pudar, R. S., and Liggett, J. A. (1992). "Leaks in pipe networks." *Journal of Hydraulic Engineering*, 118(7), 1031-1046.

Puust, R., Kapelan, Z., Savic, D. A., and Koppel, T. (2010). "A review of methods for leakage management in pipe networks." *Urban Water Journal*, 7(1), 25 - 45.

Rajani, B., and Kleiner, Y. (2001). "Comprehensive review of structural deterioration of water mains: physically based models." *Urban Water*, 3(3), 151-164.

Roinila, T., Vilkko, M., and Suntio, T. (2010). "Frequency-response measurement of switched-mode power supplies in the presence of nonlinear distortions." *IEEE Transactions on Power Electronics*, 25(8), 2179-2187.

Rose, J. L., Cho, Y., and Avioli, M. J. (2009). "Next generation guided wave health monitoring for long range inspection of pipes." *Journal of Loss Prevention in the Process Industries*, 22(6), 1010-1015.

Roubal, M. (2002). "Condition assessment of pipeline networks." American Society of Civil Engineers.

Sarin, P., Snoeyink, V. L., Bebee, J., Kriven, W. M., and Clement, J. A. (2001). "Physico-chemical characteristics of corrosion scales in old iron pipes." *Water Research*, 35(12), 2961-2969.

Sattar, A. M., Chaudhry, M. H., and Kassem, A. A. (2008). "Partial blockage detection in pipelines by frequency response method." *Journal of Hydraulic Engineering*, 134(1), 76-89.

Sattar, A. M., and Chaudhry, M. H. (2008). "Leak detection in pipelines by frequency response method." *Journal of Hydraulic Research*, 46(sup 1), 138-151.

Selvakumar, A., Clark, R. M., and Sivaganesan, M. (2002). "Costs for water supply distribution system rehabilitation." *Journal of Water Resources Planning and Management*, 128(4), 303-306.

Shamloo, H., and Haghighi, A. (2009). "Leak detection in pipelines by inverse backward transient analysis." *Journal of Hydraulic Research*, 47(3), 311-318.

Shucksmith, J. D., Boxall, J. B., Staszewski, W. J., Seth, A., and Beck, S. B. M. (2012). "Onsite leak location in a pipe network by cepstrum

analysis of pressure transients." *Journal - American Water Works Association*, 104(8), E457-E465.

Silva, R. A., Buiatti, C. M., Cruz, S. L., and Pereira, J. A. F. R. (1996). "Pressure wave behaviour and leak detection in pipelines." *Computers & Chemical Engineering*, 20(SUPPL. PT A), S491-S496.

Stephens, M. L. (2008). "Transient response analysis for fault detection and pipeline wall condition assessment in field water transmission and distribution pipelines and networks," PhD Dissertation, University of Adelaide, Adelaide, Australia.

Stephens, M. L., Lambert, M. F., and Simpson, A. R. (2013). "Determining the internal wall condition of a water pipeline in the field using an inverse transient model." *Journal of Hydraulic Engineering*, 139(3), 310–324.

Stephens, M. L., Simpson, A. R., and Lambert, M. F. (2008). "Internal wall condition assessment for water pipelines using inverse transient analysis." *Proceedings of the 10th Annual Symposium on Water Distribution Systems Analysis*, ASCE, Reston, VA.

Svingen, B. (1996). "Fluid structure interaction in slender pipes." *Proceedings of the 7th International Conference on Pressure Surges and Fluid Transients in Pipelines and Open Channels*, Mechanical Engineering Publications, London, UK, 385-396.

Swietlik, J., Raczyk-Stanisawiak, U., Piszora, P., and Nawrocki, J. (2012). "Corrosion in drinking water pipes: The importance of green rusts." *Water Research*, 46(1), 1-10.

Tafuri, A. N. (2000). "Locating leaks with acoustic technology." *Journal of American Water Works Association*, 92(7), 57-66.

Taghvaei, M., Beck, S. B. M., and Staszewski, W. J. (2006). "Leak detection in pipelines using cepstrum analysis." Institute of Physics Publishing, 367-372.

Taghvaei, S. M. (2009). "Fast leak detection and location of water pipelines based using orthogonal wavelet transform." American Society of Civil Engineers, 186-192.

Tan, A. H., and Godfrey, K. R. (2002). "The generation of binary and near-binary pseudorandom signals: An overview." *IEEE Transactions on Instrumentation and Measurement*, 51(4), 583-588.

Tijsseling, A. S. (1996). "Fluid-structure interaction in liquid-filled pipe systems: A review." *Journal of Fluids and Structures*, 10(2), 109-146.

Tran, D. H., Perera, B. J. C., and Ng, A. W. M. (2009). "Predicting structural deterioration condition of individual storm-water pipes using probabilistic neural networks and multiple logistic regression models." *Journal of Water Resources Planning and Management*, 135(6), 553-557.

Tran, D. H., Perera, B. J. C., and Ng, A. W. M. (2010). "Hydraulic deterioration models for storm-water drainage pipes: Ordered probit versus probabilistic neural network." *Journal of Computing in Civil Engineering*, 24(2), 140-150.

US EPA. (2009). "Condition Assessment of Ferrous Water Transmission and Distribution Systems - State of Technology Review Report." *Publication No. EPA/600/R-09/055*, National Risk Management Research Laboratory, Cincinnati, OH.

US EPA. (2011). "Aging Water Infrastructure Research: Addressing the Challenge Through Science and Innovation." *Publication No.*

EPA/600/F-11/010, National Risk Management Research Laboratory, Cincinnati, OH.

US EPA. (2012). "Condition Assessment Technologies for Water Transmission and Distribution Systems." *Publication No. EPA/600/R-12/017*, National Risk Management Research Laboratory, Cinccinati.

Vardy, A. E., and Brown, J. M. B. (2003). "Transient turbulent friction in smooth pipe flows." *Journal of Sound and Vibration*, 259(5), 1011-1036.

Vardy, A. E., and Brown, J. M. (1996). "On turbulent, unsteady, smooth pipe friction." *Proceedings of the 7th International Conference on Pressure Surges and Fluid Transients in Pipelines and Open Channels*, Mechanical Engineering Publications, London, UK, 289-311.

Vítkovský, J. P., Simpson, A. R., and Lambert, M. F. (2000). "Leak detection and calibration using transients and genetic algorithms." *Journal of Water Resources Planning and Management*, 126(4), 262-265.

Vítkovský, J. P., Stephens, M. L., Bergant, A., Simpson, A. R., and Lambert, M. F. (2006). "Numerical error in weighting function-based unsteady friction models for pipe transients." *Journal of Hydraulic Engineering*, 132(7), 709-721.

Vítkovský, J. P., Lambert, M. F., Simpson, A. R., and Liggett, J. A. (2007). "Experimental observation and analysis of inverse transients for pipeline leak detection." *Journal of Water Resources Planning and Management*, 133(6), 519-530.

Vítkovský, J. P., Bergant, A., Simpson, A. R., and Lambert, M. F. (2003a). "Frequency-domain transient pipe flow solution including unsteady friction." *Pumps, Electromechanical Devices and Systems Applied to Urban Water Management: Proceedings of the International*

Conference, A. A. Balkema Publishers, Lisse, The Netherlands, 773-780.

Vítkovský, J. P., Lee, P. J., Spethens, M. L., Lambert, M. F., Simpson, A. R., and Liggett, J. A. (2003b). "Leak and blockage detection in pipelines via an impulse response method." *Pumps, Electromechanical Devices and Systems Applied to Urban Water Management: Proceedings of the International Conference*, A. A. Balkema Publishers, Lisse, The Netherlands, 423–430.

Vreeburg, I. J. H. G., and Boxall, D. J. B. (2007). "Discolouration in potable water distribution systems: A review." *Water Research*, 41(3), 519-529.

Wang, X. J., Lambert, M. F., Simpson, A. R., Liggett, J. A., and Vítkovský, J. P. (2002). "Leak detection in pipelines using the damping of fluid transients." *Journal of Hydraulic Engineering*, 128(7), 697-711.

Wang, X. J., Lambert, M. F., and Simpson, A. R. (2005). "Detection and location of a partial blockage in a pipeline using damping of fluid transients." *Journal of Water Resources Planning and Management*, 131(3), 244-249.

WSAA. (2008). "WSAA Report Card 2007/2008, Performance of the Australian Urban Water Industry and projections for the future." Water Services Association of Australia (WSAA), Melbourne, Australia.

Wylie, E. B. (1983). "The microcomputer and pipeline transients." *Journal of Hydraulic Engineering, ASCE*, 109(12), 1723-1739.

Wylie, E. B., and Streeter, V. L. (1993). *Fluid Transients in Systems*, Prentice Hall Inc., Englewood Cliffs, New Jersey, USA.

Zamanzadeh, M., Kirkwood, G. C., Scheinman, S., and Bayer, G. T. (2007). "Corrosion sensors for detecting graphitization of cast iron in water

mains." *Proceedings of Corrosion Conference and Expo 2007*, Curran Associates, Inc., Red Hook, NY.

Zecchin, A. C., White, L. B., Lambert, M. F., and Simpson, A. R. (2013). "Parameter identification of fluid line networks by frequency-domain maximum likelihood estimation." *Mechanical Systems and Signal Processing*, 37(1-2), 370-387.

Zielke, W. (1968). "Frequency-dependent friction in transient pipe flow." *Journal of Basic Engineering*, 90(1), 109-115.